UNIVERSITÀ
DEGLI STUDI
FIRENZE

DOTTORATO DI RICERCA IN
AREA DEL FARMACO E TRATTAMENTI INNOVATIVI

CICLO XXX

COORDINATORE Prof.ssa Elisabetta Teodori

MODELING AND STRUCTURE-BASED APPROACHES IN THE DESIGN, SYNTHESIS AND BIOLOGICAL EVALUATION OF LIGANDS TARGETING THE METALLOENZYMES CARBONIC ANHYDRASES

Settore Scientifico Disciplinare CHIM/08

Dottorando
Dott. Alessio Nocentini

Tutore Scientifico
Prof.ssa Paola Gratteri

Tutore Teorico
Prof. Claudiu T. Supuran

Coordinatore
Prof.ssa Elisabetta Teodori

Anni 2014/2017

Abstract

Different projects pertaining computational structure-based drug design (SBDD), synthesis and biological evaluation of compounds acting as inhibitors of the enzymes carbonic anhydrase (CAs, EC 4.2.1.1) were the focus of the three-years research activity of the PhD period.

CAs are ubiquitous metalloenzymes, which catalyse a simple physiological reaction, i.e. the conversion of CO_2 to the bicarbonate ion and protons. CAs are present throughout most living organisms and encoded by seven evolutionarily unrelated gene families: the α-, β-, γ-, δ-, ζ-, η and θ-CAs. The active site of most CAs contains a zinc ion (Zn^{2+}), which is crucial for catalysis.

The CAs have gained increasing attention in the pharmaceutical field over the last decades due to the identification of a plethora of isoforms both in humans (hCA) and pathogens, where CAs are involved in many physiological and pathological processes.

This thesis work mainly deals with the rational design and synthesis of inhibitors (CAIs) of CA isoforms belonging to the α- and β- classes of carbonic anhydrases

All human CAs belong to the α-class and, up to now, sixteen isozymes have been identified. These isozymes are normally found in monomeric form, with the exception of human isoforms VI, IX and XII which occur as dimers. β-CAs, found in many bacteria and fungi, are oligomers formed by two or more identical subunits, generally dimers, tetramers and octamers.

Considering the variety of human physiological-pathological processes showing abnormal levels or activities of these enzymes, as well as the essential role of CAs in the life cycle of pathogens, CA isozymes have acquired growing interest for the design of inhibitors or activators with biomedical applications.

The “Click Chemistry approach”, which have acquired a prominent role in medicinal chemistry, was applied in order to synthesize carbonic anhydrases inhibitors (CAIs) belonging to the sulfonamide, coumarin and sulfocoumarin type. The inhibitory profile of the designed and synthesized derivatives pointed out interesting potential candidates for the treatment of pathologies, such as glaucoma or tumors. The binding mode of the triazole sulfonamide derivatives within hCAs was studied by means of computational methods and X-ray crystallography.

The particular trend of the inhibitory profile of sulfocoumarin, a prodrug class of CAIs, led us to hypothesize the involvement of the sulfocoumarin CA-mediated hydrolysis in the isoform-selective efficacy. By means of quantum-mechanics (QM) computational methods applied to a cluster CA-model, we were able to define a multi-step hydrolytic reaction mechanism.

New chemotypes were studied for CA inhibition. Despite the primary sulfonamide moiety is the ideal zinc-binding group for CA inhibition, we were interested in studying the never-investigated N-nitrosulfonamide as new CA inhibitory chemotype. Promising results obtained for an initial set of compounds, screened on different CA isoforms, were followed by computational binding mode evaluation, which depicted a novel Zn-binding approach.

The great interest of the cosmetic field on the research over new anti-dandruff agents led us to investigate a variety of hCAIs belonging to different chemotypes present in our libraries for the inhibition of the CA from *Malassezia Globosa* (MgCA), a dandruff-producing fungus. A model of MgCA was built by homology in order to evaluate the binding mode of these chemotypes, such as mono- and dithiocarbammates, phenols and benzoxaboroles.

Isoform IX of the hCA represents a validated anticancer drug target and a marker of tumor hypoxia. Considering pyrimidine and purine were widely used as anti-tumor pharmacophores in medicinal chemical research, we applied the “tail approach” by combining adenine or uracil as tails of benzenesulfonamide derivatives. Therefore, we studied the inhibitory efficacy of the synthesized compounds against the target isoform as well as off-target ones. Moreover, we reported the crystal structure of an adenine derivative both in complex with hCA II and hCA IX.

Finally, during my three-years PhD period, I dealt with additional computational studies, biological evaluation, spectroscopic measurements, as well as synthetic procedures, mainly applied to the development of new promising CAIs for different applications in the medicinal field.

TABLE OF CONTENTS

LIST OF ABBREVIATION AND SYMBOLS

4-NpA	4-nitrophenyl acetate
AAZ	acetazolamide
AG	anchoring group
AS	aminosulfonamides
B3LYP	Becke, 3-parameter, Lee-Yang-Parr
BRZ	brinzolamide
CAIs	carbonic anhydrases inhibitors
CAs	carbonic anhydrases
CuAAC	copper-catalyzed azide−alkyne cycloadditions
DBU	1,8-diazabicyclo[5.4.0]undec-7-ene
DCP	dichlorophenamide
DFT	density functional theory
DMAP	4-(dimethylamino)pyridine
DRZ	dorzolamide
DTCs	dithiocarbamates
ED	electro-donating group
EDC	N-(3-dimethylaminopropyl)-N′-ethylcarbodiimide
ESP	ElectroStatic Potential charges
EW	electro-withdrawing group
EZA	ethoxzolamide
GMQE	Global Model Quality Estimation
hCAs	human carbonic anhydrases
HOAt	1-hydroxy-7-azabenzotriazole
hp	*Helicobacter pylori*
IOP	intra ocular pressure
MgCA	*Malassezia Globosa* carbonic anhydrase
MM	molecular mechanics
MM-GBSA	Molecular Mechanics Generalized Born Surface Area
MTCs	monothiocarbammates
NHS	N-hydroxysuccinimide
PDB	Protein Data Bank
PTB	phenyltriazolylbenzenesulfonamide
QM	quantum-mechanics
QM/MM	quantum mechanics/molecular mechanics
QST	Quadratic Synchronous Transit methods
SA	sulfanilamide
SAR	structure-activity relationship
SBDD	structure-based drug design
SG	sticky group
TcCA	*Trypanosoma cruzi* carbonic anhydrase
VchCA	*Vibrio cholera* carbonic anhydrase
ZBG	zinc-binding group
ZPE	zero point energy

Understanding the binding interactions between ligands and biological targets represents a paradigm in the modern medicinal chemistry research. Over the years it has increasingly relied on the 3D structural information obtained by X-ray and NMR techniques that make it possible to investigate how a ligand recognizes its target, and to study which forces are responsible for the binding.

Many computational tools and programs are widely used as part of an early discovery process in which compounds are designed and iteratively optimized in order to improve binding affinity and pharmacokinetic properties.

In this thesis work we deal with computational structure based drug design (SBDD), synthesis and biological evaluation of compounds acting as inhibitors of the enzyme carbonic anhydrase (CAs, EC 4.2.1.1). Moreover, we used SBDD tools to evaluate and rationalize the experimental inhibitory profile measured for the synthesized and screened derivatives. Additionally, we built model by homology for those enzyme isoforms for which the 3D structure was not available.

The development of novel inhibitors for the different isoforms of carbonic anhydrase is currently of great interest in the medicinal chemistry field for the identification of new promising drug candidates useful for the treatment of various diseases.

Herefollowing, we will report some of the major results obtained in the three-year PhD research period that led to the discovery of novel inhibitors, also belonging to new chemotypes, for different isoforms of the zinc-enzymes carbonic anhydrase and to the identification of new and promising candidates for the treatment of glaucoma, cancer and bacterial/fungal/parasitic infections.

Part I - Introduction

Chapter 1. Distribution, biochemistry, and structural features of Carbonic Anhydrase classes.

1.1 Carbonic Anhydrases: an overview.

Carbonic anhydrases (CAs, EC 4.2.1.1) are ubiquitous metalloenzymes, present throughout most living organisms and encoded by seven evolutionarily unrelated gene families: the α-, β-, γ-, δ-, ζ-, η and θ-CAs.[1-12] Primarily, CAs have been identified in red blood cells of bovine [13] and subsequently found in all mammalian tissues, plants, algae and bacteria. The ubiquity of CAs is due to the catalysis of a simple, but physiologically pivotal reaction for living beings,[1] i.e. the reversible hydration of carbon dioxide to bicarbonate and protons according to the following equilibrium:

$$CO_2+H_2O \leftrightharpoons HCO_3^- + H^+$$

The reaction of hydration of CO_2 consists of four reactions:

1) $CO_2(g) \leftrightharpoons CO_2(aq)$	Reaction of dissolution in aqueous phase
2) $CO_2(aq) + H_2O \leftrightharpoons H_2CO_3$	Hydration reaction (carbonic acid production)
3) $H_2CO_3 \leftrightharpoons HCO_3^- + H^+$	Ionization reaction (bicarbonate production)
4) $HCO_3^- \leftrightharpoons CO_3^{2-} + H^+$	Dissociation reaction (carbonate formation)

The carbonic anhydrases, which are among the fastest enzymes known, effectively speeds up the rate of the overall reaction, being able to convert a million molecules of CO_2 per second, thus increasing the value of the turnover number (kcat) from 10^{-1} s^{-1},[14] in physiological conditions and in the absence of the catalyst, to 10^5 s^{-1}.

CO_2, bicarbonate, and protons are essential in a plethora of physiologic processes in organisms belonging to all life kingdoms (Bacteria, Archaea, and Eukarya) and for this reason, relatively high amounts of CAs are present in different tissues/cell compartments of most investigated organisms.

In mammals, CAs are involved in breathing and transport of CO_2 and HCO_3^- in tissues and lungs, in the homeostasis of pH and CO_2 in biosynthetic reactions such as gluconeogenesis, lipogenesis, ureagenesis.[1] Differently in microorganisms, in addition to

the transport of CO_2/HCO_3^- and its supply for biosynthetic reactions, carbonic anhydrases play a role in: i) carbon fixation in photosynthetic process; ii) metabolism of xenobiotics (e.g. degradation of the cyanate in E. coli); iii) pH regulation; iv) survival of the pathogen within the host organism; v) synthesis of purine and pyrimidine.[15]

In mammals, the carbon dioxide produced by the aerobic metabolism leaves the cells at the level of the peripheral tissue, driven by the pressure gradient, and enters the blood where it dissolves in the plasma. About 90% of the carbon dioxide enters the red blood cells where the carbonic anhydrase catalyses its hydration, forming carbonic acid, which in turn dissociates into HCO_3^- and H^+. Thereafter, HCO_3^- leaves the red blood cell by a protein antiporter which exchanges a HCO_3^- ion with a Cl^- ion. The ratio 1:1 between the two anions maintains the electrical neutrality, thus does not affect the membrane potential of the cell. The HCO_3^- ion is converted to carbonate and protons, acting as a buffer.[16] At the alveolar level the concentration of CO_2 is lower than in the peripheral tissues, while the higher concentration of HCO_3^- drives its pumping inside the red cell. Herein, the CAs catalyse the reverse reaction, converting the bicarbonate/carbonic acid in water and carbon dioxide. The CO_2 is released into the blood and is exhaled after having passed by diffusion through the walls of the alveolus. Therefore, the direction of the reaction depends on the concentration of CO_2: in case of low concentration, as in the lungs, the acid is dissociated, releasing carbon dioxide; alternatively, when the concentration is high, CO_2 is converted to carbonates, which are transported by the blood to the lungs.[16]

1.2 Carbonic Anhydrase classes.

Until now seven distinct gene families of CAs were identified.[1-12]

The α-CAs are present in vertebrates, protozoa, algae, and cytoplasm of green plants and in some bacteria;[1] the β-CAs are predominantly found in bacteria, algae and chloroplasts of both mono- as well as dicotyledons, but also in many fungi and some Archaea.[1,10,15] The γ-CAs were found in Archaea, cyanobacteria, and most types of bacteria, [1,10,15] the δ - and ζ-CAs seem to be present only in marine diatoms,[4,5] whereas the η-CAs in protozoa.[7] θ-CA has been recently identified in the marine diatom *Phaeodactylum tricornutum*.

The α-, β-, δ-, η- and, maybe θ-CAs contain a Zn(II) ion at the active site, the γ-CAs are probably Fe(II) enzymes (although it seems that the Fe(II) can be replaced by Zn(II) or

Co(II) ions), whereas the ζ-class CAs are cambialistic enzymes, active both with Cd(II) or Zn(II) bounded within the active site as cofactor.[1,4,5,7,9,12]

In addition to hydration of carbon dioxide, α-CAs were shown to be able to catalyse the hydrolysis of esters/thioesters, (for example 4-nitrophenyl acetate (4-NpA) hydrolysis, as well as other hydrolytic reactions);[2] differently no esterase activity was detected so far for enzymes belonging to the other six CA genetic families.[2]

1.3 Catalytic mechanism.

All CAs are metalloenzymes, and the metal ion is critical for catalysis, as the apoenzyme is devoid of activity. [1-3]

In all CA classes, the catalytic reaction ($CO_2+H_2O \leftrightharpoons HCO_3^- + H^+$) follows a two-step catalytic mechanism, in which a metal hydroxide species of the enzyme ($E\text{-}M^{2+}\text{-}OH^-$) is the catalytically active species. Indeed, in the first step of reaction, this species acts as strong nucleophile (at neutral pH) on the CO_2 molecule bound in a hydrophobic pocket nearby with consequent formation of HCO_3^-, which is then displaced from the active site by a water molecule (Eq. 1.1). The second step regenerates the metal hydroxide species through a proton transfer reaction from the M^{2+} bound water to an exogenous proton acceptor or to an active site residue, represented by B in Eq. 1.2. [1-3]

$$E\text{-}M^{2+}\text{-}OH^- + CO_2 \leftrightharpoons E\text{-}M^{2+}\text{-}HCO_3^- \leftrightharpoons E\text{-}M^{2+}\text{-}H_2O + HCO_3^- \quad (1.1)$$

$$E\text{-}M^{2+}\text{-}H_2O + B \leftrightharpoons -M^{2+}\text{-}OH^- + BH^+ \quad (1.2)$$

Figure 1 transfers the two-steps catalytic mechanism just depicted into a generic α-CA active site cavity. Primarily the zinc ion, present in the catalytic pocket, is bound to a hydroxyl ion (Figure 1a) in a configuration which corresponds to the active form of the enzyme.[1] The substrate CO_2 is bound in a hydrophobic pocket near the Zn(II) ion, mainly defined by residues which are Val21, Val143, Leu198 and Trp209 in the human isoform hCA II. CO_2 undergoes the hydration process in an orientation that makes it suited for the nucleophilic attack on the carbon atom by the zinc bound hydroxide ion (Figure 1a). Thereafter, the bicarbonate ion is displaced by a water molecule and released in solution. When the water molecule is coordinated to the zinc the enzyme is in its acidic,

catalytically inactive form (Figure 1a). The catalytically active form of the enzyme is regenerated through the proton transfer reaction from the active site of the enzyme to the surrounding micro-environment (Figure 1a). In the catalytically very active isozymes, (such as human isoforms CA II, IV, VI, VII, IX, XII, XIII and XIV), the process is assisted by a histidine residue placed at the entrance of the active site (His64 known as "proton shuttle residue"), or by a cluster of histidines (Figure lb), which protrudes from the rim of the active site to the surface of the enzyme, thus assuring efficient proton-transfer pathways.[1] Indeed, the absence of His64 in other CAs lowers their catalytic efficiency.

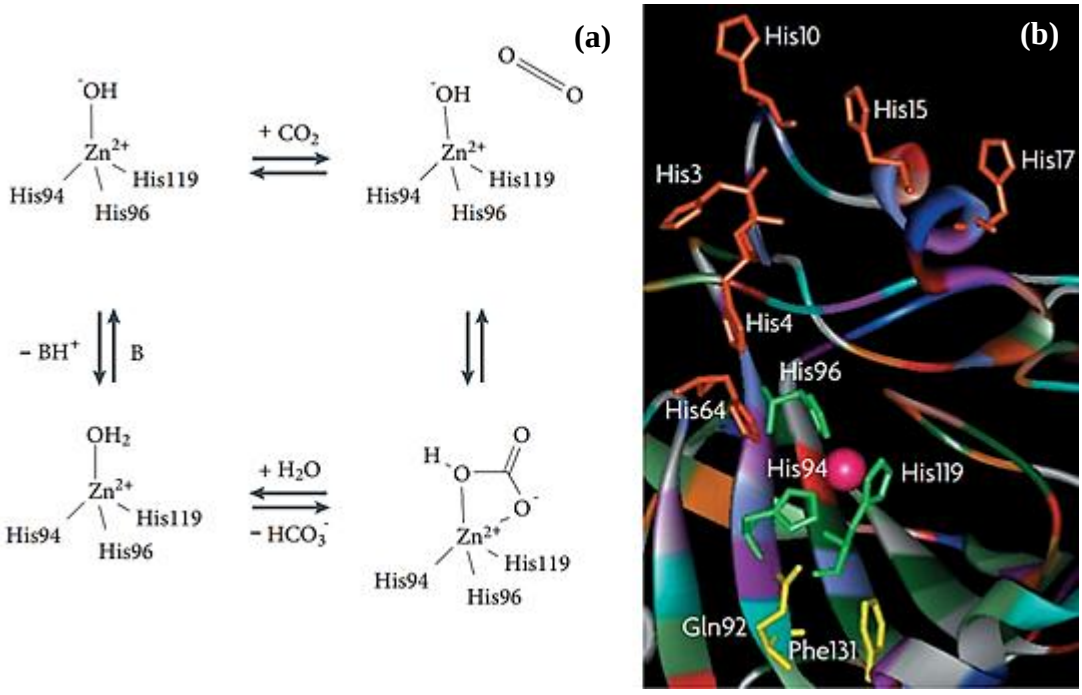

Figure 1. (a) Schematic representation of the catalytic mechanism of a α-CA; (b) His64, known as "proton shuttle residue" and cluster of histidines, which assure efficient proton-transfer pathways.

1.4 Characteristics of the Carbonic Anhydrase classes.

Since my work mainly relies on CA isoforms belonging to α and β classes, here following, I present the main features of such classes of carbonic anhydrase.

α-Carbonic Anhydrases (α-CAs).

All mammals CAs belong to the α-class and, up to now, sixteen isozymes have been identified.[1-3,17] These isoenzymes differ by molecular features, oligomeric arrangement, cellular localization, distribution in organs and tissues, expression levels, kinetic properties and response to different classes of inhibitors (Figure 2).[1-3] According to their cellular localization (h) α-CAs are classified in:

• Cytosolic (isoenzymes I, II, III, IV, VIII)
• Mitochondrial (isoenzymes VA, VB)
• Membrane-bound (isoenzymes IV, IX, XII, XIV, XV)
• Secreted in saliva (isoenzyme VI)
• Catalytically inactive isoforms (CARP VIII, X and XI).

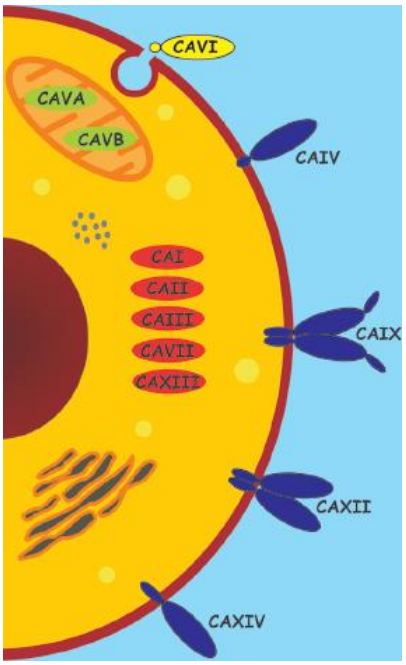

The cytosolic CA I, II, III, VII, and XIII and the mitochondrial CA VA and VB consist only of the CA domain; the membrane-associated CA IV, IX, XII, and XIV have a trans membrane anchor and, except for CA IV, also a cytoplasmic tail, while CA IX is the only isozyme with an N-terminal proteoglycan-like domain; CA VI is secreted and contains a short C-terminal extension.

Figure 2. Schematic illustration of domain composition and subcellular localization of catalytically active human α-CAs.

Table 1. Organ/Tissue Distribution, Subcellular Localization, CO_2 Hydrase Activity and involved diseases.

Isoform	Organ/tissue distribution	Subcellular localization	Catalitic Activity	Involved diseases
CA I	erythrocytes, eye, gastrointestinal tract	cytosol	low	retinal/cerebral edema
CA II	bone osteoclasts, brain, erythrocytes, eye, gastrointestinal tract, kidney, lung, testis	cytosol	high	glaucoma, edema, epilepsy, altitude sickness
CA III	adipocytes, skeletal muscle	cytosol	very low	oxidative stress
CA IV	brain capillaries, colon, eye, kidney, lung, heart muscle pancreas	membrane-bound	medium	glaucoma, retinitis pigmentosa, stroke
CA VA	liver	mitochondria	low	obesity
CA VB	Gastrointestinal tract, kidney, heart and skeletal muscle, pancreas, spinal cord	mitochondria	high	obesity
CA VI	salivary and mammary glands	secreted into saliva and milk	low	cariogenesis
CA VII	central nervous system	cytosol	high	epilepsy
CA VIII	central nervous system	cytosol	acatalytic	neurodegeneration, cancer
CA IX	tumours, gastrointestinal mucosa	transmembrane	high	cancer
CA X	central nervous system	cytosol	acatalytic	NA
CA XI	central nervous system	cytosol	acatalytic	NA
CA XII	Eye, intestine, kidney, reproductive epithelia, tumors	transmembrane	low	cancer, glaucoma
CA XIII	brain, gut, kidney, lung, reproductive tract	cytosol	low	sterility
CA XIV	eye, brain, kidney, liver,	transmembrane	low	epilepsy, retinopathy

To date the three-dimensional structures of all human isoforms except CA VB have been determined.[2] The analysis of the 3D structures shows that these enzymes exhibit similar structural features independently on their subcellular localization, characterized by a central twisted β-sheet surrounded by helical connections and additional β-strands (Figure 3a). The active site is located in a large, conical cavity, approximately wide 12 Å and deep 13 Å, which spans from the protein surface to the center of the molecule. The catalytic zinc ion is positioned at the bottom of the cavity and exhibits a tetrahedral coordination with three conserved His residues and a water molecule/hydroxide ion as ligands. The Zn^{2+}-bound water molecule/hydroxide ion is involved in a network of hydrogen bonds which enhance its nucleophilicity (Figure 3b). In particular, it establishes a hydrogen bond with the hydroxyl moiety of the conserved Thr199 residue and with two water molecules, located on two opposite sides: the first one, also called the “deep water”, is located in a hydrophobic cavity delimited by conserved residues in position 121, 143,

198, and 209, while the second one is in a hydrophilic environment toward the entrance of the active site (Figure 4).

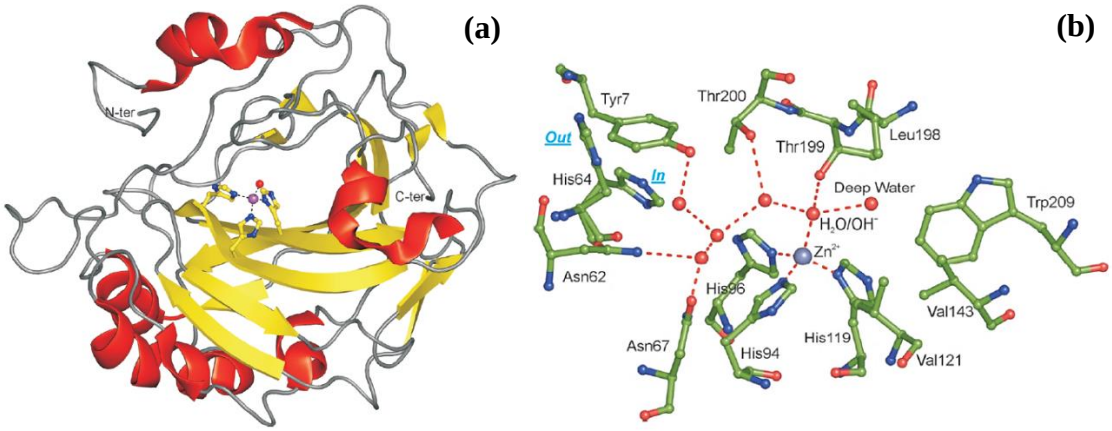

Figure 3. (a) Ribbon diagram of hCA II structure (PDB code 1CA2), which has been chosen as representative CA isoform. The active site Zn^{2+} coordination is also shown. Helix and β-strand regions are coloured in red and yellow, respectively. (b) The active site of hCA II. The Zn^{2+} is tetrahedrally coordinated by the three catalytic histidines and a water molecule/hydroxide ion, which is engaged in a well-defined network of hydrogen bonds. Water molecules are indicated as red circles. The side chain of His64 is shown in both the in and out conformations.

Several studies suggested that these two peculiar active site environments are responsible of the rapid catalytic cycling of CO_2 to bicarbonate; indeed, the hydrophobic region is necessary to sequester the CO_2 substrate and orient the carbon atom for nucleophilic attack by the zinc-bound hydroxide, while the hydrophilic region creates a well ordered hydrogen-bonded solvent network, which is necessary to allow the proton transfer reaction from the zinc-bound water molecule to the bulk solvent .

The α-CA are normally found in monomeric form with a molecular weight of approximately 29 kDa, with the exception of hCA VI, hCA IX and XII which occur as dimers.[2,17]

Differently, the bacterial α-CAs, such as those identified in the genome of *Sulfurihydrogenibium yellowstonense*, *Sulfurihydrogenibium azorense* and *Neisseriagonorrhoeae*, are dimers formed by two identical active monomers.[12]

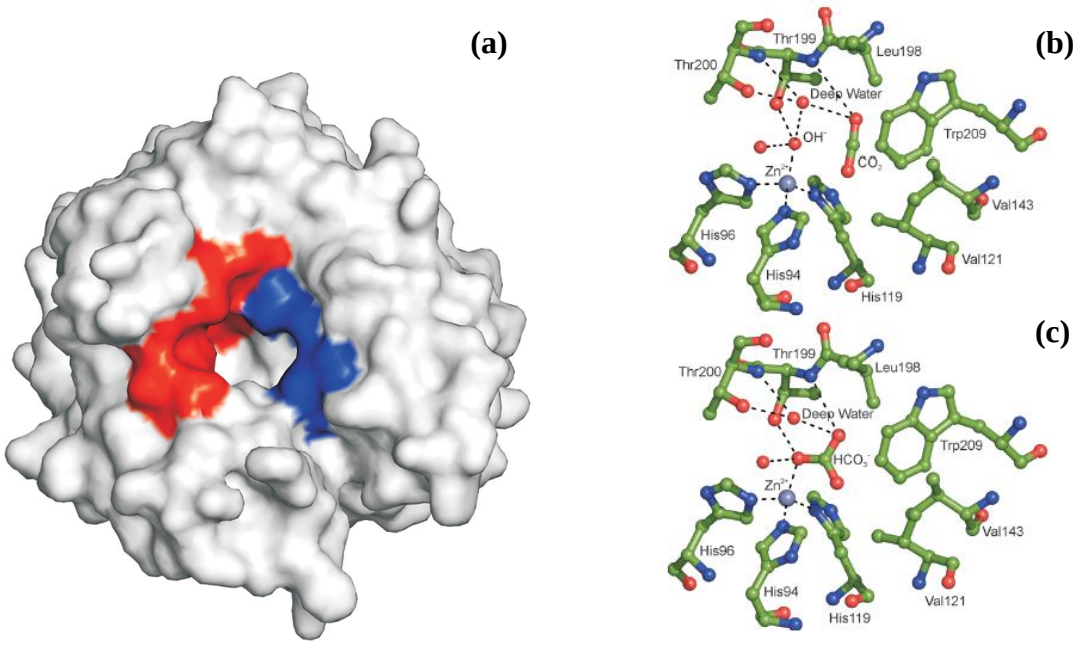

Figure 4. (a) Solvent accessible surface of hCA II. Residues delimiting the hydrophobic half of the active site cleft are shown in red (Ile91, Phe131, Val121, Val135, Leu141, Val143, Leu198, Pro202, Leu204Val207 and Trp209), while residues delimiting the hydrophilic one areshown in blue (Asn62, His64, Asn67 and Gln92); Active site of hCA II showing: (b) the position of CO_2 molecule (PDB code 2VVA), (c) the binding of the bicarbonate ion (PDB code 2VVB). The Zn^{2+} coordination and polar interactions are also reported.

Beside the great efficiency in the catalysis of carbon dioxide hydration process, α-CA show some catalytic versatility, participating in several other hydrolytic processes which presumably involve non-physiological substrates (Scheme 1). These reactions include the hydration of cyanate to carbamic acid (eq. **a**), or of cyanamide to urea (eq. **b**), the aldehyde hydration to gem-diols (eq. **c**), the hydrolysis of some carboxylic (eq. **d**) or sulfonic acid esters (eq. **e**), as well as other less investigated hydrolytic processes (eq. **f-h**).[2]
Recently, it has been shown that α-CA are endowed with a thioesterasic activity (eq. **i**).[18]

Scheme 1

a. $O=C=NH + H_2O \leftrightarrows H_2NCOOH$

b. $HN=C=NH + H_2O \leftrightarrows H_2NCONH_2$

c. $RCHO + H_2O \leftrightarrows RCH(OH)_2$

d. $RCOOAr + H_2O \leftrightarrows RCOOH + ArOH$

e. $RSO_3Ar + H_2O \leftrightarrows RSO_3H + ArOH$

f. $ArF + H_2O \leftrightarrows HF + ArOH$

g. $PhCH_2OCOCl + H_2O \leftrightharpoons PhCH_2OH + CO_2 + HCl$

h. $RSO_2Cl + H_2O \leftrightharpoons RSO_3H + HCl$

i. $PhSO_2NHCSSMe \leftrightharpoons C_6H_5SO_2NH_2 + H_2S + COS$

(Ar = 2,4-dinitrophenyl)

(R = Me; Ph)

β-Carbonic Anhydrases (β-CAs).

Most of bacteria, Archaea as *Methanobacterium thermoautotrophicum*, chloroplasts of algae, fungi and higher plants, contain CA belonging to the β-class.[10] Conversely from α-class isozymes, β-CAs are oligomers formed by two or more identical subunits, generally dimers (Figure 5a), tetramers and octamers. The monomeric subunit has a molecular weight of 25-30 kDa and the active form of the enzyme requires two subunits to reconstitute the catalytic site.[20] The residues of the catalytic triade are highly conserved among β-CA isoforms: [10,12,20,21] the Zn(II) ion is coordinated by two Cys residues, a residue of His and the carboxyl group of a residue of Asp or alternatively a water molecule/hydroxide ion (Figure 5b and Figure 6: β-CA from fungi *Cryptococcus Neoformans* (Can2) taken as representative).

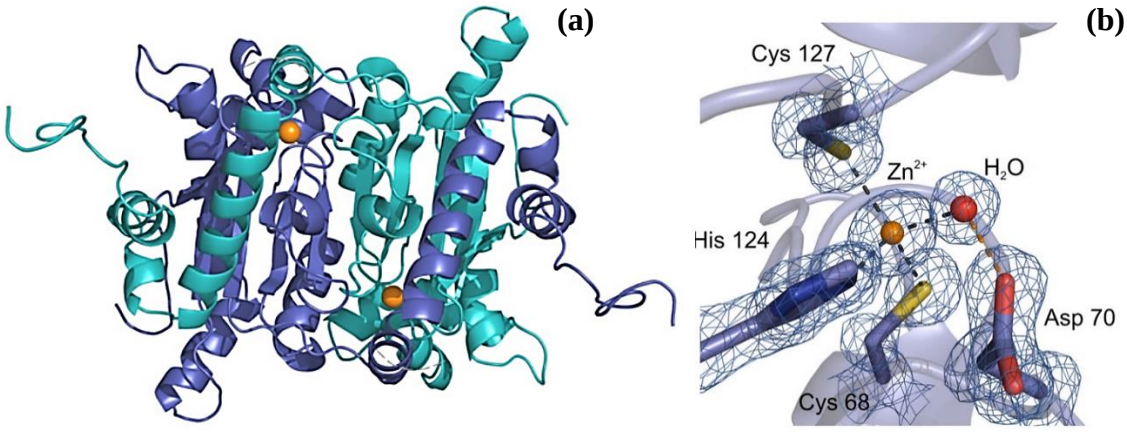

Figure 5. (a) Overall structure of the β-CA from fungi *Cryptococcus Neoformans* (Can2) dimer. One monomer is colored blue, while the other one is colored cyan. The Zn^{2+} ions are shown as orange spheres; (b) Active site of Can2 with electron density contoured at 1.0 σ. Coordination of the active-site Zn^{2+} by Cys68, His124, Cys127, and a water molecule is indicated by black broken lines, and the hydrogen bond from the water molecule to Asp70 is colored orange.

At a pH of 7.5 or lower, the active site of β-carbonic anhydrase, which is formed by residues belonging to two different subunits, is “locked, since the carboxyl group of an aspartic acid coordinates the zinc ion, thus completing the coordination pattern. For pH values higher than 8.3, the enzyme active site is instead found in its open form, due to the salt bridge that the aspartate residue forms with an arginine residue conserved in all the β-carbonic anhydrase.[19,20] A molecule of water/hydroxide ion completes the tetrahedral geometry coordination pattern of the metal ion (Figure 6). As a result, the catalytic mechanism of β-CAs with the active site in the "open" form is rather similar to α-class enzymes.

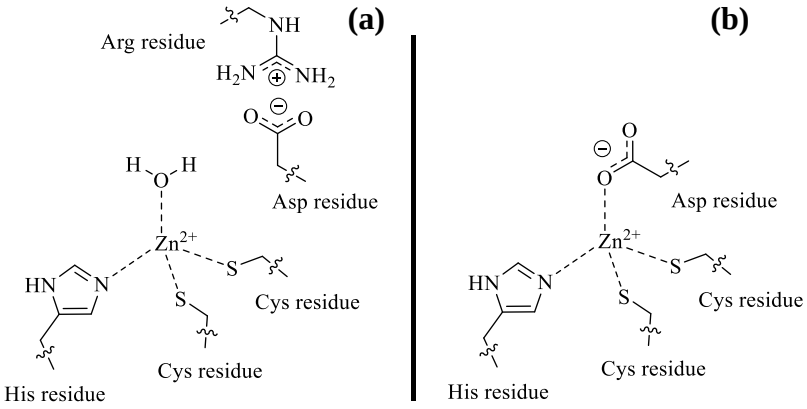

Figure 6. Active (a) and inactive (b) forms of β-CAs binding site cavity.

Chapter 2. Carbonic Anhydrases as drug targets.

2.1 Human Carbonic Anhydrases.

Several studies demonstrated the important role of hCAs in a variety of physiological processes showing that abnormal levels or activities of these enzymes have been often associated with different human diseases.[1,2,17] Consequently, in recent years CA isozymes have acquired great interest for the design of inhibitors or activators with biomedical applications.[1,22-27] CA activators may have pharmacological applications in pathologies in which learning and memory are impaired, such as Alzheimer's disease or aging.[3] On the other hand, CA inhibitors (CAIs) have been originally used as diuretics, antiglaucoma agents, antiepileptics, and in the management of altitude sickness,[3] while novel generation compounds are undergoing clinical investigation as anti-obesity, and antitumor drugs/diagnostic tools.[22-27]

Some hCAs, such as CA I and II, are ubiquitous and may be both targets for some diseases and off-targets, and in this case their inhibition should be avoided. For instance, hCA IX and XII in tumors should be inhibited by compounds, which do not affect the activity of CA I, II, VA, and VB.[22-27] Specifically CA I is found in many tissues, but Feeener's group[28] demonstrated how this enzyme is involved in retinal and cerebral edema, and its inhibition may be a valuable tool to affect these conditions. CA II is involved in several diseases, such as glaucoma, edema, epilepsy, and probably altitude sickness.[28-33] CA III plays a role in the oxidative stress, characterizing a lot of inflammatory diseases, although it is not clear whether the antioxidant effects of this protein are due to the hydration activity of CA III or to other enzyme properties, such as the presence of Cys residues on its surface. [34] CA IV is surely a drug target for several pathologies, including glaucoma (together with CA II and XII), retinitis pigmentosa, stroke and rheumatoid arthritis.[35-39] The mitochondrial isoforms CA VA and VB are targets for obtaining antiobesity agents,[40-42] whereas CA VI is implicated in cariogenesis.[43,44] CA VII has been noted for its contributions to epileptiform activity together with CA II and XIV.[1,2,31,45] CA VIII was demonstrated to be involved in neurodegenerative diseases, as it has been associated with ataxia, mild mental retardation and quadrupedal gait in humans. Moreover it was found to be involved in the development of colorectal and lung cancers in humans.[46,47] Almost

nothing is known regarding the involvement of the remaining two acatalytic isoforms, CA X and XI, in human pathologies or what is the physiological function of these two proteins conserved all over the phylogenetic tree in vertebrates.[46] CA IX and XII are well-established anticancer drug targets. CA IX is a marker of disease progression in many types of hypoxic tumors, and recently its inhibition has been shown to be associated with a significant inhibition of the growth of both primary tumors and metastases. Furthermore, CAIs targeting this isoform can also be used for imaging of hypoxic tumors.[2,48-54] CA XII is less investigated but basically it is also an antitumor target. [2,48-54] Paucity of data regards CA XIII showing that it is involved in the sperm motility processes[55], probably together with CA XIV. CA XIV is involved in epileptogenesis and, similarly to CA IV, in some retinopathies, and may be a drug target for innovative agents useful in the management of such disorders.[56,57]

None of the currently clinically used CAIs show selectivity for a specific isozyme.[1,2] Thus, developing isozyme-specific CAIs should be highly beneficial in obtaining novel classes of drugs devoid of various undesired side-effects. Recently, a large number of structural studies has provided a scientific basis for the rational drug design of more selective enzyme inhibitors.[2,58] However, although X-ray crystal structures are already available for the majority of the twelve catalytically active members of the human CA family,[58-68] most of the reported complexes with inhibitors regards just isozyme II, the most thoroughly characterized CA isoform.[2]

2.2 Carbonic Anhydrases from pathogens.

It has been demonstrated that in many microorganisms as pathogens, CAs are essential for their life cycle and their inhibition can lead to growth impairment and defects.[15,69] CA classes are differently expressed in bacteria and cyanobacteria, fungi, protozoa and simple algae.[15]

In prokaryotes, the existence of genes encoding CAs from at least three classes (α-, β- and γ-class) suggests that these enzymes play an important role in the prokaryotic physiology.[8-10,15,69]

One of the best studied bacterial α-CA is the one from the gastric pathogen provoking ulcer and gastric cancer, *H. pylori*, hpαCA.[70-72] In fact, the genome project of *H. pylori*

identified two different classes of CAs, with different subcellular localization: a periplasmic α-class CA (hpαCA) and a cytoplasmic β-class CA (hpβCA) [70-72]. These two enzymes were shown to be catalytically efficient, exhibiting an almost identical activity as the human isoform hCA I, in the CO_2 hydration reaction, and are highly inhibited by many clinically used sulfonamides/sulfamates.[72] Since the efficacy of *H. pylori* eradication therapies currently employed has been decreasing due to drug resistance and side effects of the commonly used drugs, the dual inhibition of α- and/or β-CAs of H. pylori could be applied as an alternative therapy in patients with *H. pylori* infection or for the prevention of gastroduodenal diseases provoked by this widespread pathogen.[71,72]

Recently, the purification and characterization of another interesting enzyme, the α-CA from *Vibrio cholerae* (denominated VchCA) was reported.[73,74] This Gram-negative bacterium, which is the causative agent of cholera, colonizes the upper small intestine where sodium bicarbonate, an inducer of virulence gene expression, is present at a high concentration. *V. cholera* utilizes the CA system to accumulate bicarbonate into its cells, thus suggesting a pivotal role of this metalloenzymes in the microbial virulence.[73]

CAs are abundant in fungi and yeasts,[21,75-80] but these enzymes have only recently started to be characterized and studied in detail. *Saccharomyces cerevisiae*[79], *Candida albicans*[75,76] and *C. glabrata* [76,77] each have only one β-CA, whereas multiple copies of β-CA- and α-CA-encoding genes were reported in other fungi.[78] A recent work demonstrated that these CAs play an important role in the CO_2-sensing of the fungal pathogens and in the regulation of sexual development.[77] Finally, another yeast, which has been investigated in detail for the presence of CAs is *Malassezia globosa*, which produces dandruff.[80] As the above-mentioned fungi/yeasts, it contains only one β-CA, denominated MgCA. It may be observed that prevalently the β-CAs from various fungi/yeasts have been investigated.

Few protozoan parasites have been investigated for the presence and druggability of CAs. The malaria-provoking organism *Plasmodium falciparum*, was undoubtedly the first one.[7,78-83] An α-CA has also been cloned and characterized in the unicellular protozoan *Trypanosoma cruzi*, the causative agent of Chagas disease.[74-85] The enzyme (TcCA) has a very high catalytic activity for the CO_2 hydration reaction, being similar kinetically to the human isoform hCA II.

In addition, another β-CA from the unicellular parasitic protozoan *Leishmania. donovani* chagasi, which causes visceral leishmaniasis was identified, cloned, and characterized.[86]

2.3 Structural features of Carbonic Anhydrase inhibitors (CAIs).

The main aim of the drug design campaigns in the last decades was to obtain isoform-selective CAIs for the various isoforms involved specifically in different pathologies.[1-3,23-27,87-93]

Carbonic anhydrase inhibitors can be divided into different classes depending on their inhibitory mechanism. The three main and most investigated classes are:

- Compounds possessing a zinc-binding group.
- Compounds which anchor to the zinc-coordinated water/hydroxide ion.
- Compounds which occlude the active site entrance.

2.3.1 The zinc binders as Carbonic Anhydrase inhibitors.

Up to now, the sulfonamide group (R-SO_2NH_2) is the most important and largely used zinc binding function for the design of CAIs [1,3,87-91], with at least 20 such compounds in clinical use for decades or clinical development in the last period (Figure 7) such as, sulfanilamide **SA**, acetazolamide **AAZ**, ethoxzolamide **EZA**, dichlorophenamide **DCP**, dorzolamide **DRZ** and brinzolamide **BRZ**. Since the first evidence of their CA inhibitory properties,[92] these molecules were largely investigated by means of kinetic, physiological and pharmacological studies. [1,3,87-93]

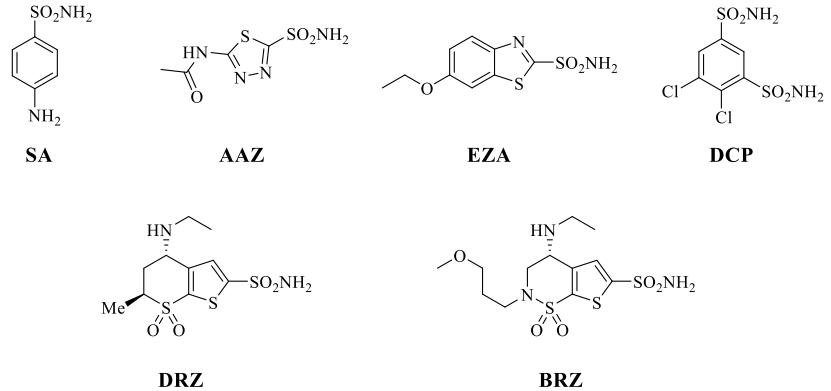

Figure 7. Examples of clinically used sulfonamides.

Many X-ray crystallographic evidences demonstrate the binding mode of the zinc-binder type CAIs, to which sulfonamides and their bioisosters sulfamates and sulfamides belong. A general CA inhibition mechanism with zinc binders, is shown in Figure 8. The zinc-binding group (**ZBG**) of these CAIs, i.e. the SO_2NH^- moieties for the three main classes of inhibitors mentioned above, bind in deprotonated form to the Zn(II) ion from the enzyme active site, so replacing the zinc-bound water molecule and mantaining tetrahedral coordination geometry.

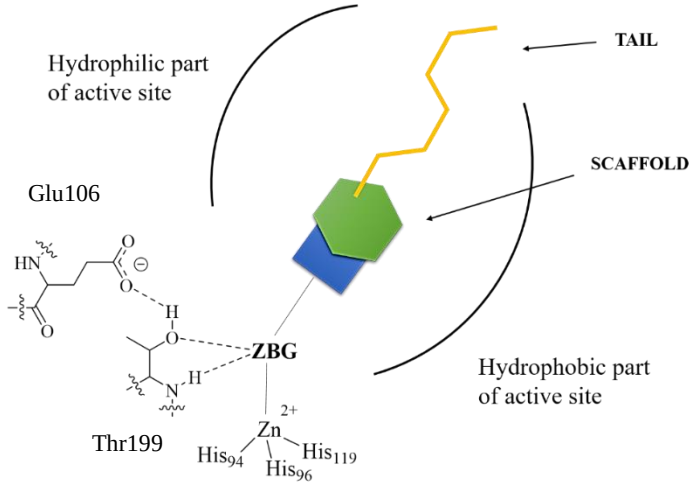

Figure 8. CAIs belonging to the zinc binders (sulfonamides, sulfamates, sulfonamides, carboxylates, hydroxamates, dithiocarbammates, monothiocarbammates).

Moreover, the **ZBG** participates in strong interactions with the gate keeper residues Thr199–Glu106, conserved in all α-CAs. The scaffold may occupy either the hydrophylic or hydrophobic (or both) halves of the active site, whereas the tails are generally orientated toward the exit of the cavity where the most variable amino acid residues among the different mammalian isoforms are found.[1,2,90,91,93] Several studies highlighted that the sulfonamide group is an ideal **ZBG** for the CA active site for two main reasons: on one hand, it combines the negative charge of the deprotonated nitrogen with the positively charged zinc ion, on the other hand, the presence of one proton on the coordinated nitrogen atom satisfies the hydrogen bond acceptor character of Thr199 OG1 atom, able to form a strong H-bond with it.

Among sulfonamide, the benzenesulfonamides constitute the most common and best characterized class. The phenyl ring establishes several Van der Waals interactions with

residues Gln92, Val121, Phe131, Leu198, and Thr200 (Figure 9; numbering as in hCA II; PDB code 2WEJ).[1-3,27]

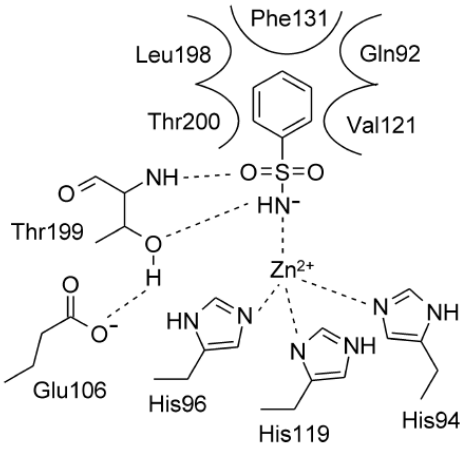

Figure 9. Schematic representation of the binding mode of benzenesulfonamide with the CA II active site (PDB code 2WEJ).

The most limiting concern of the CAIs belonging to the sulfonamide-type relies on the wide range of side effects, that they elicit by inhibiting most of the catalytically active CA isoforms found in vertebrates[1-3] Moreover, sulfonamides and sulfamates not only inhibit CAs belonging to α-class, but also CAs belonging to different families. This feature may be exploited for obtaining anti-infectives with a new mechanism of action.[15] Obtaining isoform-selective CAIs for the various isoforms is however not an easy task, considering the quite similar active site architecture of the 12 catalytically active isoforms present in primates.[1] In fact, all human isoforms have the three conserved His residues (His94, 96, and 119) acting as zinc ligands, as well as half the active site mainly lined with hydrophobic residues and, as previously mentioned the opposite one with hydrophilic residues.[1-3,20] However, there are also important differences in amino acid residues mainly in the middle and toward the exit of the active site cavity.[1-3,20,94] In the binding with the enyme, most of the inhibitors above mentioned (Figure 7) do not make extensive contacts with the aminoacids of the outer portion of the catalytic cleft, but they bind deep within the active site cavity, which is rather similar in all mammalian isoforms.[1-3,91,94] Thus, it appeared of considerable interest to devise alternative approaches for obtaining isoform selective CAIs. One of the most successful one, "the tail approach" [1-3,95,96], consists in appending molecular "tails" to the scaffolds of aromatic/heterocyclic sulfonamides possessing derivatizable moieties in such a way that an elongated molecule

is obtained with its tail being able to interact with amino acid residues from the middle and edge of the active site cavity (Figure 8). The choice of tails endowed with diverse chemical nature allows to modulate the physico-chemical properties of such CAIs, which are crucial for their biological activity. For example, this design was used for antiglaucoma agents, that should possess an appropriate hydrophilicity and water solubility in order to be formulated as eye drops but also a balanced lipophilicity for being able to penetrate through the plasma membranes and arrive at the ciliary processes where the enzymes responsible for aqueous humor secretion are found (i.e. CA II, IV, and XII).[1,2,29,96]

Another interesting approach to overcome, at least, in part the lack in isoform selectivity characteristic of the zinc-binders CAIs consists in endowing the derivative with a permanent positive charge (Figure 10a)[97] and thus, due to their cationic nature, they would be unable to penetrate through biological membranes and therefore would inhibit in vivo only CA enzymes located on the outer surface of the membranes, such as the extracellular isoforms CA IV, IX, XII, and XIV.[2,97,98]

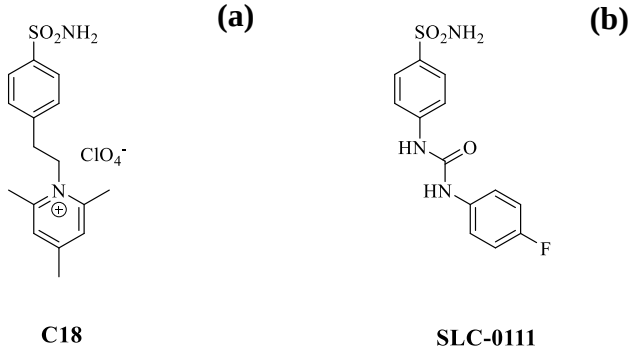

Figure 10. Structure of membrane-permemant sulfonamide (a) **C18** and (b) **SLC-0111** which successfully completed Phase I clinical trials for the treatment of advanced, metastatic hypoxic tumors over-expressing hCA IX/XII

Nevertheless, over the last few decades the "tail approach" has been the main method applied for the design of isoform-selective CA inhibitors, with an extensive application that greatly enriched the database of CAIs, though eliciting only a rather limited number of derivatives showing relevant isoform-selectivity inhibition profiles (among the zinc-binders CAIs). However, in this context, recent studies from our group led to the discovery and clinical development of **SLC-0111** (Figure 10b), a sulfonamide CAI which successfully completed Phase I clinical trials for the treatment of advanced, metastatic

hypoxic tumors over-expressing hCA IX/XII, being scheduled for Phase II trials later this year.[99-100]

Beyond sulfonamide-like inhibitors, dithiocarbamates (DTCs),[101,102] xanthates,[103] monothiocarbammates,[104] carboxylates,[105,106] and hydroxamates,[107,108] posses a zinc binding group (ZBG) and thus belong the same class of CAIs. X-ray crystal structures are available for adducts of various isoforms (mainly hCA I and II) with all these classes of CAIs except the xanthates and monothiocarbammates for which computational methods were used to assess their inhibition mechanism.[103,104]

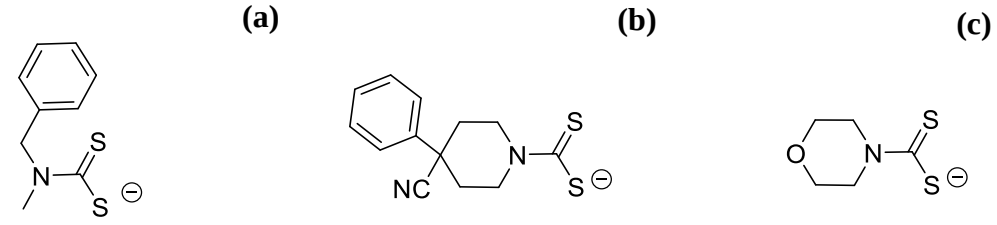

Figure 11. Stucture of hCA II - cocrystallized DTCs.

For example, the X-ray crystal structure of the adducts formed between the derivatives in Figure 11 and the hCA II are available in the PDB.[101] One of the sulfur atoms of the inhibitor is coordinated to the Zn(II) ion and makes the canonical interactions of all ZBGs with the gate keeper residues Thr199-Glu106 (Figure 12). For these DTCs, the scaffolds have very diverse orientation within the active site, which may explain their high inhibitory activity against many CA isoforms.[101,102]

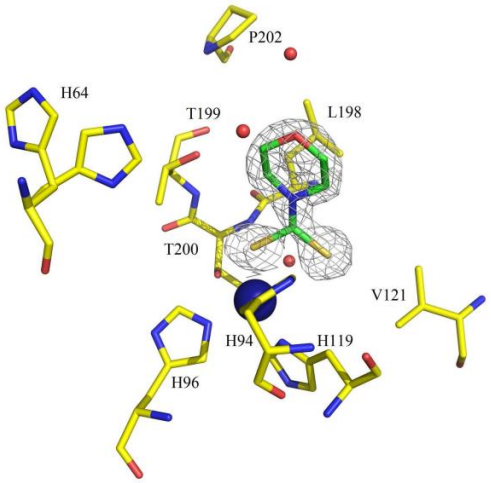

Figure 12. Stick representation of hCA II active site with a DTC (green) complexed within it. The electron density is represented by a Σ-weighted 2Fo − Fc Fourier map.

2.3.2 Carbonic Anhydrase inhibitors anchoring to the zinc-coordinated water/hydroxide ion.

The first example of inhibitor anchoring to the zinc-coordinated water molecule/hydroxideion, was reported to be phenol (Figure 13a).[109,110] The polyamine spermine (Figure 13b) was the second one.[111]

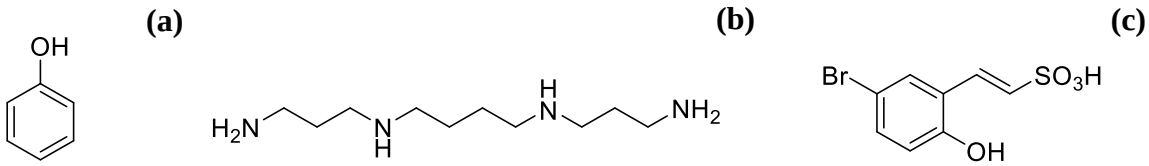

Figure 13. Stucture of phenol (a), spermine (b) and hydrolized sulfocoumarin (c).

Compounds inhibiting CAs by this mechanism (Figure 13) are characterized by the presence of an anchoring group (**AG**) attached to a scaffold possibly incorporating tails which can interact, as for the zinc binders, with the two halves of the active site (Figure 14). The main prerogative of the inhibitors anchoring to the zinc nucleophile is the absence of a direct bond between the inhibitor and the metal ion.[97,90,91]

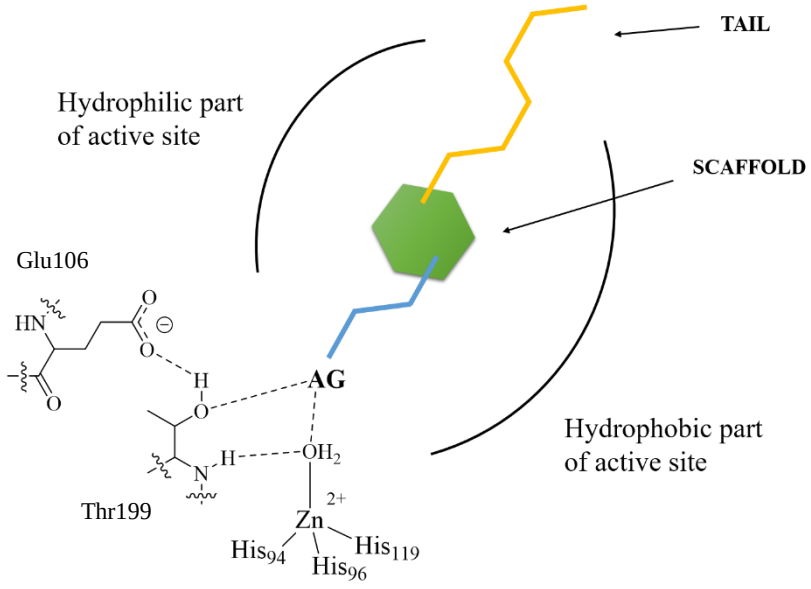

Figure 14. Compounds which anchor to the Zn(II)-coordinated water molecule/hydroxide ion. The anchoring group (**AG**) are of the OH (phenol), amino (polyamine), carboxylic acid (COOH), ester (COOR), sulfonate (sulfocoumarin) type.

As reported in the last years by several groups, the **AG**s belong to a variety of chemical functionalities. They include phenolic OH [109,112,113], primary amine,[110] COOH,[114] COOMe,[113] and SO_3H [115] moieties. Many of them display efficient inhibitory activity against CAs belonging to the α- and β-CA classes. [109-116] The phenol is anchored to the Zn-bound hydroxide ion (preponderant species at the pH at which the experiments were done) by a hydrogen bond involving the H atom of the inhibitor and the donor hydroxide ion. In addition, a second hydrogen bond involves the gate-keeping residue Thr199, whose backbone NH group participates in a second hydrogen bond with the phenol (Figure 15a).

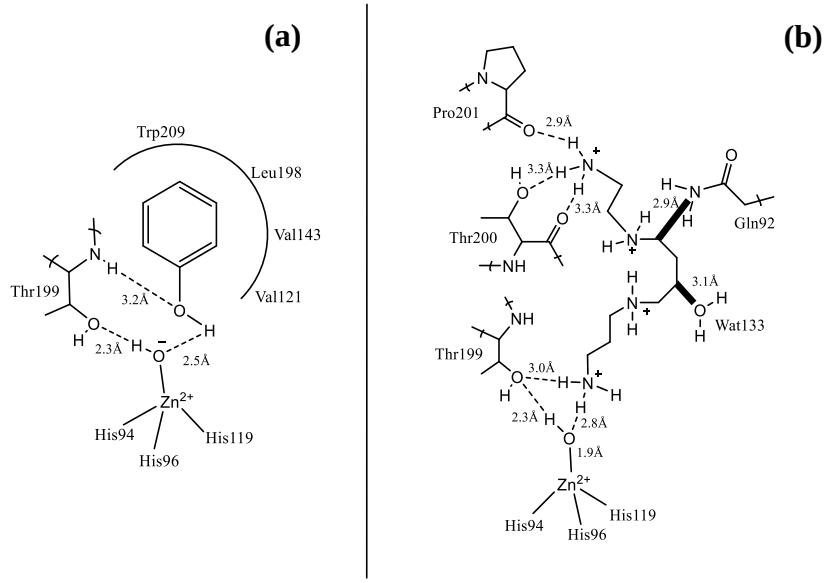

Figure 15. (a) Schematic representation of the binding of phenol to hCA II. (b) Schematic representation of interactions in which spermine (Figure 13b), as tetracation participates when bound to the hCA II active site. Figures represent distances (in Å). Hydrogen bonds are represented as dashed lines. In bold are shown two clashes involving some carbon atoms (C5 and C7) of the spermine scaffold with a water molecule (Wat113) and Gln92. The nonprotein zinc ligand is represented as a hydroxide ion, which should be the preponderant species at the pH at which the experiments were done (7.5).

Spermine (Figure 13b) binds in a rather similar manner as phenol, although with a slightly different network of hydrogen bonding (Figure 15b). Thus, one of the primary amine moieties of the inhibitor, probably as ammonium salt, anchors by means of a hydrogen bond to the zinc-coordinated water molecule/hydroxide ion, and also makes a second hydrogen bond with the side chain OH group of Thr199. The other terminal primary amine of spermine participates in hydrogen bonding with Thr200 and Pro201.[110]

The sulfonic acid from the hydrolized sulfocoumarin derivative (Figure 13c; see discussion in paragraph 3.1) was found to anchor to the Zn-bound hydroxide ion, thus making this CA inhibition mechanism much more general than initially considered when phenols were discovered as inhibitors. It should be also noted that CAs belonging to other genetic families than the α- and β-ones were not yet investigated for this type of alternative inhibition mechanism.

2.3.3 Carbonic Anhydrase inhibition by occlusion of the active site entrance.

The third main CA inhibition mechanism consists in the active site entrance occlusion. These inhibitors bind further away from the metal ion compared to the zinc binders in Figure 8 and 9 or to the compounds anchoring to the zinc coordinated water molecule in Figure 14, basically at the entrance of the active site cavity, which is the most variable region between various isoforms as the 16 mammalian ones.[1,2,90-94] Compounds acting by occluding the active site entrance possess a sticky group (**SG**) attached to a scaffold which can be aromatic, heterocyclic, or aliphatic (Figure 16). They may also incorporate a tail, which can extend away from the active site.

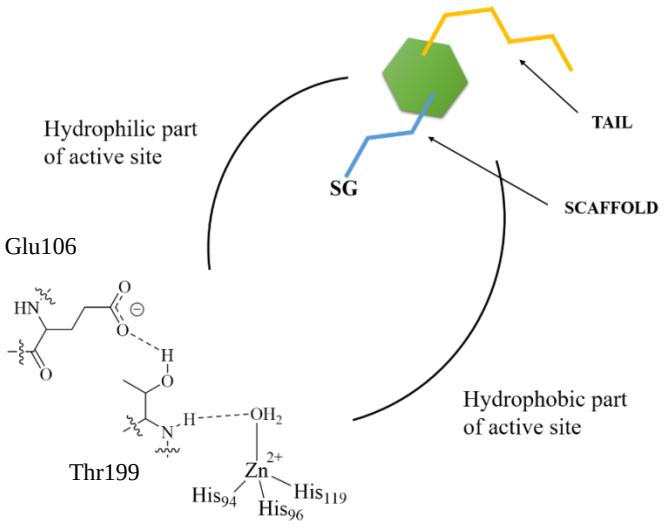

Figure 16. Binding representation of compounds occluding the entrance to the active site. **SG** represents a sticky group, of the phenol, carboxylic acid or amide type. The compound binds at

the entrance of the active site cavity and a tail, if present, interacts with residues on the surface of the protein.

This inhibition mechanism has been evidenced for the first time for coumarins [117,118] but thereafter other compounds such as the antiepileptic drug lacosamide [119] and substituted coumarins[120-124] were observed to possess significant CA inhibitory properties probably sharing a common mechanism of action. The first compound with this interesting CA inhibition mechanism was the natural product coumarin (Figure 17b), isolated from the Australian plant Leionema ellipticum.[117]

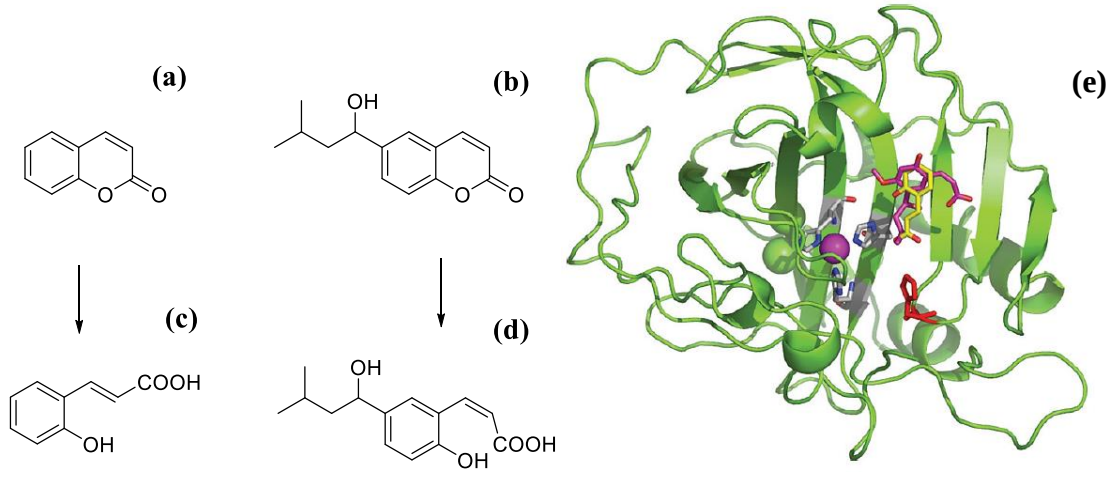

Figure 17. Coumarins (a,b) and their CA-mediated hydrolysis (c,d), respectively. (e) Binding of the coumarin **a** hydrolysis product (trans-2-hydroxy-cinnamic acid **c**, in yellow) and coumarin **b** hydrolysis product (cis- 2-hydroxycinnamic acid **d**, magenta) to the hCA II active site. The protein backbone is shown as green ribbon, the catalytic Zn(II) ion as violet sphere, with its three protein ligands (His94, 96, and 119, CPK colors) also evidenced. The proton shuttle residue (His64) is shown in red.

Unexpectedly the electron density data for the adduct hCA II/coumaris revealed that the real enzyme inhibitors are the hydrolized forms in Figure 17c and 17d of coumarins in Figure 17a and 17b respectively and their formation is related to the α-CAs esterase activity. However, the rather bulky nature of the obtained hydrolysis products interferes with their binding in the neighbourhood of the metal ion. Thus, the obtained 2-hydroxycinnamicacids may bind as cis isomers (17d[118]) or as trans-isomers (17c[117]) depending on how bulky the moieties present on the scaffold are. Indeed, for less bulky groups the trans isomer was observed, whereas for bulkier such groups the isomerization did not occur (Figure 17e).

The most notable aspect of this inhibition mechanism is the fact that the inhibitors bind in an active site region which is the most variable between the various isoforms, i.e. the entrance to the cavity.[1-3,20] This has important consequences for the drug design of CAIs, since compounds binding in that region should in principle interact differently with the various CAs and thus show isoform-selective inhibitory profiles. In fact, larger series of diversely substituted coumarin/thiocoumarin derivatives were investigated and showed a high level of isoform selective behavior against many isoforms such as CA IX,XII, XIII, XIV, etc.[120-124] The replacement of the CO moiety of the coumarin lactone with a SO_2 group led to sulfocoumarins.[115] Differently from coumarins, whose hydrolized forms bind at the entrance of the active site, as previousy mentioned, the hydrolized form of sulfocoumarins anchors to the Zn-bound water molecule. Likewise coumarins, many derivatives belonging to this bioisosteric class showed a very high degree of isoform selectivity toward the trans-membrane tumor-associated isoforms hCA IX and XII compared to the cytosolic ones hCA I and II. [115]

Part II - Research of the three-years PhD period

Chapter 3. SBDD approaches, synthesis and biological evaluation of carbonic anhydrase inhibitors.

The knowledge of most CA isoforms structural features, nowadays available, represents a valuable aid for exploring the binding ligand/target interactions.
SBDD tools were used to evaluate and rationalize the experimental inhibitory profile measured for the synthesized and screened derivatives. Additionally, models were built by homology for those enzyme isoforms for which the 3D structure was not available.
Methods belonging to molecular mechanics (MM), quantum mechanics (QM) as well as mixed approaches (QM/MM) were widely used to gain insight into the interaction behaviour of the planned CAIs and their enzymatic targets.
The discussion of the research carried out and the results obtained during the three years PhD period will be herein presented according to the different projects they belong to.

3.1 "Click chemistry" approach applied to the design of novel CAIs belonging to first, second and third classes of inhibitors.

The copper-catalyzed azide−alkyne cycloadditions (CuAAC), better known as "Click Chemistry", have acquired a prominent role in medicinal chemistry,[125-129] thus becoming a versatile and useful synthetic tool to generate 1,4-disubstituted-1,2,3-triazoles to be used as biologically uncleavable linker between valuable molecular fragments and/or as moiety that can actively contribute to additional enzyme-inhibitor interaction points. The 1,2,3-triazole ring is an amide bioisoster endowed with a moderate dipole character, hydrogen bonding capability, rigidity, stability in the *in vivo* environment and an aromatic character able to establish π-stacking interactions with appropriate aminoacid residues within the binding cavities.
In the last years, click chemistry has often been used to obtain CAIs belonging to the sulfonamide or coumarin classes.[125-128] For example, aromatic sulfonamides incorporating glycosyl moieties as well as aromatic-heteroaromatic or aliphatic groups by means of a triazole linker, were obtained and showed to be potent inhibitors against physiologically/pathologically relevant isoforms such as hCA I, II, IX, and XII.[125,126] Noteworthy, Pala et al. recently reported two subsets of benzene and tetrafluorobenzene

sulfonamides bearing aliphatic or aromatic moieties through the Click Chemistry approach.[128]

During my PhD period, we continue the exploration of this type of derivatives, including a molecular flexibility element in the structure of compounds belonging to the sulfonamide, coumarin and sulfocoumarin type.

Series A: sulfonamides

Primary sulfonamides such as sulfanilamide, acetazolamide, ethoxzolamide and dichlorphenamide (Figure 7) are clinically used for almost 70 years as anti-glaucoma agents for systematic administration, although they show a range of side effects due to the lack of enzymatic as well as tissue selectivity. The second generation antiglaucoma drugs, such as dorzolamide and brinzolamide, act topically, thus leading to significant reduction of the side effects (Figure 7).[130-134]

Glaucoma is a chronic, degenerative eye disease characterized by elevated intra ocular pressure (IOP), that causes irreversible damage to the optic nerve. The hCA II isoform, along with the IV and XII are largely expressed in the eye and involved in the disease.

In the context of the "Click Chemistry approach" application, we primarily carried out a deeper investigation based on the benzenesulfonamide-containing 1,2,3-triazolyl moieties previously reported from Pala et al.[128] in order to design new potent CAIs as potential candidates for the treatment of pathologies, such as glaucoma or tumors. Compounds of the phenyltriazolylbenzenesulfonamide (**PTB)**-type (Figure 18), were considered as analogues of **SLC-0111** (Figure 18), which successfully completed Phase I clinical trials for the treatment of advanced, metastatic hypoxic tumors over-expressing hCA IX/XII.[99-100] In fact, these compounds incorporate the 1,2,3-triazolyl moiety as bioisoster of the ureido group and were all characterized by the direct connections between three main molecular fragments: the benzenesulfonamide head (**α**), the triazolyl spacer (**β**) and the aromatic tailing portion (**γ**). **PTB**-based structures possess a rather low conformational freedom (Figures 18 and 19).

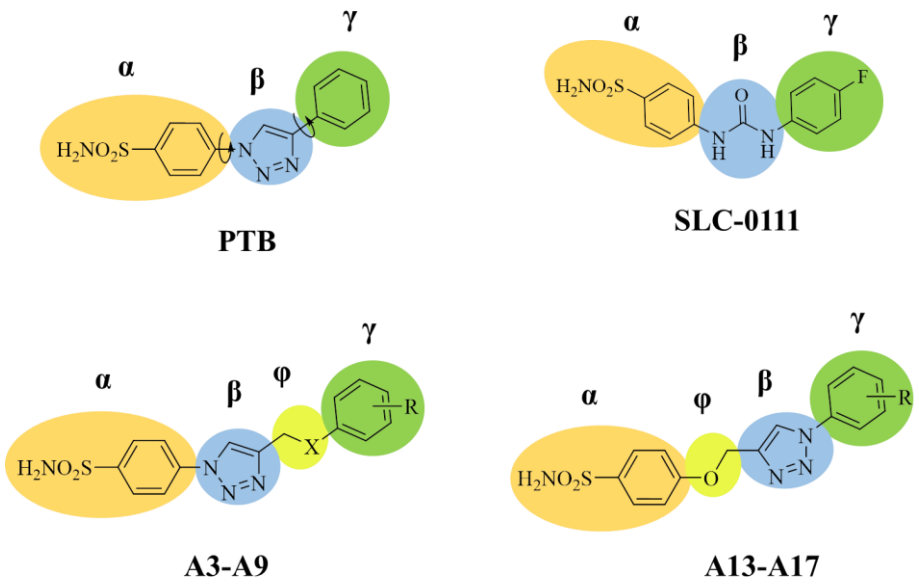

Figure 18. General structures of the designed benzenesulfonamides in the present study.

Starting from these considerations new derivatives were rationally designed with the aim to investigate whether an enhanced flexibility between these three molecular fragments will produce better interactions within the CAs active sites, and thus will reinforce inhibitory properties, as well as the selectivity profiles for the different isoforms. The enhanced flexibility will reduce the molecular constrain and increase the degree of freedom, thus allowing the aromatic tail to better interact with the most energetically favourable enzymatic sub-pocket(s).[100]

Prior to carry out the synthesis, docking experiments were performed to evaluate the binding interactions of the planned sulfonamides with the hCA II (PDB ID: 4Q6E, Figure 19). As expected, poses coming from docking pointed out analogies in the binding mode of the lead **PTB** and the newly designed triazoles: the NH^- moiety of the sulfonamide group was involved in coordination interaction with the zinc ion, and in hydrogen bond distance with OG1 atom of Thr199 (2.48Å), whereas one oxygen atom of sulfonamide group formed another hydrogen bond with the backbone NH of Thr199 (1.94Å). A π-π interaction was established between the triazole ring and the phenyl group of Phe131 side chain.

By inspection of the reported poses it was clear that the presence of more flexible "tails" allowed a more extended network of interactions at the outer rim of the binding site

cavity. In addition, substituents on the triazole ring could locate both in the hydrophobic (red) and in the hydrophilic half (blue) of hCAII active site.

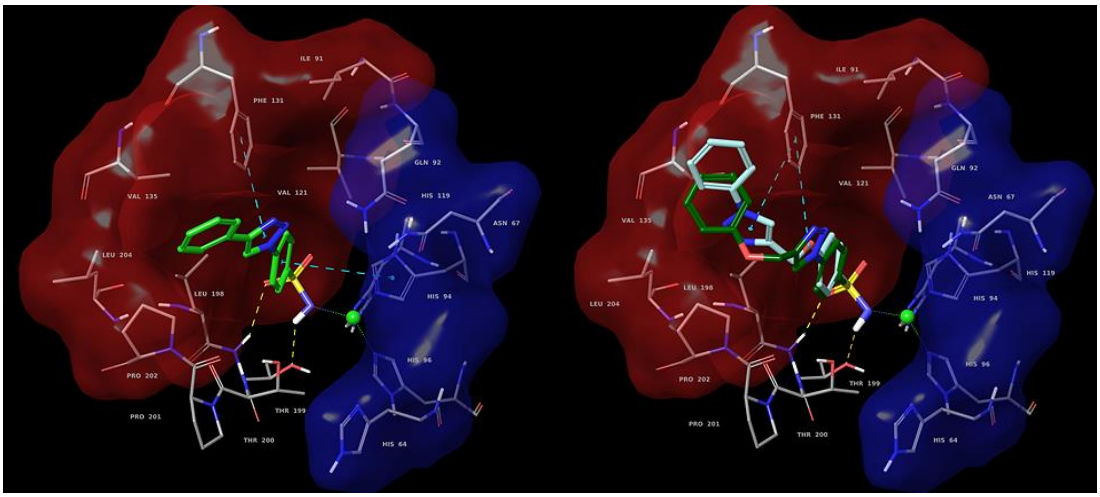

Figure 19. Computed binding modes of **PTB** (green, a), first (**A3**, dark green) and second (**A13**, aquamarine) subset designed lead compounds (b) within hCA II active site (PDB 4Q6E).

Once confirmed the rational, the two subsets of triazole derivatives were synthesized and investigated for the inhibition of the physiologically dominant, cytosolic isoforms hCA I and II, as well as the transmembrane, tumor-associated hCA IX and XII. In addition, we confirmed the predicted binding mode by means of high resolution X-ray crystal structure and subsequently expanded the investigation to all synthesized derivatives by docking them in hCA II and IX. Finally, considering the interesting water solubility the reported triazoles were endowed with, some of them were screened for their anti-glaucoma activity in an animal model of the disease. Indeed, water solubility is a basic requirement for a topical intra-ocular formulation.

As shown in Figure 18, the enhanced "tail" flexibility was achieved by the introduction of a CH_2X (X = O, S, NH) linker (**φ**) between **β** and **γ** (derivatives A**3-A9**) and **α** and **β** (derivatives A**13-A17**). In comparison to the reference **PTB**, a larger set of substituents on the aromatic tail has been explored, obtaining two novel sets of benzenesulfonamide not investigated as CAIs up to now.

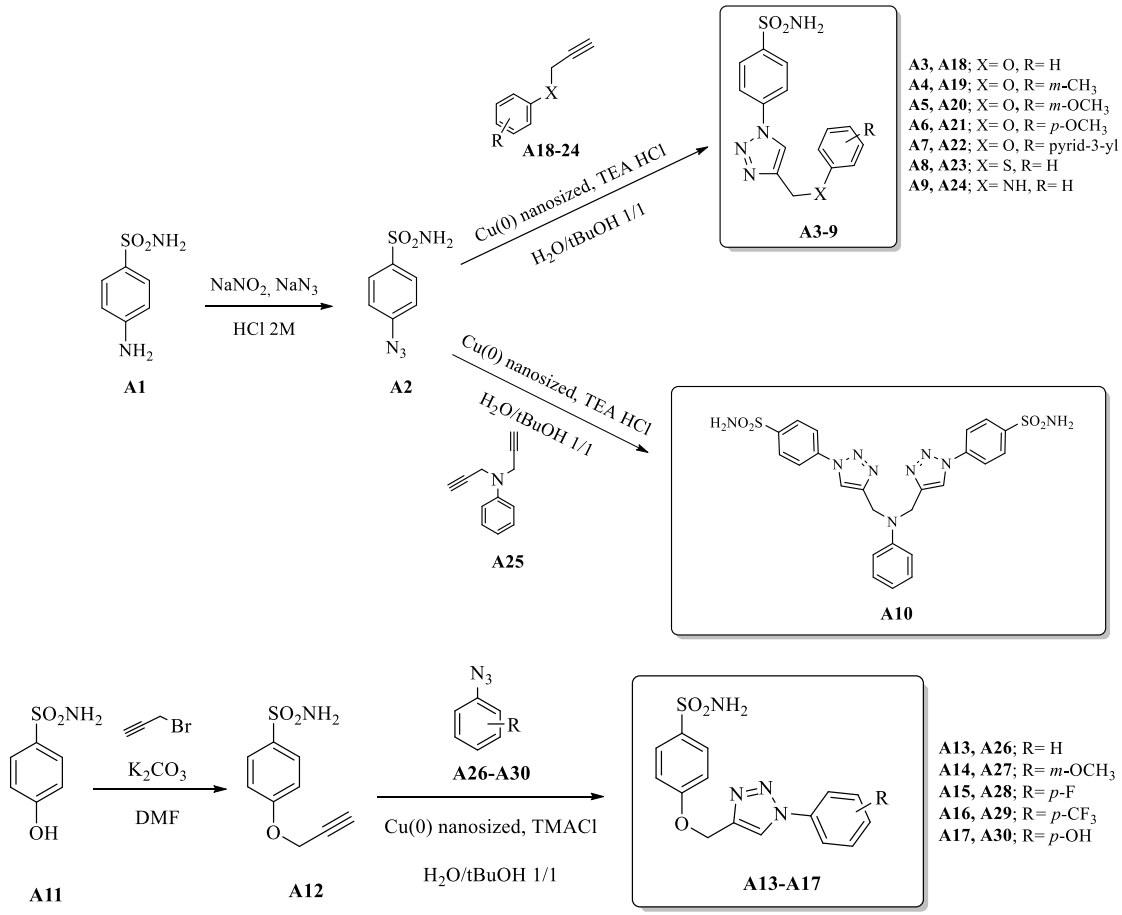

Scheme 2. General synthetic procedure for compounds **A3-A10, A13-A17**.

Two different synthetic strategies were used for obtaining the above-mentioned derivatives, both involving the application of the Click chemistry approach (Scheme 2). For the first subset (**A3-A9**), the key intermediate 4-azidobenzenesulfonamide **A2** was obtained from sulfanilamide treated with $NaNO_2$ and NaN_3 in acid aqueous media. Reaction of **A2** with the propargyl amino, thioether or ethers derivatives **A18-A24** afforded the first subset of triazoles, **A3-A9**, incorporating diverse aryl groups at the triazole-benzenesulfonamide moiety by means of the linker CH_2X. A double propargylation which occurred at aniline NH_2 suggested to react the dipropargyl derivate **A25** with key intermediate **A2** in order to obtain the novel double head, twin-tailed sulfonamide **A10**.

For the second subset (**A13-A17**), starting from 4-hydroxy-benzenesulfonamide, the propargyl ether key intermediate **A12** was obtained as alkyne to use in the "click chemistry". Reaction of **A12** with freshly prepared aromatic azides **A26- A30** afforded

the second subset of triazoles, **A13-A17**, that on the contrary to the preceding one, incorporated diverse aryl-triazole tails appended to the zinc-binding group (ZBG) scaffold through a CH_2O linker.

The CA inhibitory activities of compounds **A3-A10**, and **A13-A17** was investigated by means of the stopped flow carbon dioxide hydrase assay,[135] in comparison to the lead compound **PTB** [128] and acetazolamide (**AAZ**) as standard CAI, against four physiologically significant isoforms, the cytosolic, hCA I and II, as well as the transmembrane, tumor-associated hCA IX and XII. The rational for the choice of these four isoforms is that hCA II and XII (upregulated in the eyes of glaucomatous patients)[2,132-135] are targets for antiglaucoma drugs, whereas hCA IX (and XII) have been validated as targets for the treatment and prognosis of hypoxic cancers.[2,48-54] Otherwise hCA I is one of the main off-target isoforms both for the antiglaucoma or anticancer CAIs therapeutic application.[1,2]

The following SAR can be unveiled from the inhibition data shown in Table 2:

(i) The cytosolic isoforms hCA I was moderately inhibited by most of the sulfonamides of the first subset with inhibition constants (K_Is) ranging between 123.0 and 512.6 nM and comparable to the lead **PTB** (K_I 342.0 nM) and to the reference **AAZ** (K_I 250 nM). The only exceptions were derivative **A9**, which was an effective hCA I inhibitor (K_I of 7.9 nM), and the double head derivative **A10** which resulted inactive (K_I > 10000 nM). We may hypothesize that the presence of hydrophilic moieties in these molecular structures is well tolerated within the hCA I active site. Indeed, the substitution of the phenyl with a more hydrophilic pyridyl ring (**A7**) or the substitution of the oxymethylene linker with a strongly hydrophilic aminomethylene one (**A9**) increased the inhibitory activity up to 123.0 and 7.91 nM respectively.

The sulfonamides belonging to the second subset showed a diminished hCA I inhibitory action. Indeed, only derivate **A17** which incorporates a hydroxy group to the phenyl ring acted as a strong hCA I inhibitor, with K_I of 92.8 nM, whereas the remaining compounds possessed inhibition constants ranging between 278.1 and 949.8 nM. Derivative **A16** did not inhibit hCA I up to 10000 nM.

Table 2: Inhibition data of human CA isoforms hCA I, II, IX and XII with sulfonamides **A3- A10**, **A13- A17** reported here and the standard sulfonamide inhibitor acetazolamide (**AAZ**) by a stopped flow CO_2 hydrase assay.[135]

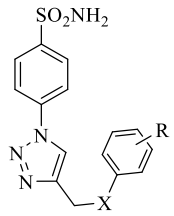

A3-9

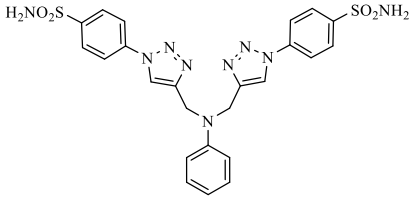

A10

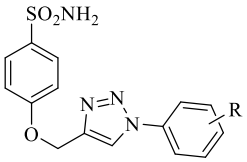

A13-A17

			K_I (nM)			
Compound	X	R	hCA I	hCA II	hCA IX	hCA XII
A3	O	H	349.9	1.0	2.1	1.1
A4	O	*m*-CH_3	406.8	1.5	2.3	5.4
A5	O	*m*-OCH_3	351.1	1.5	9.3	1.1
A6	O	*p*-OCH_3	512.6	4.3	14.3	1.0
A7	O	Pyridyl-3-yl	123.0	1.4	17.2	6.0
A8	S	H	195.7	1.5	2.4	4.9
A9	NH	H	7.9	0.83	2.2	1.1
A10	-	-	>10000	>10000	12.1	10.2
A13	-	H	565.6	1.2	2.6	1.1
A14	-	*m*-OCH_3	278.1	12.4	20.5	101.6
A15	-	*p*-F	949.8	2.6	16.2	3.2
A16	-	*p*-CF_3	>10000	15.7	23.6	4.3
A17	-	*p*-OH	92.8	1.0	18.7	7.1
PTB			342.0	43.9	25.9	6.0
AAZ			250.2	12.0	25.2	5.7

* Mean from 3 different assays, by a stopped flow technique (errors were in the range of ± 5-10 % of the reported values).

ii) The physiologically dominant isoform hCA II was very potently inhibited by all the investigated compounds (K_I values ranging between 0.83 and 15.7 nM, Table 1), with the exception of the double head derivative **A10** which did not inhibit hCA II up to 10000 nM. The definition of a proper SAR for hCA II is not feasible, considering that the remaining derivatives showed rather similar affinities. However, it could be stressed that the presence of a hydrophilic aminomethylene linker in the first subset of derivatives led

to the strongest inhibitor reported here (**A9**) with its subnanomolar activity of 0.83 nM for this isoform, whereas the presence of a *para* substituent on the phenyl ring, represented herein by the methoxy group of **A6**, reduced the inhibitory potency by four times.

Within the second subset of derivatives, the incorporation of a methoxy or trifluoromethyl group in *meta* or *para* positions to the sulfamoyl ZBG, respectively, led to a ten-fold decrease of the inhibitory activity. Generally, all the investigated compounds (except derivative **A10**) were better inhibitors compared to the lead **PTB** or the clinically used **AAZ** (K_I values of 43.9 and 12.1 nM), thus proving that compounds endowed with enhanced flexibility between their molecular fragments act as more effective hCA II inhibitors compared to the rigid compound **PTB**.

iii) All the reported derivatives acted as very efficient inhibitors for the tumor-associated isoform hCA IX. The general inhibitory tendency was slightly less compact compared to the behaviour observed against hCA II, with K_Is ranging between 2.1 and 23.6 nM. The data in Table 2 allowed us to draw a very clear-cut SAR: for both reported subsets, the derivatives bearing an unsubstituted phenyl ring are the most efficient inhibitors regardless on the nature of the XCH_2 linker. Indeed derivatives **A3**, **A8**, **A9** and **A13** were low nanomolar hCA IX inhibitors, with K_Is of 2.1, 2.4, 2.2 and 2.6 nM respectively. Only compound **A4** represented the exception to this general rule with a K_I of 2.34 nM, although it has a methyl substituent at position 3 of the aromatic tail. Conversely, for the first subset of derivatives, the insertion of a methoxy group on the ring or its substitution with a pyridyl moiety decreased the inhibitory potency to the range of 9.3-17.3 nM. Within the second subset of CAIs, the incorporation of *p*-F-, *p* -OH-, *m*-MeO- and *p* -CF_3- moiety on the tail drove to K_Is ranging between 16.2 and 23.6 nM. It should be also highlighted the potent inhibitory activity of the double head derivate **A10** against this isoform with a K_I of 12.1 nM, in comparison to its ineffective activity on the cytosolic isoforms hCA I and hCA II, making this compound selective for the tumor-associated over the cytosolic isoforms.

All the reported derivatives were more potent inhibitors compared to the lead **PTB** or the clinically used **AAZ** (K_I values of 25.9 and 25.0 nM), especially the unsubstituted compounds **A3**, **A8**, **A9** and **A13** which showed a more than ten times better inhibitory

activity, confirming the importance of the flexible features to better interact with the CA IX active site.

iv) The reported derivatives showed a very efficient inhibitory activity also against the other tumor-associated isoform hCA XII (which is also involved in glaucoma). However in this case the outline of a straightforward SAR, as for CA IX, was not observed. Indeed within the first subset, compounds **A3** and **A9**, unsubstituted on the external phenyl ring and compounds **A5** and **A6**, incorporating a methoxy group respectively at the *meta* and *para* positions, acted as low nanomolar inhibitors with K_Is ranging between 1.0 and 1.1 nM. On the contrary, derivative **A8**, bearing a -CH_2S- linker, showed in this case a five-fold reduction in the inhibitory activity. The insertion of a methyl group at the *meta* position (**A4**) or the substitution of the phenyl ring with a pyridyl one (**A7**) reduced the activity by five and six times respectively.

Conversely, for the second group of compounds, the unsubstituted derivative **A13** acted as the most potent inhibitor with a K_I of 1.1 nM, whereas the insertion of substituents on the phenyl ring generally reduced the inhibitory efficiency. In particular derivative **A17**, bearing a *meta* methoxy group showed a K_I increased by a hundred times compared to its unsubstituted counterpart.

Differently from the previously discussed isoforms, not all the new sulfonamides inhibited CA XII better than the lead **PTB** or the clinically used **AAZ** (K_I values of 6.0 and 5.7 nM). These data suggested that the enhancement of the molecular flexibility did not generally increase the interaction with the CA XII active site, but depending on the nature and position of the substituents on the external phenyl ring, a more intricate interaction was probably in act between the enzyme and the inhibitor.

Finally it should be stressed the potent inhibitory activity of the double head derivate **A10** against this isoform too, with a K_I of 10.2 nM. Although its inhibitory potency was slightly reduced in comparison to lead **PTB** or **AAZ**, this data was surprising and extremely interesting when merged with the K_I of compound **A10** against CA I, II and IX. In fact, **A10** acted as a strong and selective inhibitor of the tumor-associated isoform hCA IX and XII over the cytosolic isoforms hCA I and II.

An experimental validation of the docking estimated interactions mode was achieved by the X-ray crystallographic structures of the adducts formed by hCA II with compounds

A3 and **A13** (at 1.0 Å atomic resolution), carried out by Dr. Marta Ferraroni, Università degli Studi di Firenze.

The Fo-Fc electron density maps (Figure 20) show a well-defined density for all the atoms of the inhibitors **A3** and **A13** bound within the hCA II active site, which are coordinated to the Zn(II) ion by means of the sulfonamide moiety. The sulfonamide nitrogen coordinated to the zinc ion also makes a strong H-bond with the OH of Thr199. These interactions are common to all CA - sulfonamide adducts reported to date.[2] The scaffold of the inhibitors occupied the entire available space inside the cavity and were oriented toward the hydrophobic part of the active site cleft, establishing strong van der Waals interactions. In particular the phenyl ring attached to the sulfonamide group made hydrophobic interactions with residues Val121 and Leu198. The 1,2,3-triazole ring forms hydrogen bonds with water molecules and in the inhibitor **A13** an edge-to-face π- π stacking interaction with the phenyl group of the Phe131 side chain. Furthermore the terminal phenyl ring of inhibitors **A3** and **A13** forms strong hydrophobic interactions with Val135 and Phe131.

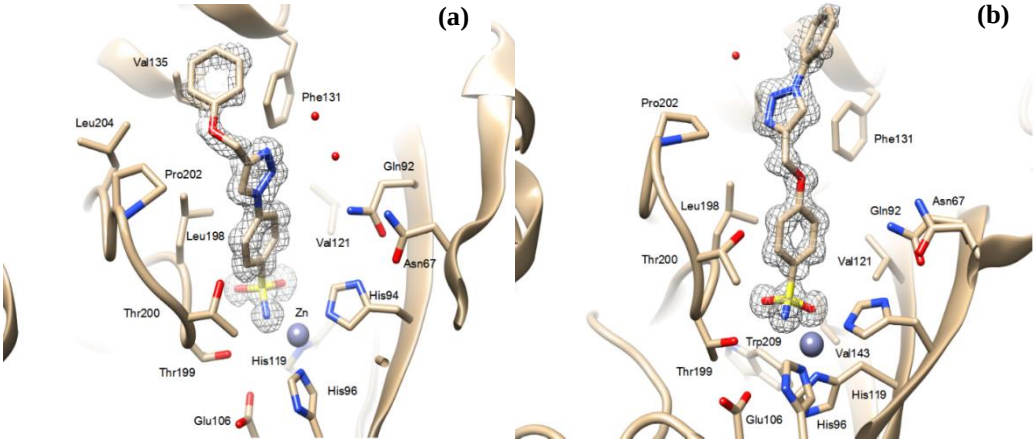

Figure 20. Active site region in the hCA II-**A3** (a) and **A13** (b) complexes. The omit Fo-Fc electron density maps (contoured at 2.0 σ) for the two inhibitors are also shown. Coordinates and structure factors for hCA II complexes with **A3** and **A13** have been deposited in the Protein Data Bank (PDB) accession code: 5LJQ and 5LJT.

Indeed the superposition of the experimental X-ray and the *in silico* poses highlight a very good matching (Figure 21).

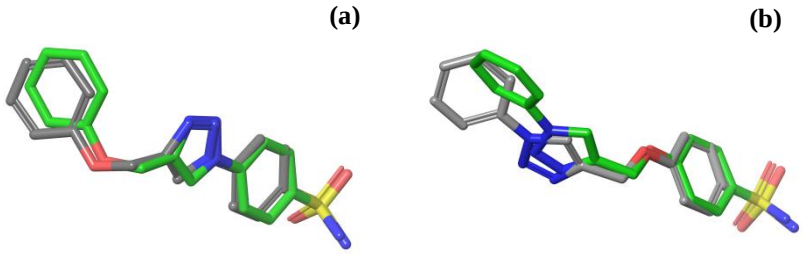

Figure 21. Docking (grey) vs. X-ray (green) orientation in hCA II active site for compounds **A3** (a) and **A13** (b).

In order to gain a better understanding on the binding modes of all the synthesized compounds, docking studies were carried out for the overall of two subsets inhibitors **A3-A9** and **A13-A17** with hCA II (PDB ID: 4Q6E) and hCA IX (PDB ID: 3IAI)[67]. In hCA II, all compounds were predicted to orient the aromatic sulfonamide moiety deeply into the catalytic cleft of the active site forming a hydrogen bond with the hydroxyl group of T199 side chain, while the NH^- coordinates the zinc ion and the phenyl ring is neighboured by several hydrophobic residues (Val121, His94 and Leu198). The 1,2,3-triazole ring, linked to the position 4 of the benzosulfonamide directly (first subset: compounds **A3-A9**), or through an oxymethylene linker (second subset: compounds **A13-A17**), mostly forms edge-to-face π- π interactions with the phenyl group of the Phe131 side chain. The flexible hydrophobic tail of the compounds is oriented towards the lipophilic half of the CA active site, in the region delimited by residues Phe131, Gly132, Val135, Gln136, Pro202 and Leu204 (Figure 22).

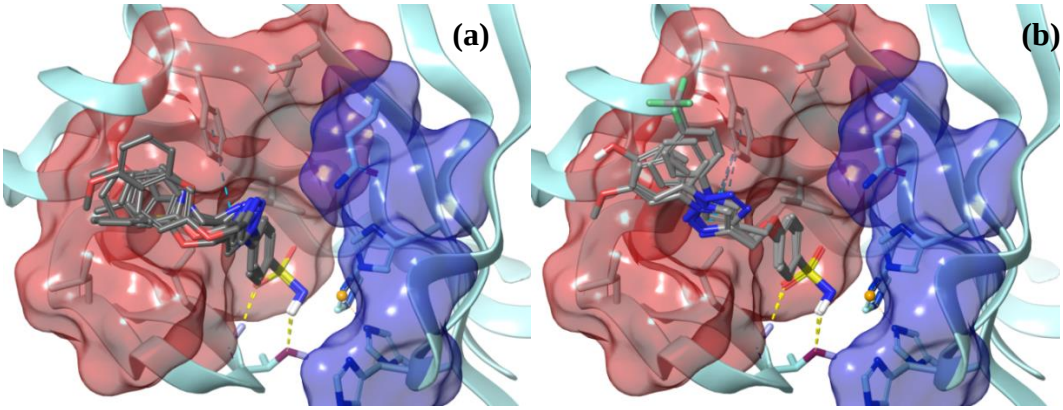

Figure 22. Representation of the binding orientation of compounds (a) **A3-A9** and (b) **A13-A17** in hCA II (PDB code 4Q6E). The hydrophobic half of the active site cleft is shown as a red surface, while the hydrophilic half as a blue one.

As mentioned above, docking studies were also performed in the hCA IX active site (PDB ID: 3IAI).[67] Compounds **A3- A9** oriented themselves in quite similar poses as observed for hCA II. The triazole ring established hydrophobic interactions with Val131, whereas the tail aryl groups extended in a partly exposed pocket formed by hydrophobic residues. The different orientation of the aromatic tails could be correlated to the mutation of Phe131 replaced by Val131 in hCA IX active site. Conversely compounds **A13- A17**, which bear the aryltriazole moieties linked to benzenesulfonamide through an oxymethylene linker, extend their tails towards the hydrophilic region delimited by residues Asn62, His64, Gln67 and Gln92, where the triazole forms polar interactions with Gln67 and Gln92. The different orientation assumed by such moieties within hCA IX active site is likely due to the Phe131V CAII/IX mutation. In absence of the π- π interaction driving force the aromatic tails were not driven near the hydrophobic side anymore, but instead found good interaction points on the hydrophilic region (Figure 23b).

The different set of interactions established by the aromatic tails of the two subsets of compounds within hCA II and hCA IX active sites could explain the general reduced inhibitory activity against the tumor-associated isoforms compared to the cytosolic one.

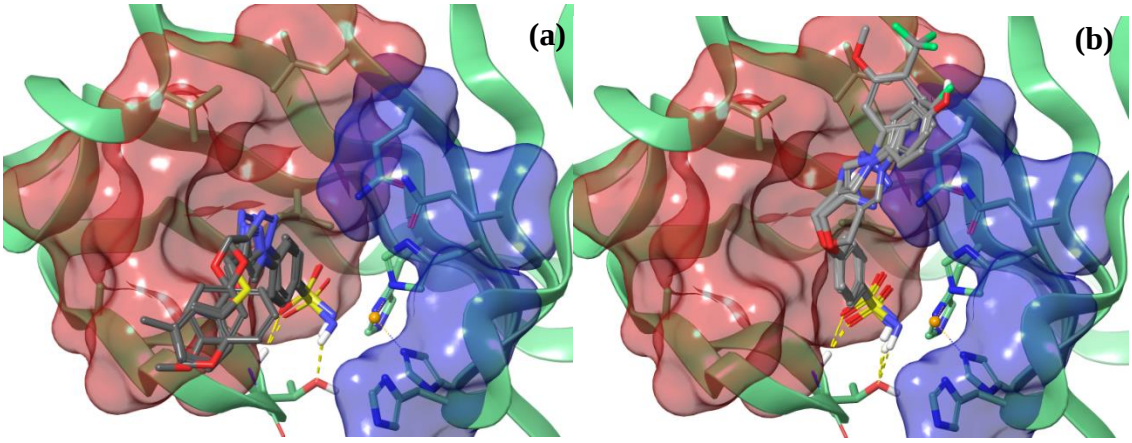

Figure 23. Representation of the binding orientation of compounds (a) **A3- A8** and (b) **A13- A17** in hCAIX (PDB code 3IAI). The hydrophobic half of the active site cleft is shown as a red surface, while the hydrophilic half as a blue one.

The intraocular pressure (IOP) lowering properties of some of the derivatives of this series, **A3**, **A13** (for which the X-ray structures of the adducts with hCA II were reported) and **A9** (which showed a unique sub-nanomolar inhibitory activity against hCA II) were measured in an animal model of glaucoma [135] by the group of Prof. Masini, Università degli Studi di Firenze.

The three compounds showed a sufficient water solubility to be formulated as 1% eye drops at the neutral pH value (dorzolamide, **DRZ**, the clinically used drug is a hydrochloride salt with a pH of the eye drops of 5.5 which produces eye irritation and stinging as side effects).[7b-d, 10b] The compounds were administered to rabbits with high IOP, induced by the injection of 0.1 mL of hypertonic saline solution (5% in distilled water) into the vitreous of both eyes (Figure 24). **DRZ** hydrochloride was used as a standard drug, whereas the control experiments were done by using the vehicle (hydroxypropylcellulose at 0.05%). The selected derivatives were very potent inhibitors of isoforms hCA II (responsible for aqueous humor secretion; K_I of 0.83-1.2 nM, Table 1) and hCA XII (isoform that is overexpressed in the eyes of glaucomatous patients;[17] K_I of 1.1 nM, Table 1).

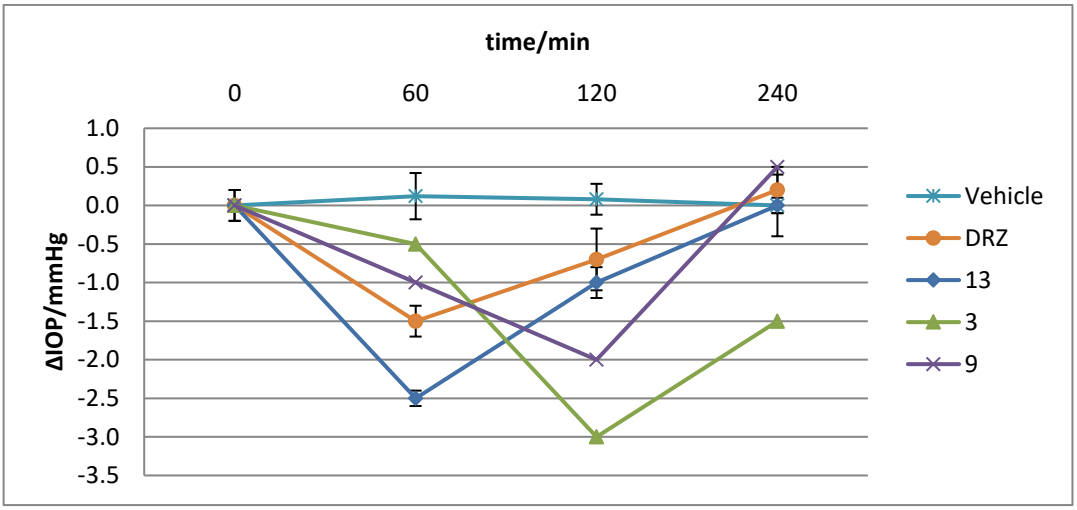

Figure 24. Drop of intraocular pressure (ΔIOP, mmHg) versus time (min) in hypertonic saline-induced ocular hypertension in rabbits, treated with 50 μL of 1 % solution of compounds **A3**, **A9** and **A13** and **DRZ** as the standard drug and vehicle. Errors were within 10−15% of the reported IOP values (from three different measurements for each of the four animals in the study group) and were statistically significant ($p = 0.045$ by the Student's t test).

As seen from the data of Figure 24, all three compounds proved to be more effective than **DRZ**, even if at different times post-administration. Indeed, a comparable behaviour to **DRZ**, which caused an IOP drop of 1.5 mm Hg at 60 min post-administration, emerged only for derivative **A13**, that effected an IOP drop increased to 2.5 mmHg after the same time. Another analogy between **A13** and **DRZ** was the IOP rise in short-term, so that after 4 h no IOP decrease was seen. Conversely for derivatives **A3** and **A9**, the peak of IOP drop, that reached 3.0 and 2.0 mm Hg respectively, was at 2 h post-administration, whereas their IOP lowering activity after 1h was reduced in comparison to DRZ. In addition, while for compound **A9** after 4 h no IOP decrease was seen, **A3** showed the ability to protract its IOP lowering action up to the same time point.

It should be mentioned that the animal model employed for these estimations is of normotensive rabbits, and this is why the absolute IOP drops are not very high. However the advantage of this model is that the measurements can be done rapidly and are highly reproducible.

The sulfonamides of the series, designed in order to be endowed with an enhanced flexibility between their molecular fragments in comparison to their lead **PTB**, have been screened for the inhibition of four physiologically relevant CA isoforms: hCA I, II, IX, and XII. Hence, interesting SAR have been extrapolated and afterwards the X-ray crystal

structures of two of them bound to hCA II shed light on their inhibitory behaviour at the molecular level, which was in agreement with the results of the preliminary computations. The crystallographic results supported a deeper molecular modelling analysis concerning all the reported derivatives and both hCA II and hCA IX. Three of these compounds also showed highly effective *in vivo* antiglaucoma activity in an animal model of the disease being more effective compared to the clinically used drug dorzolamide, even if at different time post-administration.

The data and results of this research were published in Nocentini, A. et al. *J. Med. Chem*. **2016**, *59*, 10692-10704. The experimental procedures are reported in Chapter 4.

Series B: coumarins

The "Click Chemistry" approach was applied also to coumarins.[118-124] Indeed, although a large number of synthetic approaches were reported to date for derivatizing coumarins in order to obtain CAIs, the "click chemistry" one has been not investigated in detail for this class of compounds. Again a flexibility element was introduced in the triazolic "tails" of the designed derivatives.

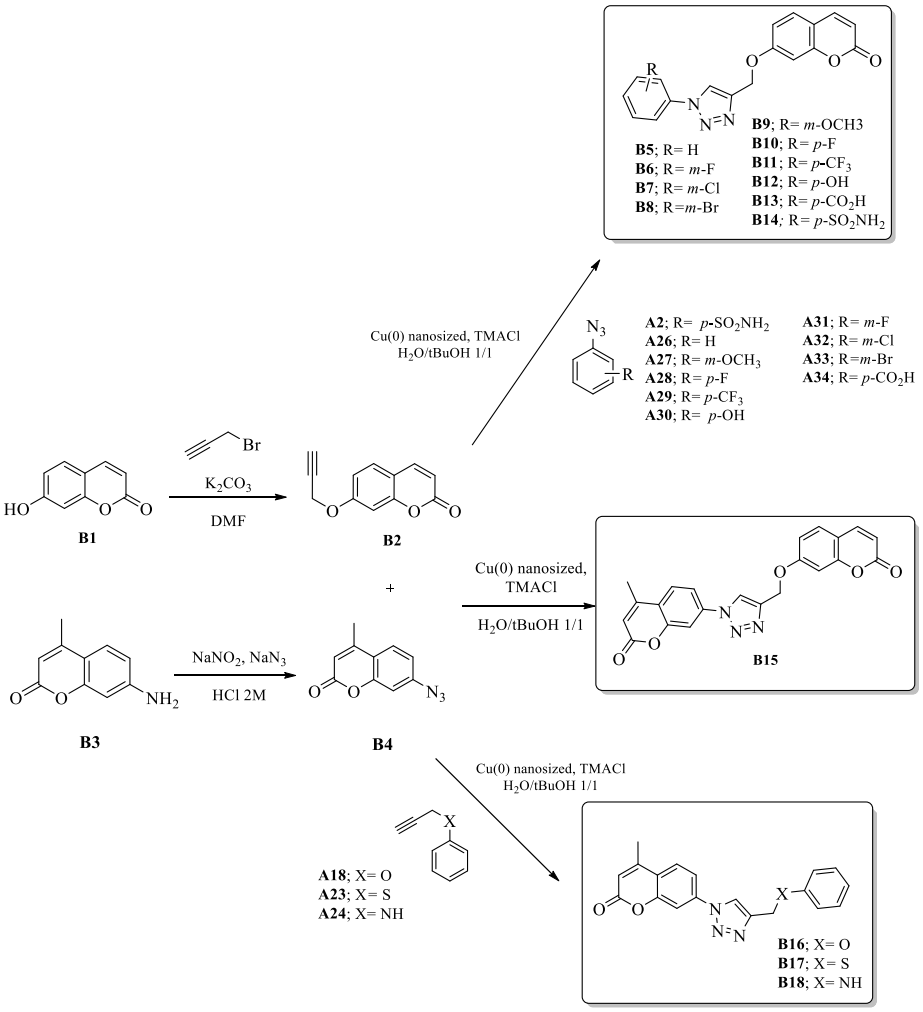

Scheme 3. General synthetic scheme of compounds **B5-B18**.

Starting from 7-hydroxy-coumarin **B1**, the propargyl ether key intermediate **B2** was obtained as an alkyne for the click chemistry. Reaction of **B2** with aromatic azides (**A2, A26-A34**, in common with the synthetic pathway of sulfonamides of series A) afforded a first subset of triazoles, **B5-B14**, incorporating the coumarin ring and diverse aryl groups at the triazole moiety (Scheme 3).

4-Methyl-7-amino-coumarin **B3** was transformed into the corresponding azide **B4** by diazotization followed by reaction with sodium azide, and was subsequently used for cycloaddition reactions with alkyne **B2** (leading to a bis-coumarin derivative, **B15**) or propargyl derivatives **A18, A23, A24** (in common with the synthetic pathway of sulfonamides of series A), leading to derivatives **B16-B18** (Scheme 3).

The rationale for derivatizing the 7-hydroxy-/amino coumarins was furnished by earlier works in which it was shown that coumarins incorporating various functionalities in this position are effective and isoform-selective CAIs.[118-124] Thus, compounds incorporating substituted-aromatic moieties either directly attached to the triazole ring (as in **B5-B14**) or via a CH_2X linker (as in **B16-B18**, in which X = O, S or NH) were synthesized. For the first sub-group of derivatives (**B5-B14**), the aryl azides used incorporated various 3- or 4-substituted groups (halogens, OH, OMe, carboxyl, sulfamoyl, etc.) in order to delineate the structure-activity relationship (SAR) for the inhibition of various CA isoforms with the obtained derivatives.

Coumarins **B5-B18** were screened for the inhibition of four hCA isoforms involved in important physiologic/pathologic processes, i.e., the cytosolic, hCA I and II (off-targets in this case) and the transmembrane, tumor-associated hCA IX and XII (anticancer drug targets). [2,48-54] Table 3 shows inhibition data of coumarins **B5-B18** and the sulfonamide acetazolamide **AAZ** (as standard inhibitor) against hCA I, II, IX and XII, after a period of 6 h of incubation of the enzyme and inhibitor solutions, which is used for assaying all coumarins as CAIs. [118-124]

The following SAR should be noted regarding the inhibition data of Table 3.

(i) Isoform hCA I was moderately or poorly inhibited by coumarins 5-18 investigated here. Five derivatives (**B9, B11-B14**) showed K_Is in the range of 172.8 -246.7 nM (the same range as the sulfonamide acetazolamide, **AAZ**) whereas the remaining ones were weaker, micromolar inhibitors (**B6, B10, B16** and **B17**) or did not inhibit significantly the enzyme up until 10 μM (Table 3). The compounds showing some inhibitory activity, had the following substitution patterns at the aryl moiety linked to the triazole ring: 3-methoxyphenyl, 4-trifluoromethylphenyl, 4-hydroxy-/carboxy-and sulfamoyl-phenyl.

(ii) Isoform II, the physiologically dominant one was poorly inhibited by the new coumarins reported here except the carboxylate derivative **B13** which showed K_I of 99.6 nM. The other derivatives did not inhibit significantly the enzyme up until 10 μM (Table 3). Carboxylates may have a multitude of inhibition mechanisms towards CAs, as the COO^- moiety may be a zinc-binding group, it may anchor to the zinc-coordinated water molecule or even promotes binding outside the active site.[114]

Table 3: Inhibition data of human CA isoforms hCA I, II, IX and XII with coumarins **B5-B18** reported here and the standard sulfonamide inhibitor acetazolamide (**AAZ**) by a stopped flow CO_2 hydrase assay.[135]

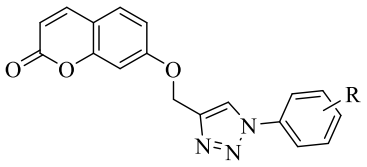

B5-B14

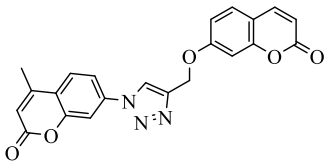

B15

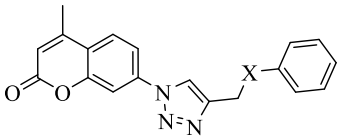

B16-B18

			K_I (nM)			
Compound	R	X	hCAI	hCA II	hCA IX	hCA XII
B5	H	-	>10000	>10000	24.5	4.8
B6	3-F	-	921	>10000	24.9	5.1
B7	3-Cl	-	>10000	>10000	31.2	5.5
B8	3-Br	-	>10000	>10000	27.5	27.1
B9	3-OCH_3	-	210.7	>10000	23.6	5.2
B10	4-F	-	1568	>10000	24.0	4.7
B11	4-CF_3	-	239.5	>10000	23.0	5.5
B12	4-OH	-	242.5	>10000	26.9	5.3
B13	4-COOH	-	240.9	99.6	28.8	4.9
B14	4-SO_2NH_2	-	172.8	>10000	14.3	9.9
B15	-	-	>10000	>10000	22.8	37.8
B16	-	O	1243.2	>10000	33.1	5.0
B17	-	S	2137.9	>10000	29.6	5.1
B18	-	NH	246.7	9743	34.4	4.9
AAZ		250	12	25	5.7	

* Mean from 3 different assays, by a stopped flow technique (errors were in the range of ± 5-10 % of the reported values).

(iii) The transmembrane isoform hCA IX was effectively inhibited by all coumarins reported here, with K_Is in the range of 14.3 – 34.4 nM. It may be observed that the range of the inhibitory power is very small, meaning that all the substitution patterns explored in the paper lead to highly effective CAIs.

(iv) A similar situation to what mentioned above for hCA IX has also been observed for the inhibition of hCA XII with the coumarins investigated here, which showed highly effective inhibitory action, with K_Is in the range of 4.7 – 37.8 nM. Only the bis-coumarin

B15 was slightly less inhibitory (K_I of 37.8 nM) whereas the remaining derivatives showed K_Is < 10 nM (except one compound, **B8**, which has a K_I of 27.1 nM). Overall, the coumarins reported here show excellent inhibitory action against both tumor-associated isoforms hCA IX and XII.

(v) As many coumarins, the derivatives investigated here are hCA IX/XII selective inhibitors over hCA I and II, which constitutes a very important feature for this class of compounds. Indeed, one of the main problems with CAIs is constituted by their wide range of side effects, mainly due to inhibion of the off target isoforms such as hCA I and II.

The series of 7-substituted coumarins incorporating aryl-triazole moieties were prepared by click chemistry procedures and was assayed for the inhibition of the cytosolic, widespread human hCA I and II isoforms, and the transmembrane, tumor-associated ones hCA IX and XII, reporting selective low nanomolar inhibitory action against the transmembrane isoforms (K_I of 14.3 – 34.4 nM against hCA IX and of 4.7 – 37.8 nM against hCA XII). Since many hypoxic tumors overexpress hCA IX/XII, and as these targets were recently validated for obtaining antitumor/antimetastatic agents, with one inhibitor that successfully completed Phase I clinical trials, the present findings constitute an interesting extension to the knowledge of non-sulfonamide, selective inhibitors of CA isoforms involved in serious pathologies.

The data and results of this research were published in Nocentini, A. et al. *Bioorg. Med. Chem.* **2015**, *23*, 6955-66. The experimental procedures are reported in Chapter 4.

Series C

Finally, we applied the analogue concept to the sulfocoumarin scaffold, namely 1,2-benzoxathiines-2,2-dioxides that were recently validated as a novel class of CAIs.[115] As mentioned in paragraphs 2.3.2 and 2.2.3, the design of sulfocoumarins as CAIs was inspired by their corresponding bioisosters coumarins, whose inhibition mechanism has been previously depicted. Indeed the sulfocoumarins, as well as coumarins, undergo a CA-mediated hydrolysis within the active site cavity with the generation of the inhibitory species (Figure 25a). The inhibition mechanism of such hydrolysis products is different

at the molecular level when compared to the classical sulfonamide-based CAI.[2] The 2-hydroxyphenyl-ω-ethenyl sulfonic acids which are formed from the original sulfocoumarins, tightly bind to the zinc-coordinated water molecule by means of hydrogen bonding, whereas the scaffold of the inhibitor establishes additional favourable interactions within the cavity (Figure 25b).

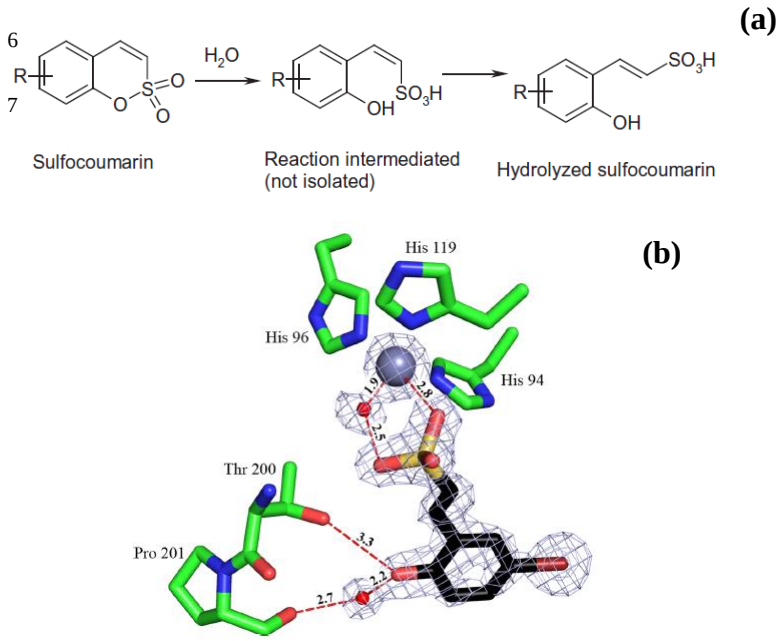

Figure 25 CA inhibition mechanism of sulfocoumarins. (a) The sulfocoumarin undergoes an enzyme-mediated hydrolysis with formation of the trans-2-hydroxy-phenyl-ω-ethenylsulfonic acid. (b) The sulfonic acid binds to the CA II active site, by anchoring of the sulfonic acid group to the zinc-coordinated water molecule. The Zn(II) ion (central larger sphere), its three His ligands (His94, 96 and 119), the water molecule coordinated to the zinc (small sphere) as well as active site residues Thr200 and Pro201 involved in the binding of the hydrolyzed sulfocoumarin are shown, as determined by X-ray crystallography (PDB file 4BCW).[115]

In analogy to coumarins, the substitution pattern at the sulfocoumarins scaffold strongly influences the potency and selectivity profile against different human CA isoforms for this class of inhibitors.[115,136-139] Indeed, in our previous reports[115,137-139] we investigated a large series of sulfocoumarins bearing tetrazolyl, triazolyl or small moieties at position 6, which were shown to act as low nanomolar hCAIX/XII inhibitors, but do not inhibit hCAI and II. On the contrary, derivates bearing small substituents and benzyl esthers at the 7-position of the scaffold act as low nanomolar hCAII inhibitors, but do not significantly inhibit hCAI, IX and XII.[136]

To date, sulfocoumarins incorporating bulky, flexible moieties at position 7 were not reported; thus, we performed the synthesis and evaluated the inhibition properties against four relevant hCA isoforms (hCAI, II, IX and XII) of a small series of 7-substituted sulfocoumarins bearing aryl-triazolyl moieties via a CH_2O linker and synthesized by means of Click chemistry procedures (Scheme 4).

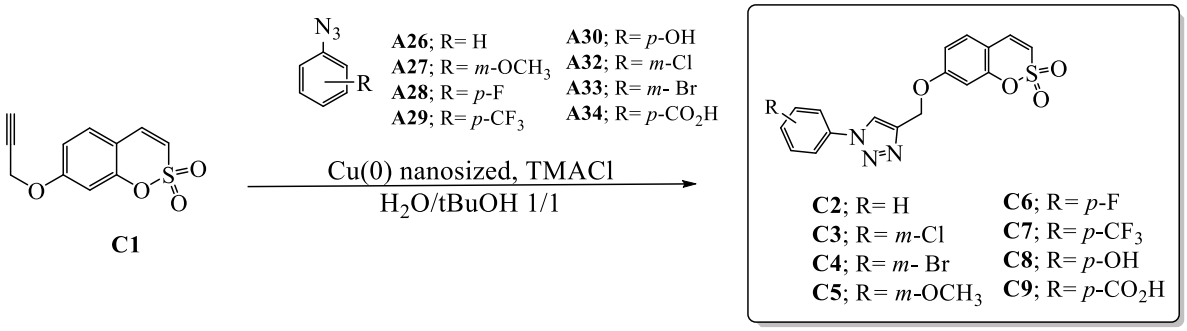

Scheme 4. General synthetic scheme of compounds **C2-C9**

The general strategy of Zalubovski's group[140,141] for the preparation of 6-substituted sulfocoumarins was recently validated for the synthesis of 7-substituted such derivates.[140] Reaction of 2,4-dihydroxybenzaldehyde **C10** with benzylbromide afforded the benzyl derivate **C11**, which was treated with methanesulfonyl chloride followed by cyclization of the sulfonate **C12**, in presence of 1,8-diazabicyclo[5.4.0]undec-7-ene (DBU), with formation of the racemic 4-hydroxy-7-benzyloxy-3,4-dihydrosulfocoumarin **C13**. The alcohol **C13** was deprotected at the 7 position by hydrogenation, with formation of the 7-hydroxy derivative **C14**, which by dehydration and alkylsulfonylation of the phenol group in presence of mesyl chloride led to C**15**. Hydrolysis of the methylsulfonate ester **C15** in the presence of tetraethylammonium hydroxide led to the formation of 7-hydroxysulfocoumarin **C16**, which was converted to the propargyl derivate **C1** through reaction with the proper bromide (Scheme 5). Alkyne **C1** was reacted with various freshly prepared arylazides (**A26-A34**, in common with the synthetic pathway of series **A** and **B**) in presence of copper(0) nanosized as catalyst[128] to afford the 1,2,3-triazolyl derivates **C2-C9** (Scheme 4).

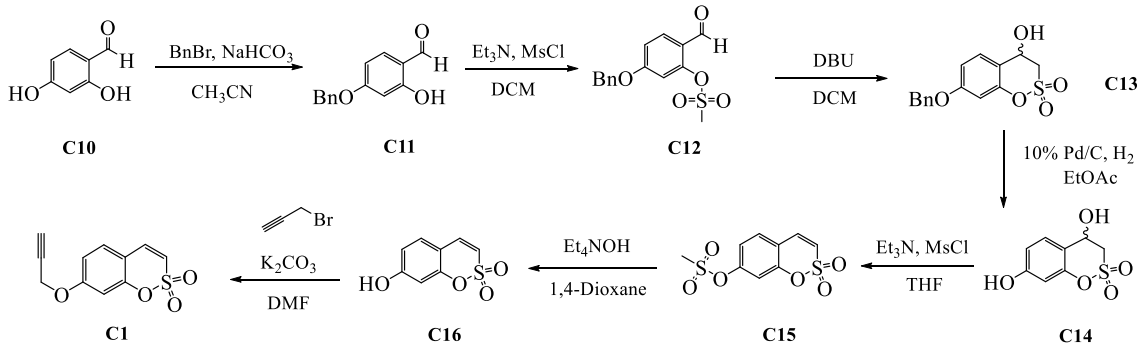

Scheme 5. Synthesis of 7-propargyloxysulfocoumarin **C1**

Sulfocoumarins **C2-C9** were screened for the inhibition of four physiologically relevant human CA isoforms, the cytosolic hCAI and II and the trasmembrane tumor-associated hCAIX and XII. Table 1 shows inhibition data of sulfocoumarins **C2-C9** and the sulfonamide acetazolamide AAZ (as standard inhibitor) against hCA I, II, IX and XII, after a period of 6 h of incubation of the enzyme and inhibitor solutions, which is used for assaying all sulfocoumarins as CAIs.

The following SAR should be noted regarding the inhibition data of Table 4.

(i) According to previous reports,[115,136-139] isoform hCA I was not or poorly inhibited by sulfocoumarins **C2-C9** investigated here. Compounds **C3** and **C6** are high micromolar inhibitors, whereas the remaining ones did not inhibit significantly the enzyme up until 10 μM.

(ii) The inhibition profiles shown by sulfocoumarins **C2-C9** on the remaining three isoforms was quite surprising and unexpected. Indeed, although the 7-substituted sulfocoumarins reported earlier[137] were effective and totally selective inhibitors for hCA II over the tumor-associated isoforms IX and XII, surprisingly derivates **C2-C9** do not exhibit any inhibitory activity against the cytosolic isoform hCA II, but were low nanomolar inhibitors for the transmembrane isoforms (Table 4). It should be mentioned that the previously sinthesized derivates incorporated small moieties or benzyl esthers at the 7 position, whereas sulfocoumarins **C2-C9** bear flexible and bulky aryl-triazolyl moieties via a CH_2O linker.

Table 4: Inhibition data of human CA isoforms hCA I, II, IX and XII with sulfocoumarins **C2-C9** reported here and the standard sulfonamide inhibitor acetazolamide (**AAZ**) by a stopped flow CO_2 hydrase assay.[135]

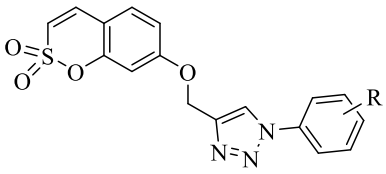

C2-C9

		K_I (nM)			
Compound	R	hCAI	hCA II	hCA IX	hCA XII
C2	-	>10000	>10000	25.3	4.5
C3	3-Cl	2301	>10000	25.6	4.5
C4	3-Br	>10000	>10000	36.5	5.5
C5	3-OCH_3	>10000	>10000	24.1	4.3
C6	4-F	984	>10000	26.8	5.5
C7	4-CF_3	>10000	>10000	19.0	5.2
C8	4-OH	>10000	>10000	19.6	19.1
C9	4-COOH	>10000	>10000	19.2	4.6
AAZ	-	250	12	25	5.7

***** Mean from 3 different assays, by a stopped flow technique (errors were in the range of ± 5-10 % of the reported values).

(iii) As mentioned, the transmembrane isoforms hCA IX and XII were strongly inhibited by the new sulfocoumarins **C2-C9**, here reported, with K_I values of 19.0-36.5 nM against hCAIX and 4.3-19.1 nM against hCAXII, respectively. These values were comparable with the clinically used sulfonamide **AAZ** (Table 4). The definition of a proper structure-activity relationship (SAR) for hCA IX and hCA XII is not feasible, considering that all these compounds showed high and similar affinity for such these isoforms. Thus, the nature of the substituent R on the phenyl moiety has a weak influence on the inhibitory properties. On the contrary, these data demonstrate that the nature of the substituent at position 7 of the sulfocoumarins scaffold is a pivotal factor to address the selectivity profile of such derivates.

Therefore, unlike 7-substituted sulfocoumarins investigated earlier, which were potent and selective hCA II inhibitors and ineffective as hCA I, IX and XII inhibitors, compounds from this new series exhibit effective and selective inhibitory properties for the tumor-associated isoforms over hCAIX and XII.
These results are of interest and highlight the need of an in-depth investigation of the inhibitory mechanism of such class of CAIs.

The data and results of this research were published in Nocentini, A et al. *J. Enzyme Inhib. Med. Chem.* **2016**, *31*, 1226-33. The experimental procedures are reported in Chapter 4.

3.2 Deciphering the mechanism of human Carbonic Anhydrase inhibition with sulfocoumarins (Serie D).

As mentioned, the esterase activity shown by the α-CAs,[2] recently allowed the discover of two novel classes of CAIs.[115,117] In detail, the coumarins and their bioisoster sulfocoumarins represent two aromatic scaffold directly not able to inhibit the CA activity, but, on the other hand, showed to act as substrates for the esterase activity of the enzymes undergoing a CA-mediated hydrolysis. The formed cinnamic and sulfonic acids, respectively, inhibits the CAs. [115,117] The prodrug features of coumarin and sulfocoumarin were confirmed by the inhibitory activity registered after a 6h incubation time. [115,116,117]
The detailed reaction mechanism of the CA-mediated prodrug hydrolysis has not been established yet and its knowledge would be meaningfull to further design CAIs belonging to these prodrugs classes.
In recent studies, we reported a variety of sulfocoumarins bearing electro-withdrawing (EW) or electro-donating (ED) groups at the 6- and 7- position, which showed different efficacy against the screened CA-isoforms. [136-140] The series of 6- and 7-substituted sulfocoumarins were implemented with compounds exhibiting groups endowed different electronic (EW or ED) or steric properties.
The novel CA inhibitory profiles were integrated and compared with the previously reported ones. The inhibition profile of the benzo[e][1,2]oxathiine 2,2-dioxide arose as hard to rationalize by simple SAR study and pointed out a raising conviction that such an

isoform-selective efficacy might unlikely derive from simple enzyme-ligand interaction after the hydrolysis process, whereas it could pertain and involve the mechanism through which sulfocoumarin were hydrolysed by the different CAs esterase activity.

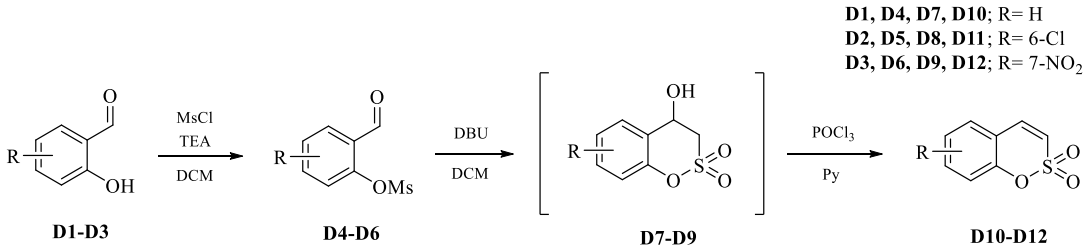

Scheme 6. General synthetic procedure of sulfocoumarin **D10-D12**.

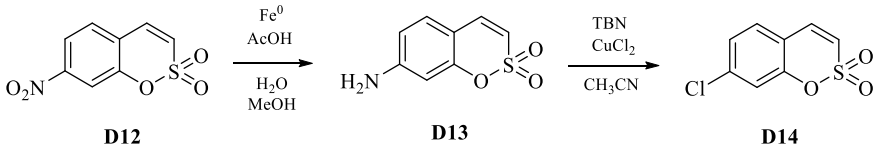

Scheme 7. Synthetic procedure of sulfocoumarin **D13-D14**.

The general strategy of designed by Zalubovski's group and extended by us, as previously reported, [136-140] was exploited for the synthesis of the novel sulfocoumarins. Reaction of the proper 2-hydroxybenzaldehyde **D1-D2** with mesyl chloride afforded the mesylates derivate **D4-D6**, which were treated with 1,8-diazabicyclo[5.4.0]undec-7-ene (DBU), with formation of the racemic 4-hydroxy-3,4-dihydrosulfocoumarin **D7-D9** in mixture with their dehydration products **D10-D12** (Scheme 7). The dehydration was concluded by treating the mixtures with $POCl_3$ in pyridine. 7-NH_2-sulfocoumarin **D13** was obtained by reducing the correspondent nitro-derivative **D12** with iron (0) and that was therefore converted to the chlorine compound **D14** through Sandmeyer reaction with $CuCl_2$ in presence of tert-butyl nitrite (Scheme 7).

Sulfocoumarins **D10-D14** were screened for the inhibition of four physiologically relevant human CA isoforms, the cytosolic hCAI and II and the trasmembrane tumor-associated hCAIX and XII. The following SAR should be noted regarding the inhibition data of Table 5.

Table 5: Inhibition data of human CA isoforms hCA I, II, IX and XII with sulfocoumarins **D** reported here and the standard sulfonamide inhibitor acetazolamide (**AAZ**) by a stopped flow CO_2 hydrase assay.[135]

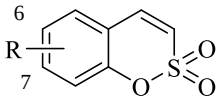

		K_I (nM) [a]			
Compound	R	hCAI	hCA II	hCA IX	hCA XII
D10	H	>100000	>100000	432.2	69.5
6-NO_2-sulfocoumarin [b]		92000	>100000	3770	3160
6-NH_2-sulfocoumarin [b]		6780	8890	46.0	23.0
D11	6-Cl	>100000	>100000	136.3	89.5
D12	7-NO_2	>100000	>100000	37.0	81.7
D13	7-NH_2	>100000	>100000	33.5	38.4
D14	7-Cl	>100000	>100000	33.7	60.9
AAZ	-	250	12	25	5.7

[a] Mean from 3 different assays, by a stopped flow technique (errors were in the range of ± 5-10 % of the reported values). [b] From ref 115.

(i) Not surprisingly, isoform hCA I and II were not significantly inhibited by sulfocoumarins **D10**-**D14** investigated here up until 10 μM.

(ii) Conversely transmembrane isoforms hCA IX and XII were strongly inhibited by the new sulfocoumarins **D10**-**D14** in the low-medium nanomolar range, with K_I values of 33.5-432.2 nM against hCA IX and 38.4-89.5 nM against hCA XII, respectively.

Considering the aforementioned hypothesis regarding the isoform-selectivity exhibited by sulfocoumarins, in the present study, we used the B3LYP hybrid density functional theory (DFT) to study and deduce the sulfocoumarin hydrolysis upon the CA esterase activity.

Indeed, the computational studies represent a valid tool to provide insights into the enzymatic reaction mechanism, [142-147] The knowledge of such mechanism might further aid in the design of novel specific enzymatic modulators.

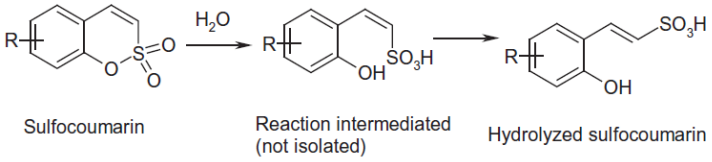

The ligand conformation present in the unique crystallographic structure of the sulfocoumarin/CA complex known to date (PDB ID 4BCW) [115] represents the final stage of the hydrolysis process. The sulfocoumarin is crystallized in the hydrolysed form, with the sulfonate anchored to the Zn(II) and hydroxide ions, and interacting with the NH of the Thr199 backbone. The phenol moiety establishes H-bond with Thr200 side chain.

Quantum mechanics-based simulation (e.g. density functional theory, DFT) and the cluster approach, i.e. a simplified model system which enables to overcome the complexity of the enzyme overall[142-146], was used to elucidate the catalysis pathway and the hydrolysis mechanism of the sulfocoumarin.

The cluster model includes the essential elements involved in the reaction: (i) the Zn ion; (ii) the Zn-bound OH^- (as present in the active form of the enzyme); (iii) three imidazole nuclei representative of the three side chains His residues; (iv) the truncated Thr199 residue that established a H-bond with the sulfonate moiety; (v) an additional water molecule taken from the X-ray structure (only in the last two steps as described later).

Docking simulation were used in order to position the not hydrolized sulfocoumarin into the binding cleft of the hCA II (pdb code: 4BCW). The docked pose was prepositioned in the model system, fully minimized at the DFT/B3LYP level of theory, LACVP* basis set, and then a transition state search with Jaguar was undertaken in the same experimental conditions.

Starting from the fully minimized reactant and product structures, a guess at the transition state was built and optimized. Single point calculations have been carried out at the DFT/B3LYP level of theory, LACVP**$^+$ basis set, and the nature of stationary points as true minima or first order saddle points was checked by frequency calculations and unscaled ZPE corrections were applied to the energy values.

The reaction energy, computed as the difference between the product and reactant energies, was determined. In a similar fashion, the activation barrier was determined as the difference between the transition state energy and the energy of the reactants.

The CA esterase reaction that led to the hydrolysis of sulfocoumarin is a multistep process comprising four steps:

Step 1: Nucleophilic attack of the hydroxide ion on the cyclic sulfonate (sulphur atom) and double bond protonation.

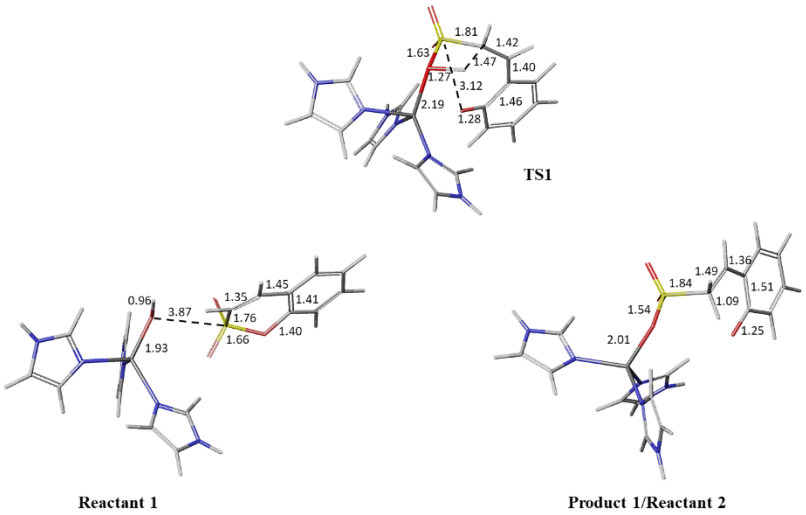

Figure 26. Reaction path for the first step. Thr199 omitted for clarity

The distance between the negative oxygen atom of the hydroxide present in the active form of the enzyme and the sulfonate ester sulphur atom (d= 3.87 Å) is proper to elicit a nucleophilic attack, which began the cycle opening alongside with the double bond protonation. This latter event is fundamental to offer the molecule the degree of freedom necessary to lose the planarity and ease the ring opening. The formed intermediate is a carbocation which was stabilized by resonance with the phenoxide ion deriving from the sulfonic ester.

The activation barrier for the first step was calculated to be 36.77 kcal/mol

Step 2: Formation of the E geometric isomer, through intramolecular acid-base reaction.

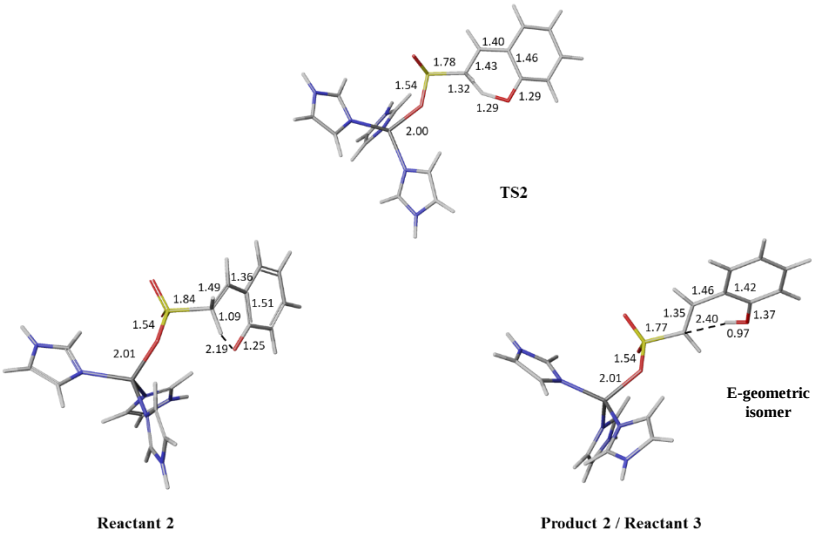

Figure 27. Reaction path for the second step. Thr199 omitted for clarity.

The second step pertains the formation of the E geometric isomer. It is determined by a intramolecular acid-base reaction, where the phenoxide moiety act as a base to deprotonate the CH_2 linked to the sulfur atom. The most energetically stable isomer (E) is formed.

The activation barrier for this step was calculated to be 16.053 kcal/mol.

Step 3: Entrance of an additional water molecule (pentameric zinc coordination pattern)

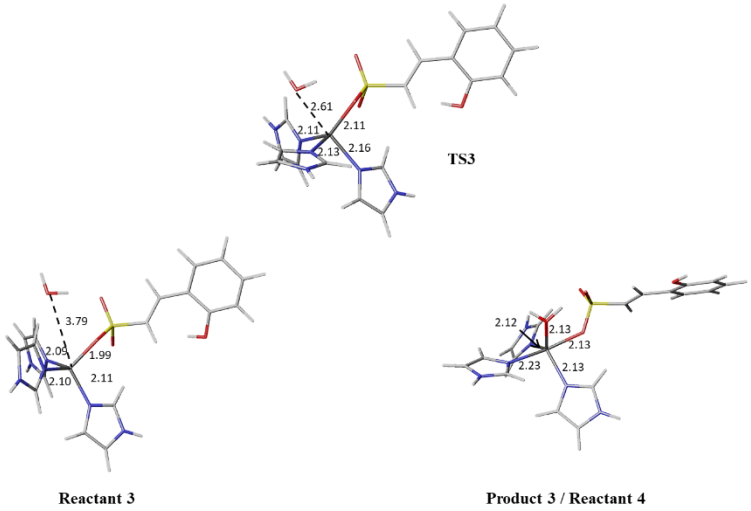

Figure 28. Reaction path for the third step. Thr199 omitted for clarity.

The additional water molecule present in the built cluster model approaches the Zn ion, eliciting a reorganization of the coordination pattern components (imidazoles and sulfonate), by which an intermediate between a trigonal bipyramid (water oxygen and its opposite histidine nitrogen in apical positions) and a square pyramid (sulfonate oxygen, water oxygen, its opposite histidine nitrogen, and histidine nitrogen which forms a 2.15 Å coordination bond defining the basal plane) is formed.
The activation barrier for this step was calculated to be 0.373 kcal/mol.

Step 4: Sulfonate exit and formation of the pseudo-tetrahedrical system

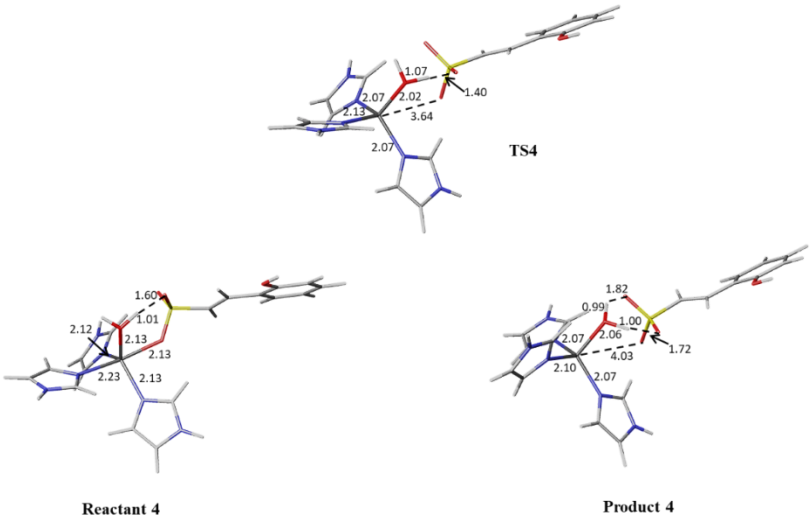

Figure 29. Reaction path for the fourth step. Thr199 omitted for clarity.

Finally, the sulfonate moiety slightly moves away from the Zn ion and the remaining components of the trigonal bipyramide rearrange forming a pseudo a tetrahedrical coordination system. The activation barrier for this step was calculated to be 9 kcal/mol. At least in the chosen model, the anchoring of the sulfonate to the coordinated water molecule does not allow it to totally depart from the inner part of the active site and restore the zinc bound hydroxide ion. Nevertheless, it could be possible that in the real active site, other residues and/or water molecules are involved to remove the product and deprotonate the coordinated water.

A four-steps CA-mediated hydrolytic process was depicted for sulfocoumarins by means of QM computational methods applied to a cluster model of the CAs binding site. This study was carried out in collaboration with Prof. C. Bazzicalupi, University of Florence.

The transfer of hydrolysis reaction from the system model to the overall of CAs active sites is currently on going by means of mixed MM/QM methods.

The experimental procedures are reported in Chapter 4.

3.3 N-Nitrosulfonamides: a new chemotype for Carbonic Anhydrase inhibition (Series E).

Nowadays the generally previous accepted theory[148] that only unsubstituted sulfonamides may act as inhibitors has been extensively shown to be incorrect. If compared to the high number of tails appended at the aromatic ring incorporating the sulfonamide ZBG, [1-3,95,96] only few modifications have been carried out on this group itself.[149-152] Indeed this could seem counterproductive, considering that the negative charge on nitrogen and the presence of a proton on it themselves make this group the ideal ligand for CA, but on the other hand a such functionalization could lead to novel inhibition mechanisms.[2]

It should be considered that secondary sulfonamides maintain the possibility to coordinate the Zn ion in the deprotonated form, as confirmed by X-ray crystallography. Di Fiore et. al demonstrated that N-hydroxy and N-methoxy sulfonamides are able to bind the Zn ion in the deprotonated form.[152] An analogous inhibition mechanism has been identified for the cyclic secondary sulfonamide saccharin and its derivatives by several groups.[153,154]

On the other hand, tertiary sulfonamides lose their acid peculiarity, paving the way to novel inhibition mechanism. Carradori et al [155-158] recently synthesized different series of tertiary sulfonamides, among which probenecid and saccharin derivatives, obtaining interesting and selective inhibition profiles, although the inhibition mechanisms of these compounds were not investigated yet in detail, as no X-ray crystallographic structures were obtained so far for adducts of these CAIs with various CA isoforms.

Although few examples of N-nitro sulfonamide are present in literature,[159,160] their CAs inhibitory properties have never been investigated and studied. Thus, it appeared to be stimulating to investigate a series of N-nitro aromatic sulfonamide, which showed strong as well as selective inhibitory activity on the tumor-associated isoform hCA IX over the cytosolic hCA II. In addition these derivatives were shown to inhibit the pathogenic fungal MgCA in the low micromolar range.

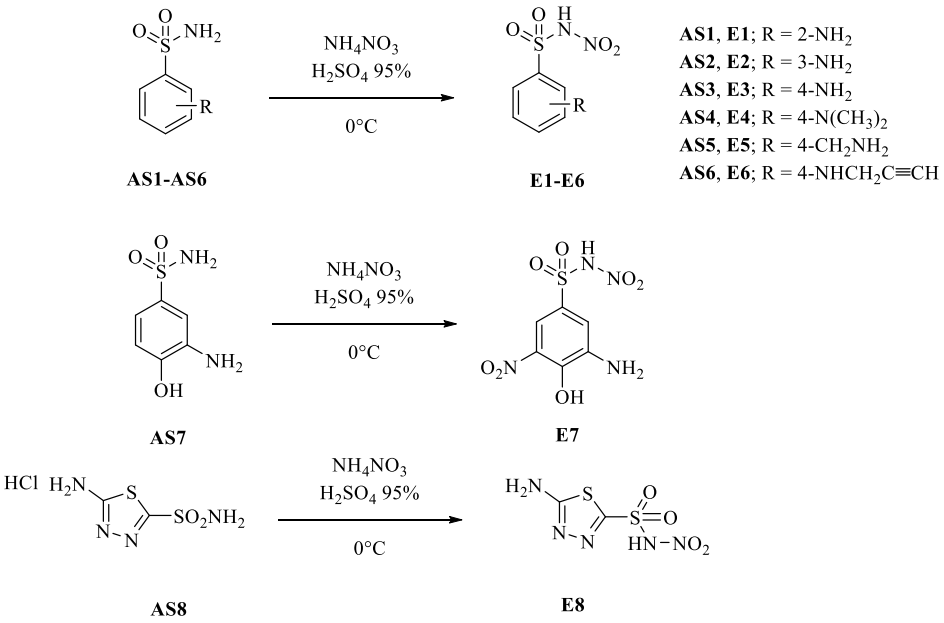

Scheme 8. General synthetic procedure for compounds **E1-E8**

The rationale of this work relies on the salient features of the nitro moiety, a strongly electro-withdrawing (EW) group able to enhance the acidity of the sulfonamide, and thus the interaction with the positive zinc ion. Furthermore, it allows for two additional H-bond acceptor atoms for possible interactions with active site residues.

The general synthetic strategy reported by Minksztym[159] for the chemoselective mononitration of aminosulfonamides (**AS**) has been applied and extended here (Scheme 8). The strongly acidic reaction conditions deactivate the amino moiety against nitration ensuring the exclusive functionalization of the sulfonamide nitrogen. The presence of the amino group ensures the stability of the zwitterion adduct. In fact, in absence of a basic counterpart, the strong acid N-nitrosulfonamide is not stable and rapidly decomposes to the corresponding sulfonic acid releasing N_2O.[159] The presence of a basic function in such a molecule, not too distant from the substituted sulfonamide, stabilizes it through the formation of a zwitterion. The evidence for the formation of the zwitterion was found in the solid state by means of IR.[159]

The synthesis was carried out treating the amino sulfonamides with NH_4NO_3 in concentrated H_2SO_4 (Scheme 8) and the obtained nitro derivatives were purified by means of crystallization in a polar solvent. The strong acidic character of the nitrosulfonamide reflects in the ^{1}H NMR spectra, where the signals were located with the signals of residual

water contained in DMSO-d_6. The ^{1}H NMR spectrum the 4-(2-aminomethyl)benzenesulfonamide N^1-nitro derivative **E5** further reveals the presence of the zwitterion through a three protons broad signal at 8.19 ppm representing the ammonium positive moiety. In the case of 3-amino-4-hydroxybenzenesulfonamide **A40**, the more activated aromatic ring undergoes an additional nitration at the 5 position, affording derivative **E7**, which has two NO_2 moieties in its molecule (Scheme 8).

N^1-Nitro sulfonamides **E1-E8** were screened for the inhibition of the *Malassezia globosa* CA[80] and two human (h) CA isoforms: the cytosolic hCA II and the tumor-associated hCA IX. Table 6 shows inhibition data of compounds **E1-E8** in addition to acetazolamide (AAZ) used as standard inhibitor and a clinically used drug.

The following structure-activity relationship (SAR) can be extrapolated from the inhibition data shown in Table 6:

(i) Most of the compounds of the series were efficient and selective inhibitors of the tumor-associated isoform hCA IX over the cytosolic one hCAII. Indeed, only derivatives **E2**, **E6** and **E8** exhibited low micromolar inhibitory activity against hCA II, whereas the remaining ones did not significantly inhibit the enzyme up to 50 μM inhibitor concentration. These data may suggest that the N-nitrosulfonamide group does not fit well within the hCA II active site, but the presence of some key elements on the molecular structure may improve the good contacts with the enzyme active site, thus leading to an increased inhibitory activity. Repositioning of the amino group in position 3 of the aromatic scaffold, a three carbon atoms alkyl substituent on the para amino moiety or the substitution of the benzene ring with the heterocyclic 1,3,4-thiadiazole, respectively contributed to make derivatives **E2**, **E6** and **E8** low micromolar inhibitors for hCA II (K_I values spanning between 1.35 and 5.11 μM, Table 6).

Table 6: Inhibition data of human CA isoforms hCA II, IX, *Malassezia globosa* CA (MgCA) with N-nitrosulfonamides and the standard sulfonamide inhibitor acetazolamide (**AAZ**) by a stopped flow CO_2 hydrase assay.[135]

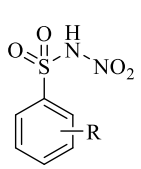

E1-E6

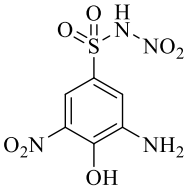

E7

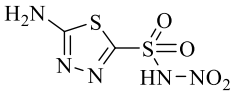

E8

		K_I (µM)		
Compound	R	hCA II	hCA IX	MgCA
E1	2-NH_2	>50	0.42	0.66
E2	3-NH_2	5.11	>50	2.75
E3	4-NH_2	>50	8.19	0.71
E4	4-$N(CH_3)_2$	>50	2.79	0.22
E5	4-(CH_2NH_2)	>50	5.99	8.09
E6	4-$NHCH_2C{\equiv}CH$	1.35	2.00	3.49
E7	-	>50	8.72	0.67
E8	-	4.52	0.84	4.50
AAZ		0.012	0.025	74.00

* Mean from 3 different assays, by a stopped flow technique (errors were in the range of ± 5-10 % of the reported values).

(ii) As mentioned above, the tumor-associated isoform hCA IX was inhibited in the low micromolar range by all the new N^1-nitro sulfonamides reported here with K_Is ranging between 0.42 and 8.72 µM, with the exception of compound **E2**, which did not significantly inhibit the enzyme up to 50 µM inhibitor concentration. Thus, the peculiarity that enable derivative **E2** as a micromolar inhibitor against hCA II, that is the amino group in *meta* position towards the N-nitro moiety, did not fit well within the hCA IX active site. Instead the analogue derivative incorporating an additional hydroxy and nitro group at the 4 and 5 positions of the benzene ring (derivative **E7**) acted as a micromolar inhibitor of hCA IX, with a K_I of 8.72 µM. The definition of a proper SAR for hCA IX is not feasible at the moment, considering that the remaining derivatives showed similar affinities (Table 6). However, we can speculate that the presence of the aromatic amino

moiety in position 2 with respect to the substituted sulfonamide or appended to a hetearomatic core is better tolerated within the active site cavity, as highlighted by the sub-micromolar K_Is values of compounds **E1** and **E8**.

(iii) The fungal enzyme MgCA was effectively inhibited by all N-nitro sulfonamides **E1-E8** investigated here, with K_Is ranging between 0.22 and 8.09 μM (Table 6). These values were from 10 to 300 times lower than the K_I of the clinically used sulfonamide **AAZ** (K_Is 74.0 μM).[80] The presence of small hydrophilic substituents at position 4 of the benzene ring (compounds **E3**, **E4** and **E7**) positively influenced the MgCA inhibitory properties of this class of derivatives. Indeed, compounds **E3** and **E4**, which incorporate at that position an unsubstituted or dimethyl substituted amino moiety, showed K_Is of 0.71 - 0.22 μM, whereas derivative **E7**, which incorporates a hydroxy moiety with an additional amino and nitro group in its *ortho* positions, showed a K_I of 0.67 μM. Thus, all the N-nitro sulfonamides reported here showed interesting inhibitory properties against this fungal enzyme, making them interesting candidates as lead molecules for fungal CAIs.

Due to the promising inhibitory profile of the compounds **E1-E8**, computational investigations were undertaken in order to get more insight into the binding mode of the new class of CA inhibitors.

Compouds **E2**, **E3** and **E8**, chosen as representative of the overall series, were submitted to QM geometry optimization (B3LYP/6-31G*) and ESP charges computation prior to dock the molecules into hCA II (PDB 5JLT) and IX (PDB 3IAI)[50] active site pockets.

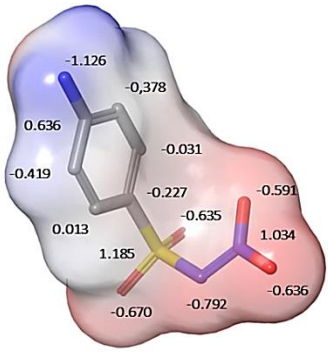

Figure 30. DFT-based geometry optimization. QM-ESP charges were derived from a single point calculation (B3LYP/6-31G* level of theory)

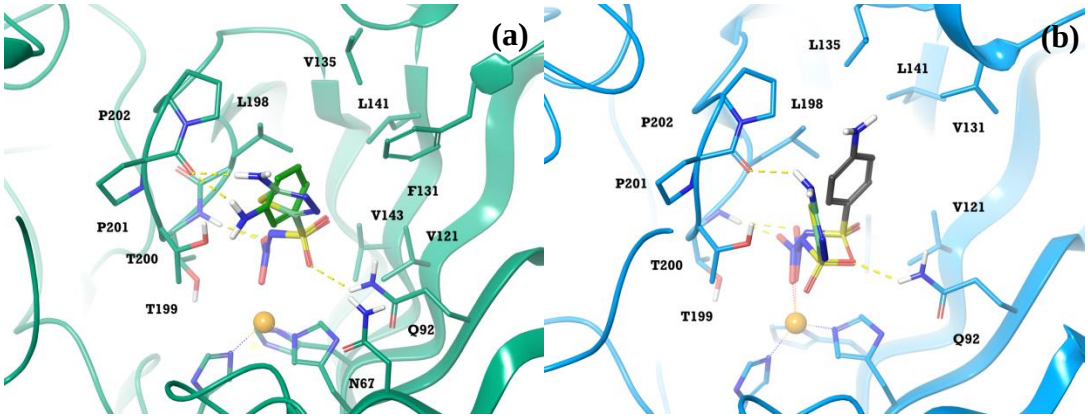

Figure 31. Binding mode of N^1-nitro derivate **E2** and **E8** within hCA II active site (a) and **E3** and **E8** within hCA IX binding site (b).

Binding interaction mode of N-nitrosufonamides in hCAII (**E2** and **E8**) and CAIX (**E3** and **E8**) was investigated by docking procedures using the calculated ESP atomic charges. Surprisingly, in none of the poses obtained, the negatively charged nitrogen atom of the sulfonamide group coordinates the Zn ion as expected. It is likely that the steric hindrance and, mostly, the electronic properties of the nitro group prevent the canonical binding mode observed in other sulfonamide derivatives.

Conversely the best pose obtained within both the II- and IX-CA active sites concerned a network of interactions not reported up to now. One of the negatively charged oxygen atoms of the nitro moiety coordinated the metal ion, whereas the other one acts as H-bond acceptor interacting with the NH of T199 backbone. This set of contacts was reinforced by an additional H-bond between one oxygen atom of sulfonamide group and Q92 side chain (Figure 31). The analogue set of interactions with a different ZBG positioning was found for **E8** within hCA IX. The aromatic scaffolds establish additional hydrophobic contacts within the lipophilic cavity, whereas NH_2 moieties are involved in H-bonds with the carbonyl group of Pro201.

The series of N^1-nitro aromatic sulfonamides, obtained by applying a selective sulfonamide nitration synthetic strategy[153] was investigated for the inhibition of two hCA isoforms, the cytosolic hCA II and the transmembrane hCA IX, in addition to the fungal MgCA, reporting rather interesting inhibitory profiles and innovative binding mode according instead to computational studies. Therefore, the N-nitro sulfonamide moiety can be considered as a new chemotype for CA inhibition. Due to the ease of preparation,

additional series of derivatives should be prepared, in order to better understand the SAR for this under-investigated class of sulfonamides.
Moreover, X-ray crystallographic studies are currently ongoing to validate the binding mode predicted by docking simulations.

The data and results of this research were published in Nocentini, A et al. *Bioorg. Med. Chem.* **2016**, *24*, 3612-7. The experimental procedures are reported in Chapter 4.

3.4 Structure-based evaluation of the binding mode of several chemotypes within the β-CA from the dandruff-producing fungi Malassezia globose (Series F, G, H, I).

Dandruff represents a serious problem worldwide, being present in more than 50% of the population. It is characterized by an excessive shedding of dead skin cells from the scalp,[161] leading to unpleasant and unesthetical consequences for the affected patient. This condition is triggered by several factors, including an increase in sebum production, irritation by pathogenic organisms, particularly fungi belonging to the genus Malassezia, as well as hereditary, susceptibility factors.[161-162] Recently, inhibition of the β- CA found in these organisms was proposed as novel anti-dandruff strategies, using M. globosa as model organism.[80]
Our group cloned and characterized MgCA,[164] which was shown to be an effective catalyst for the physiologic reaction, CO_2 hydration to bicarbonate and protons, and that its inhibition with sulfonamide containing compounds lead to growth defects of the fungus in vivo. Such results showed for the first time relevant anti-dandruff effects by targeting MgCA, which were equivalent to those of the standard azole drug ketoconazole.[165] Our research group subsequently developed a different cloning and purification strategy for this enzyme,[164] and showed that apart sulfonamides, anions and amino acids also constitute interesting modulators of its activity.[163,164] However, one of the main drawbacks of this research was that few compounds tested so far showed an inhibitory efficacy with K_Is under 100 nM (typically in the 60–90 nM range), and all of them were sulfonamides which have permeability problems through biological membranes, and also may give rise to allergic reactions in some patients.[164,165] Thus,

finding non-sulfonamide, effective CAIs targeting MgCA seems to be a challenge not very easy to address

Hence, in the context of a project aimed to the identification of novel chemotypes for MgCA inhibition as anti-dandruff agents, we screened several hCAIs inhibitors present in our libraries. Moreover, we undertook a structure-based drug design program in order to investigate the interaction mode of such chemotypes within MgCA binding site.

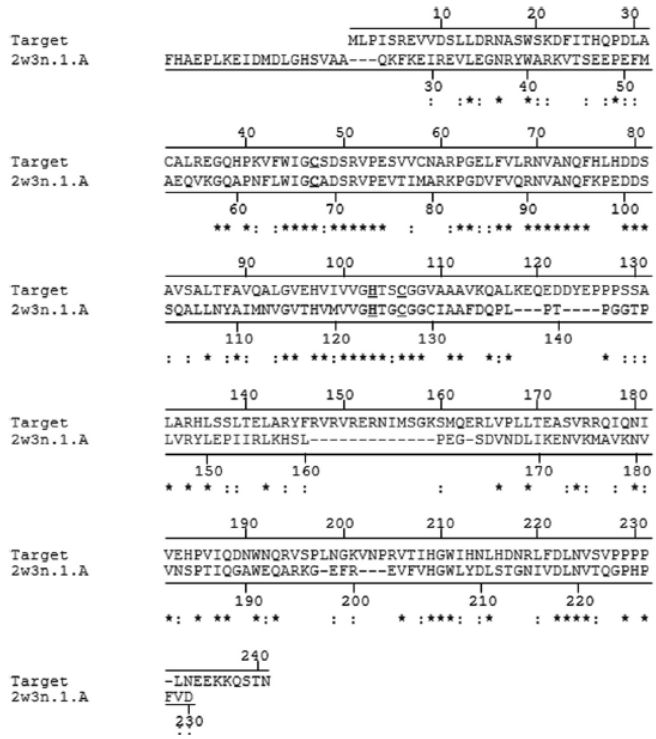

Figure 32. Sequence alignment of MgCA (target) and Can2 (PDB file 2W3N) [21] used as template. Asterisk marks identical amino acid residues. Residues with similar properties are marked with the sign ‘’:”. In bold and underlined are the zinc ion ligands. The insertions or gaps in the sequence of Can2, file 2W3N, did not influence the secondary structures of the two proteins.

Since the 3D structure of MgCA is not available, we built by homology a model taking as template the X-ray crystal structure of Can2, the β-CA from *Cryptococcus neoformans*.[21] The sequence alignment from Figure 32, shows the conservation degree between MgCA and Can2. The residues which coordinate the catalytic zinc ion in MgCA, C47, H103, and C106, corresponds to C68, H124, and C127 in Can2. The fourth coordination site is occupied by a water molecule. Other important residues of the active site are conserved in the two enzymes (D49, R51, Q38, F66, F88 corresponding to C.

neoformans residues D70, R72, Q59, F87, Y109). The alignment of the Can2 residue Y109 corresponds to F88 in MgCA.

Figure 33 reports the obtained MgCA homology model. The GMQE (Global Model Quality Estimation) score of 0.68 reflected a good quality of the model. Details on the homology built procedure are reported in Chapter 4.

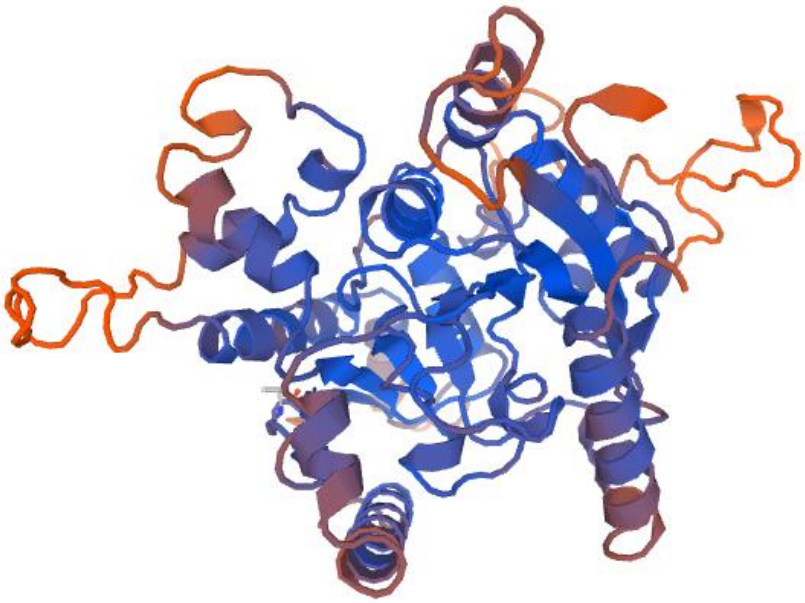

Figure 33. MgCA homology model coloured by Local Quality Score (Orange: 0.0 – Blue: 1.0).

Several chemical scaffolds were taken into account as new chemotypes to be evaluated for their inhibitory profile against MgCA. In the following paragraphs four series of compounds will be described, namely DTCs, MTCs, phenols and benzoxaboroles.

Series F: Dithiocarbammates (DTCs)

The dithiocarbammates (DTCs) were found rather recently to act as zinc-binding CAIs, by using a combination of structure-based crystallographic and kinetic drug design approach.[101] The CS_2 moiety present in these compounds was shown to coordinate to the Zn(II) ion from the enzyme active site of human isoform hCA II, whereas the organic scaffold of the inhibitor participated in various favourable interactions with amino acid residues from the cavity.

A series of DTCs, which were reported earlier by our group as hCAIs, were investigated as inhibitors of MgCA.[101,102]

Table 8. Inhibition of the human isoforms hCA I and II, and the fungal enzyme MgCA with DTCs **F1–F21**, and acetazolamide (**AAZ**) as standard drug, by a stopped-flow CO2 hydrase assay.[135]

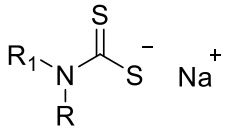

F1-F21

N°	R	R_1	K_I (nM)*		
			hCA I	hCA II	MgCA
F1	$Me_2N(CH_2)_2$	H	85.9	35.8	2980
F2	$HO(CH_2)_3$	H	706	41.7	3190
F3	$HO(CH_2)_4$	H	295	24.3	6235
F4	$HO(CH_2)_5$	H	66.5	17.3	383
F5	Quinuclidin-3-yl	H	494	48.7	643
F6	(R)-Quinuclidin-3-yl	H	240	18.9	490
F7	(S)-Quinuclidin-3-yl	H	615	65.9	724
F8	$-(CH_2)_5-$		252	30.1	773
F9	$-(CH_2)_3-CH(OH)CH_2-$		428	60.7	678
F10	$-(CH_2)_4-CH(COONa)-$		485	80.1	2400
F11	$-(CH_2)_3-CH(COONa)CH_2-$		290	45.4	718
F12	(*R*) $-(CH_2)_3-CH(COONa)CH_2-$		496	80.5	577
F13	(*S*) $-(CH_2)_3-CH(COONa)CH_2-$		109	8.9	929
F14	$-(CH_2)_2-CH(COONa)(CH_2)_2-$		337	78.7	556
F15	$-(CH_2)_3-CH(NHAc)CH_2-$		910	47.9	885
F16	$-(CH_2)_3-CH(NHBoc)CH_2-$		683	13.2	644
F17	$-CH(Me)CH_2-O-(CH_2)_2-$		434	60.2	660
F18	$-CH(COONa)CH_2-O-(CH_2)_2-$		84.7	78.5	4745
F19	$-(CH_2)_2N(CH_2CONHC_6H_{11})(CH_2)_2-$		415	67.2	801
F20	$Ph(CH_2)_2$	H	425	107	4625
F21	$H_2NO_2SC_6H_4(CH_2)_2$	H	97.5	48.1	914
AAZ	-	-	250	12.1	74000

* Mean from 3 different assays, by a stopped flow technique (errors were in the range of ± 5-10 % of the reported values)

Two strong and one weak inhibitors from Table 8, i.e., compounds **F4**, **F6** and **F20**, were selected as representative of the overall synthesized DTCs and docked within the

homology model built for MgCA (Figures 34). The compounds were all predicted to bind to the zinc ion with one sulphur atom of the dithiocarbamate moiety positioned in the fourth coordination site, since this binding mode has been observed for DTCs complexed to α-CAs, by means of X-ray crystallography (Figure 12). The coordination bond was observed to be reinforced by two H-bonds formed by a second sulphur atom and the residues S48 (chain B) and Q38 (chain A) (it should be stressed that MgCA is active as a homodimer, similarly to all β-CAs). The aliphatic tail of derivative **F4** was observed to establish additional hydrophobic interactions with V71, L136, L132 (chain B) and F88 (chain A), whereas its hydroxyl moiety was in H-bond distance with the backbone carbonyl group of S84 (chain A) (Figure 34a).

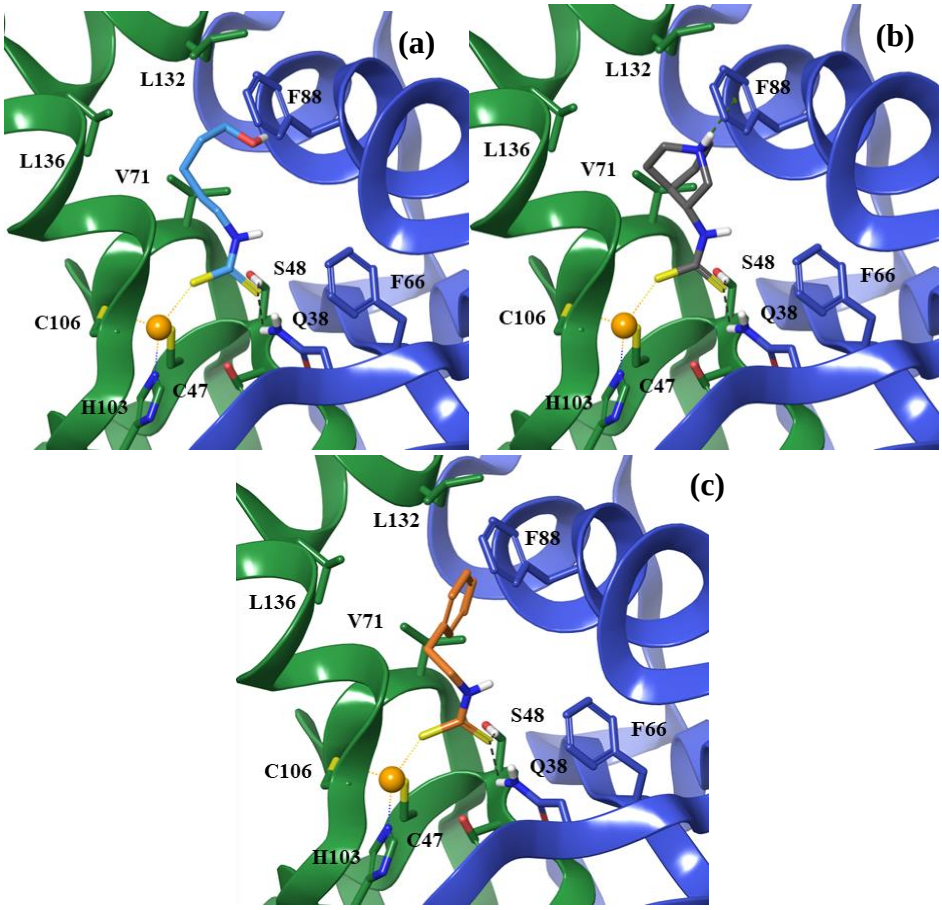

Figure 34. Compounds **F4** (a), **F6** (b) and **F20** (c) docked within the homology model built for MgCA. Monomers A and B of the enzyme are coloured in blue and green, respectively.

The quinuclidine scaffold of compound **F6** was observed to establish hydrophobic contacts with the same lipophilic residues mentioned above for DTC **F4**, whereas the positively charged amino function is involved in a π-cation interaction with F88 of chain

A (Figure 34b). Despite the hydrophobic interactions with V71, L132 (chain B) and F88 (chain A), derivative **F20** showed a conformational strain within the catalytic cleft, determined by the phenethyl group which was not able to properly fit within the tight binding area of the active site (Figure 34c). This strain also affected the coordination bond of the dithiocarbamate moiety with the zinc ion, explaining its reduced inhibitory properties against MgCA compared to the other two inhibitors (Table 8).

The data and results of this research were published in Vullo, D. et al. *Bioorg. Med. Chem.* **2017**, *25*, 1260-1265.

Series G: Phenols

We continue our interest in finding alternative CAIs targeting MgCA by considering a panel of phenols, which were evaluated as inhibitor of MgCA (Table 9).

Docking simulation were performed to unveil the interaction mode of phenols within the fungal enzyme. Differently from dithiocarbamates and sulfonamides, phenols belong to the second class of CAIs and bind to hCA II by anchoring to the zinc-bound water/ hydroxide ion[109] that, together with the nitrogen atoms from H94, H96, H119, defines the tetrahedral coordination of the metal ion. (Figure 15a). Hence, the homology-built model of MgCA was integrated with the 3D coordinates of the Zn coordinated water molecule in 2W3Q and used as target for docking experiments.

The computations were able to highlight a rather interesting inhibitory mechanism of phenols against the fungal enzyme MgCA.

Indeed, all derivatives were predicted to anchor to the catalytic cleft establishing a wide network of H-bonds, as observed in the hCA II – phenol **G1** complex X-ray crystal structure. The computations were done at pH of 7.4 ± 1. At this pH value, all phenols are neutral except **G9**. The pKa value for this compound was found to be 7.86, thus making equilibrium with the phenoxide ion possibile.

Table 9: Inhibition data of MgCA, hCA I and II with phenols **G1-G22** and the standard sulfonamide inhibitor acetazolamide (**AAZ**) by a stopped flow CO_2 hydrase assay.[135]

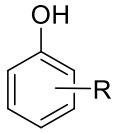

G1-G22

Phenol	R	K_I (μM)*		
		MgCA	hCA I	hCA II
G1	H	65.0	10.2	5.5
G2	2-OH	7.0	>100	5.5
G3	3-OH	6.1	>100	9.4
G4	4-OH	6.3	10.7	0.1
G5	2,4-OH	7.4	>100	>100
G6	3-NH_2	3.9	4.9	4.7
G7	4-NH_2	32.0	>100	>100
G8	4-$NHCOCH_3$	2.5	10.0	6.2
G9	4-CN	0.7	>100	0.1
G10	2-COOH	6.6	9.9	7.1
G11	4-COOH	4.9	9.8	10.6
G12	4-CH_2OH	6.1	68.9	95.3
G13	3-NH_2-4-Cl	44.9	6.3	4.9
G14	4-NH_2-2-Cl	>100	57.8	57.5
G15	2,5-F	29.7	>100	>100
G16	3,5-F	8.8	38.8	33.9
G17	2,4,6-F	36.4	>100	>100
G18	4-COOH-2-OH	6.5	1.1	0.5
G19	2-COOH-3-OH	5.9	5.7	5.2
G20	2-COOH-4-OH	4.5	4.2	4.1
G21	4-(HOOCCH=CH)	3.3	1.1	1.0
G22	2-OH-4-(HOOCCH=CH)	0.6	2.4	1.6
AAZ	-	74.0	0.25	0.012

* Mean from 3 different assays, by a stopped flow technique (errors were in the range of ± 5-10 % of the reported values)

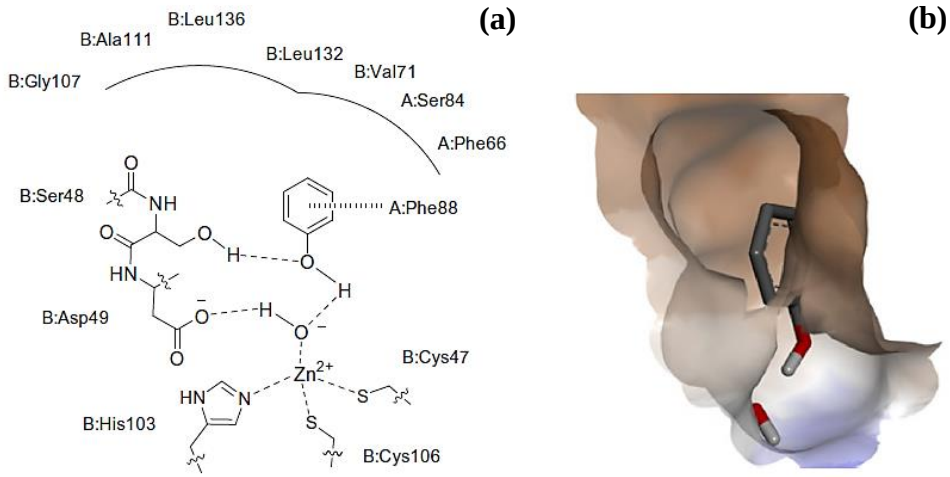

Figure 35. (a) Schematic representation of the binding mode of phenol **G1** into the MgCA active sites. (b) Hydrophobic surface of binding site receptor area; hydrophobicity increases from blue to brown.

Docking experiment pointed out that the OH function acted as H-bond donor towards the Zn^{2+} bound hydroxide group which, in turn, was further stabilized by an additional hydrogen bond to the OD2 of B:D49. Moreover, common to all studied derivatives, an OA-O hydrogen bond was observed between the side chain hydroxyl group of B:S48, acting as donor, and the oxygen atom of the hydroxyl in position 1. The aromatic moiety accommodated in a hydrophobic cavity delimited by A:F66, B:V71 and B:L132 (Figure 35a). This positioning was strengthened by π-π (face to face) and π-alkyl interactions with the side chains of A:F88 and A: V71, respectively, which sandwiched the aromatic portion. Substituted phenols displayed some additional interactions, both within the hydrophobic cleft and the catalytic cavity, which improved the inhibitory effectiveness as clearly shown by the data in Table 9.

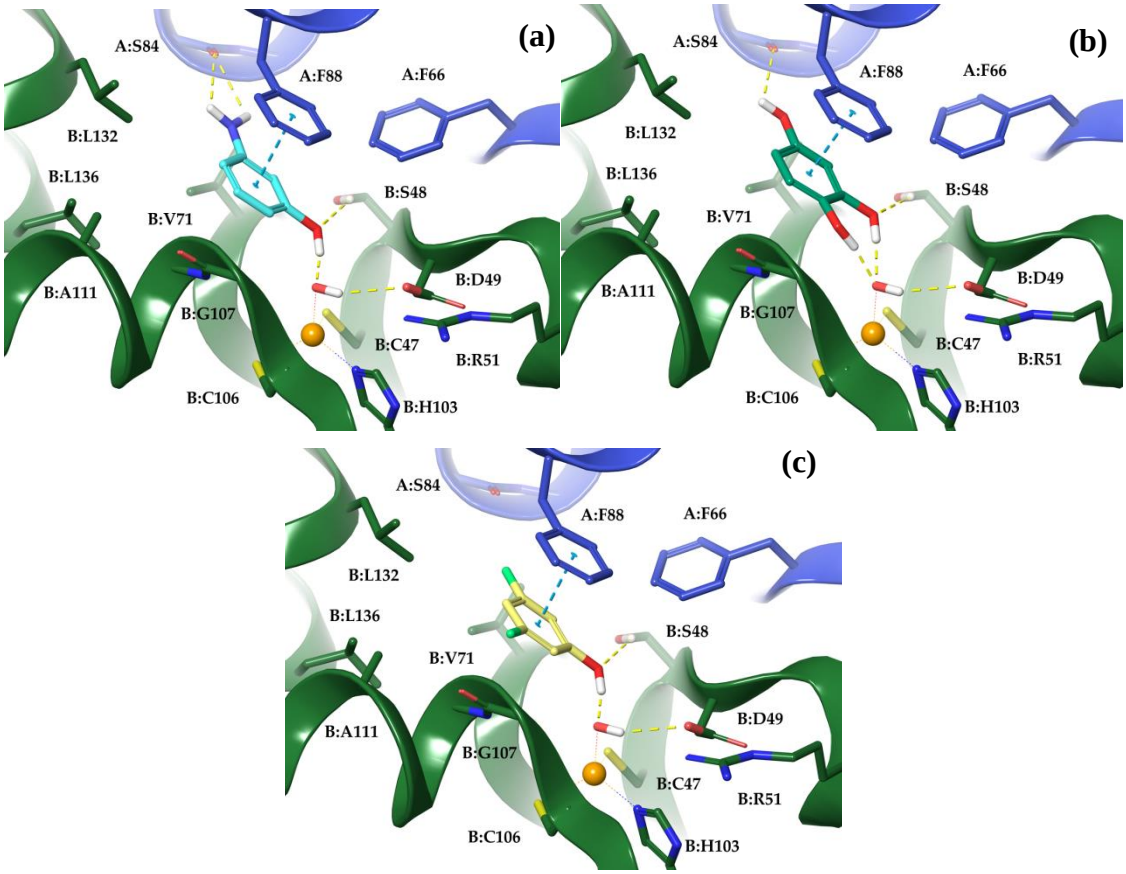

Figure 36. Simulated binding modes of compounds (a) **G6**, (b) **G5**, (c) **G16** within MgCA active site. Monomer A and B are coloured blue and green, respectively.

Compounds **G1, G5, G6, G8, G9, G12, G16** were taken as representatives of the tested phenol derivatives due the chemical features and size of the substituents appended at the aromatic ring. The aminic function of compound **G6** was predicted to orient towards A:S84 forming a bifurcated hydrogen bond O···(H1-N, H2-N) with the backbone carbonyl of the residue (Figure 36a). Also the derivative **G5** formed a three-center hydrogen bond involving the Zn^{2+} bound hydroxide group as acceptor and the hydroxyl in position 1 and 2 as donor groups (Figure 36b). Both fluorine atoms of compound **G16** established favorable halogen hydrophobic interactions with A:S84 and B:G107 (Figure 36c). This latter residue was also in H-bond distance with the hydroxymethyl group of compound **G12** (Figure 37b).

The aromatic rings of derivatives **G8**, **G9** and **G12**, bearing slightly bulky substituents in position 4, oriented in a slightly different way than those of the other studied compounds (Figure 37a). This reflected on a greater distance from the side chain of A:V71 and in a weakening of the π-alkyl interaction. However, the acetamidic and cyano groups of **G8**

and **G9** were able to go more in depth within the area of the hydrophobic pocket lined by residues B:L132, B:L136, B:A111 and B:G107 (Figure 37b). It is likely that substitutions of the aromatic ring with groups able to fit better this area leads to an improved inhibitory activity for this series of derivatives.

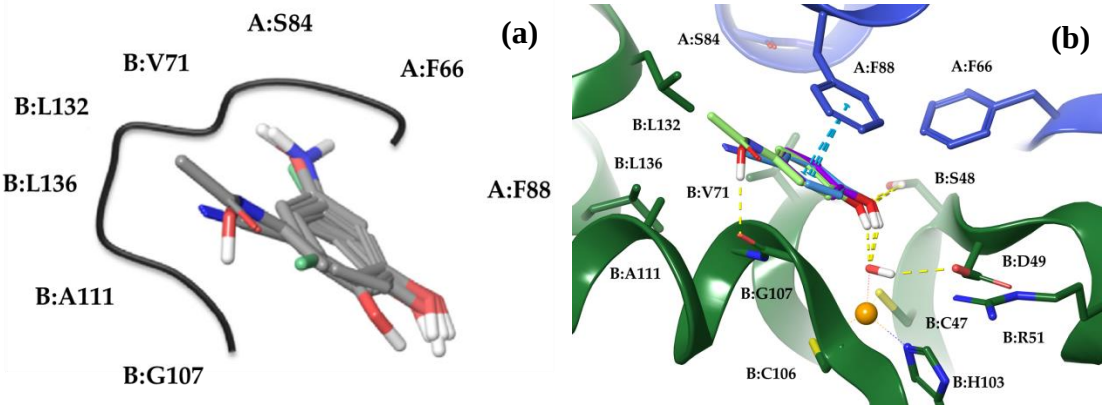

Figure 37. (a) Schematic representation of the aligned derivatives **G5, G6, G8, G9, G12, G16** in the hydrophobic pocket and (b) simulated binding modes of compounds **G8, G9, G12** within MgCA active site. Monomer A and B are coloured blue and green, respectively.

The data and results of this research were published in Entezari, H. Y. et al. *Bioorg. Med. Chem.* **2017**, *25*, 2577-2582.

Series H: Monothiocarbammates (MTCs)

Monothiocarbammates (MTCs), [104] derivatives of the DTCs (Series F), were also investigated and their inhibitory profile against MgCA compared to the one previously reported against hCA I and II. [104] Similarly to DTCs, MTCs possess a zinc-binding group which may coordinate effectively to the catalytical metal ion from the MgCA active site.

Table 10. hCA I, II and MgCA inhibition data with MTCs **H1-H15** by a stopped-flow CO_2 hydrase assay.[135]

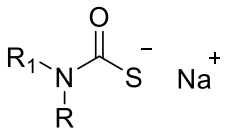

H1-H15

No.	R	R_1	K_I * hCA I (nM)	hCA II(nM)	MgCA(μM)
H1	H	CH_2CH_2(3,4-di-MeO–C_6H_4)	891	26.7	14.1
H2	H	CH_2CH_2Ph	>2000	43.7	18.9
H3	H	-N(CH_2CH_2)N(CH_3)CH_2CH_2-	>2000	35.0	7.81
H4	*n*-Pr	*n*-Pr	>2000	46.7	1.85
H5	*n*-Bu	*n*-Bu	909	>2000	7.52
H6	*i*-Bu	*i*-Bu	681	43.0	8.61
H7	Et	*n*-Bu	700	>2000	5.26
H8	Me	CH_2COOEt	827	44.5	9.16
H9	Me	CH_2Ph	>2000	>2000	7.61
H10	–(CH_2CH_2)–O–(CH_2CH_2)–		569	>2000	7.65
H11	–(CH_2CH_2)–NH–(CH_2CH_2)–		876	22.4	7.41
H12	–(CH_2CH_2)–N(4–F–C_6H_4)–(CH_2CH_2)–		895	46.8	8.33
H13	–(CH_2CH_2)–N(4–CF_3–C_6H_4)–(CH_2CH_2)-		>2000	43.6	4.22
H14	–(CH_2CH_2)–N(3–Cl–C_6H_4)–(CH_2CH_2)–		686	>2000	15.9
H15	–(CH_2CH_2)–N($CH_2CONHC_6H_{11}$)–(CH_2CH_2)–		949	45.9	6.13
AAZ			250	12	74

* Mean from 3 different assays, by a stopped flow technique (errors were in the range of ± 5-10 % of the reported values).

Docking simulations were performed to elucidate the binding mode of MTCs within the MgCA active site. Four inhibitors from Table 10 (compounds **H2**, **H8**, **H9** and **H10**) endowed with acceptable inhibitory properties and a varied structure were selected as representatives of the synthesized MTCs. These derivatives were submitted to quantum mechanics optimization (B3LYP/6–31G) in order to compute the charge distribution and optimal geometry, prior to dock the molecules into the homology- built model of MgCA. According to previously reported evidence,[104,166] points of high electron density surface are located close to the sulfur atom of the MTC (as in the DTCs previously investigated). The lowest energy docking solutions suggest that the fourth Zn coordination position can be occupied either by sulfur or oxygen atoms of the MTC inhibitor. However, based on

the findings obtained by QM calculations (Figure 38a) and on the previous spectroscopic and crystallographic studies,[166] which agreed in indicating that the negative charge distribution is mainly localized on sulfur, poses were selected in which the sulphur atom binds in tetrahedral coordination geometry to the catalytic zinc ion from the enzyme active site.

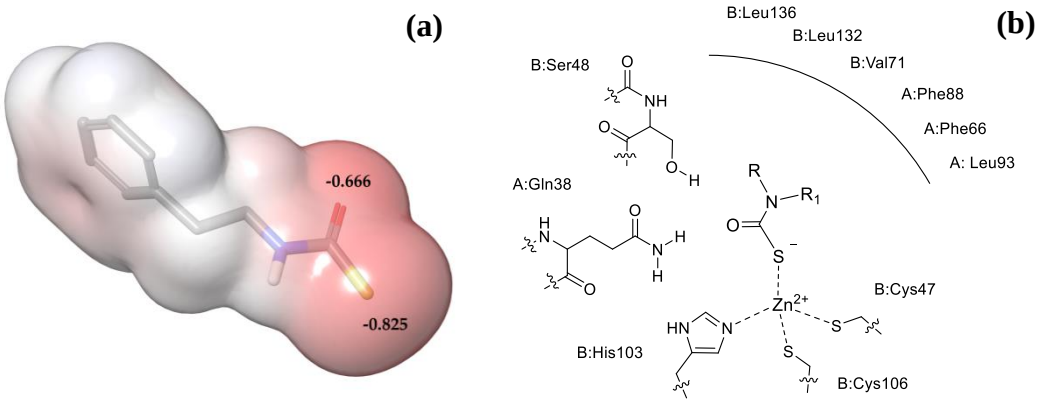

Figure 38. (a) ESP atomic charges of **H2** derived from a B3LYP/6–31G. Red colour represents negative values of the electrostatic potential (b) Schematic representation of the binding mode of MTCs into the MgCA active site.

The oxygen atom of the MTC moiety was, on the other hand, found in H-bond distance from residues S48(B) and Q38(A), depending on the selected pose (Figure 38b). The scaffold fragments of the four derivatives accommodate into a hydrophobic pocket defined by residues from both monomers. π–π interactions occur between the phenyl moieties of derivatives **H2** and **H9** and the side chain of F88(A). The benzyl and phenethyl tails of these derivatives were further stabilized by the π-alkyl interactions established with the aliphatic side chain of V71(B) and L132(B) (Figure 39a). These same three residues and L136(B) were involved in hydrophobic interactions with the ethyl group of the ester function of **H8** (Figure 39b). CH-π interactions were also observed for the N-methyl group of the zinc-binding group moiety of **H8** and **H9** and the side chains of F66 and L93 from monomer A. Alkyl- and π-alkyl interactions were also observed for the morpholine ring of **H10** and the side chains of V71(B) and F88(A), respectively (Figure 39c). Compared to the predicted binding mode of DTCs, which form H-bond with both S48 (chain B) and Q38 (chain A) residues, the oxygen atom of the MTC was able to bind only to the side chain OG atom of S48 or NE2 atom of Q38. Hence, it is reasonable to hypothesize that the shorter length of the CO bond (1.25 Å) compared to that of the CS

(1.75 Å) may contribute to the generally worse inhibitory profile of MTCs compared to DTCs.

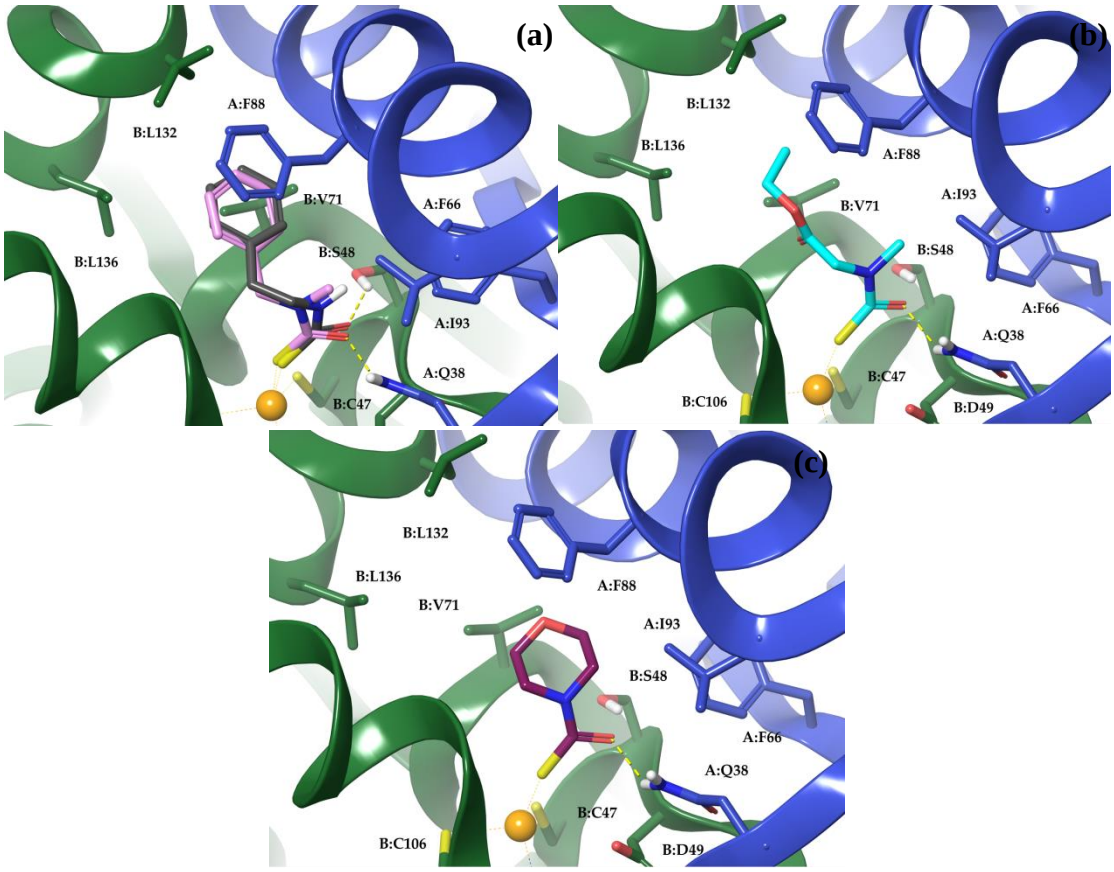

Figure 39. Docked orientations of compounds **H2** and **H9** (a); **H8** (b) and **H10**(c) within MgCA active site. Monomer A and B are coloured blue and green, respectively.

The data and results of this research were published in Nocentini, A. et al. *J. Enzyme Inhib. Med. Chem.* **2017**, *32*, 1064-1070.

Series I: Benzoxaboroles.

The last chemotype we investigated against MgCA was the benzoxaborole one. Benzoxaboroles were recently validated as efficient new and alternative class of CAIs, presenting interesting inhibition properties and a completely new binding mode to the hCA II active site.

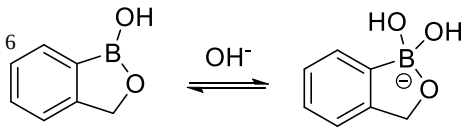

I1 **I1-T**

Figure 40. General structure of benzoxaborole **I1** and its tetrahedral derivative **I1-T.**

Two alternative ligand binding modes were found within the binding cleft of hCA II, both referring to the tetrahedral derivative **I1-T.**[167] Figures 41b and 41c show the details of the two possibile coordination modes of **I1-T** to the catalytic zinc ion.

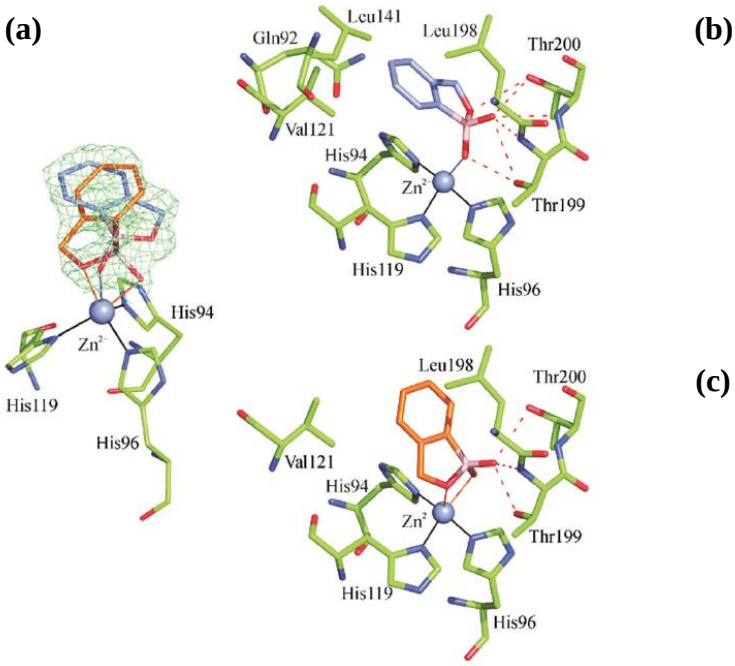

Figure 41. (a) σ_A-Weighted |2Fo-Fc| map relative to the inhibitor molecule in the hCA II/**I1** adduct. The two possible coordination modes of the inhibitor are depicted. The zinc ion coordination is drawn in black for the histidines, in blue for binding mode A and in orange for binding mode B. (b) Details of the interactions of inhibitor **I1** with the enzyme active site in binding mode A. (c) Details of the interactions of inhibitor **I1** with the enzyme active site in binding mode B.

In this contest, we screened the previously reported benzoxaboroles, [167] i.e. mainly ureas and thioureas, for the inhibition of MgCA and additionally against two other fungal β-CAs, Can2 and CgNce103,[75,77] by means the Stopped-Flow technique.[135]

Table 11. Inhibition data of hCA I, hCA II and β-CA isoforms, MgCA, Can2 and CgNce103 with benzoxaboroles **I1-I23** and Tavaborole and the standard sulfonamide inhibitor Acetazolamide by a stopped flow CO_2 hydrase assay.[135]

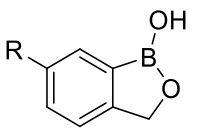

I1-I23

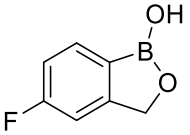

Tavaborole

		K_I (nM)*				
Cmpds	**R=**	**MgCA**	**Can2**	**CgNce103**	**hCA I**	**hCA II**
I1	H	109130	174	260	5690	8180
I2	NO_2	91276	88	89	6352	504
I3	NH_2	44603	93	244	9435	590
I4	NHCONH-CH_2Ph	58214	602	201	557	439
I5	NHCONH-CH_2-(3-Cl,5-CH_3-Ph)	86833	400	79	570	276
I6	NHCONH-Ph	63687	81	86	654	730
I7	NHCONH-(4-Cl-Ph)	77855	92	81	3465	707
I8	NHCONH-CH_2-2-furyl	55637	283	96	613	841
I9	NHCONH-(4-F-Ph)	76193	78	75	235	480
I10	NHCONH-(4-CF_3-Ph)	73614	84	96	487	456
I11	NHCONH-(2,4,6-Cl-Ph)	98557	73	81	450	272
I12	NHCONH-(2-OMe,5-CH_3-Ph)	71221	248	78	98	89
I13	NHCONH-(4-$COCH_3$-Ph)	62187	65	203	288	797
I14	NHCSNH-CH_2CH_2Ph	22531	676	467	639	1547
I15	NHCSNH-(4-CH_3-Ph)	24906	181	89	318	1253
I16	NHCSNH-napht-2-yl	30625	573	339	548	1148
I17	NHCSNH-(4-OCH_3-Ph)	28765	89	86	514	1250
I18	NHCSNH-(4-NO_2-Ph)	8675	79	96	385	>10000
I19	NHCSNH-CH_2Ph	5346	537	334	380	1305
I20	NHCSNH-(4-F-Ph)	30100	86	86	355	1500
I21	NHCSNH-CH_2-2-furyl	6095	236	229	258	2230
I22	NHCSNH-(4-CF_3-Ph)	49762	275	112	417	1838
I23	NHCSNH-Ph	21319	198	97	532	1625
Tavaborole		99022	89	72	2015	462
Acetazolamide		76000	10	11	250	12

* Mean from 3 different assays, by a stopped flow technique (errors were in the range of ± 5-10 % of the reported values).

Molecular modelling investigations were undertaken to in-depth investigate the interesting inhibitory profiles of the benzoxaboroles against the β-CAs from *Malassezia globosa* (MgCA) and *Cryptococcus neoformans* (Can2). A common feature of the studied compounds is the presence of the benzoxaborole core functionalized in position 6 by groups with different size and chemical properties. As the tetrahedral anionic form of benzoxaboroles was found to coordinate the hCA II zinc ion, the charged hydroxylated (e.g $B(OH)_2^-$) forms of some representative derivatives in Table 11 were submitted to QM geometry optimization (B3LYP/6-31G^{*+}) and ESP charges computation prior to dock the molecules into the homology-built model of MgCA and into the X-ray solved structure of Can2 (PDB 2W3N). The active pockets of these enzymes comprise residues from the two monomers (chain A and B) and share many common features, as well as some differences that modulate the inhibitory activities of the benzoxaboroles against the two fungal isoforms (Table 12).

Table 12. Non-conserved residues in MgCA and Can2 within 6Å from the benzoxaborole core

MgCA	Can2
A:S84	A:A105
A:T87	A:N108
A:F88	A:Y109
A:A92	A:N113
A:L93	A:V114
B:S48	B:A69
B:S105	B:G126
B:V109	B:C130
B:A110	B:I131
B:H135	B:Y152

Differently from the zinc-coordination geometries found in the X-ray structures of hCA II-benzoxaborole adducts, findings from docking within the MgCA and Can2 only revealed that the boron-bonded OH of derivatives in Table 11 occupied the fourth coordination position, so defining the tetrahedral coordination sphere of the Zn ion

(Figure 42). The coordination environment of the catalytic metal ion is completed by the side chains of two cysteine and a histidine residues (i.e. MgCA: C47, H103 and C106; Can2: C68, H124 and C127).

The tendency of inhibitory efficacy of derivatives in Table 11, two orders of magnitude greater for Can2 than MgCA, is likely to depend on the different network of H-bonds to which the anionic form of the boronic ester moiety takes part. This network includes, together with others, residues that are mutated in the two enzymes and in particular B:S48/A69 and A:F88/Y109 (Table 12). Within the MgCA binding site (Figure 42a) the Zn-coordinated OH group was involved in three H-bonds, acting as bifurcated acceptor in the interaction with the backbone NH of B:G107 and B:G108 and as donor with the OD of B:D49. The second hydroxyl group was in H-bond distance with A:Q38 (O···HE), whereas the cyclic boronic ester oxygen accept the HG hydrogen atom from the B:S48 side chain (Table 13). In addition to this set of interactions, the molecule is further stabilized by face to face π-π and π-alkyl interactions occurring with the side chains of A:F88, B:V71 and B:L132.

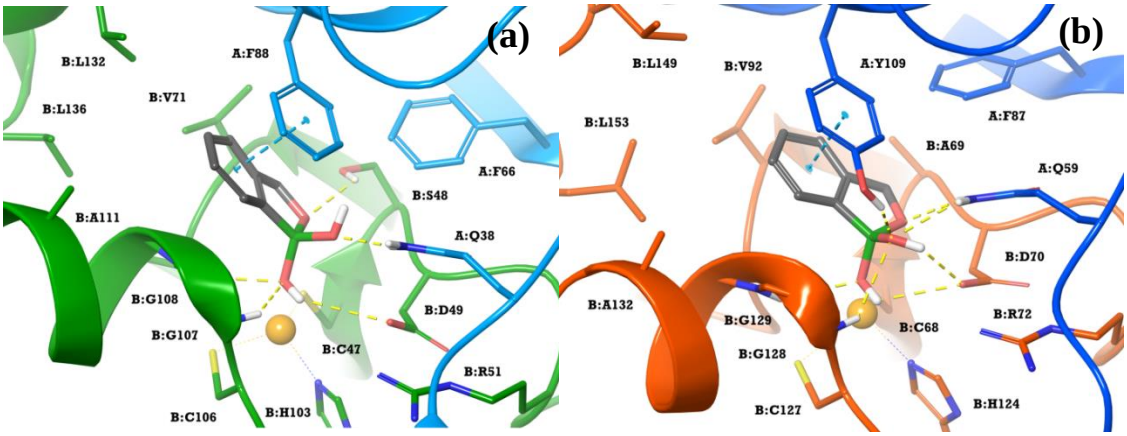

Figure 42. Docking orientations of benzoxaborole **I1** within (a) MgCA and (b) Can2 active sites. Monomer A and B are coloured light blue and green (MgCA) and blue and orange (Can2), respectively. H-bonds and π-π interactions are highlighted by yellow and blue dashed lines, respectively.

Table 13 Hydrogen bonds between benzoxaborole and β-CA isoforms MgCA and Can2

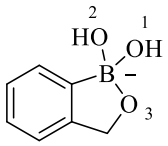

MgCA		Can2	
atoms	d(H···A) (Å)	atoms	d(H···A) (Å)
O1···HN B:G107	2.3	O1···HN B:G129	2.8
O1···HN B:G108	2.8	O1-H···OD B:D70	2.8
O1-H···OD B:D49	3.1	O2···HH B:Y109	2.2
O2··· HE A:Q38	2.1	O2···HN B:G128	2.8
O3···HG B:S48	2.5	O2···HE A:Q59	2.7
		O2-H···OD B:D70	2.4
		O2···HA B:G128	2.9
		O3···HE A:Q59	2.3

The two residues mutation modifies the chemical features and the size of the Can2 binding pocket which in turn cause a different position of the benzoxaborole scaffold if compared to what observed in MgCA (Figure 42b). The Zn-coordinated OH group mostly holds the same interactions described for the MgCA, whereas the second OH is H-bonded to the B:D70 (OH···OD) to which it donates the proton while accepts the HH and HE hydrogens from the B:Y109 and A:Q59, respectively. Additionally it gives rise either to conventional and non-conventional H-bonds with B:G128. The A:Q59 side chain donates the hydrogen HE to the cyclic boronic ester oxygen (Table 13). The aromatic portion of the ligand is sandwiched between the hydrophobic surface of B:Y109 on one side and B:V92 on the other, establishing π-π and π-alkyl contacts.

The set of interactions described above applies to the benzoxaborole core of all the studied derivatives. Results from docking within MgCA indicate that the pendants at position 6 point out towards the outer part of the binding site and all give rise to almost the same kind of interactions with the residues of the enzymatic counterpart (Figure 43a). This is

consistent with the inhibitory profile of derivatives in Table 11 that, as a matter of fact, do not vary considerably throughout the set of the synthesized compounds.

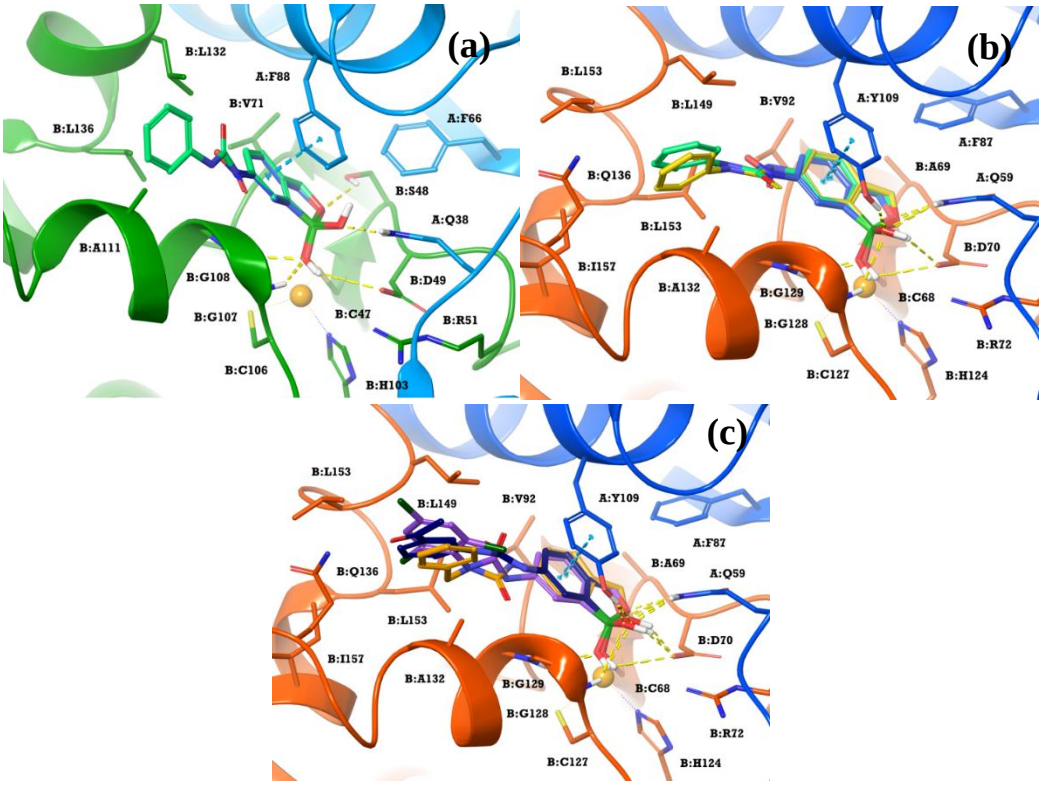

Figure 43 (a) Predicted binding modes of (a) **I2** (light blue) and **I6** (green), within MgCA active site. The nitro group of **I2** established lipophilic contacts with B:A111, B:L132 and B:G107. The ureido group of **I6** was involved in three-centre H-bond with B:G107. Predicted binding modes of (b) **I2** (light blue), **I6** (green), **I23** (yellow) and (c) **I4** (orange), **I11** (purple), **D13** (blue) within CAN2 active site. Monomer A and B are coloured light blue and green (MgCA) and blue and orange (Can2), respectively. H-bonds and π-π interactions are highlighted respectively by yellow and blue dashed lines.

Conversely, because of the orientations adopted by the benzoxaborole scaffold within Can2, the substituents in position 6 accommodate in an area lined by the residues A132, Q136, L149, V150, L153, I157, all belonging to the chain B (Figures 43b-c and 44). The NO_2 and NH_2 groups of derivatives **I2** and **I3**, as well as Tavaborole, just face to this hydrophobic cleft (Figure 44). Instead, the aryl ureido/thioureido moieties of the remaining derivatives accommodate deeper into the hydrophobic pocket and their aromatic portions establish extensive van der Waals interactions with the surrounding residues (Figures 43b-c and 44). Within this pocket **I13** positions its acetyl group at hydrogen bond distance from B:Q136. Due to the presence in **I4** of the CH_2 spacer between the urea and the aromatic tail, the position of this latter slightly differs from that

of the other derivatives, moving away from the hydrophobic pocket and thus losing stabilizing interactions (Figure 43c). The replacement of the urea oxygen with a sulphur atom (**I23**) did not substantially modify the pose assumed by the compounds.

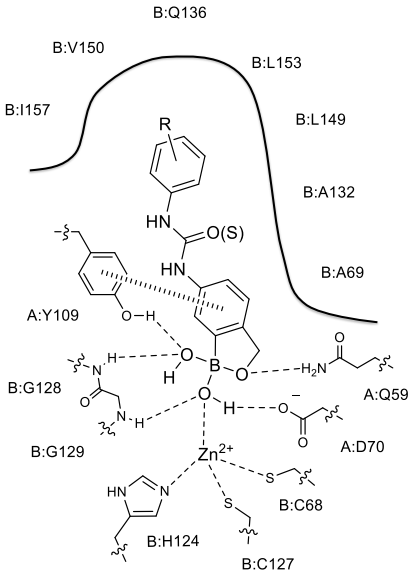

Figure 44 Schematic representation of the binding mode of 6-substituted benzoxaboroles into the CAN2 active site.

The data and results of this research were published in Nocentini, A. et al. *ACS Med. Chem. Lett.* **2017** DOI: 10.1021/acsmedchemlett.7b00369

Concluding, the variety of hCAIs described in paragraph 3.4, all present in our libraries and belonging to different chemotypes, were screened as inhibitors of the β-CA from the fungus *Malassezia Globosa*. A homology model of MgCA was built using the crystal structure of Can2 as template in order to evaluate the binding mode of such chemotypes within MgCA. The large series of benzoxaboroles was tested additionally as inhibitors of CgNce103 and Can2 and their binding mode in this latter evaluated by means of computational investigations.

The SBDD binding mode evaluation carried out to rationalize the inhibitory profile exhibited by four different chemotypes toward MgCA (also Can2 and CgNce103 for benzoxaboroles) shed light on the ligand/target interactions established at the molecular level and represents a starting point to further the research of non-sulfonamide, effective CAIs targeting MgCA or different fungal isoforms.

3.5 Nitrogenous bases-bearing benzenesulfonamides as Carbonic Anhydrase IX inhibitors (Serie J).

Isoform IX (hCA IX) represents a validated anticancer drug target recognized as a marker of tumor hypoxia and prognostic factor for several types of cancers. In tumors, the activity of extracellular hCA IX, whose expression is strongly induced by hypoxia via the hypoxia inducible factor-1α (HIF-1α), maintains the external pH, supporting an acidic extracellular microenvironment suited for hypoxic tumor cell survival and proliferation, but detrimental to normal cells.[2,48-54] Since hCA IX plays a crucial role in pH regulation in several tumors (e.g. breast, brain, colorectal, etc.) and expression is limited in normal tissues, this isozyme has become an attractive target for the design of antineoplastic therapies, as recently proposed by many groups.[53] Hence, it is not surprising that hCA IX has been the main focus of the last decade of research over other hCA isoforms.

The purine and pyrimidine scaffolds are among the most abundant N-based heterocycles in nature and have been involved in many metabolic and cellular processes.[168,169] The pyrimidine and purine moieties are considered privileged structures in drug discovery with a wide array of synthetic accessibility and ability to confer drug-like properties to the compound libraries based on them.[168-171] Thus, nitrogenous bases such as uracil and adenine are components of a number of useful drugs and are associated with many biological, pharmaceutical, and therapeutic activities.[168-171] In particular, pyrimidine and purine were widely used as anti-tumor pharmacophores in medicinal chemical research, considering their ability to interfere with DNA function in diverse manners. [168,169] Modified pyrimidine nucleosides were among the first chemotherapeutic agents introduced into the medical treatment of cancer.[170] Antiviral and anti-tumor actions are two of the most widely reported activities of uracil analogues.[168] Moreover, many pyrimidine-like scaffolds have been developed that exhibit potent anti-tumor cytotoxic activity *in vitro* against different human cell lines, interfering with DNA synthesis in the case of tumors or RNA/DNA synthesis in antiviral activity.[171]

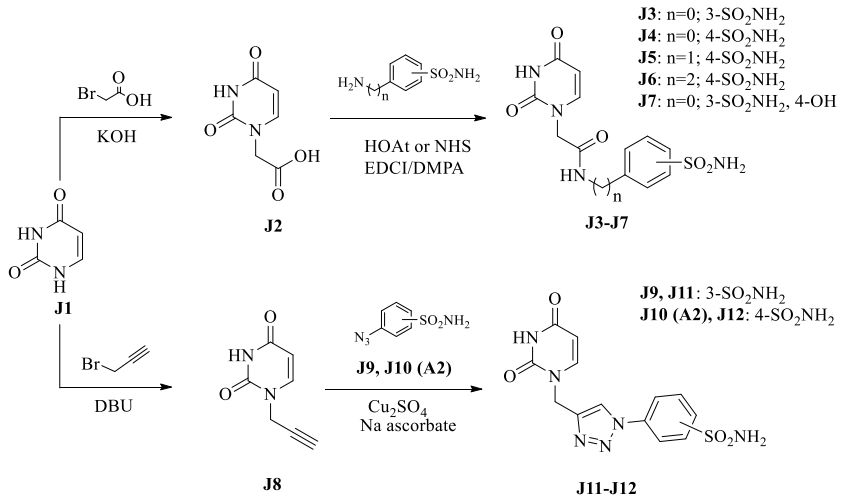

Scheme 9. General synthetic procedure for uracil derivatives **J3-J12**.

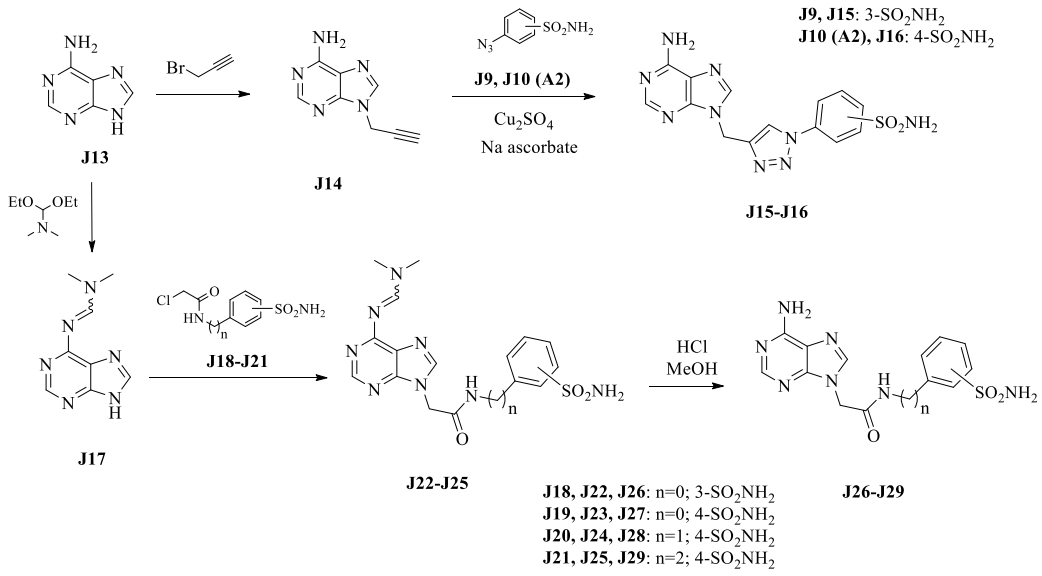

Scheme 10. General synthetic procedure for adenine derivatives **J15-J29**.

Hence, we report two novel series of derivatives combining the benzenesulfonamide ZBG pharmacophore with uracil and adenine scaffolds.

The rationale of the presented work is the incorporation of the purine/pyrimidine pharmacophore as the tail of a classical CAI with a benzenesulfonamide ZBG scaffold. Uracil and adenine moieties were used to modulate the interaction with the different CA isozymes and exploit their intrinsic anti-tumor effect in parallel and synergic to the inhibition of hCA IX. Indeed, molecular hybridization, which covalently combines two

or more drug pharmacophores into a single molecule, have proven to be an effective tool for designing novel entities as potent antitumor agents.[172-174] It should also be stressed that such scaffolds confer drug like properties to the compounds in which they are present and exhibit enhanced solubility in water due to their polar nature.[168]

The uracil and adenine moieties were incorporated at various positions of the benzenesulfonamide scaffold by means of different length spacer of the ether, amide and its bioisoster triazole types, to elicit diverse positioning of the purine and pyrimidine groups within the CAs binding pockets. The bioisosteric amide/triazole substitution was pursued due to the anticancer activity of 1,2,3-triazoles and their derivatives reported in the literature in addition to the *in vivo* stability of this linker.[175] It should be stressed that uracil and adenine were appended at the compounds' tails through the N1 and N9 moieties, respectively, in order to maintain the pharmacophore and the connection by which such nitrogenous bases are incorporated in nucleotides and nucleic acids.[168,169]

The triazole derivatives (**J11-J12**, **J15-J16**) were prepared through analogue synthetic strategies both for the uracil and adenine scaffold, consisting in "Click Chemistry", between N1-propargyluracil (**J8**) and the N9-propargyladenine (**J14**) and freshly prepared azides of sulfanilamide and metanilamide (Scheme 9,10).

Conversely, different synthetic pathways had to be designed for the amide-bearing derivatives considering the diverse reactivity of these nitrogenous bases. For the pyrimidine ring, it was feasible to obtain the 1-carboxymethyl derivative (**J2**) in one step with good yields and no need of protection by reacting uracil with bromoacetic acid in NaOH(aq) environment. The carboxy intermediate was activated in situ with 1-hydroxy-7-azabenzotriazole or N-hydroxysuccinimmide in the presence of 1-ethyl-3-(3-dimethylaminopropyl)carbodiimide and 4-dimethylaminopyridine and subsequently coupled with different amino benzenesulfonamides to give the uracil bearing compounds **J3-J7**.

The synthetic pathway planned for adenine involves the selective and fast protection of its amino group with DMF diethyl acetal (**J17**), followed by SN1 reaction with the chloroacetamido derivatives of amino-benzenesulfonamides (**J18-J21**) (Scheme 10). The obtained intermediates bearing the N-protected adenine (**J22-J25**) were evaluated for their CA inhibitory activity and thereafter submitted to an acidic treatment to free the sulfonamide group and produce the planned adenine-incorporating derivatives (**J26-J29**).

The CA inhibitory activities of the compounds, in addition to acetazolamide (**AAZ**) as standard inhibitor, were measured against four isoforms hCA I II, IV, and IX by a stopped flow CO_2 hydrase assay.[135]

The following structure–activity relationship (SAR) were obtained from the inhibition data reported in Table 14.

(i) The inhibitory profile of the screened derivatives against the four CA isoforms was dependent on the length and positioning of the spacer at the benzenesulfonamide scaffold more than on the nature of both the spacer and the nitrogenous base. In this context, the para-substitution at the benzenesulfonamide scaffold was more favourable than meta (**J3**, **J7**, **J11**, **J15**, **J22** and **J26**) in inducing effective CA inhibitory properties. Moreover, in the case of the amidic linker at position 4, a direct or two carbon spacer between the amide and the benzene ring led to better inhibitory profiles over a single carbon atom connection in the uracil derivatives (**J4** and **J6**) and to a lesser extent for adenines (**J23**, **J25**, **J27** and **J29**).

(ii) Weak hCA I inhibitory potency can be ascribed to most of the adenine- and uracil-bearing compounds reported, with KIs ranging between 256.2 and 9840.2 nM. Within the pyrimidine subset, derivatives **J4**, **J6** and **J12**, incorporating a direct or two carbon atoms spacer amide or triazole linker at the 4 position of the ZBG scaffold, respectively, were weak nanomolar inhibitors (KIs of 645.5, 658.9 and 256.2 nM). The adenines showed a similar tendency such that the derivatives with the privileged spacer were the best hCA I inhibitors, whereas the m-substituted **J15**, **J22** and **J26** did not inhibit the isozyme to 10 μM. It is worth highlighting the better effectiveness of the free amine adenines than the N-protected derivatives. Furthermore, compounds **J12** (first series) and **J16** (second series), incorporating the triazole linker at the 4-position, were the best hCA I inhibitors.

(iii) Isoform II was greatly affected by most sulfonamide-bearing nitrogenous bases, with KIs spanning in the subnanomolar to medium nanomolar range (0.85-889.2 nM), except for compound J7, incorporating the spacer at the 3-position of the scaffold and an additional OH group in para, which inhibited hCA II in the micromolar range (KI 4357.7 nM).

Table 14: Inhibition data of human CA isoforms hCA I, II, IV and IX with sulfonamides reported here and the standard sulfonamide inhibitor acetazolamide (AAZ) by a stopped flow CO2 hydrase assay.[135]

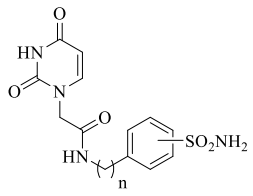

J3-J7

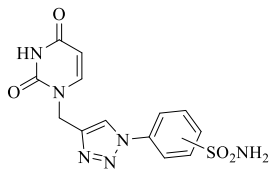

J11-J12

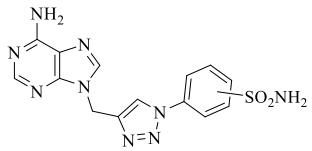

J15-J16

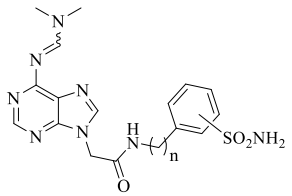

J22-J25

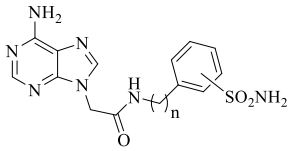

J26-J29

			K_I (nM)			
Compound	*meta/para*	n	hCAI	hCA II	hCA IV	hCA IX
J3	*m*	0	7966.7	704.3	2940.3	3121.2
J4	*p*	0	645.5	17.7	469.6	25.7
J5	*p*	1	1565.7	495.4	1180.7	405.2
J6	*p*	2	658.9	42.1	1780.0	46.0
J7	*m*, 4-OH	0	9840.2	4357.7	2296.5	439.2
J11	*m*	-	4871.0	388.1	299.5	460.3
J12	*p*	-	256.2	0.85	386.7	4.8
J15	*m*	-	>10000	655.3	311.1	1310.1
J16	*p*	-	410.9	5.6	211.4	1.9
J22	*m*	0	>10000	756.2	3837.7	2805.5
J23	*p*	0	966.3	30.7	395.4	40.0
J24	*p*	1	4721.4	87.0	1164.6	165.8
J25	*p*	2	1962.6	57.8	1974.3	112.7
J26	*m*	0	>10000	889.2	3347.0	428.5
J27	*p*	0	666.6	8.4	156.1	16.9
J28	*p*	1	977.1	59.2	277.4	45.2
J29	*p*	2	811.8	8.2	2246.9	11.4
AAZ	-	-	250	12	74	25

* Mean from 3 different assays, by a stopped flow technique (errors were in the range of ± 5-10 % of the reported values).

Further details may be inferred from the results reported for hCA I, but two orders of magnitude below. Indeed, the para-substituted compounds **J4**, **J6** and **J12** were the most potent within the uracil series, showing K_I values ranging between 0.85 and 42.1 nM. The equally substituted adenines, both N-protected (**J23-J25**) or not (**J16**, **J27-J29)** within the second series (KIs in the range 30.7-87.0 nM and 5.6-59.2 nM, respectively) confirmed the efficacy of this substitution pattern, being the most active within their subsets. A methylene linker between the amide and benzene ring consistently reduced the CA inhibition efficacy in the uracil series, and slightly influenced the adenines. Again, the triazoles **J12** (K_I of 0.85 nM) and **J16** (K_I of 5.6 nM) possessed the most efficient hCA II inhibitory properties.

(iv) The reported hCA IV inhibitory profiles of the sulfonamides deviate from the general tendency observed for the other isoforms tested. Beside the 3-substituted amides **J3**, **J7**, **J22** and **J26** that showed ineffective inhibition (K_Is in the range 2296.5-3837.7 nM), compounds **J4**, **J23** and **J27**, which incorporate the amide group directly appended at the benzene ring, were the most efficient amide-bearing compounds, regardless the uracil or adenine moiety present in their molecules. Inversely, the amides of methyl-aminobenzenesulfonamide (**J5**, **J24** and **J28**) were better hCA IV inhibitors than the ethylaminobenzenesulfonamide derivatives (**J6**, **J25** and **J29**), with the biggest extent in case of the free amine adenines **J28** and **J29**, with a ratio approaching 10 (KIs of 277.4 and 2246.9 nM, respectively). The uracil (**J11-J12**) and adenine (**J15-J16**) compounds bearing a triazole linker inhibited hCA IV in the medium nanomolar range, regardless of the positioning at the benzene ring (KIs in the range 211.4-386.7 nM).

(v) The targeted tumor-associated isoform hCA IX was potently inhibited by most sulfonamides reported with binding affinities comparable to hCA II. Therefore, the general tendencies described above were also applicable for this isoform. The 3-substituted derivatives were shown to act as the weakest hCA IX inhibitors, regardless of the nature of the tails (K_Is in the range 428.5-3121.2 nM). The data in Table 14 demonstrates triazoles **J12** and **J16** as the most efficacious in inhibiting the isozyme (K_Is of 4.8 and 1.9 nM). The addition of a carbon atom spacer between the amide moiety and the benzene ring decreased the hCA IX inhibition for the uracil bearing derivative **J5** (from 25.7 to 405.2 nM) and adenines **J24** (from 40.0 to 165.8 nM) and **J28** (from 16.9 to 45.2 nM). Conversely, the increase of the spacer to two carbon atoms improved the

inhibitory potency, mostly for the NH_2 free adenine **J29** (KI of 11.4 nM). It is worth mentioning the KIs reported for the free adenines **J27-J29** (Kis in the range 40.0-165.8 nM) were lower than the N-protected ones **J23-J25** (Kis in the range 16.9-45.2 nM). Compound 32 bearing the adenine moiety through an ether linker was a potent hCA IX inhibitor, with a KI of 31.1 nM.

Some of the reported derivatives (e.g. **J5**, **J7**, **J16**, **J26**, **J28**) exhibited a preferential inhibitory profile for the tumor-associated isoform hCA IX over the ubiquitous hCA II. Noteworthy, more than two-fold IX/II selectivity was observed for adenine **J26**. We focus on the three-fold selectivity shown by the potent triazole **J16** and on the ten-fold IX/II selective efficacy of 3-amido-4-hydroxy uracil bearing compound **J7** though it exerted its action only in the high nanomolar range.

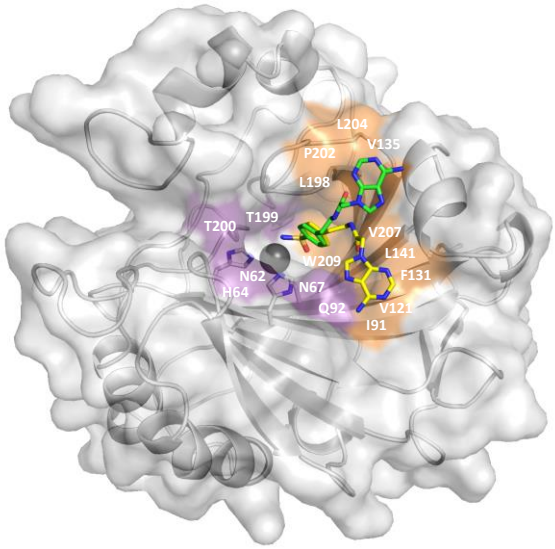

Figure 45. Superimposition of compound **J29** in complex with hCA II and hCA IX-mimic. The overlay is shown in a surface representation of hCA II (gray) with inhibitor shown as sticks (green in hCA II and yellow in hCA IX-mimic). Hydrophobic and hydrophilic active site residues are labelled and colored orange and purple, respectively.

In collaboration with the group of Prof. McKenna from University of Florida, the crystal structures of hCA II and hCA IX-mimic were each solved in complex with compound **J29** to a resolution of 1.6 Å (Figures 45, 46). The benzenesulfonamide ZBG was observed to displace the zinc-bound solvent, binding directly to the catalytic zinc. The orientation of this pharmacophore was conserved in both isoforms (Figure 45) with a hydrogen bond

between the oxygen of the sulfonamide and the amide of T199 (3.1 Å) (Figure 46A, B). The tail of compound **J29** therefore dictates the differences in binding between CA isoforms.

In complex with hCA II, the free amine of the adenine ring in **J29** forms a weak hydrogen bond with the carbonyl oxygen of G132 (3.5 Å). The tail is further supported by van der Waals interactions with residues Q92, F131, V135, L198, and P202 (Figure 46A). In CA IX-mimic, the decrease in steric hindrance of residue V131 in relation to F131 of hCA II allows the rotation of the adenine ring to form two hydrogen bonds with an active site solvent molecule that is anchored to Q92 (3.0 Å). The bonds between the carbonyl oxygen and N7 of adenine in compound **J29** with this water molecule are 2.6 and 3.1 Å, respectively. Similar to hCA II, binding of **J29** in the hCA IX active site is further stabilized by van der Waals interactions with residues Q67, V131, V135 and L198 (Figure 46B).

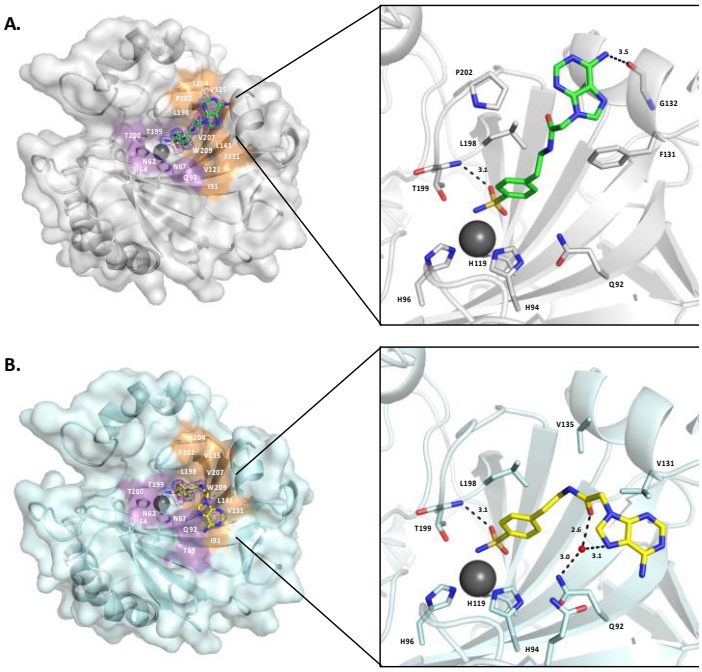

Figure 46. Active site interactions of compound **J29**. A. HCA II (gray) and B. hCA IX-mimic (pale cyan) in complex with **J29** (green and yellow, respectively). Hydrogen bonds are shown as black dashes with distances labelled in angstroms.

Compound **J29** exhibited approximately 80 and 200-fold selectivity for both hCA II and hCA IX over hCA I and hCA IV, respectively (Table 14). The hCA I active site contains larger, aromatic residues H67, F91, H200, and Y204 that may cause steric

hindrance with the nitrogenous base of the compound tail. In hCA II and hCA IX-mimic, side chains of the alpha helix containing residues 126-136 stabilize the tail of the inhibitor through hydrogen bonds and van der Waals interactions. However, in CA IV, this helix is replaced by a loop that extends away from the active site, decreasing the number of possible interactions with the inhibitor.

In collaboration with the group of Prof. Ghelardini from University of Firenze, some selected compounds (**J4**, **J27** and **J29**), chosen among those possessing the best CA inhibitory profile, were tested (30 – 300 μM) to evaluate their effects on viability of human colon cancer HT-29 cells. Measurements were performed after 16 and 48 h incubation in both normoxic and hypoxic conditions. The efficacy of tested compounds is represented in Figure 47. After 16 h incubation in normoxic condition, J**27,** J**29** were significantly active (300 μM) inducing cell mortality by about 10-15%. Hypoxia favored J**27** activity at all concentration tested. Incubation prolonged up to 48 h, highlighted the efficacy of **J4** and **J27**, particularly in hypoxic condition (25-30% cell viability decrease). Compound **J4** showed the best potency.

It is worth commenting on the trend of the cytotoxic effect shown by the screened derivatives. Indeed, compounds **J27** and **J29** showed comparable cytotoxic effect both after 16 and 48 h in normoxia. It is reasonable to ascribe the small observed effect to alternative, not yet identified, mechanisms of action beyond hCA IX inhibition (hCA IX is not upregulated in these cells), which are likely to be related to the adenine pharmacophore.

In hypoxic conditions, derivative **J27** uniquely maintained its anti-proliferative activity after 16 h, whereas **J29** totally lost the efficacy shown in normoxia. Whereas after 48 h in hypoxia, the cytotoxic profile was distinctly different due to the strong upregulation of hCA IX. Indeed, the uracil-bearing **J4**, which showed total inactivity up to now, aroused with the best efficacy herein reported. Conversely, **J29** slightly lost its efficacy after a prolonged hypoxia. Therefore, both in normoxic and hypoxic conditions, derivative **J29** exhibits a cytotoxic efficacy that likely relies on an adenine-related alternative mechanism of action. In contrast, since compound **J4** show greater efficacy after prolonged hypoxia, it is reasonable to ascribed their relevant anti-proliferative activity to the inhibition of the over-expressed hCA IX.

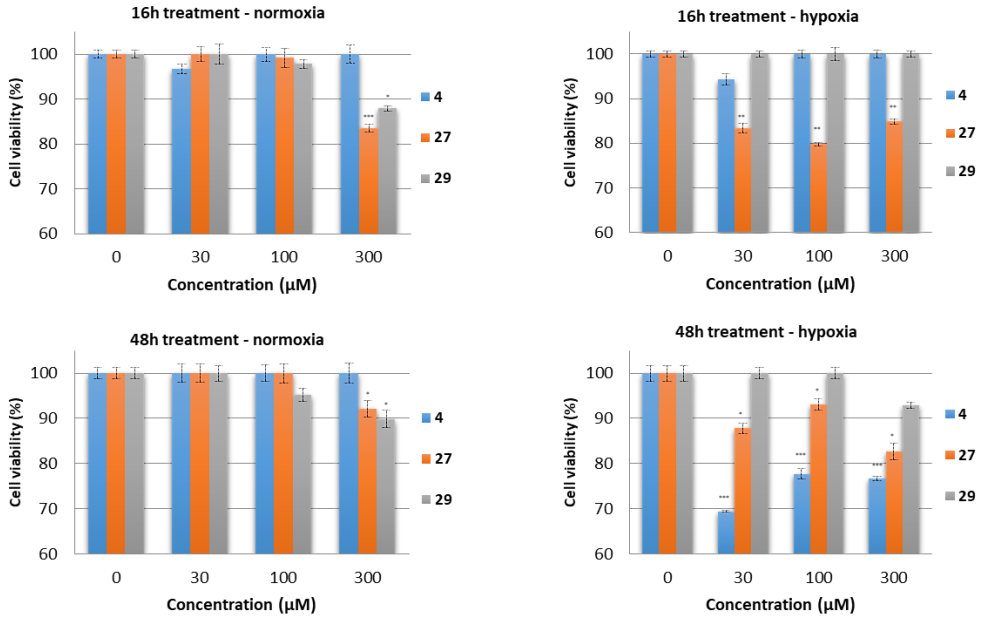

Figure 47. HT-29 cells (1.10^4/well) were treated with of compounds **J4**, **J27**and **J29** (30 - 300 µM). Incubation was allowed for 16 and 48 h in normoxic (20% O_2) and hypoxic conditions (0.1% O_2). Cell viability was measured by the reduction of 3-(4,5-dimethylthiozol-2-yl)-2,5-diphenyltetrazolium bromide (MTT) as an index of mitochondrial compartment functionality. Formazan crystals produced by the reaction were dissolved in DMSO and the absorbance measured at 550 nm. Control condition was arbitrarily set as 100% and values are expressed as the mean ± S.E.M. of three experiments. *P<0.05, **P<0.01 and ***P<0.001 in comparison to control (0 µM).

Two series of nitrogenous bases-bearing benzenesulfonamides were obtained according to the molecular hybridization design approach. The incorporation of the purine/pyrimidine pharmacophore as the tail of a classical CAI with a benzenesulfonamide ZBG scaffold was considered both to modulate the interaction with CA isozymes and exploit an intrinsic anti-tumor effect in parallel and synergic to the inhibition of hCA IX. The compounds were investigated for their inhibition of cytosolic hCA I and II and transmembrane hCA IV and IX. In addition, X-ray crystallography demonstrates the binding mode of a nitrogenous base within the active site of hCA II and a hCA IX-mimic. Finally, the most effective compounds were evaluated for their anti-proliferative activity against HT-29 colon cancer cell lines.

The data and results of this research were published in *ACS Med. Chem. Lett.* **2017**, *8*, 1314−1319.

3.6 In vitro evaluation and computational studies on novel 4/3-((4-oxo-5-(2-oxoindolin-3-ylidene)thiazolidin-2-ylidene)amino) benzenesulfonamides (series K).

Over the last few years, isatin (1*H*-indole-2,3-dione) stood out as a promising tail scaffold to design compounds with interesting inhibitory activity profiles towards different carbonic anhydrase isoforms. Numerous studies have developed diverse isatin-based derivatives as potent CA inhibitors.[176-179] Moreover, isatin, as a privileged scaffold, is endowed with excellent anticancer profile[180,181] and represents an important pharmacophore in two clinically approved anticancer drugs: Sunitinib (Sutent®) and Nintedanib (Ofev®).[182,183] Consequently, design and synthesis of various effective isatin-based anticancer agents have attracted considerable attention in the current medical era.[184-186] Several research groups explored the anti-proliferative activity of many isatin-thiazolidine/thiazolidinone analogs.[190-193]

Taking the above into account, the group of Prof. W.M. Eldehna from Kafrelsheikh University, (Kafrelsheikh, Egypt) reported novel 4/3-((4-oxo-5-(2-oxoindolin-3-ylidene)thiazolidin-2-ylidene)amino)benzenesulfonamides (**K4a-m** and **K7a-g**) (Figure 48), with the prime aim of combining a strong hCAIX inhibition together with the intrinsic anti-tumor activity of the isatin scaffold. My contribution to this work dealt with the evaluation *in vitro* of their inhibitory activity against a panel of hCA I, II, IV and IX isoforms, using stopped-flow CO_2 hydrase assay as well as with computational studies to investigate the inhibitory profiles of the reported derivatives against hCA II and IX.

Furthermore, compounds **K4a-m** and **K7a-g** were evaluated for their anti-proliferative activity against breast cancer MCF-7 and colorectal cancer Caco-2 cell lines. Compound **K4c**, which highlighted the best anti-proliferative efficacy was further investigated for its apoptosis induction potential in MCF-7 cells, to gain mechanistic insights into the anti-proliferative activity of the newly prepared sulfonamides.

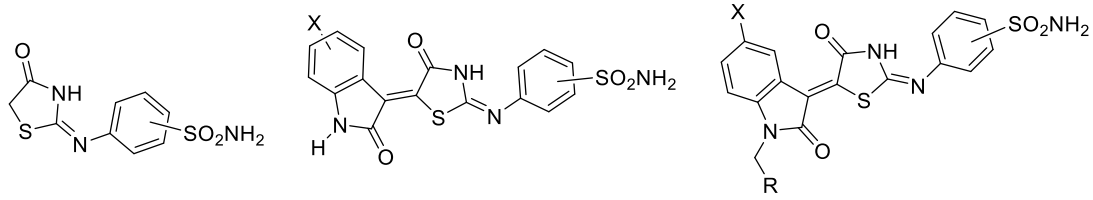

K3a, b **K4a-m** **K7a-g**

Figure 48. Structures of isatin derivatives of the present study

Sulfonamides **K3a-b**, **K4a-m** and **K7a-g** were evaluated for their ability to inhibit the physiologically relevant hCA isoforms, hCA I, II, IV and IX by the stopped-flow CO_2 hydrase assays,[135] in comparison to the clinically used acetazolamide (**AAZ**) as standard CAI.

The following structure–activity relationship (SAR) can be compiled from the inhibition data reported in Table 15:

(i) The cytosolic isoform hCA I was moderately inhibited by most of the sulfonamides with inhibition constants (K_Is) ranging in the high nanomolar - low micromolar range, in detail, between 513.7 and 9269.7 nM, except for the p-substituted precursor **K3a** which arose as the best hCA I inhibitor with a K_I of 91.9 nM.

(ii) The physiologically dominant isoform hCA II was very potently inhibited by most of the p-substituted derivatives **K3a, K4a-h, K7a-7f** (K_I values ranging between 1.8 and 69.6 nM, Table 15), apart from the N-unsubstituted 5-Br and 5,7-(CH3)2 isatin-bearing derivatives **K4d** and **K4h**, which exhibited a slightly reduced inhibitory efficacy (K_I values of 210.5 and 466.0 nM). The incorporation of a methyl group on the isatin core (**K7a-c**) did not substantially interfere with the derivatives hCA II inhibitory potency, whereas an analogue benzylic substitution (**K7d-f**) led to a three-fold to twenty-fold efficacy enhancement likened to the N-unsubstituted compounds (**K4a-4g**). Conversely, it is noteworthy that all the m-substituted derivatives (**K4i-m**) were found to possess a generally ten-fold diminished hCA II inhibition efficacy (K_Is ranging between 176.4 and 598.2 nM) in comparison to their p-substituted analogues. Likewise, the meta-substituted precursor **K3b** (K_I of 73.2 nM) was forty times less potent than **K3a** (K_I of 1.8 nM). On the other hand, the N-benzyl moiety furnished the 3-substituted **K7g** with a comparable inhibitory potency likened to the 4-substituted N-benzyl analogues (**K7d-f**).

Table 15. Inhibition data of human CA isoforms hCA I, II, IV and IX with sulfonamides **K3a-b**, **K4a-m** and **K7a-g** and the standard sulfonamide inhibitor acetazolamide (**AAZ**) by a stopped flow CO_2 hydrase assay.[135]

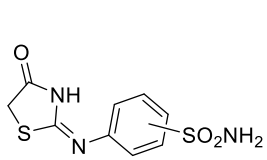

K3a, b

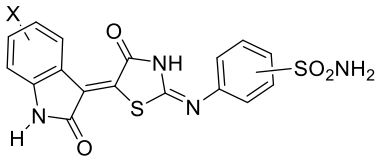

K4a-m

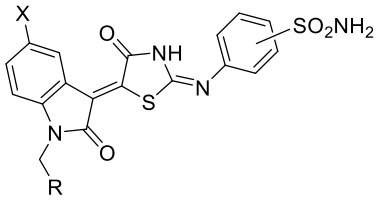

K7a-g

Cmpd	*p/m*	X	R	K_I (nM)*			
				hCA I	hCA II	hCA IV	hCA IX
K4a	*p*	H	-	630.8	23.0	>10000	47.0
K4b	*p*	5-F	-	513.7	7.1	4290.5	26.6
K4c	*p*	5-Cl	-	2290.4	69.6	3256.1	62.4
K4d	*p*	5-Br	-	3611.4	210.5	2986.4	66.6
K4e	*p*	5-OCH_3	-	2881.6	24.3	>10000	23.1
K4f	*p*	5-CH_3	-	4243.7	57.4	2864.4	72.1
K4g	*p*	5-NO_2	-	2883.7	35.7	3682.3	34.1
K4h	*p*	5,7-$(CH_3)_2$	-	7602.0	466.0	4751.0	100.1
K4i	*m*	H	-	2662.6	273.8	1972.7	16.1
K4j	*m*	5-Cl	-	728.5	598.2	395.5	62.0
K4k	*m*	5-Br	-	718.7	416.0	235.0	15.9
K4l	*m*	5-OCH_3	-	3424.4	176.4	2526.6	24.7
K4m	*m*	5-NO_2	-	884.2	506.6	441.9	48.0
K7a	*p*	H	H	4001.7	43.5	4712.2	146.3
K7b	*p*	5-Cl	H	923.9	38.4	3040.7	123.3
K7c	*p*	5-Br	H	872.7	17.8	2634.0	38.9
K7d	*p*	H	C_6H_5	5630.7	8.3	3299.6	117.5
K7e	*p*	5-Cl	C_6H_5	881.1	2.6	4305.8	90.6
K7f	*p*	5-Br	C_6H_5	9269.7	59.8	2897.3	321.1
K7g	*m*	H	C_6H_5	856.4	18.2	2244.6	169.8
K3a	*p*		-	91.9	1.8	348.3	4.5
K3b	*m*		-	741.4	73.2	101.9	17.7
AAZ	-	-	-	250	12	74	25

* Mean from 3 different assays, by a stopped flow technique (errors were in the range of ± 5-10 % of the reported values).

(iii) The data reported in Table 15 ascribed to the most reported sulfonamides poor efficacy in inhibiting the trans-membrane isoform hCA IV. Indeed, the p-substituted

derivatives **K4a-h**, **K7a-f** were shown to inhibit such isozyme in the micromolar range (K_Is ranging between 2634.0 and 4751.0 nM), except **K4a** and **K4e** which did not inhibit hCA IV up to 10000 nM. It is worth highlighting that the 3-substituted **K4i-m** showed a generally improved inhibitory profile against hCA IV, in particular derivatives **K4j**, **K4k** and **K4m (**K_Is of 395.5, 235.0 and 441.9 nM), which were endowed with electro-withdrawing substituents at the 5- position of the isatin scaffold (respectively 5-Cl, 5-Br, 5-NO_2). The precursors **K3a** and **K3b**, devoid of the isatin core appended at the oxothiazolidin-2-ylidene moiety, arose among the best inhibitors against such trans-membrane isozyme, again with the 3-substitution preferred to the 4-substituted one (K_Is of 348.3 vs 101.9 nM).

(iv) The target tumor-associated isoform hCA IX was effectively inhibited by all the isatin-bearing sulfonamides herein reported. Furthermore, the inhibition profiles were found to be rather flat, since the measures K_Is ranged between 15.9 and 169.8 nM, aside from derivative **K7f** whose efficacy raised at slightly higher concentration (K_I of 321.1 nM). It is worth stressing the comparable inhibitory effectiveness of the N-unsubstituted 3- and 4- pendant bearing derivatives (although slightly heightened for derivatives **K4i-4m**; K_Is ranging between 16.1 and 62.0 nM), unlike arose for the cytosolic hCA II.

The incorporation of a methyl or benzyl group on the isatin N atom elicit a worsening of effectiveness against hCA IX both for the p-substituted derivatives **K7a-7f** (except **K7c**, 5-Br; K_I of 38.9 nM) and the m-pendant bearing **K7g** (K_I 169.8 nM). Finally, the isatin-devoid precursor **K3a** and **K3b** inhibited hCA IX in the low nanomolar range with K_Is of 4.5 and 17.7 nM.

(v) The inhibitory profiles reported in Table 15 undeniably ascribed to the m-substituted amminobenzenesulfonamide **K4i-4m** a rather selective hCA IX/II inhibitory efficacy. Indeed, it is satisfying to note that such compounds displayed a selectivity ratio hCA IX/hCA II which spanned from 7.1 and 26.2. Considering that isoform hCA IX is a validated target for the diagnosis and treatment of cancers, discovery of selective inhibitors represents a promising step to unveil a more effective cancer therapy devoid of the classical side effects owing to hCA I/II inhibition.

The inhibitory profiles of the derivatives in Table 15 were further investigated carrying out docking and Molecular Mechanics Generalized Born Surface Area (MM-GBSA)

calculation to predict their binding mode and free energy as inhibitors of the hCA II (PDB 5LJT) and IX (PDB 5FL4)[176] isoforms.

As it could be foreseen, all docking solutions oriented the benzenesulfonamide moieties deeply into the active site region of both the isozymes. Indeed, it is worth highlighting that all the reported derivatives were found to inhibit both hCA II and IX in the nanomolar range. In detail, the sulfonamide established two hydrogen bonds with the T199 residue, its negatively charged nitrogen atom coordinated the zinc ion and the phenyl ring was involved in several hydrophobic contacts (V121, H94 and L198).

Despite the different size of the hydrophobic pocket in hCA II and hCA IX isoforms, mainly due to the F131/V131 mutation, the tails of the 4-substituted derivatives **K3a**, **K4a-4h** and **K7a-7f** located comparably within the two isozyme binding sites (Figures 49a and 50a). In detail, the eterocyclic tails were found to lie in the hydrophobic areas defined by F131, I91, V121, Q92 and V131, L91, V121 in hCA II and hCA IX, respectively. The C=O moiety of the oxothiazolidin-2-ylidene was involved in a three-centre H-bond involving the HE/Q92 and HD/N67 (hCA II) or HE/Q71 (hCA IX) hydrogen atoms as donor groups. The isatin scaffolds was stabilized by edge-to-face and π-alkyl hydrophobic interactions occurring with F131 (V131 in hCA IX) and I91. X-substitution on the isatin benzene ring did not substantially affect ligands positioning within the hydrophobic pockets, although they differently interacted with the residues nearby (Figure 49b and 50b). It is worth noting that the contacts involving the N-methyl and N-benzyl groups of derivatives **K7a-7f** within the aforementioned hydrophobic regions contributed in increasing the inhibitory efficacy against the cytosolic isozyme, whereas they had no, or at least little, influence on the inhibitory efficacy of the hCA IX.

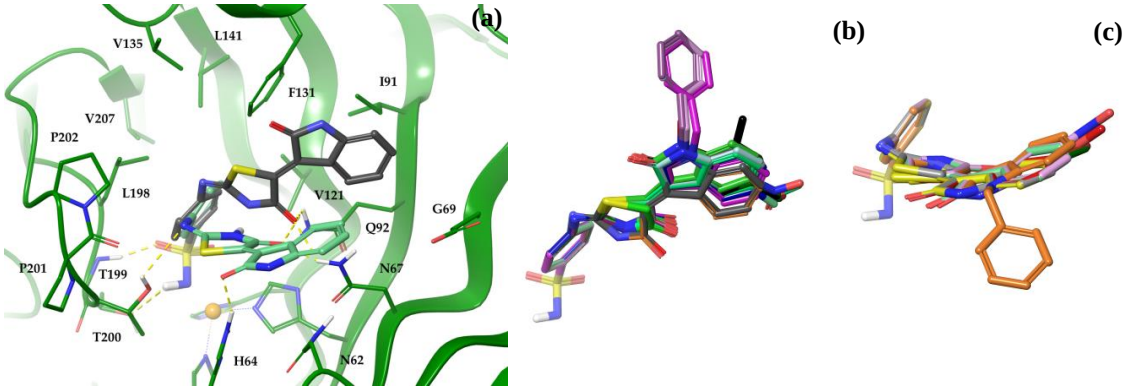

Figure 49. (a) Simulated binding modes of compounds **K4a** (4-substituted, grey) and **K4i** (3-substituted, acquamarine) within hCA II active site; (b) 4-substituted and (c) 3-substituted benzenesulfonamides docked within hCA II active site.

Conversely, docking solutions found for the 3- substituted derivatives **K3a**, **K4i-4m** and **K7g** identified two cavities, which differ depending on the enzyme isoform considered, within which the N-pendant on the amminobenzensulfonamide moieties locate (Figures 49a and 50a). In hCA IX, the pocket defined by V131, L91, Q67, S69 and Q92 is roomy enough to accommodate the N-pendant, though rotated by 90° (Figure 50a). Again the endocyclic carbonyl of the oxothiazolidin-2-ylidene acts as H-bond acceptor to HE/Q67 which, in turn, is involved in weak C-H···π H-bonds with V121 and L91 (Figure 50a). The isatin benzene ring additional formed π-alkyl hydrophobic interactions with S69.

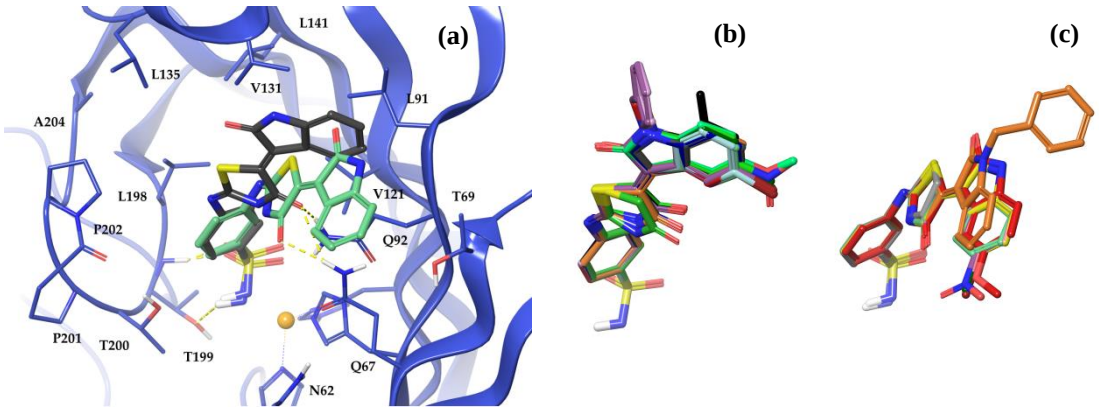

Figure 50. (a) Simulated binding modes of compounds **K4a** (4-substituted, grey) and **K4i** (3-substituted, acquamarine) within hCA IX active site; (b) 4-substituted and (c) 3-substituted benzenesulfonamides docked within hCA IX active site.

In hCA II, the N-pendant of the amminobenzensulfonamide was oriented towards N62 and H64, and was engaged in several H-bonds (Figure 49a). The imine nitrogen act as H-

bond acceptor from HG/T200, the carbonyl of the oxothiazolidin-2-ylidene was part of bifurcated H-bonds with donor being HE/Q92 and HD/N67, whereas the C=O of the isatin accepts the HE/H64. The isatin benzene ring formed additional π- alkyl hydrophobic contacts with L60. The introduction of a benzyl group on the nitrogen atom of the isatin provided the 3-substituted compound **K7g** with an inhibitory efficacy against hCA II comparable to the one observed for the 4-substituted N-benzyl derivatives **K7d**-**7f**. Again, the type and nature of the X-substitution at the isatin benzene ring did not substantially affect ligands positioning within both the isozymes binding pockets.

Analysing the results obtained from docking simulations, it is possible to assume that switching the substituents from the para to the meta position caused the increase in the steric hindrance that, together with a torsional strain, prevent the eterocyclic tails of the 3-substituted derivatives to lie within the hCA II hydrophobic cavity, thus worsening the inhibitory efficacy of the compounds against such isoform.

Basing on the enzyme-inhibitor complexes obtained from molecular docking, ΔG binding energy were calculated using the MM-GBSA approach, either or not defining a 4Å shell from the ligands within which hCA II and hCA IX residues were relaxed during the computations (Table 16).

For all derivatives, but **K7d-f** in the case of hCA II, the ranking of the ligands based on the calculated MM-GBSA $\Delta G_{binding}$ values substantially agreed with ranking based on experimental inhibition data. As far as it concerns the hCA IX isoform, the ΔG binding values found reflected the experimental inhibition data in Table15 (Figure 51). In the case of hCA II, a better agreement was achieved not considering the **K7d-f** (featured by the N-benzyl substitution at the isatine scaffold).

Within the here considered congeneric series of sulfonamides, the MM-GBSA approach has shown good success in rank-ordering the inhibitor potencies of the studied compounds making it possible to prioritize derivatives for synthesis as inhibitors against hCA II and hCA IX enzyme isoforms.

Moreover, all sulfonamides were examined by the group of Prof. Eldehna for their anti-proliferative activity against breast cancer MCF-7 and colorectal cancer Caco-2 cell lines. In particular, compound **K4c** was the most potent derivative against MCF-7 (IC_{50} = 3.96 ± 0.21)**,** while **K4j** was the most active member against Caco-2 cells (IC_{50} = 5.87 ± 0.37). Interestingly, compound **K4c** provoked the intrinsic apoptotic mitochondrial

pathway in MCF-7 cells, evidenced by the enhanced expression of the pro-apoptotic protein Bax and the reduced expression of the anti-apoptotic protein Bcl-2, and the up-regulated active caspase-3 and caspase-9, cytochrome C and p53 levels.

Table 16. Results of the MM-GBSA calculation on hCA II (5LJT) and hCA IX (5FL4)

	ΔG_{exp} (kcal/mol)			
Compound	5LJT	5LJT 4Å [(a)]	5FL4	5FL4 4Å[(a)]
K3a	-33.965	-42.301	-34.196	-34.543
K3b	-37.229	-39.449	-37.523	-36.224
K4a	-48.294	-51.442	-51.102	-54.033
K4b	-47.054	-51.073	-49.334	-54.442
K4c	-53.238	-58.898	-56.486	-59.021
K4d	-52.393	-61.659	-55.364	-56.322
K4e	-52.470	-58.807	-54.195	-55.507
K4f	-51.247	-59.706	-55.772	-57.587
K4g	-49.431	-58.535	-53.066	-56.657
K4h	-51.580	-59.519	-56.823	-59.265
K4i	-49.434	-52.147	-47.805	-46.780
K4j	-54.111	-54.874	-51.015	-52.226
K4k	-54.057	-56.809	-51.408	-57.458
K4l	-52.317	-52.146	-50.098	-53.287
K4m	-52.289	-52.928	-49.969	-49.812
K7a	-50.096	-52.559	-53.794	-58.783
K7b	-54.387	-63.293	-59.336	-56.696
K7c	-52.935	-62.923	-58.048	-60.361
K7d	-58.443	-71.069	-60.630	-70.339
K7e	-62.064	-69.749	-59.418	-64.349
K7f	-61.063	-69.790	-58.381	-63.488
K7g	-53.362	-58.269	-54.903	-56.508

[(a)] Residues within 4Å from the ligand were treated as flexible

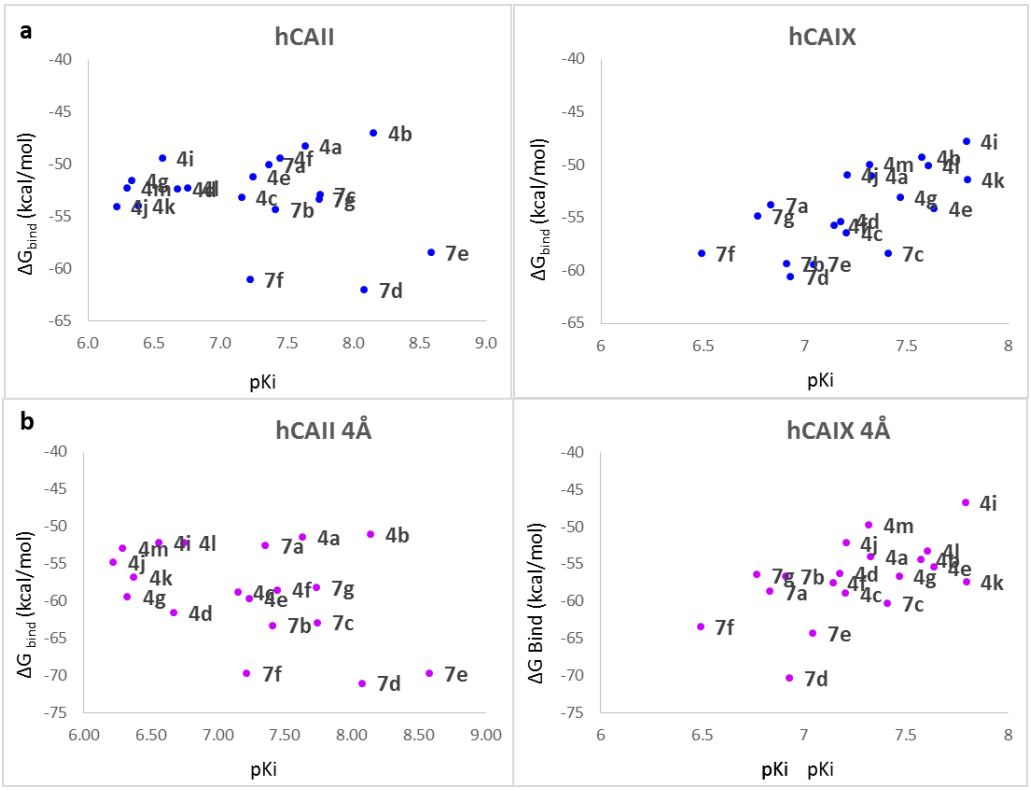

Figure 51. MMGBSA ΔG binding energy vs. pKi values of series K derivatives. Because of the absence of the isatine moiety, derivatives **K3a** and **K3b**, were not considered. Energy values were computed (a) not allowing residues to relax and (b) defining an enzyme flexible region (4Å from the ligand).

The data and results of this research were published in Eldehna, W.M. et al. *Eur. J. Med. Chem.* **2017**,*139*, 250-262. The experimental procedures are reported in Chapter 4.

3.7. Projects under further investigation.

Some relevant projects I worked on in this three-years PhD period are currently under further and detailed investigations. Two of them were started during stages I attended during my PhD period. The discussion about these projects will be only mentioned briefly, reporting only some key points, without going into details of structures, synthesis and in vitro screenings.

Stage at the laboratory of Prof. Silviu T. Balaban in the Institut des sciences moléculaires de Marseille, Aix-Marseille Universitè.

During my second PhD year, I attended a stage guest of Prof. Balaban and his group in Marseille. Their research focuses on the design of fluorescent probes or dyes for a variety of applications, mainly light-harvesting. I had the opportunity to learn much about fluorescence study and apply this to the evaluation of novel fluorescent probes-bearing CAIs.

Fluorescence emission by organic molecules is a phenomenon strictly dependent on the surrounding microenvironment. The formation of discrete host/guest complexes of fluorescent dyes with macrocyclic structures has been widely documented and was generally found to elicit a consistent change in the micro-environmental parameters, which subsequently perturbs the fluorescence phenomenon. Fluorescence probes and their supramolecular complexes possess a variety of potential analytical, environmental and mostly biological applications as diagnostics and imaging tools.[196]

During the stage, I designed and synthesize a set of 4-[4-(dimethylamino)styryl]pyridium based fluorescent dyes bearing classical zinc binding groups such as the sulfonamides, sulfamates and sulfamides to address their spectrum of action to the inhibition of the CAs. The proper pyrillium salts were used as precursors (Figure 53).[197]

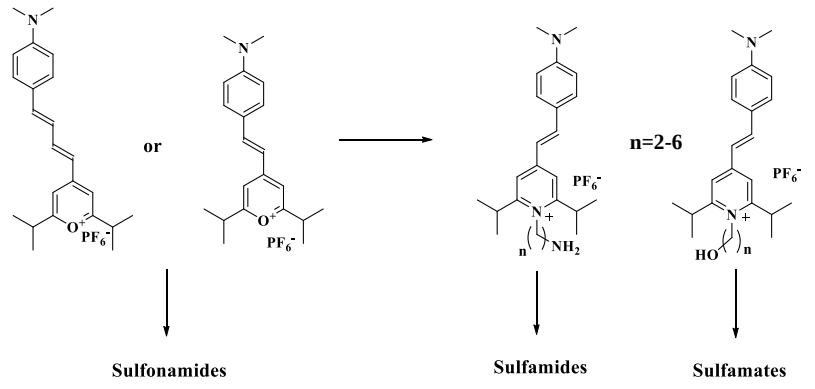

Figure 53. General structures and design of fluorescent dyes CAIs.

The reported derivatives were evaluated for their inhibition profiles against four physiologically relevant hCAIs: i.e. I, II, IV and XII. The synthesized dyes demonstrated to possess diverse inhibitory potency depending on the nature of the exhibited ZBG and

on the length of the spacer between the fluorescent core and the ZBG itself. Moreover, I studied the formation of supramolecular host/guest biological complexes by means of UV-vis absorption and fluorescence emission measurements, which were carried out for all the reported derivatives alone and in presence of the ubiquitous isoforms hCA I and hCA II. Changes in the spectroscopic properties of the dyes after incubation with the two enzymatic isoforms were measured and correlated to the inhibitory profiles of the evaluated derivatives and mostly to the length of the spacer between the ZGB and the fluorescent portion, which elicits different micro-environment for the different probes. The X-ray crystal structures of four of the aforementioned host-guest CA-inhibitors complexes were obtained in collaboration with Dr. Tom Peat (CSIRO, Australia) and provided for a valid explanation for the spectroscopic changes the dyes revealed upon their binding to human carbonic anhydrase isoforms. To validate this innovative proof of concept, additional studies are currently ongoing in collaboration with Prof. Ilies from Temple University, Philadelphia.

Hypoxia activated nitrobenzenesulfonamides

Hypoxia, a state of low oxygen, is a common feature of solid tumors and is associated with disease progression as well as resistance to radiotherapy and certain chemotherapeutic drugs.[198] Bioreductive prodrugs can be designed for selective activation under low oxygen conditions typical of many solid tumors. These hypoxia-activated prodrugs can target and kill hypoxic cells. Hypoxia-activated prodrugs are deactivated or masked cytotoxins that undergo biotransformation following reductive metabolism by endogenous human cellular oxidoreductases. This activation step is catalysed by a variety of oxidoreductases and differs depending on the bioreductive drug class. Five classes of bioreductive compounds that can undergo enzymatic reduction to active species have been developed. Several nitroaromatic compounds have been evaluated in clinical trials, including the nitroimidazoles.[182]

As mentioned, hCA IX and XII are over-expressed in hypoxic tumour, where they play a main role in their growth, tuning the pH to support an extracellular hypoxic microenvironment suited for hypoxic tumor cell survival and proliferation.

In this project I designed and synthesized novel derivatives with the aim to endow them with the ability of both inhibiting the tumour-associated hCA isoforms and being bio-reduced by oxidoreductases in hypoxic condition.

As the "tail" approach [1-3,95,96] is widely and successfully applied in designing new CAIs, varied molecular "tails" were appended to a nitrobenzenesulfonamide scaffold (Figure 54).

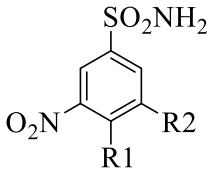

R1: Groups to enhance water solubility

R2: Molecular "tail" to modulate the interaction with different CAs

Figure 54. General structures of hypoxya-activated nitrobenzenesulfonamides

The series of twenty derivatives was evaluated for their inhibition profiles against four hCAs, I, II, IX and XII. Some selected compounds, chosen among those possessing the best CA inhibitory profile, were tested (30 – 300 μM) to evaluate their effects on viability of human colon cancer HT-29 cells after 16 and 48 h incubation in both normoxic and hypoxic conditions. According to ration design, several derivatives demonstrated a strongly enhanced efficacy in hypoxic conditions. X-ray crystallography and computational studies are currently ongoing to evaluate the binding mode the nitro-derivatives with hCA II and IX.

Since nitroimidazole derivatives are widely studied for the treatment of Neglected tropical diseases such as Leishmaniasis and Chagas diseases caused by protozoan *Leishmania donovani* and *Trypanosoma cruzi*,[84,86] I screened the synthesized nitro-derivatives for the inhibition of the CAs from these two pathogens (paragraph 2.1.1). The measured inhibition in the micromolar range lead us to further evaluate their efficacy *in vitro* against the two protozoans in collaboration with Prof. A. Vermelho, from Universidade Federal do Rio de Janeiro.

Stage at the laboratory of Prof. Jean-Yves Winum in Institut des Biomolécules Max Mousseron in Montpellier.

Finally, during my third PhD year, I attended a stage, guest of Prof. Jean-Yves Winum and his group in Montpellier. There I focused on the synthesis of novel benzoxaboroles to further explore the SAR of this new chemotype, only recently validated as CAI. As the "Click Chemistry" approach has been not investigated in detail for this class of compounds, we proceeded with its evaluation, reporting a new set of derivatives, which were screened for the inhibition of human and pathogenic CA. Their binding mode within such isoforms is currently under investigation.

Regarding the enzymatic assays reported in Chapter 3, I performed those of Series D, I, J and K.
Moreover, other studies in which I was involved regarded the computational evaluation of the binding behaviour of different molecular systems, as well as the inhibitory profile evaluation for derivatives of our collaborators by means of the Stopped Flow Assay.[135]
The data and results of these studies were reported in:

Altug, C. et al. *Bioorg. Med. Chem.* **2017**, *25*, 1456-1464.

Eldehna, W.M., et al. *Eur. J. Med. Chem.* **2017**, *127*, 521-530.

Fares, M. et al. *Bioorg. Med. Chem.* **2017**, *25*, 2210-2217.

Bibi, D, et al. *Neurochem. Res.* **2017**, *42*,1972-1982.

Zhang, Z. et al. *J. Enzyme Inhib. Med. Chem.* **2017**, *32*, 722-730.

Akocak, S. et al. *Bioorg. Med. Chem.* **2017**, *25*, 3093-3097.

Angeli, A. et al. *Bioorg. Med. Chem.* **2017**, *25*, 5373-5379.

Diuzheva, A. et al. *Phytochem. Anal.* **2017** DOI: 10.1002/pca.2737

Fragai, M. et al. *J. Med. Chem.* **2017**, 60, 9003-9011.

Chapter 4. Experimental section

General Protocols

Chemistry

Anhydrous solvents and all reagents were purchased from Sigma-Aldrich, Alfa Aesar and TCI. All reactions involving air- or moisture-sensitive compounds were performed under a nitrogen atmosphere using dried glassware and syringes techniques to transfer solutions. Nuclear magnetic resonance (^{1}H-NMR, ^{13}C-NMR, ^{19}F-NMR) spectra were recorded using a Bruker Advance III 400 MHz spectrometer in DMSO-d_6 or $CDCl_3$. Chemical shifts are reported in parts per million (ppm) and the coupling constants (*J*) are expressed in Hertz (Hz). Splitting patterns are designated as follows: s, singlet; d, doublet; t, triplet; q, quadruplet; sept, septet; m, multiplet; bs, broad singlet; dd, double of doubles, appt, apparent triplet, appq, apparent quartet. The assignment of exchangeable protons (O*H* and N*H*) was confirmed by the addition of D_2O. Analytical thin-layer chromatography (TLC) was carried out on Merck silica gel F-254 plates. Flash chromatography purifications were performed on Merck Silica gel 60 (230-400 mesh ASTM) as the stationary phase and ethyl acetate/*n*-hexane or MeOH/DCM were used as eluents. Melting points (mp) were measured in open capillary tubes with a Gallenkamp MPD350.BM3.5 apparatus and are uncorrected. HPLC was performed by using a Waters 2690 separation module coupled with a photodiode array detector (PDA Waters 996) and as column a Nova-Pak C18 4 μm 3.9 mm × 150 mm (Waters), silica-based reverse phase column. Sample was dissolved in acetonitrile 10%, and an injection volume of 45 μL was used. The mobile phase, at a flow rate of 1 mL/min, was a gradient of water + trifluoroacetic acid (TFA) 0.1% (A) and acetonitrile + TFA 0.1% (B), with steps as follows: (A% : B%), 0−10 min 90:10, 10−25 min gradient to 60:40, 26:28 min isocratic 20:80, 29−35 min isocratic 90:10. TFA 0.1% in water as well in acetonitrile was used as counterion. All compounds reported here were >96% HPLC pure. The solvents used in MS measures were acetone, acetonitrile (Chromasolv grade), purchased from Sigma-Aldrich (Milan - Italy), and mQ water 18 MΩ, obtained from Millipore's Simplicity system (Milan-Italy). The mass spectra were obtained using a Varian 1200L triple

quadrupole system (Palo Alto, CA, USA) equipped by Electrospray Source (ESI) operating in both positive and negative ions. Stock solutions of analytes were prepared in acetone at 1.0 mg mL^{-1} and stored at 4°C. Working solutions of each analyte were freshly prepared by diluting stock solutions in a mixture of mQ H_2O/ACN 1/1 (*v/v*) up to a concentration of 1.0 μg mL^{-1} The mass spectra of each analyte were acquired by introducing, via syringe pump at 10 μL min^{-1}, of the its working solution. Raw-data were collected and processed by Varian Workstation Vers. 6.8 software.

Carbonic Anhydrase Inhibition

α-CAs

An Applied Photophysics stopped-flow instrument has been used for assaying the CA catalysed CO_2 hydration activity. Phenol red (at a concentration of 0.2 mM) has been used as indicator, working at the absorbance maximum of 557 nm, with 20 mM Hepes (pH 7.5) as buffer, and 20 mM Na_2SO_4 (for maintaining constant the ionic strength), following the initial rates of the CA-catalyzed CO_2 hydration reaction for a period of 10-100 s.[135] The CO_2 concentrations ranged from 1.7 to 17 mM for the determination of the kinetic parameters and inhibition constants. For each inhibitor, at least six traces of the initial 5-10% of the reaction have been used for determining the initial velocity. The uncatalyzed rates were determined in the same manner and subtracted from the total observed rates. Stock solutions of inhibitor (0.1 mM) were prepared in distilled-deionized water and dilutions up to 0.01 nM were done thereafter with the assay buffer. Inhibitor and enzyme solutions were preincubated together for 15 min (sulfonamides) or 6h (coumarins and sulfocoumarins) at room temperature prior to assay, in order to allow for the formation of the E-I complex. The inhibition constants were obtained by non-linear least-squares methods using PRISM 3 and the Cheng-Prusoff equation, as reported earlier,[1-3,95,96] and represent the mean from at least three different determinations. All CA isofoms were recombinant ones obtained in-house as reported earlier.[1-3,95,96]

β-CAs

An Applied Photophysics stopped-flow instrument has been used for assaying the CA catalyzed CO_2 hydration activity.[135] Bromothymol blue (at a concentration of 0.2 mM) has been used as indicator, working at the absorbance maximum of 557 nm, with 10–20 mM TRIS (pH 8.3) as buffer, and 20 mM $NaBF_4$ for maintaining constant the ionic strength, following the initial rates of the CA catalyzed CO_2 hydration reaction for a period of 10–100 s. The CO_2 concentrations ranged from 1.7 to 17 mM for the determination of the kinetic parameters and inhibition constants. For each inhibitor, at least six traces of the initial 5–10% of the reaction have been used for determining the initial velocity. The uncatalyzed rates were determined in the same manner and subtracted from the total observed rates. Stock solutions of inhibitor (10 mM) were prepared in distilled-deionized water and dilutions up to 0.01M were done thereafter with the assay buffer. Inhibitor and enzyme solutions were preincubated together for 15 min at room temperature prior to assay, in order to allow for the formation of the E-I complex. The inhibition constants were obtained by non-linear least-squares methods using the Cheng-Prusoff equation whereas the kinetic parameters for the uninhibited enzymes from Lineweaver-Burk plots, as reported earlier, [12,80,86] and represent the mean from at least three different determinations determinations. MgCA was a recombinant protein, obtained and purified by a diverse procedure as the one reported earlier.[12,80,86]

Modeling

Hardware

- Workstation SO Linux
  - Distribution: Linux version 3.2.0-4-amd64 - gcc version 4.6.3 (Debian 4.6.3-14)
  - Intel® 2x CPU Xeon® 6-core E5-2620v2 @ 2.10 GHz (1200 MHz) 15MB
  - 4x DDR3-1600 ECC 8GB module

Software

- Schrödinger Suite Release 2016-1, Schrödinger, LLC, New York, NY, 2016 www.schroedinger.com
  - Maestro v.10.5;
  - Epik, v.3.5;
  - Impact, v.7.0;
  - Prime, v.4.3;
  - Macromodel v. 11.1.
  - Glide, v.7.0;
  - Jaguar, v.9.1;
- Swiss-PdbViewer, v. 4.1;
- BioEdit; v. 7.2.6.

All crystal structures used for computational studies were prepared according to the Protein Preparation module in Maestro - Schrödinger suite, assigning bond orders, adding hydrogens, deleting water molecules, and optimizing H-bonding networks. Finally, energy minimization with a root mean square deviation (RMSD) value of 0.30 was applied using an Optimized Potentials for Liquid Simulation (OPLS_2005) force field.[199a-c,200]

This procedure was applied to the following structures (PDB ID):
4Q6E, 5LJT, 3IAI, 5FL4, 4BCW, 2W3N and MgCA homology built model (paragraph 4.4.3).

3D ligand structures were prepared by Maestro,[199a] evaluated for their ionization states at pH 7.4 ± 0.5 (α-CAs) or ± 1.0 (β-CAs) with Epik. [199b] OPLS-2005 force field in Macromodel[199g] was used for energy minimization for a maximum number of 2500 conjugate gradient iterations and setting a convergence criterion of 0.05 kcal $mol^{-1}Å^{-1}$. Grids for docking were centred in the centroid of the complexed ligand. Docking studies were carried out with the program Glide.[199f] The standard precision (SP) mode of the GlideScore function was applied to evaluate the predicted binding poses.

For compounds of the series **E**, **H** and **I**, the atomic electrostatic charges of the ligands were computed with Jaguar [199g] fitting them to an electrostatic potential calculated at the B3LYP/ 6–31G*$^{+}$ level of theory. ESP atomic charges were used in docking simulations.

For compounds of the series **K**, the best three poses for each compound were re-docked by means of Prime MM-GBSA calculations[199d] with a VSGB solvatation model.[201]

Figures were generated with Maestro.[199a]

4.1. "Click chemistry" approach applied to the design of novel CAIs belonging to first, second and third classes of inhibitors (Series A, B, C)

4.1.1 Chemistry.

The general chemistry protocols are reported at the beginning of the experimental section.

Sulfonamides (series A) - General synthetic procedure of compounds A3-A10, A13-A17.[128]

The appropriate alkyne **A12, A18-A24** (1.0 eq) was added to a suspension of aryl azide **A2, A26-A30** (1.1 eq) in H_2O/*tert*-BuOH 1/1 (4 ml) at r.t., followed by copper (0) nanosized (0.1 eq) and TEA HCl or TMACl (1.0 eq). The suspension was stirred at r.t. or 60°C until starting materials were consumed (TLC monitoring), then quenched with H_2O (20 ml) and the formed precipitate was filtered-off and washed with H_2O. The residue was purified by silica gel column chromatography eluting with ethyl acetate in *n*-hexane or alternatively was dissolved in a minimal amount of acetone, the obtained solution was filtered through Celite 521® and then concentrated under *vacuo* to give a residue that was triturated with Et_2O to afford the titled compounds **A3-A10, A13-A17.**

Synthesis of 4-(4-phenoxymethyl-[1,2,3]triazol-1-yl)-benzenesulfonamide **A3**.

Compound **A3** was obtained according the general procedure earlier reported using prop-2-ynyloxy-benzene **A18** (1.0 eq), 4-azido-benzenesulfonamide **A2** (0.12 g, 1.1 eq) in *tert*-ButOH/H_2O 1/1 (4 ml), triethylamine hydrochloride (1.0 eq) and copper nanosize (0.1 eq). The reaction mixture was stirred for 27h at r.t. to give the titled compound **A3** as a light yellow solid.

4-(4-Phenoxymethyl-[1,2,3]triazol-1-yl)-benzenesulfonamide A3: 72% yield; m.p. 200-202°C; silica gel TLC R_f 0.22 (EtOAc/*n*-hexane 50 % *v/v*); δ_H (400 MHz, DMSO-d_6): 5.29 (s, 2H, CH_2), 7.01 (t, *J* = 7.2, 1H), 7.12 (d, *J* = 7.6, 2H), 7.37 (t, *J* = 7.6, 2H), 7.57 (s, 2H, exchange with D_2O, SO_2NH_2), 8.07 (d, *J* = 8.8, 2H), 8.19 (d, *J* = 8.8, 2H), 9.10 (s, 1H); δ_C (100 MHz, DMSO-d_6): 61.7, 115.6, 121.3, 121.9, 124.0, 128.4, 130.5, 139.5, 144.8, 145.3, 158.9; *m/z* (ESI positive) 331.0 $[M+H]^+$

Synthesis of 4-(4-m-tolyloxymethyl-[1,2,3]triazol-1-yl)-benzenesulfonamide **A4.**

Compound **A4** was obtained according the general procedure earlier reported using 1-methyl-3-prop-2-ynyloxy-benzene **A19** (1.0 eq), 4-azido-benzenesulfonamide **A2** (0.12 g, 1.1 eq) in *tert*-ButOH/H_2O 1/1 (4 ml), triethylamine hydrochloride (1.0 eq) and copper nanosize (0.1 eq). The reaction mixture was stirred for 24h at r.t. to give the titled compound **A4** as a yellow solid.

4-(4-m-Tolyloxymethyl-[1,2,3]triazol-1-yl)-benzenesulfonamide A4: 68% yield; m.p. 176-178°C; silica gel TLC R_f 0.13 (EtOAc/*n*-hexane 50 % *v/v*); δ_H (400 MHz, DMSO-d_6): 2.33 (s, 3H, CH_3), 5.27 (s, 2H, CH_2), 6.83 (d, *J* = 7.6, 1H), 6.91 (d, *J* = 7.6, 1H), 6.94 (s, 1H), 7.23 (t, *J* = 7.6, 1H), 7.57 (s, 2H, exchange with D_2O, SO_2NH_2), 8.07 (d, *J* = 8.8, 2H), 8.19 (d, *J* = 8.8, 2H), 9.09 (s, 1H); δ_C (100 MHz, DMSO-d_6): 22.1, 61.8, 112.6, 116.3, 121.3, 122.7, 124.0, 128.5, 130.3, 139.5, 140.0, 144.8, 145.4, 158.9; *m/z* (ESI positive) 345.0 $[M+H]^+$

Synthesis of 4-[4-(3-methoxy-phenoxymethyl)-[1,2,3]triazol-1-yl]-benzenesulfonamide **A5.**

Compound **A5** was obtained according the general procedure earlier reported using 1-methoxy-3-prop-2-ynyloxy-benzene **A20** (1.0 eq), 4-azido-benzenesulfonamide **A2** (0.12

g, 1.1 eq) in *tert*-ButOH/H_2O 1/1 (4 ml), triethylamine hydrochloride (1.0 eq) and copper nanosize (0.1 eq). The reaction mixture was stirred for 17h at r.t. to give the titled compound **A5** as a yellow solid.

4-[4-(3-Methoxy-phenoxymethyl)-[1,2,3]triazol-1-yl]-benzenesulfonamide A5: 70% yield; m.p. 159-161°C; silica gel TLC R_f 0.14 (EtOAc/*n*-hexane 50 % *v/v*); δ_H (400 MHz, DMSO-d_6): 3.78 (s, 3H, CH_3), 5.28 (s, 2H, CH_2), 6.60 (dd, *J* = 2.0, 8.0, 1H), 6.68 (s, 1H), 6.70 (dd, *J* = 2.0, 8.0, 1H), 7.25 (t, *J* = 8.0, 1H), 7.59 (s, 2H, exchange with D_2O, SO_2NH_2), 8.07 (d, *J* = 8.8, 2H), 8.19 (d, *J* = 8.8, 2H), 9.11 (s, 1H); δ_C (100 MHz, DMSO-d_6): 56.1, 61.9, 102.0, 107.7, 107.8, 121.3, 124.0, 128.5, 131.0, 139.5, 144.9, 145.2, 160.1, 161.5; *m/z* (ESI positive) 361.0 $[M+H]^+$

Synthesis of 4-[4-(4-methoxy-phenoxymethyl)-[1,2,3]triazol-1-yl]-benzenesulfonamide **A6.**

Compound **A6** was obtained according the general procedure earlier reported using 1-methoxy-4-prop-2-ynyloxy-benzene **A21** (1.0 eq), 4-azido-benzenesulfonamide **A2** (0.12 g, 1.1 eq) in *tert*-ButOH/H_2O 1/1 (4 ml), triethylamine hydrochloride (1.0 eq) and copper nanosize (0.1 eq). The reaction mixture was stirred for 24h at r.t. to give the titled compound **A6** as a yellow solid.

4-[4-(4-Methoxy-phenoxymethyl)-[1,2,3]triazol-1-yl]-benzenesulfonamide A6: 68% yield; m.p. 209-210°C; silica gel TLC R_f 0.18 (EtOAc/*n*-hexane 50 % *v/v*); δ_H (400 MHz, DMSO-d_6): 3.74 (s, 3H, CH_3), 5.22 (s, 2H, CH_2), 6.92 (d, *J* = 8.8, 2H), 7.05 (d, *J* = 8.8, 2H), 7.58 (s, 2H, exchange with D_2O, SO_2NH_2), 8.06 (d, *J* = 8.0, 2H), 8.19 (d, *J* = 8.0, 2H), 9.09 (s, 1H); δ_C (100 MHz, DMSO-d_6): 56.3, 62.4, 115.6, 116.7, 121.3, 123.9, 128.5, 139.5, 144.8, 145.5, 152.9, 154.6; *m/z* (ESI positive) 361.0 $[M+H]^+$

Synthesis of 4-(4-((pyridin-3-yloxy)methyl)-1H-1,2,3-triazol-1-yl)benzenesulfonamide **A7.**

Compound **A7** was obtained according the general procedure earlier reported using 2-prop-2-ynyloxy-pyridine **A22** (1.0 eq), 4-azido-benzenesulfonamide **A2** (0.12 g, 1.1 eq) in *tert*-ButOH/H_2O 1/1 (4 ml), triethylamine hydrochloride (1.0 eq) and copper nanosize

(0.1 eq). The reaction mixture was stirred for 48h at r.t. to give the titled compound **A7** as a yellow solid.

4-[4-(Pyridin-2-yloxymethyl)-[1,2,3]triazol-1-yl]-benzenesulfonamide A7: 51% yield; m.p. 277-280d; silica gel TLC R_f 0.09 (EtOAc/*n*-hexane 50 % *v/v*); δ_H (400 MHz, DMSO-d_6): 5.29 (s, 2H, CH_2), 6.31 (t, *J* = 6.4, 1H), 6.45 (d, *J* = 9.4, 1H), 7.48 (t, *J* = 9.4, 1H), 7.55 (s, 2H, exchange with D_2O, SO_2NH_2), 7.90 (d, *J* = 6.4, 1H), 8.04 (d, *J* = 8.8, 2H), 8.17 (d, *J* = 8.8, 2H), 8.89 (s, 1H); δ_C (100 MHz, DMSO-d_6): 44.1, 106.5, 120.6, 121.2, 123.2, 128.4, 139.4, 140.1, 141.2, 144.8, 152.8, 162.1; *m/z* (ESI negative) 330.0 $[M-H]^-$

Synthesis of 4-(4-phenylsulfanylmethyl-[1,2,3]triazol-1-yl)-benzenesulfonamide **A8.**

Compound **A8** was obtained according the general procedure earlier reported using prop-2-ynylsulfanyl-benzene **A23** (1.0 eq), 4-azido-benzenesulfonamide **A2** (0.12 g, 1.1 eq) in *tert*-ButOH/H_2O 1/1 (4 ml), triethylamine hydrochloride (1.0 eq) and copper nanosize (0.1 eq). The reaction mixture was stirred for 24h at r.t. to give the titled compound **A8** as a yellow solid.

4-(4-Phenylsulfanylmethyl-[1,2,3]triazol-1-yl)-benzenesulfonamide A8: 63% yield; m.p. 202-204°C; silica gel TLC R_f 0.62 (EtOAc/*n*-hexane 50 % *v/v*); δ_H (400 MHz, DMSO-d_6): 4.43 (s, 2H, CH_2), 7.25 (t, *J* = 7.2, 1H), 7.37 (t, *J* = 7.6, 2H), 7.45 (d, *J* = 7.6, 2H), 7.53 (s, 2H, exchange with D_2O, SO_2NH_2), 8.04 (d, *J* = 8.4, 2H), 8.12 (d, *J* = 8.4, 2H), 8.82 (s, 1H); δ_C (100 MHz, DMSO-d_6): 28.1, 121.1, 122.6, 127.0, 128.4, 129.8, 130.0, 136.4, 139.4, 144.7, 146.2; *m/z* (ESI positive) 347.0 $[M+H]^+$

Synthesis of 4-(4-phenylaminomethyl-[1,2,3]triazol-1-yl)-benzenesulfonamide **A9.**

Compound **A9** was obtained according the general procedure earlier reported using phenyl-prop-2-ynyl-amine **A24** (1.0 eq), 4-azido-benzenesulfonamide **A2** (0.12 g, 1.1 eq) in *tert*-ButOH/H_2O 1/1 (4 ml), triethylamine hydrochloride (1.0 eq) and copper nanosize (0.1 eq). The reaction mixture was stirred for 20h at r.t. to give the titled compound **A9** as a yellow solid.

4-(4-Phenylaminomethyl-[1,2,3]triazol-1-yl)-benzenesulfonamide A9: 78% yield; m.p. 221-223°C; silica gel TLC R_f 0.57 (EtOAc/*n*-hexane 50 % *v/v*); δ_H (400 MHz, DMSO-d_6): 4.42 (d, J = 5.6, 2H, CH_2), 6.20 (t, J = 5.6, 1H, exchange with D_2O, N*H*) , 6.59 (t, J = 7.2, 1H), 6.71 (d, J = 8.0, 2H), 7.12 (t, J = 8.0, 2H), 7.57 (s, 2H, exchange with D_2O, SO_2NH_2), 8.04 (d, J = 8.4, 2H), 8.16 (d, J = 8.4, 2H), 8.85 (s, 1H); δ_C (100 MHz, DMSO-d_6): 39.5, 113.3, 117.1, 121.0, 122.2, 128.5, 129.8, 139.6, 144.6, 148.3, 149.2; *m/z* (ESI positive) 330.0 $[M+H]^+$

Synthesis of N,N-di-(1-(4-sulfamoylphenyl)-[1,2,3]triazol-4-yl-methyl)-aniline **A10.**

Compound **A10** was obtained according the general procedure earlier reported using phenyl-di-prop-2-ynyl-amine **A25** (1.0 eq), 4-azido-benzenesulfonamide **A2** (0.12 g, 2.2 eq) in *tert*-ButOH/H_2O 1/1 (4 ml), triethylamine hydrochloride (2.0 eq) and copper nanosize (0.2 eq). The reaction mixture was stirred for 72h at r.t. to give the titled compound **A10** as a yellow solid.

***N,N*-Di-(1-(4-sulfamoylphenyl)-[1,2,3]triazol-4-yl-methyl)-aniline A10:** 65% yield; m.p. 253-254°C; silica gel TLC R_f 0.14 (EtOAc/*n*-hexane 50 % *v/v*); δ_H (400 MHz, DMSO-d_6): 4.83 (s, 4H, 2 x CH_2) , 6.59 (t, J = 7.6, 1H), 6.96 (d, J = 7.8, 2H), 7.16 (t, J = 7.8, 2H), 7.52 (s, 4H, exchange with D_2O, 2 x SO_2NH_2), 8.05 (d, J = 8.4, 4H), 8.17 (d, J = 8.4, 4H), 8.94 (s, 2H); δ_C (100 MHz, DMSO-d_6): 46.6, 113.9, 117.8, 121.1, 122.5, 128.4, 130.0, 139.6, 144.7, 147.2, 148.6; *m/z* (ESI negative) 564.0 $[M-H]^-$

Synthesis of 4-(1-phenyl-1H-[1,2,3]triazol-4-ylmethoxy)-benzenesulfonamide **A13.**

Compound **A13** was obtained according the general procedure earlier reported using 4-prop-2-ynyloxy-benzenesulfonamide **A12** (0.05g, 1.0 eq), phenylazide **A26** (1.1 eq) in *tert*-ButOH/H_2O 1/1 (3.5 ml), tetramethylamonium chloride (1.0 eq) and copper nanosize (0.1 eq). The reaction mixture was stirred at 60°C for 2.5h and the obtained residue was purified by silica gel column chromatography eluting with 50% ethyl acetate in *n*-hexane to afford **A13** as a white solid.

4-(1-Phenyl-1*H*-[1,2,3]triazol-4-ylmethoxy)-benzenesulfonamide A13: 70% yield; m.p. 200-202°C; silica gel TLC R_f 0.24 (EtOAc/*n*-hexane 50 % *v/v*); δ_H (400 MHz, DMSO-d_6): 5.38 (s, 2H, CH_2), 7.26 (s, 2H, exchange with D_2O, SO_2NH_2) 7.28 (m, 2H,

overlap with signal at 7.26), 7.55 (t, *J* = 7.6, 1H), 7.65 (t, *J* = 7.6, 2H), 7.81 (d, *J* = 8.4, 2H), 7.95 (d, *J* = 7.6, 2H), 9.03 (s, 1H); δ_C (100 MHz, DMSO-d_6): 62.3, 115.7, 121.1, 124.0, 128.6, 129.8, 130.9, 137.5, 137.6, 144.3, 161.2; *m/z* (ESI positive) 331.0 $[M+H]^+$.

Synthesis of 4-[1-(3-methoxy-phenyl)-1H-[1,2,3]triazol-4-ylmethoxy]-benzenesulfonamide **A14.**

Compound **A14** was obtained according the general procedure earlier reported using 4-prop-2-ynyloxy-benzenesulfonamide **A12** (0.05g, 1.0 eq), 1-azido-3-methoxybenzene **A27** (1.1 eq) in *tert*-ButOH/H_2O 1/1 (3.5 ml), tetramethylamonium chloride (1.0 eq) and copper nanosize (0.1 eq). The reaction mixture was stirred at 60°C for 3h and the obtained residue was purified by silica gel column chromatography eluting with 50% ethyl acetate in *n*-hexane to afford **A14** as a white solid.

4-[1-(3-Methoxy-phenyl)-1*H*-[1,2,3]triazol-4-ylmethoxy]-benzenesulfonamide A14 72% yield; m.p. 184-186°C; silica gel TLC R_f 0.21 (EtOAc/n-hexane 50 % *v/v*); δ_H (400 MHz, DMSO-d_6): 3.90 (s, 3H, CH_3), 5.37 (s, 2H, CH_2), 7.11 (d, *J* = 6.8, 1H), 7.27 (s, 2H, exchange with D_2O, SO_2NH_2), 7.28 (m, 2H, overlap with signal at 7.27), 7.54 (m, 3H), 7.82 (d, *J* = 8.8, 2H), 9.05 (s, 1H); δ_C (100 MHz, DMSO-d_6): 56.6, 62.3, 106.7, 113.1, 115.5, 115.7, 124.1, 128.6, 131.8, 137.6, 138.5, 144.2, 161.1, 161.2; *m/z* (ESI positive) 361.0 $[M+H]^+$.

Synthesis of 4-[1-(4-fluoro-phenyl)-1H-[1,2,3]triazol-4-ylmethoxy]-benzenesulfonamide **A15.**

Compound **A15** was obtained according the general procedure earlier reported using 4-prop-2-ynyloxy-benzenesulfonamide **A12** (0.05g, 1.0 eq), 1-azido-4-fluorobenzene **A28** (1.1 eq) in *tert*-ButOH/H_2O 1/1 (3.5 ml), tetramethylamonium chloride (1.0 eq) and copper nanosize (0.1 eq). The reaction mixture was stirred at 60°C for 2h and the obtained residue was purified by silica gel column chromatography eluting with 50% ethyl acetate in *n*-hexane to afford **A15** as a white solid.

4-[1-(4-Fluoro-phenyl)-1*H*-[1,2,3]triazol-4-ylmethoxy]-benzenesulfonamide A15: 70% yield; m.p. 211-213°C; silica gel TLC R_f 0.29 (EtOAc/*n*-hexane 50 % *v/v*); δ_H (400 MHz, DMSO-d_6): 5.37 (s, 2H, CH_2), 7.27 (s, 2H, exchange with D_2O, SO_2NH_2), 7.28 (m,

2H, overlap with signal at 7.27), 7.51 (t, *J* = 8.4, 2H), 7.81 (d, *J* = 8.4, 2H), 8.00 (m, 2H), 9.00 (s, 1H); δ_F (376 MHz, DMSO-*d*$_6$): -112.97 (s, 1F); δ_C (100 MHz, DMSO-*d*$_6$): 62.2, 115.8, 117.8 (d, J^2_{CF} = 23.1), 123.6 (d, J^3_{CF} = 8.8), 124.4, 128.7, 134.1, 137.6, 144.3, 161.2, 162.7 (d, J^1_{CF} = 244.5); *m/z* (ESI positive) 349.0 $[M+H]^+$.

Synthesis of 4-[1-(4trifluoromethyl-phenyl)-1H-[1,2,3]triazol-4-ylmethoxy]-benzenesulfonamide **A16.**

Compound **A16** was obtained according the general procedure earlier reported using 4-prop-2-ynyloxy-benzenesulfonamide **A12** (0.05g, 1.0 eq), 1-azido-4-trifluoromethylbenzene **A29** (1.1 eq) in *tert*-ButOH/H_2O 1/1 (3.5 ml), tetramethylamonium chloride (1.0 eq) and copper nanosize (0.1 eq). The reaction mixture was stirred at 60°C for 1.5h and the obtained residue was purified by silica gel column chromatography eluting with 50% ethyl acetate in *n*-hexane to afford **A16** as a white solid.

4-[1-(4-Trifluoromethyl-phenyl)-1*H*-[1,2,3]triazol-4-ylmethoxy]-benzenesulfonamide A16: 69% yield; m.p. 198-199°C; silica gel TLC R_f 0.16 (EtOAc/n-hexane 50 % *v/v*); δ_H (400 MHz, DMSO-*d*$_6$): 5.36 (s, 2H, C*H*$_2$), 7.23 (s, 2H, exchange with D_2O, SO_2NH_2), 7.24 (m, 2H, overlap with signal at 7.23), 7.78 (d, *J* = 8.8, 2H), 8.00 (d, *J* = 8.6, 2H), 8.18 (d, *J* = 8.6, 2H), 9.14 (s, 1H); δ_F (376 MHz, DMSO-*d*$_6$): -61.03 (s, 3F); δ_C (100 MHz, DMSO-*d*$_6$): 62.2, 115.8, 121.6, 124.3, 124.7 (d, J^1_{CF} = 270.6), 128.2 (q, J^3_{CF} = 3.8), 128.6, 129.8 (q, J^2_{CF} = 32.2), 137.6, 140.3, 144.7, 161.2; *m/z* (ESI positive) 399.0 $[M+H]^+$.

Synthesis of 4-[1-(4-Hydroxy-phenyl)-1H-[1,2,3]triazol-4-ylmethoxy]-benzenesulfonamide **A17.**

Compound **A17** was obtained according the general procedure earlier reported using 4-prop-2-ynyloxy-benzenesulfonamide **A12** (0.05g, 1.0 eq), 1-azido-4-hydroxybenzene **A30** (1.1 eq) in *tert*-ButOH/H_2O 1/1 (3.5 ml), tetramethylamonium chloride (1.0 eq) and copper nanosize (0.1 eq). The reaction mixture was stirred at 60°C for 1h and the obtained

residue was purified by silica gel column chromatography eluting with 60% ethyl acetate in *n*-hexane to afford **A17** as a white solid.

4-[1-(4-Hydroxy-phenyl)-1*H*-[1,2,3]triazol-4-ylmethoxy]-benzenesulfonamide A17: 49% yield; m.p. 229-231°C; silica gel TLC R_f 0.09 (EtOAc/*n*-hexane 50 % *v/v*); δ_H (400 MHz, DMSO-d_6): 5.34 (s, 2H, CH_2), 6.97 (d, J = 8.8, 2H), 7.26 (m, 2H, overlap with signal at 7.27), 7.27 (s, 2H, exchange with D_2O, SO_2NH_2), 7.71 (d, J = 8.8, 2H), 7.81 (d, J = 8.8, 2H), 8.84 (s, 1H), 10.02 (s, 1H, exchange with D_2O, O*H*); δ_C (100 MHz, DMSO-d_6): 62.3, 115.8, 117.0, 123.0, 123.9, 128.6, 129.6, 137.6, 143.9, 158.8, 161.3; *m/z* (ESI positive) 347.0 $[M+H]^+$.

General synthetic procedure of alkynes **A12, A18- A24**[202]

Propargyl bromide (1.2 eq) was added to a suspension of the proper phenol, thiophenol or aniline (0.5 g, 1.0 eq) and K_2CO_3 (2.0 eq) in dry DMF (4 ml) under a nitrogen atmosphere and that was stirred at r.t. until starting material was consumed (TLC monitoring). The reaction mixture was quenched with H_2O (20 ml) and extracted with Et_2O or EtOAc (25 ml). The organic layer was washed with brine (4x15ml), dried over Na_2SO_4 filtered-off and concentrated under *vacuo* to give the titled compounds **A18- A24.**

Synthesis of prop-2-ynyloxy-benzene **A18.**

Compound **A18** was obtained according the general procedure earlier reported. The reaction mixture was stirred at r.t. for 2h to give the titled compound **A18.**

Prop-2-ynyloxy-benzene A18: 74% yield; silica gel TLC R_f 0.68 (EtOAc/*n*-hexane 20 % *v/v*); δ_H (400 MHz, $CDCl_3$): 2.58 (t, J = 2.4, 1H), 4.76 (d, J = 2.4, 2H), 7.06 (m, 3H), 7.37 (t, J = 8.8, 2H); δ_C (100 MHz, $CDCl_3$): 56.1, 75.8, 79.0, 115.3, 121.9, 129.8, 157.9. Experimental in agreement with reported data.[202]

Synthesis of 1-methyl-3-prop-2-ynyloxy-benzene **A19.**

Compound **A19** was obtained according the general procedure earlier reported. The reaction mixture was stirred at r.t. for 2h to give the titled compound **A19.**

1-Methyl-3-prop-2-ynyloxy-benzene A19: 81% yield; silica gel TLC R_f 0.48 (EtOAc/*n*-hexane 20 % *v/v*); δ_H (400 MHz, DMSO-d_6): 2.45 (s, 3H, CH_3), 2.52 (t, J = 2.4, 1H), 4.69 (d, J = 2.4, 2H), 6.81 (m, 3H), 7.20 (t, J = 7.2, 1H); δ_C (100 MHz, $CDCl_3$): 21.9, 56.0, 75.7, 79.1, 112.0, 116.1, 122.8, 129.5, 139.9, 157.9.
Experimental in agreement with reported data.[203]

Synthesis of 1-methoxy-3-prop-2-ynyloxy-benzene **A20.**

Compound **A20** was obtained according the general procedure earlier reported. The reaction mixture was stirred at r.t. for 2h to give the titled compound **A20.**
1-Methoxy-3-prop-2-ynyloxy-benzene A20: 78% yield; silica gel TLC R_f 0.78 (EtOAc/n-hexane 50 % *v/v*); δ_H (400 MHz, $CDCl_3$): 2.53 (t, J = 2.4, 1H), 3.80 (s, 3H, CH_3), 4.68 (d, J = 2.4, 2H), 6.57 (m, 3H), 7.20 (t, J = 7.4, 1H); δ_C (100 MHz, $CDCl_3$): 55.6, 56.2, 75.8, 78.9, 101.9, 107.2, 107.6, 103.2, 159.2, 161.2.
Experimental in agreement with reported data.[203]

Synthesis of 1-methoxy-4-prop-2-ynyloxy-benzene **A21.**

Compound **A21** was obtained according the general procedure earlier reported. The reaction mixture was stirred at r.t. for 2h to give the titled compound **A21.**
1-Methoxy-4-prop-2-ynyloxy-benzene A21: 71% yield; silica gel TLC R_f 0.65 (EtOAc/*n*-hexane 50 % *v/v*); δ_H (400 MHz, $CDCl_3$): 2.51 (t, J = 2.4, 1H), 3.78 (s, 3H, CH_3), 4.64 (d, J = 2.4, 2H), 6.85 (d, J = 9.2, 2H), 6.93 (d, J = 9.2, 2H); δ_C (100 MHz, $CDCl_3$): 56.0, 56.9, 75.6, 79.2, 114.9, 116.5, 152.0, 154.8.
Experimental in agreement with reported data.[204]

Synthesis of 2-prop-2-ynyloxy-pyridine **A22.**

Compound **A22** was obtained according the general procedure earlier reported. The reaction mixture was stirred at r.t. for 3h to give to an oil that was purified by silica gel column chromatography eluting with 5% MeOH in DCM to afford **A22.**

2-Prop-2-ynyloxy-pyridine A22: 50% yield; silica gel TLC R_f 0.49 (MeOH/CH_2Cl_2 10 % *v/v*); δ_H(400 MHz, $CDCl_3$): 2.49 (t, *J* = 2.4, 1H), 4.76 (d, *J* = 2.4, 2H), 6.25 (t, *J* = 6.8, 1H), 6.61 (d, *J* = 9.2, 1H), 7.35 (m, 1H), 7.64 (d, *J* = 6.8, 1H); δ_C (100 MHz, $CDCl_3$): 31.3, 41.2, 73.5, 79.0, 116.6, 121.0, 129.6, 147.5.
Experimental in agreement with reported data.[204]

Synthesis of prop-2-ynylsulfanyl-benzene **A23.**

Compound **A23** was obtained according the general procedure earlier reported. The reaction mixture was stirred at r.t. for 2h to give the titled compound **A23**.
Prop-2-ynylsulfanyl-benzene A23: 96% yield; silica gel TLC R_f 0.61 (EtOAc/*n*-hexane 10 % *v/v*); δ_H (400 MHz, $CDCl_3$): 2.30 (t, *J* = 2.4, 1H), 3.67 (d, *J* = 2.4, 2H), 7.32 (m, 1H), 7.39 (t, *J* = 7.6, 2H), 7.52 (m, 2H); δ_C (100 MHz, $CDCl_3$): 22.9, 71.9, 80.2, 127.3, 129.3, 129.4, 130.4.
Experimental in agreement with reported data.[205]

Synthesis of phenyl-prop-2-ynyl-amine **A24** a*nd phenyl-di-prop-2-ynyl-amine* **A25.**

Compound **A24** and compound **A25** were obtained according the general procedure earlier reported. The reaction mixture was stirred at r.t. for 4h and the obtained oil was purified by silica gel column chromatography eluting with 5% EtOAc in petroleum ether to afford the titled compounds **A24** and **A25** as two yellow liquids.
Phenyl-prop-2-ynyl-amine A24: 35% yield; silica gel TLC R_f 0.76 (EtOAc/*n*-hexane 20 % *v/v*); δ_H (400 MHz, DMSO-d_6): 2.24 (t, *J* = 2.4, 1H), 3.96 (d, *J* = 2.4, 2H), 6.78 (d, *J* = 7.4, 2H), 6.85 (t, *J* =7.4, 1H), 7.31 (t, *J* =7.4, 2H); δ_C (100 MHz, $CDCl_3$): 34.4, 72.1, 80.8, 114.5, 119.7, 129.6, 146.3.
Experimental in agreement with reported data. [206]
Phenyl-di-prop-2-ynyl-amine A25: 19% yield; silica gel TLC R_f 0.88 (EtOAc/*n*-hexane 20 % *v/v*); δ_H (400 MHz, DMSO-d_6): 2.27 (t, *J* = 2.4, 2H), 4.14 (d, *J* = 2.4, 4H), 6.93 (t, *J* = 7.6, 1H), 7.02 (d, *J* =7.6, 2H), 7.24 (t, *J* = 7.6, 2H); δ_C (100 MHz, $CDCl_3$): 41.1, 73.4, 79.1, 116.5, 120.8, 129.6, 147.6.
Experimental in agreement with reported data.[207]

Synthesis of 4-prop-2-ynyloxy-benzenesulfonamide **A12.**

Compound **A12** was obtained according the general procedure earlier reported. The reaction mixture was stirred at 60°C for 5h and then was quenched with H_2O (20 ml). The obtained suspension was stirred overnight at r.t.. The formed precipitate was filtered-off and purified by silica gel column chromatography eluting with 50 % EtOAc in *n*-hexane to afford the title compound **A12**.

4-Prop-2-ynyloxy-benzenesulfonamide A12: 71% yield; m.p. 131-132°C; silica gel TLC R_f 0.47 (EtOAc/*n*-hexane 50 % *v/v*); δ_H (400 MHz, DMSO-d_6): 3.66 (t, J = 2.4, 1H), 4.94 (d, J = 2.4, 2H), 7.17 (d, J = 8.8, 2H), 7.26 (s, 2H, exchange with D_2O, SO_2NH_2), 7.80 (d, J = 8.8, 2H); δ_C (100 MHz, DMSO-d_6): 56.7, 79.6, 79.7, 115.9, 128.6, 137.8, 160.4.

Experimental in agreement with reported data.[208]

General synthetic procedure of phenylazides **A2, A26- A34, B4**.[209]

The proper aniline (0.5g, 1.0eq) was dissolved in a 4M HCl aqueous solution (5 ml) at 0°C. $NaNO_2$ (1.2 eq) was slowly added and the resulting solution was stirred at the same temperature for 0.5h. Then NaN_3 (1.5 eq) was added portion-wise and the mixture was stirred at r.t. for 0.5h. Reaction mixture was filtered-off or extracted with Et_2O (2 x 15 ml) and the combined organic layers were dried over Na_2SO_4, filtered-off and the solvent evaporated in *vacuo* to afford the corresponding phenylazide which was used without further purification.

Synthesis of 4-azido-benzenesulfonamide **A2.**

Compound **A2** was obtained according the general procedure earlier reported. Sulfanilamide was treated with $NaNO_2$ and NaN_3 in a HCl 2M aqueous solution and the formed precipitate was filtered-off to afford the titled compound **A2** as a yellow solid.

4-Azidobenzenesulfonamide A2: 60% yield; m.p. 120-121°C; silica gel TLC R_f 0.47 (EtOAc/*n*-hexane 50 % *v/v*); δ_H (400 MHz, DMSO-d_6): 7.33 (d, J = 8.8, 2H), 7.41 (s, 2H,

exchange with D_2O, SO_2NH_2), 7.87 (d, J = 8.8, 2H); δ_C (100 MHz, DMSO-d_6): 120.5, 128.6, 141.5, 143.9.
Experimental in agreement with reported data.[128]

Synthesis of phenylazide **A26.**

Compound **A26** was obtained according the general procedure earlier reported.
Phenylazide A26: 60% yield; silica gel TLC R_f 0.76 (EtOAc/*n*-hexane 50 % *v/v*); δ_H (400 MHz, DMSO-d_6):7.12 (d, J = 7.6, 2H), 7.20 (t, J = 7.6, 1H), 7.42 (t, J = 7.6, 2H); δ_C (100 MHz, DMSO-d_6): 120.0, 126.1, 131.0, 140.3.
Experimental in agreement with reported data.[209]

Synthesis of 3-methoxyphenylazide **A27.**

Compound **A27** was obtained according the general procedure earlier reported.
3-Methoxyphenyl azide A27: 74% yield; silica gel TLC R_f 0.78 (EtOAc/*n*-hexane 50 % *v/v*); δ_H (400 MHz, DMSO-d_6): 3.80 (s, 3H, CH_3), 6.66 (t, J = 2.4, 1H), 6.74 (ddd, J = 0.8, 2.4, 8.2, 1H), 6.81 (ddd, J = 0.8, 2.4, 8.2, 1H), 7.36 (t, J = 8.2, 1H); δ_C (100 MHz, DMSO-d_6): 56.3, 105.7, 112.0, 112.1, 131.7, 141.5, 161.5.
Experimental in agreement with reported data.[209]

Synthesis of 4-fluorophenylazide **A28.**

Compound **A28** was obtained according the general procedure earlier reported.
4-Fluorophenylazide A28: 89% yield; silica gel TLC R_f 0.79 (EtOAc/*n*-hexane 50 % *v/v*); δ_H (400 MHz, DMSO-d_6): 67.19 (m, 2H), 7.29 (t, J = 8.8, 2H); δ_F (376 MHz, DMSO-d_6): -117.77 (s, 1F); δ_C (100 MHz, DMSO-d_6): 117.7 (d, J^2_{CF} = 23), 121.8 (d, J^3_{CF} = 9.0), 136.4, 160.3 (d, J^1_{CF} = 241.0).
Experimental in agreement with reported data.[210]

Synthesis of 4-trifluoromethyl-phenyl azide **A29.**

Compound **A29** was obtained according the general procedure earlier reported.

4-Trifluoromethylphenylazide A29: 67% yield; silica gel TLC R_f 0.84 (EtOAc/*n*-hexane 50 % *v/v*); δ_H (400 MHz, DMSO-d_6): 7.35 (d, J = 8.8, 2H), 7.78 (d, J = 8.8, 2H); δ_F (376 MHz, DMSO-d_6): -56.18 (s, 3F); δ_C (100 MHz, DMSO-d_6): 120.8, 125.0 (d, J^1_{CF} = 269.6), 126.2 (q, J^2_{CF} = 32.0), 130.0, 144.7.

Experimental in agreement with reported data.[211]

Synthesis of 4-hydroxy-phenyl azide **A30.**

Compound **A30** was obtained according the general procedure earlier reported.

4-Hydroxyphenylazide A30: 46% yield; silica gel TLC R_f 0.84 (EtOAc/*n*-hexane 50 % *v/v*); δ_H (400 MHz, DMSO-d_6): 6.84 (d, J = 8.8, 2H), 6.97 (d, J = 8.8, 2H), 9.56 (bs, 1H, exchange with D_2O, O*H*); δ_C (100 MHz, DMSO-d_6): 117.5, 121.1, 130.6, 156.0.

Experimental in agreement with reported data.[212]

Coumarins (series B) - *General synthetic procedure of compounds* B5-B18.[128]

The appropriate alkyne **A18, A23-A24** (previously reported in series **A** experimental section) or **B2** (1.0 eq) was added to a suspension of aryl azide **A2, A26-A30** (previously reported in series **A** experimental section) or **A31-A34** (1.1 eq) in H_2O/*tert*-BuOH 1/1 (3.5 ml) at r.t., followed by copper (0) nanosized (0.1 eq) and TMACl (1.0 eq). The suspension was stirred at 60°C until starting materials were consumed (TLC monitoring), then quenched with H_2O (20 ml) and the formed precipitate was filtered-off and washed with H_2O. The solid was dissolved in a minimal amount of acetone, the obtained solution was filtered through Celite 521® and then concentrated under *vacuo* to give a residue that was triturated with Et_2O or DCM to afford the titled compounds **B5-B18.**

Synthesis of 7-(1-phenyl-1H-[1,2,3]triazol-4-ylmethoxy)-chromen-2-one **B5.**

7-(1-Phenyl-1*H*-[1,2,3]triazol-4-ylmethoxy)-chromen-2-one **B5** was obtained according the general procedure earlier reported using phenylazide **A26** (1.1eq), 7-(prop-2-ynyloxy)-2*H*-chromen-2-one **B2** (0.05g, 1.0 eq) in *tert*-ButOH/H_2O (1/1, 3.5 ml),

tetramethylamonium chloride (1.0 eq) and copper nanosize (0.1 eq). The reaction mixture was stirred for 5h to give the titled compound **B5** as a white solid.

7-(1-Phenyl-1*H*-[1,2,3]triazol-4-ylmethoxy)-chromen-2-one B5: 74 % yield; m.p. 172-175°C; silica gel TLC R_f 0.52 (EtOAc/*n*-hexane 50 % *v/v*); δ_H (400 MHz, DMSO-d_6): 5.41 (s, 2H, CH_2), 6.35 (d, *J* = 9.6, 1H), 7.11 (dd, *J* = 2.4, 8.6 , 1H), 7.25 (d, *J* = 2.4, 1H), 7.56 (t, *J* = 7.6, 1H), 7.66 (t, *J* = 7.6, 2H), 7.70 (d, *J* = 8.6, 1H), 7.96 (d, *J* = 7.6, 2H), 8.05 (d, *J* = 9.6, 1H), 9.05 (s, 1H); δ_C (100 MHz, DMSO-d_6): 63.0, 102.6, 113.6, 113.7, 113.8, 121.2, 124.1, 129.8, 130.5, 130.9, 138.0, 144.1, 145.2, 156.2, 161.2, 162.0; *m/z* (ESI positive) 320.0 $[M+H]^+$.

Synthesis of 7-[1-(3-fluoro-phenyl)-1H-[1,2,3]triazol-4-ylmethoxy]-chromen-2-one **B6.**

7-[1-(3-Fluoro-phenyl)-1*H*-[1,2,3]triazol-4-ylmethoxy]-chromen-2-one **B6** was obtained according the general procedure earlier reported using 3-fluorophenylazide **A31** (1.1 eq), 7-(prop-2-ynyloxy)-2*H*-chromen-2-one **B2** (0.05g, 1.0 eq) in *tert*-ButOH/H_2O (1/1, 3.5 ml), tetramethylamonium chloride (1.0 eq) and copper nanosize (0.1 eq). The reaction mixture was stirred for 1.5h to give the titled compound **B6** as a white solid.

7-[1-(3-Fluoro-phenyl)-1*H*-[1,2,3]triazol-4-ylmethoxy]-chromen-2-one B6: 77 % yield; m.p. 158-160°C; silica gel TLC R_f 0.45 (Ethyl acetate/*n*-hexane 50 % *v/v*); δ_H (400 MHz, DMSO-d_6): 5.42 (s, 2H, CH_2), 6.36 (d, *J* = 9.6, 1H), 7.11 (dd, *J* = 2.4, 8.6 , 1H), 7.25 (d, *J* = 2.4, 1H), 7.42 (m, 1H), 7.71 (m, 2H), 7.86 (m, 1H), 7.91 (m, 1H), 8.05 (d, *J* = 9.6, 1H), 9.10 (s, 1H); δ_F (376 MHz, DMSO-d_6): -110.52 (s, 1F); δ_C (100 MHz, DMSO-d_6): 62.5, 102.5, 108.1 (d, J^2_{CF} = 26.3), 113.6, 113.7, 113.8, 116.4 (d, J^2_{CF} = 21.0), 117.0, 124.2, 130.5, 132.8 (d, J^3_{CF} = 9.0), 138.6 (d, J^3_{CF} = 10.4), 144.3, 145.1, 156.2, 161.2, 161.9, 162.8 (d, J^1_{CF} =262.7); *m/z* (ESI positive) 338.0 $[M+H]^+$.

Synthesis of 7-[1-(3-chloro-phenyl)-1H-[1,2,3]triazol-4-ylmethoxy]-chromen-2-one **B7.**

1-Azido-3-chlorobenzene **A32** (1.1 eq) and 7-(prop-2-ynyloxy)-2*H*-chromen-2-one **B2** (0.05g, 1.0 eq) were dissolved in *tert*-ButOH/H_2O 1/1 (3.5ml) and then tetramethylamonium chloride (1.0 eq) and copper nanosize (10 % mol) were added. The

mixture was stirred at 60°C for 3.5h and then treated as described in general procedure to afford **B7** as a white solid.

7-[1-(3-Chloro-phenyl)-1*H*-[1,2,3]triazol-4-ylmethoxy]-chromen-2-one B7: 77 % yield; m.p. 182-183°C; silica gel TLC R_f 0.41 (Ethyl acetate/*n*-hexane 50 % *v/v*); δ_H (400 MHz, DMSO-d_6): 5.41 (s, 2H, CH_2), 6.36 (d, *J* = 9.6, 1H), 7.10 (dd, *J* = 2.4, 8.6 , 1H), 7.24 (d, *J* = 2.4, 1H), 7.66 (m, 3H), 7.97 (d, *J* = 8.1, 1H), 8.05 (d, *J* = 9.6, 1H), 8.11 (d, *J* = 2.0, 1H), 9.12 (s, 1H); δ_C (100 MHz, DMSO-d_6): 62.5, 102.3, 113.6, 113.7, 113.8, 119.7, 120.9, 124.3, 129.6, 130.5, 132.6, 135.1, 138.5, 144.3, 145.2, 156.2, 161.1, 161.9*; m*/z (ESI positive) 354.0 $[M+H]^+$.

Synthesis of 7-[1-(3-bromo-phenyl)-1H-[1,2,3]triazol-4-ylmethoxy]-chromen-2-one **B8.**

1-Azido-3-bromobenzene **A33** (1.1 eq) and 7-(prop-2-ynyloxy)-2*H*-chromen-2-one **B2** (0.05g, 1.0 eq) were dissolved in *tert*-ButOH/H_2O 1/1 (3.5 ml) and then tetramethylamonium chloride (1.0 eq) and copper nanosize (10 % mol) were added. The mixture was stirred at 60°C for 6h and then treated as described in general procedure to afford **B8** as a white solid.

7-[1-(3-Bromo-phenyl)-1*H*-[1,2,3]triazol-4-ylmethoxy]-chromen-2-one B8: 78 % yield; m.p. 170-172°C ; silica gel TLC R_f 0.41 (Ethyl acetate/*n*-hexane 50 % *v/v*); δ_H (400 MHz, DMSO-d_6): 5.41 (s, 2H, CH_2), 6.36 (d, *J* = 9.6, 1H), 7.10 (dd, *J* = 2.4, 8.6, 1H), 7.24 (d, *J* = 2.4, 1H), 7.61 (t, *J* = 8.2, 1H), 7.71 (d, *J* = 8.6, 1H), 7.76 (d, *J* = 8.2, 1H), 8.02 (d, *J* = 8.2, 1H), 8.05 (d, *J* = 9.6, 1H), 8.23 (s, 1H), 9.12 (s, 1H); δ_C (100 MHz, DMSO-d_6): 62.5, 102.6, 113.6, 113.7, 113.8, 120.1, 123.4, 123.7, 124.3, 130.5, 132.5, 132.8, 138.5, 144.3, 145.2, 156.0, 161.1, 161.9; *m/z* (ESI positive) 398.0 $[M+H]^+$.

Synthesis of 7-[1-(3-methoxy-phenyl)-1H-[1,2,3]triazol-4-ylmethoxy]-chromen-2-one **B9.**

1-Azido-3-methoxybenzene **A27** (1.1 eq) and 7-(prop-2-ynyloxy)-2*H*-chromen-2-one **B2** (0.05, 1.0 eq) were dissolved in *tert*-ButOH/H_2O 1/1 (3.5ml) and then tetramethylamonium chloride (1.0 eq) and copper nanosize (10 % mol) were added. The

mixture was stirred at 60°C for 2.5h and then treated as described in general procedure to afford **B9** as a white solid.

7-[1-(3-Methoxy-phenyl)-1*H*-[1,2,3]triazol-4-ylmethoxy]-chromen-2-one B9: 81 % yield; m.p. 131-133°C; silica gel TLC R_f 0.36 (Ethyl acetate/*n*-hexane 50 % *v/v*); δ_H (400 MHz, DMSO-d_6): 3.89 (s, 3H, CH_3), 5.40 (s, 2H, CH_2), 6.36 (d, J = 9.6, 1H), 7.11 (m, 2H), 7.24 (d, J = 2.4, 1H), 7.54 (m, 3H), 7.70 (d, J = 8.6, 1H), 8.05 (d, J = 9.6, 1H), 9.07 (s, 1H); δ_C (100 MHz, DMSO-d_6): 56.6, 62.7, 102.6, 106.6, 113.1, 113.6, 113.7, 113.8, 115.5, 124.2, 130.5, 131.8, 138.5, 144.0, 145.2, 156.2, 131.1, 161.2, 162.0; *m/z* (ESI positive) 350.0 $[M+H]^+$.

Synthesis of 7-[1-(4-fluoro-phenyl)-1H-[1,2,3]triazol-4-ylmethoxy]-chromen-2-one **B10.**

7-[1-(4-fluoro-phenyl)-1*H*-[1,2,3]triazol-4-ylmethoxy]-chromen-2-one **B10** was obtained according the general procedure earlier reported using 1-azido-4-fluorobenzene **A28** (1.1 eq), 7-(prop-2-ynyloxy)-2*H*-chromen-2-one **B2** (0.05g, 1.0 eq) in *tert*-ButOH/H_2O 1/1 (3.5 ml), tetramethylamonium chloride (1.0 eq) and copper nanosize (0.1 eq).The reaction mixture was stirred for 7.5h to give the titled compound **B10** as a white solid.

7-[1-(4-Fluoro-phenyl)-1*H*-[1,2,3]triazol-4-ylmethoxy]-chromen-2-one B10: 68 % yield; m.p. 201-203°C; silica gel TLC R_f 0.34 (Ethyl acetate/*n*-hexane 50 % *v/v*); δ_H (400 MHz, DMSO-d_6): 5.40 (s, 2H, CH_2), 6.36 (d, J = 9.2, 1H), 7.10 (dd, J = 2.4, 8.6, 1H), 7.24 (d, J = 2.4, 1H), 7.51 (m, 2H), 7.70 (d, J = 8.6, 1H), 8.00 (m, 2H), 8.05 (d, J = 9.2, 1H), 9.02 (s, 1H); δ_F (376 MHz, DMSO-d_6): -112.94 (s, 1F); δ_C (100 MHz, DMSO-d_6): 62.4, 102.4, 113.5, 113.6, 113.7, 117.6 (d, J^2_{CF} = 23.1), 123.4 (d, J^3_{CF} = 8.8), 124.3, 130.7, 133.9 (d, J^4_{CF} = 2.9), 144.0, 145.1, 156.1, 161.0, 161.8, 162.5 (d, J^1_{CF} = 244.4); *m/z* (ESI positive) 338.0 $[M+H]^+$.

Synthesis of 7-[1-(4-trifluoromethyl-phenyl)-1H-[1,2,3]triazol-4-ylmethoxy]-chromen-2-one **B11.**

7-[1-(4-trifluoromethyl-phenyl)-*1H*-[1,2,3]triazol-4-ylmethoxy]-chromen-2-one **B11** was obtained according the general procedure earlier reported using 1-azido-4-

trifluoromethylbenzene **A29** (1.1 eq), 7-(prop-2-ynyloxy)-2*H*-chromen-2-one **B2** (0.05g, 1.0 eq) in *tert*-ButOH/H_2O 1/1 (3.5 ml), tetramethylamonium chloride (1.0 eq) and copper nanosize (0.1 eq). The reaction mixture was stirred for 2.5h to give the titled compound **B11** as a white powder.

7-[1-(4-Trifluoromethyl-phenyl)-1*H*-[1,2,3]triazol-4-ylmethoxy]-chromen-2-one B11: 70 % yield; m.p. 185-187°C; silica gel TLC R_f 0.50 (Ethyl acetate/*n*-hexane 50 % *v/v*); δ_H (400 MHz, DMSO-d_6): 5.43 (s, 2H, CH_2), 6.35 (d, *J* = 9.6, 1H), 7.10 (dd, *J* = 2.4, 8.6 , 1H), 7.24 (d, *J* = 2.4, 1H), 7.70 (d, *J* = 8.6, 1H), 8.05 (m, 3H), 8.22 (d, *J* = 8.4, 2H), 9.19 (s, 1H); δ_C (100 MHz, DMSO-d_6): 62.5, 102.6, 113.7, 113.7, 113.8, 121.6, 123.9 (d, J^1_{CF} = 270.6), 124.4, 128.2 (q, J^3_{CF} = 3.4), 129.8 (d, J^2_{CF} = 32.7), 130.5, 140.2, 144.5, 145.2, 156.2, 161.2, 161.9; *m/z* (ESI positive) 388.0 $[M+H]^+$.

Synthesis of 7-[1-(4-hydroxy-phenyl)-1H-[1,2,3]triazol-4-ylmethoxy]-chromen-2-one **B12.**

1-Azido-4-hydroxybenzene **A30** (1.1 eq) and 7-(prop-2-ynyloxy)-2*H*-chromen-2-one **B2** (0.05g, 1.0 eq) were dissolved in *tert*-ButOH/H_2O 1/1 (3.5ml) and then tetramethylamonium chloride (1.0 eq) and copper nanosize (10 % mol) were added. The mixture was stirred at 60°C for 1.5h and then treated as described in general procedure to afford **B12** as a white solid.

7-[1-(4-Hydroxy-phenyl)-1*H*-[1,2,3]triazol-4-ylmethoxy]-chromen-2-one B12: 77 % yield; m.p. 241-242°C; silica gel TLC R_f0.21 (Ethyl acetate/*n*-hexane 50 % *v/v*); δ_H (400 MHz, DMSO-d_6): 5.37 (s, 2H, CH_2), 6.35 (d, *J* = 9.6, 1H), 6.98 (d, *J* = 8.6, 2H), 7.10 (dd, *J* = 2.4, 8.6 , 1H), 7.24 (d, *J* = 2.4, 1H), 7.70 (m, 3H), 8.05 (d, *J* = 9.6, 1H), 8.85 (s, 1H), 10.00 (s, 1H, exchange with D_2O, O*H*); δ_C (100 MHz, DMSO-d_6): 62.6, 102.6, 113.6, 113.7, 113.8, 117.0, 123.0, 124.0, 129.6, 130.5, 143.7, 145.2, 156.2, 158.8, 161.2, 162.0; *m/z* (ESI positive) 336.0 $[M+H]^+$.

Synthesis of 7-[1-(4-carboxy-phenyl)-1H-[1,2,3]triazol-4-ylmethoxy]-chromen-2-one **B13.**

1-Azido-4-carboxybenzene **A34** (1.1 eq) and 7-(prop-2-ynyloxy)-2*H*-chromen-2-one **B2** (0.05, 1.0 eq) were dissolved in *tert*-ButOH/H_2O 1/1 (3.5ml) and then tetramethylamonium chloride (1.0 eq) and copper nanosize (10 % mol) were added. The mixture was stirred at 60°C for 12h and treated as described in general procedure to afford **B13** as a white solid.

7-[1-(4-Carboxy-phenyl)-1*H*-[1,2,3]triazol-4-ylmethoxy]-chromen-2-one B13: 55 % yield; m.p. 290-292°C d; silica gel TLC R_f 0.34 (MeOH/CH_2Cl_2 10 % *v/v*); δ_H (400 MHz, DMSO-d_6): 5.42 (s, 2H, CH_2), 6.36 (d, *J* = 9.2, 1H), 7.10 (dd, *J* = 2.4, 8.6 , 1H), 7.25 (d, *J* = 2.4, 1H), 7.71 (d, *J* = 8.6, 1H), 8.05 (d, *J* = 9.2, 1H), 8.15 (m, 4H), 9.16 (s, 1H), 13.34 (bs, 1H, exchange with D_2O, COO*H*); *m/z* (ESI negative) 362.17 $[M-H]^-$.

Synthesis of 4-[4-(2-oxo-2H-chromen-7-yloxymethyl)-[1,2,3]triazol-1-yl]-benzenesulfonamide **B14.**

4-Azidobenzenesulfonamide **A2** (1.1 eq) and 7-(prop-2-ynyloxy)-2*H*-chromen-2-one **B2** (0.05, 1.0 eq) were dissolved in *tert*-ButOH/H_2O 1/1 (3.5ml) and then tetramethylamonium chloride (1.0 eq) and copper nanosize (10 % mol) were added. The mixture was stirred at 60°C for 2.5h and then treated as described in general procedure to afford **B14** as a light yellow solid.

4-[4-(2-Oxo-2*H*-chromen-7-yloxymethyl)-[1,2,3]triazol-1-yl]-benzenesulfonamide B14: 80 % yield; m.p. 279-281°C; silica gel TLC R_f 0.43 (MeOH/CH_2Cl_2 10 % *v/v*); δ_H (400 MHz, DMSO-d_6): 5.43 (s, 2H, CH_2), 6.36 (d, *J* = 9.2, 1H), 7.10 (dd, *J* = 2.4, 8.6, 1H), 7.25 (d, *J* = 2.4, 1H), 7.59 (s, 2H, exchange with D_2O, SO_2NH_2), 7.71 (d, *J* = 8.6, 1H), 8.06 (m, 3H), 8.19 (d, *J* = 8.8, 2H), 9.15 (s, 1H); δ_C (100 MHz, DMSO-d_6): 62.5, 102.6, 113.7, 113.8, 113.9, 121.4, 124.4, 128.5, 130.5, 139.4, 144.5, 144.9, 145.2, 156.3, 161.2, 161.9; *m/z* (ESI negative) 397.0 $[M-H]^-$.

Synthesis of 4-methyl-7-[4-(2-oxo-2H-chromen-7-yloxymethyl)-[1,2,3]triazol-1-yl]-chromen-2-one **B15.**

4-Methyl-7-[4-(2-oxo-2*H*-chromen-7-yloxymethyl)-[1,2,3]triazol-1-yl]-chromen-2-one **B15** was obtained according the general procedure earlier reported using 7-azido-4-

methyl-2*H*-chromen-2-one **B4** (1.1 eq) and 7-(prop-2-ynyloxy)-2*H*-chromen-2-one **B2** (0.05g, 1.0 eq) in *tert*-ButOH/H_2O 1/1 (3.5ml), tetramethylamonium chloride (1.0 eq) and copper nanosize (10 % mol). The reaction mixture was stirred for 6h to give a solid that was purified by silica gel column chromatography eluting with ethyl acetate in *n*-hexane from 20 % to 50 % to afford the title compound **B15** as a yellow solid.

4-Methyl-7-(4-((2-oxo-2*H*-chromen-7-yloxy)methyl)-1*H*-1,2,3-triazol-1-yl)-2*H*-chromen-2-one B15: 88 % yield; silica gel TLC R_f 0.32 (EtOAc/*n*-hexane 50% *v/v*); δ_H (400 MHz, DMSO-d_6) 2.11 (s, 3H, CH_3), 5.44 (s, 2H, CH_2), 6.35 (d, *J* = 9.6, 1H), 6.53 (d, *J* = 1.2, 1H), 7.11 (dd, *J* = 2.4, 8.4, 1H), 7.25 (d, *J* = 2.4, 1H), 7.71 (d, *J* = 8.4, 1H), 8.06 (m, 4H), 9.22 (s, H); δ_C (100 MHz, DMSO-d_6) 32.2, 62.5, 102.6, 108.0, 108.6, 113.7, 113.9, 115.8, 116.6, 120.6, 124.4, 128.2, 130.5, 139.3, 144.5, 145.2, 153.7, 154.3, 156.2, 160.3, 161.0, 161.9; *m/z* (ESI positive) 402.0 $[M+H]^+$.

Synthesis of 4-methyl-7-(4-phenoxymethyl-[1,2,3]triazol-1-yl)-chromen-2-one **B16).**

7-Azido-4-methyl-2*H*-chromen-2-one **B4** (1.1 eq) and prop-2-ynyloxy-benzene **A18** (0.05g, 1.0 eq) were dissolved in *tert*-ButOH/H_2O 1/1 (3.5ml) and then tetramethylamonium chloride (1.0 eq) and copper nanosize (10 % mol) were added. The mixture was stirred at 60°C for 2h and then treated as described in general procedure to afford **B16** as a yellow solid.

4-Methyl-7-(4-phenoxymethyl-[1,2,3]triazol-1-yl)-chromen-2-one B16: 70 % yield; m.p. 208-209°C; silica gel TLC R_f 0.40 (EtOAc/*n*-hexane 50 % *v/v*); δ_H (400 MHz, DMSO-d_6): 2.51 (s, 3H, CH_3), 5.30 (s, 2H, CH_2), 6.53 (d, *J* = 1.2, 1H), 7.02 (t, *J* = 7.6, 1H), 7.13 (d, *J* = 7.6, 2H), 7.37 (t, *J* = 7.6, 2H), 8.06 (m, 3H), 9.18 (s, 1H); δ_C (100 MHz, DMSO-d_6): 19.0, 61.8, 108.5, 115.6, 115.7, 116.5, 120.5, 121.9, 124.0, 128.2, 130.5, 139.4, 145.3, 153.7, 154.5, 158.9, 160.3; *m/z* (ESI positive) 334.0 $[M+H]^+$.

Synthesis of 4-methyl-7-(4-phenylsulfanylmethyl-[1,2,3]triazol-1-yl)-chromen-2-one **B17.**

7-Azido-4-methyl-2*H*-chromen-2-one **B4** (1.1 eq) and prop-2-ynylsulfanyl-benzene **A23** (0.05g, 1.0 eq) were dissolved in *tert*-ButOH/H_2O 1/1 (3.5ml) and then tetramethylamonium chloride (1.0 eq) and copper nanosize (10 % mol) were added. The

mixture was stirred at 60°C for 2h and then treated as described in general procedure to afford **B17** as a yellow solid.

4-Methyl-7-(4-phenylsulfanylmethyl-[1,2,3]triazol-1-yl)-chromen-2-one B17: 68 % yield; m.p. 178-179°C; silica gel TLC R_f 0.44 (EtOAc/n-hexane 50 % *v/v*); δ_H (400 MHz, DMSO-d_6): 2.51 (s, 3H, CH_3), 4.44 (s, 2H, CH_2), 6.52 (d, J = 1.2, 1H), 7.24 (t, J = 7.6, 1H), 7.37 (t, J = 7.6, 2H), 7.45 (d, J = 7.6, 2H), 8.00 (m, 3H), 8.94 (s, 1H); δ_C (100 MHz, DMSO-d_6): 19.0, 28.1, 108.3, 115.6, 116.3, 120.3, 122.6, 127.0, 128.2, 129.3, 130.2, 136.4. 139.3, 146.2, 153.7, 154.6, 160.4; *m/z* (ESI positive) 350.0 $[M+H]^+$.

Synthesis of 4-Methyl-7-(4-phenylaminomethyl-[1,2,3]triazol-1-yl)-chromen-2-one **B18.**

7-Azido-4-methyl-2*H*-chromen-2-one **B4** (1.1 eq) and phenyl-prop-2-ynyl-amine **A24** (0.05g, 1.0 eq) were dissolved in *tert*-ButOH/H_2O 1/1 (3.5ml) and then tetramethylamonium chloride (1.0 eq) and copper nanosize (10 % mol) were added. The mixture was stirred at 60°C for 2.5h and then treated as described in general procedure to afford **B18** as a yellow solid.

4-Methyl-7-(4-phenylaminomethyl-[1,2,3]triazol-1-yl)-chromen-2-one B18: 85% yield; m.p. 197-200°C; silica gel TLC R_f 0.30 (EtOAc/*n*-hexane 50 % *v/v*); δ_H (400 MHz, DMSO-d_6): 2.51 (s, 3H, CH_3), 4.43 (d, J = 6.0, 2H, CH_2), 6.20 (t, J = 6.0, 1H, exchange with D_2O, NH), 6.52 (d, J = 1.2, 1H), 6.60 (t, J = 7.8, 1H), 6.71 (d, J = 7.8, 2H), 7.12 (t, J =7.8, 2H), 8.03 (m, 3H), 8.94 (s, 1H); δ_C (100 MHz, DMSO-d_6): 19.0, 39.5, 108.2, 113.3, 115.5, 116.2, 117.1, 120.2, 122.3, 128.2, 129.8, 139.5, 148.3, 149.2, 153.7, 154.6, 160.4; *m/z* (ESI positive) 333.0 $[M+H]^+$.

Synthesis of 7-prop-2-ynyloxy-chromen-2-one **B2.**

Propargyl bromide (1.2 eq) was added to a suspension of compound **B1** (0.5 g, 1.0 eq) and K_2CO_3 (2.0 eq) in dry DMF (4 ml) under a nitrogen atmosphere and that was stirred at r.t. until starting material was consumed (TLC monitoring). The reaction mixture was quenched with H_2O (20 ml) and extracted with Et_2O or EtOAc (25 ml). The organic layer was washed with brine (4x15ml), dried over Na_2SO_4, filtered-off and concentrated under *vacuo* to give the titled compounds **B2.**

7-Prop-2-ynyloxy-chromen-2-one B2: 73% yield; m.p. 118-119°C; silica gel TLC R_f 0.56 (EtOAc/*n*-hexane 50 % *v/v*); δ_H (400 MHz, DMSO-d_6): 3.69 (t, J = 2.4, 1H), 4.97 (d, J = 2.4, 2H), 6.36 (d, J = 9.6, 1H), 7.03 (dd, J = 2.4, 8.6, 1H), 7.09 (d, J = 2.4, 1H), 7.70 (d, J = 8.6, 1H), 8.04 (d, J = 9.6, 1H); δ_C (100 MHz, DMSO-d_6): 57.0, 79.4, 79.8, 102.7, 113.7, 113.8, 113.9, 130.4, 145.1, 156.0, 161.0, 161.1.
Experimental in agreement with reported data. [213]

Synthesis of 7-azido-4-methyl-chromen-2-one **B4**

7-Azido-4-methyl-chromen-2-one **B4** was obtained according the general procedure reported earlier for aromatic azides (in series **A** experimental section). 7-Amino-4-methyl-coumarin **B3** was treated with $NaNO_2$ and NaN_3 in a HCl 2M aqueous solution and the formed precipitate was filtered-off to afford the title compound **B4** as a yellow solid.
7-Azido-4-methyl-chromen-2-one B4: 88% yield; m.p. 122-124°C; silica gel TLC R_f 0.57 (EtOAc/*n*-hexane 20 % *v/v*); δ_H (400 MHz, DMSO-d_6): 2.46 (d, J = 1.2, 3H, CH_3), 6.38 (d, J = 1.2, 1H), 7.18 (m, 2H), 7.83 (d, J = 8.4, 1H); δ_C (100 MHz, DMSO-d_6): 19.0, 107.7, 114.1, 116.5, 117.7, 127.9, 144.2, 153.8, 155.0, 160.4.
Experimental in agreement with reported data.[214]

Synthesis of 3-fluorophenylazide **A31**

3-Fluorophenylazide **A31** was obtained according to the general procedure reported earlier for aromatic azides (in series **A** experimental section).
3-Fluorophenyl azide A31: 62% yield; silica gel TLC R_f 0.81 (EtOAc/*n*-hexane 50 % *v/v*); δ_H (400 MHz, DMSO-d_6): 7.06 (m, 3H), 7.46 (q, J = 7.2, 1H); δ_F (376 MHz, DMSO-d_6): -110.52 (s, 1F); δ_C (100 MHz, DMSO-d_6): 107.6 (d, J^2_{CF} = 25.0), 112.8 (d, J^2_{CF} = 21.0), 116.2, 132.5 (d, J^3_{CF} = 9.0), 142.5 (d, J^3_{CF} = 9.0), 163.7 (d, J^1_{CF} = 245.0).
Experimental in agreement with reported data.[215]

Synthesis of 3-chlorophenylazide **A32**

3-Chlorophenylazide **A32** was obtained according to the general procedure reported earlier for aromatic azides (in series **A** experimental section).

3-Chlorophenyl azide A32: 86% yield; silica gel TLC R_f 0.84 (EtOAc/*n*-hexane 50 % *v/v*); δ_H (400 MHz, DMSO-d_6): 7.14 (dd, J = 2.2, 8.0, 1H), 7.24 (t, J = 2.2, 1H), 7.30 (d, J = 2.2, 1H), 7.46 (t, J = 8.0, 1H); δ_C (100 MHz, DMSO-d_6): 118.9, 120.1, 126.0, 132.4, 135.1, 142.2.

Experimental in agreement with reported data.[215]

Synthesis of 3-bromophenylazide **A33**

3-Bromophenylazide **A33** was obtained according to the general procedure reported earlier for aromatic azides (in series **A** experimental section).

3-Bromophenylazide A33. 88% yield; silica gel TLC R_f 0.83 (EtOAc/*n*-hexane 50 % *v/v*); δ_H (400 MHz, DMSO-d_6): 7.18 (dt, J = 1.6, 7,2, 1H), 7.38 (m, 3H); δ_C (100 MHz, DMSO-d_6): 119.3, 122.8, 123.5, 128.9, 132.7, 142.3.

Experimental in agreement with reported data.[215]

Synthesis of 4-azidobenzoic acid **A34**

4-Azidobenzoic acid **A34** was obtained according the general procedure reported earlier for aromatic azides (in series **A** experimental section). 4-Aminobenzoic acid was treated with $NaNO_2$ and NaN_3 in a 4M HCl aqueous solution and the formed precipitate was filtered-off to afford the title compound **A34** as a yellow solid.

4-Azidobenzoic acid A34: 73% yield; m.p. 188-190°C d; silica gel TLC R_f 0.71 (EtOAc/*n*-hexane 50 % *v/v*); δ_H (400 MHz, DMSO-d_6): 7.25 (d, J = 8.4, 2H), 7.99 (d, J = 8.4, 2H), 13.02 (bs, 1H, exchange with D_2O, COOH); δ_C (100 MHz, DMSO-d_6): 120.2, 128.3, 132.2, 144.9, 167.6.

Experimental in agreement with reported data.[216]

Sulfocoumarins (series C) - *General Synthetic procedure of compounds* C2-C9.[128]

7-Prop-2-ynyloxy-benzo[e][1,2]oxathiine 2,2-dioxide **C1** (1.0 eq) was added to a suspension of aryl azide **A26-A34** (previously reported in series **A** and **B** experimental section) (1.1 eq) in H_2O/^{t}BuOH 1/1 (3.5 ml) at r.t., followed by copper (0) nanosized (0.1 eq) and TMACl (1.0 eq). The suspension was stirred at 60°C until starting materials were consumed (TLC monitoring), then quenched with H_2O (20 ml) and the formed precipitate was filtered-off and washed with H_2O. The solid was dissolved in a minimal amount of acetone, the obtained solution was filtered through Celite 521® and then concentrated under *vacuo* to give a residue that was triturated with Et_2O or DCM to afford the titled compounds **C2-C9.**

Synthesis of 4-(2,2-dioxo-2H-2λ^6-benzo[e][1,2]oxathiin-7-yloxymethyl)-1-phenyl-1H-[1,2,3]triazole **C2.**

4-(2,2-Dioxo-2H-2λ6-benzo[e][1,2]oxathiin-7-yloxymethyl)-1-phenyl-1H-[1,2,3]triazole **C2** was obtained according the general procedure earlier reported using phenylazide **A26** (1.1eq), 7-prop-2-ynyloxy-benzo[e][1,2]oxathiine 2,2-dioxide **C1** (0.05g, 1.0 eq) in *tert*-ButOH/H_2O (1/1, 3.5 ml), tetramethylamonium chloride (1.0 eq) and copper nanosize (0.1 eq).The reaction mixture was stirred for 7h to give the titled compound **C2** as a white solid.

4-(2,2-Dioxo-2*H*-2λ^6-benzo[e][1,2]oxathiin-7-yloxymethyl)-1-phenyl-1*H*-[1,2,3]triazole C2: 72% yield; m.p. 141-143°C; silica gel TLC R_f 0.39 (EtOAc/*n*-hexane 50 % *v/v*); δ_H (400 MHz, DMSO-d_6): 5.41 (s, 2H, CH_2), 7.16 (dd, J = 2.4, 8.8 , 1H), 7.30 (d, J = 2.4, 1H), 7.37 (d, J = 10.4, 1H), 7.55 (t, J = 7.6, 1H), 7.67 (m, 4H), 7.95 (d, J = 7.6, 2H), 9.05 (s, 1H); δ_C (100 MHz, DMSO-d_6): 62.7, 105.6, 113.2, 114.4, 120.3, 121.2, 124.2, 129.8, 130.7, 132.2, 137.4, 137.4, 143.9, 153.2, 161.9; *m/z* (ESI positive) 356.0 $[M+H]^+$.

Synthesis of 1-(3-chloro-phenyl)-4-(2,2-dioxo-2H-2λ^6-benzo[e][1,2]oxathiin-7-yloxymethyl)-1H-[1,2,3]triazole **C3.**

1-Azido-3-chlorobenzene **A32** (1.1 eq) and 7-prop-2-ynyloxy-benzo[e][1,2]oxathiine 2,2-dioxide **C1** (0.05g, 1.0 eq) were dissolved in *tert*-ButOH/H_2O 1/1 (3.5 ml) and then tetramethylamonium chloride (1.0 eq) and copper nanosize (10 % mol) were added. The

mixture was stirred at 60°C for 3.5h and then treated as described in general procedure to afford **C3** as a white solid.

1-(3-Chloro-phenyl)-4-(2,2-dioxo-2*H*-2λ⁶-benzo[e][1,2]oxathiin-7-yloxymethyl)-1*H*-[1,2,3]triazole C3: 71% yield; m.p. 174-176°C; silica gel TLC R_f 0.26 (EtOAc/*n*-hexane 50 % *v/v*); δ_H (400 MHz, DMSO-d_6): 5.41 (s, 2H, CH_2), 7.16 (dd, *J* = 2.4, 8.8, 1H), 7.28 (d, *J* = 2.4, 1H), 7.37 (d, *J* = 10.4, 1H), 7.66 (m, 4H), 7.97 (d, *J* = 8.8, 1H), 8.10 (s ,1H), 9.11 (s, 1H); δ_C (100 MHz, DMSO-d_6): 62.6, 105.6, 113.2, 114.4, 119.7, 120.3, 121.0, 124.4, 129.6, 132.2, 132.6, 135.2, 137.4, 138.5, 144.1, 153.2, 161.8; *m/z* (ESI positive) 390.0 $[M+H]^+$.

Synthesis of 1-(3-bromo-phenyl)-4-(2,2-dioxo-2H-2λ⁶-benzo[e][1,2]oxathiin-7-yloxymethyl)-1H-[1,2,3]triazole **C4.**

1-Azido-3-bromobenzene **A33** (1.1 eq) and 7-prop-2-ynyloxy-benzo[e][1,2]oxathiine 2,2-dioxide **C1** (0.05g, 1.0 eq) were dissolved in *tert*-ButOH/H_2O 1/1 (3.5 ml) and then tetramethylamonium chloride (1.0 eq) and copper nanosize (10 % mol) were added. The mixture was stirred at 60°C for 3.5h and then treated as described in general procedure to afford **C4** as a white solid.

1-(3-Bromo-phenyl)-4-(2,2-dioxo-2*H*-2λ⁶-benzo[e][1,2]oxathiin-7-yloxymethyl)-1*H*-[1,2,3]triazole C4: 79% yield; m.p. 171-173°C; silica gel TLC R_f 0.49 (EtOAc/*n*-hexane 50 % *v/v*); δ_H (400 MHz, DMSO-d_6): 5.41 (s, 2H, CH_2), 7.16 (dd, *J* = 2.4, 8.8 , 1H), 7.30 (d, *J* = 2.4, 1H), 7.37 (d, *J* = 10.4, 1H), 7.61 (t, *J* = 8.4, 1H), 7.69 (m, 2H), 7.76 (d, *J* = 8.4, 1H), 8.01 (d, *J* = 8.4, 1H), 8.23 (t, *J* = 2.0, 1H), 9.11 (s, 1H); δ_C (100 MHz, DMSO-d_6): 62.7, 105.6, 113.3, 114.4, 120.2, 120.4, 123.4, 123.8, 124.4, 132.2, 132.6, 132.8, 137.4, 138.6, 144.1, 153.2, 161.9; *m/z* (ESI positive) 434.0 $[M+H]^+$.

Synthesisof 4-(2,2-Dioxo-2H-2λ⁶-benzo[e][1,2]oxathiin-7-yloxymethyl)-1-(3-methoxy-phenyl)-1H-[1,2,3]triazole **C5.**

4-(2,2-Dioxo-2H-2λ6-benzo[e][1,2]oxathiin-7-yloxymethyl)-1-(3-methoxy-phenyl)-1H-[1,2,3]triazole **C5** was obtained according the general procedure earlier reported using 1-azido-3-methoxybenzene **A27** (1.1 eq), 7-prop-2-ynyloxy-benzo[e][1,2]oxathiine 2,2-

dioxide **C1** (0.05g, 1.0 eq) in *tert*-ButOH/H_2O 1/1 (3.5 ml), tetramethylamonium chloride (1.0 eq) and copper nanosize (0.1 eq). The reaction mixture was stirred for 6.5h to give the titled compound **C5** as a white solid.

4-(2,2-Dioxo-2*H*-2λ⁶-benzo[e][1,2]oxathiin-7-yloxymethyl)-1-(3-methoxy-phenyl)-1*H*-[1,2,3]triazole C5 : 68% yield; m.p. 129-131°C; silica gel TLC R_f 0.40 (EtOAc/*n*-hexane 50 % *v/v*); δ_H (400 MHz, DMSO-d_6): 3.90 (s, 3H, CH_3), 5.41 (s, 2H, CH_2), 7.11 (d, *J* = 7.2, 1H), 7.16 (dd, *J* = 2.4, 8.8 , 1H), 7.30 (d, *J* = 2.4, 1H), 7.37 (d, *J* = 10.4, 1H), 7.54 (m, 3H), 7.69 (m, 2H), 9.06 (s, 1H); δ_C (100 MHz, DMSO-d_6): 56.6, 62.7, 105.6, 106.8, 113.1, 113.2, 114.3, 115.5, 120.3, 124.3, 131.8, 132.1, 137.4, 138.5, 143.9, 153.2, 161.1, 161.9; *m/z* (ESI positive) 386.0 $[M+H]^+$.

Synthesis of 4-(2,2-dioxo-2H-2λ⁶-benzo[e][1,2]oxathiin-7-yloxymethyl)-1-(4-fluoro-phenyl)-1H-[1,2,3]triazole **C6.**

1-Azido-4-fluorobenzene **A28** (1.1 eq) and 7-prop-2-ynyloxy-benzo[e][1,2]oxathiine 2,2-dioxide **C1** (0.05g, 1.0 eq) were dissolved in *tert*-ButOH/H_2O 1/1 (3.5 ml) and then tetramethylamonium chloride (1.0 eq) and copper nanosize (10 % mol) were added. The mixture was stirred at 60°C for 2.5h and then treated as described in general procedure to afford **C6** as a white solid.

4-(2,2-Dioxo-2*H*-2λ⁶-benzo[e][1,2]oxathiin-7-yloxymethyl)-1-(4-fluoro-phenyl)-1*H*-[1,2,3]triazole C6: 63% yield; m.p. 168-170°C ; silica gel TLC R_f 0.33 (EtOAc/*n*-hexane 50 % *v/v*); δ_H (400 MHz, DMSO-d_6): 5.41 (s, 2H, CH_2), 7.16 (dd, *J* = 2.4, 8.8, 1H), 7.29 (d, *J* = 2.4, 1H), 7.37 (d, *J* = 10.4, 1H), 7.51 (t, *J* = 8.8, 2H), 7.69 (m, 2H), 8.00 (m, 2H), 9.01 (s, 1H); δ_F (376 MHz, DMSO-d_6): -112.92 (s, 1F); δ_C (100 MHz, DMSO-d_6): 62.7, 105.6, 113.2, 114.4, 117.7 (d, $J\ ^2_{CF}$ = 23.0), 120.3, 123.6 (d, $J\ ^1_{CF}$ = 8.9), 124.5, 132.2, 134.0, 137.4, 144.0, 153.2, 161.9, 162.7 (d, $J\ ^1_{CF}$ = 245.2); *m/z* (ESI positive) 374.0 $[M+H]^+$.

Synthesis of 4-(2,2-dioxo-2H-2λ⁶-benzo[e][1,2]oxathiin-7-yloxymethyl)-1-(4-trifluoromethyl-phenyl)-1H-[1,2,3]triazole **C7.**

1-Azido-4-trifluoromethylbenzene **A29** (1.1 eq) and 7-prop-2-ynyloxy-benzo[e][1,2]oxathiine 2,2-dioxide **C1** (0.05g, 1.0 eq) were dissolved in *tert*-ButOH/H_2O 1/1 (3.5 ml) and then tetramethylamonium chloride (1.0 eq) and copper nanosize (10 % mol) were added. The mixture was stirred at 60°C for 5h and then treated as described in general procedure to afford **C7** as a white solid.

4-(2,2-Dioxo-2*H*-2λ^6-benzo[e][1,2]oxathiin-7-yloxymethyl)-1-(4-trifluoromethyl-phenyl)-1*H*-[1,2,3]triazole C7: 74% yield; m.p. 210-212°C; silica gel TLC R_f 0.40 (EtOAc/*n*-hexane 50 % *v/v*); δ_H (400 MHz, DMSO-d_6): 5.43 (s, 2H, CH_2), 7.16 (dd, *J* = 2.4, 8.8 , 1H), 7.29 (d, *J* = 2.4, 1H), 7.37 (d, *J* = 10.4, 1H), 7.69 (m, 2H), 8.04 (d, *J* = 8.4, 2H), 8.22 (d, *J* = 8.4, 2H), 9.19 (s, 1H); δ_C (100 MHz, DMSO-d_6): 62.7, 105.6, 113.3, 114.4, 120.4, 121.7, 124.5, 124.8 (d, J^1_{CF} = 270.4), 128.2, 129.8 (d, J^2_{CF} = 32.0), 132.2, 137.4, 140.3, 144.4, 153.3, 161.9; *m/z* (ESI positive) 324.0 $[M+H]^+$.

Synthesis of 4-(2,2-dioxo-2H-2λ^6-benzo[e][1,2]oxathiin-7-yloxymethyl)-1-(4-hydroxy-phenyl)-1H-[1,2,3]triazole **C8.**

1-Azido-4-hydroxybenzene **A30** (1.1 eq) and 7-prop-2-ynyloxy-benzo[e][1,2]oxathiine 2,2-dioxide **C1** (0.05g, 1.0 eq) were dissolved in *tert*-ButOH/H_2O 1/1 (3.5 ml) and then tetramethylamonium chloride (1.0 eq) and copper nanosize (10 % mol) were added. The mixture was stirred at 60°C for 4h and then treated as described in general procedure to afford **C7** as a white solid.

4-(2,2-Dioxo-2*H*-2λ^6-benzo[e][1,2]oxathiin-7-yloxymethyl)-1-(4-hydroxy-phenyl)-*1H*-[1,2,3]triazole C8: 82% yield; m.p. 244-246°C; silica gel TLC R_f 0.35 (EtOAc/*n*-hexane 50 % *v/v*); δ_H (400 MHz, DMSO-d_6): 5.38 (s, 2H, CH_2), 6.98 (d, *J* = 8.8, 2H), 7.15 (dd, *J* = 2.4, 8.8 , 1H), 7.28 (d, *J* = 2.4, 1H), 7.37 (d, *J* = 10.4, 1H), 7.69 (m, 4H), 8.84 (s, 1H), 10.00 (s, 1H, exchange with D_2O, O*H*); δ_C (100 MHz, DMSO-d_6): 62.7, 105.6, 113.2, 114.3, 117.0, 120.3, 123.0, 124.1, 129.6, 132.1, 137.42, 143.5, 153.2, 158.8, 161.9; *m/z* (ESI positive) 372.0 $[M+H]^+$.

Synthesis of 1-(4-carboxy-phenyl)-4-(2,2-dioxo-2H-2λ^6-benzo[e][1,2]oxathiin-7-yloxymethyl)-1H-[1,2,3]triazole **C9.**

1-Azido-carboxybenzene **A34** (1.1 eq) and 7-prop-2-ynyloxy-benzo[e][1,2]oxathiine 2,2-dioxide **C1** (0.05g, 1.0 eq) were dissolved in *tert*-ButOH/H_2O 1/1 (3.5 ml) and then tetramethylamonium chloride (1.0 eq) and copper nanosize (10 % mol) were added. The mixture was stirred at 60°C for 12.5h and then treated as described in general procedure to afford **C9** as a white solid.

1-(4-Carboxy-phenyl)-4-(2,2-dioxo-2*H*-2λ^6-benzo[e][1,2]oxathiin-7-yloxymethyl)-1*H*-[1,2,3]triazole C9: 22% yield; m.p. >300°C; silica gel TLC R_f 0.42 (MeOH/CH_2Cl_2 10 % *v/v*); δ_H (400 MHz, DMSO-d_6): 5.43 (s, 2H, CH_2), 7.17 (dd, *J* = 2.4, 8.8 , 1H), 7.30 (d, *J* = 2.4, 1H), 7.38 (d, *J* = 10.4, 1H), 7.69 (m, 2H), 8.11 (d, *J* = 8.4, 2H), 8.19 (d, *J* = 8.4, 2H), 9.16 (s, 1H), 13.31 (bs, 1H, exchange with D_2O, COO*H*); *m/z* (ESI positive) 400.0 $[M+H]^+$.

Synthesis 7-prop-2-ynyloxy-benzo[e][1,2]oxathiine 2,2-dioxide **C1**

Propargyl bromide (1.2 eq) was added to a suspension of compound **C16** (0.5 g, 1.0 eq) and K_2CO_3 (2.0 eq) in dry DMF (4 ml) under a nitrogen atmosphere and that was stirred at r.t. for 2h. The reaction mixture was quenched with H_2O (20 ml) and extracted with EtOAc (25 ml). The organic layer was washed with brine (4x15ml), dried over Na_2SO_4, filtered-off and concentrated under *vacuo* to give a residue that was triturated with Et_2O to afford the titled compound **C1** as a white powder.

7-Prop-2-ynyloxy-benzo[e][1,2]oxathiine 2,2-dioxide C1: 54% yield; m.p. 150-151°C; silica gel TLC R_f 0.83 (EtOAc/n-hexane 50 % *v/v*); δ_H (400 MHz, DMSO-d_6): 3.70 (t, *J* = 2.4, 1H), 4.98 (d, *J* = 2.4, 2H), 7.07 (dd, *J* = 2.4, 8.4, 1H), 7.15 (d, *J* = 2.4, 1H), 7.37 (d, *J* = 10.4, 1H), 7.68 (m, 2H); δ_C (100 MHz, DMSO-d_6): 57.21, 79.28, 80.03, 105.70, 113.43, 114.42, 120.51, 132.11, 137.40, 153.07, 161.03.

Synthesis 7-hydroxybenzo[e][1,2]oxathiine 2,2-dioxide **C16**

7-Hydroxybenzo[e][1,2]oxathiine 2,2-dioxide **C16** was synthesized as previously reported by Zalubovski's group.[141]

4.1.2 Carbonic Anhydrase Inhibition.

The CA inhibitory profiles of compounds belonging to series **A**, **B** and **C** were obtained according to the general procedures described at the beginning of the experimental section.

4.1.3 Computational studies.

Computational studies for compounds belonging to series **A** were performed according to the general procedures described at the beginning of the experimental section.

4.1.4 Co-crystallization and X-ray data collection.

Crystals of hCA II complexed with compounds **A3** and **A13** were obtained using the sitting drop vapor diffusion method. An equal volume of 0.8 mM solution of hCA II in Tris pH=8.0 and 1.6 mM of the inhibitors in Hepes 20mM pH=7.4 was mixed and incubated for 15 minutes. 2 µl of the complex solution were mixed with 2 µl of a solution of 1.5, 1.6 and 1.7 M sodium citrate, 50 mM Tris pH 8.0 and were equilibrated against 500 µl of the same solution at 296 K in 24 well Linbro plate. Crystals of the complexes grew in a few days. The crystals were flash-frozen at 100K using a solution obtained by adding 25% (v/v) glycerol to the mother liquor solution as cryoprotectant. Data on crystals of the complexes with compounds **A3** and **A13** were collected using synchrotron radiation at the ID-23-1 beamline at ESRF (Grenoble, France) with a wavelength of 0.976 Å and a PILATUS 6M-F detector, to a maximum resolution of 1.05 and 1.00, respectively. Data were integrated and scaled using the program XDS.[217] Data processing statistics are showed in Table EXP1.

Table EXP1.

Summary of Data Collection and Atomic Model Refinement Statistics.[a]

	HCAII + *A*3	**HCAII + *A*13**
PDB ID	5LJQ	5LJT
Wavelength (Å)	0.976	0.976
Space Group	$P2_1$	$P2_1$
Unit cell (a,b,c,β) (Å, °)	42.37, 41.44, 72.22, 104.45	42.36, 41.40, 72.17 104.41
Limiting resolution (Å)	40.0-1.05 (1.11-1.05)	41.0-1.00 (1.06-1.00)
Unique reflections	109788	121936
Rsym (%)	6.1 (57.9)	6.0 (67.2)
Redundancy	4.75 (3.77)	3.5 (2.6)
Completeness overall (%)	97.1 (86.1)	93.7 (75.6)
<I/(I)>	12.61 (2.07)	10.22 (1.30)
Refinement statistics		
Resolution range (Å)	30.0-1.05	30.0- 1.00
Unique reflections, working/free	104237/5466	115805/6012
Rfactor (%)	13.35	13.82
Rfree(%)	14.85	15.72
No. of protein atoms	4176	4328
No. of water molecules	418	439
No. of heterogen atoms	52	66
r.m.s.d. bonds(Å)	0.0046	0.0047
r.m.s.d. angles (°)	1.176	1.189
Average B factor (Å²)		
All atoms	12.48	11.84
inhibitor	14.33	10.81
solvent	26.55	26.07

[a] Values in parentheses are for the highest resolution shell.

The crystal structure of hCA II (PDB accession code: 4FIK) without solvent molecules and other heteroatoms was used to obtain initial phases of the structures using Refmac5.[218] 5% of the unique reflections were selected randomly and excluded from the refinement data set for the purpose of Rfree calculations. The initial |Fo - Fc| difference electron density maps unambiguously showed the inhibitor molecules.

Atomic models for the inhibitors were calculated and energy minimized using the program JLigand 1.0.39. Geometrical restraints for the inhibitors were generated using

the Grade Web Server (http://grade.globalphasing.org). During the refinement, anisotropic temperature factors were introduced and hydrogen atoms were added to the models. Manual building of the models was performed using COOT.[219] Solvent molecules were introduced automatically using the program ARP.[220] The quality of the final models were assessed with COOT and Rampage.[221] Crystal parameters and refinement data are summarized in Table EXP1. Atomic coordinates were deposited in the Protein Data Bank (PDB accession codes: 5LJQ, 5LJT). Graphical representations were generated with Chimera.[222]

4.1.5 Hypertensive Rabbit IOP Lowering Studies.

Male New Zealand albino rabbits weighing 1500−2000 g were used in these studies. Animals were anesthetized using zoletil (tiletamine chloride plus zolazepam chloride, 3 mg/kg body weight, im) and injected with 0.1 mL of hypertonic saline solution (5% in distilled water) into the vitreous of both eyes. IOP was determined using a tonometer (Tono-pen Avia tonometer, Reichhert Inc., Depew, NY 14043, USA) prior to hypertonic saline injection (basal) at 1, 2, 3, and 4 h after administration of the drug. Vehicle (phosphate buffer 7.00 plus DMSO 2%) or drugs were instilled immediately after the injection of hypertonic saline. Eyes were randomly assigned to different groups. Vehicle or drug (0.50 mL) was directly instilled into the conjunctive pocket at the desired doses (1−2%).[226] The IOP was followed for 4 h after drug administration. Four different animals were used for each tested compound. All animal manipulations were carried out according to the European Community guidelines for animal care [DL 116/92, application of the European Communities Council Directive of 24 November 1986 (86/609/EEC)]. The ethical policy of the University of Florence complies with the Guide for the Care and Use of Laboratory Animals of the US National Institutes of Health (NIH Publication No. 85-23, revised 1996; University of Florence assurance number A5278-01). Formal approval to conduct the experiments described was obtained from the Animal Subjects Review Board of the University of Florence. Experiments involving animals have been reported according to ARRIVE - Animal Research: Reporting of in Vivo Experiments–guidelines.[225] All efforts were made to minimize animal suffering and to reduce the number of animals used.

4.2. Deciphering the mechanism of human carbonic anhydrase inhibition with sulfocoumarins

4.2.1 Chemistry.

The general chemistry protocols are reported at the beginning of the experimental section.

***General synthetic procedure of derivatives* D4-D6**.[141]

MsCl (1.2 eq) was added to a solution of the proper 2-hydroxybenzaldehyde **D1-D3** (0.5 g, 1.0 eq) and TEA (1.4 eq) in dry DCM (10 ml) at 0°C under a nitrogen atmosphere and the reaction mixture was stirred at r.t. until the consumption of the starting material (TLC monitoring). The reaction was quenched with H_2O (25 mL) and extracted with EtOAc (2 x 30 mL). The combined organic layers were washed with brine, dried over Na_2SO_4, filtered-off and concentrated under *vacuo* to yield the titled compounds **D4-D6**.

Synthesis of 2-formylphenyl methanesulfonate **D4.**

2-Formylphenyl methanesulfonate **D4** was obtained according the general procedure earlier reported using 2-hydroxybenzaldehyde **D1** (0.6 g, 1.0 eq), MsCl (1.2 eq) and TEA (1.4 eq) in dry DCM (10 ml).

2-Formylphenyl methanesulfonate D4: 73% yield; silica gel TLC R_f 0.67 (EtOAc/n-hexane 50 % v/v); δ_H (400 MHz, DMSO-d_6): 3.59 (s, 3H, CH_3), 7.58 (m, 2H, Ar), 7.82 (m, 1H, Ar), 7.92 (m, 1H, Ar), 10.24 (s, 1H, C*H*O); δ_C (100 MHz, DMSO-d_6): 37.8, 123.8, 128.0, 129.0, 129.2, 136.1, 149.7, 188.7.

Experimental data in agreement with reported data.[141]

Synthesis of 4-chloro-2-formylphenyl methanesulfonate **D5.**

4-Chloro-2-formylphenyl methanesulfonate **D5** was obtained according the general procedure earlier reported using 5-chloro-2-hydroxybenzaldehyde **D2** (0.6 g, 1.0 eq), MsCl (1.2 eq) and TEA (1.4 eq) in dry DCM (10 ml).

4-Chloro-2-formylphenyl methanesulfonate D5: 85% yield; silica gel TLC R_f *0*.38 (EtOAc/n-hexane 30 % v/v); δ_H (400 MHz, DMSO-*d*$_6$): 3.61 (s, 3H, C*H*$_3$), 7.31 (dd, *J* = 0.8, 8.4, 1H, Ar), 7.90 (m, 2H, Ar), 10.18 (s, 1H, C*H*O); δ_C (100 MHz, DMSO-*d*$_6$): 38.8, 127.0, 129.3, 131.5, 133.4, 136.5, 149.2, 188.6; GC-MS (EI): m/z 234 $[M]^{+*}$.

Synthesis of 2-formyl-5-nitrophenyl methanesulfonate **D6.**

2-Formyl-5-nitrophenyl methanesulfonate **D6** was obtained according the general procedure earlier reported using 2-hydroxy-4-nitrobenzaldehyde **D3** (0.6 g, 1.0 eq), MsCl (1.2 eq) and TEA (1.4 eq) in dry DCM (10 ml).

2-Formyl-5-nitrophenyl methanesulfonate D6: 82% yield; silica gel TLC R_f 0.27 (EtOAc/n-hexane 30 % v/v); δ_H (400 MHz, DMSO-*d*$_6$): 3.73 (s, 3H, C*H*$_3$), 8.18 (d, *J* = 9.2, 1H, Ar), 8.40 (m, 2H, Ar), 10.32 (s, 1H, C*H*O); δ_C (100 MHz, DMSO-*d*$_6$): 38.7, 120.2, 123.5, 131.2, 134.4, 150.4, 152.0, 188.6; GC-MS (EI): m/z 245 $[M]^{+*}$.

Synthesis of 2-hydroxy-4-nitrobenzaldehyde **D3.**[226]

BBr_3 1.0M in DCM (1.8 eq) was added dropwise to a solution of 2-methoxy-4-nitrobenzaldehyde (0.5 g, 1.0 eq) in dry DCM (15 ml) cooled to -78°C. The reaction mixture was allowed to slowly reach r.t., stirred o.n. and then quenched with slush. The aqueous layer was separated and extracted with ethyl acetate (15 ml). The combined organic layers were washed with brine, dried over anhydrous Na_2SO_4 and concentrated under *vacuo* the titled compound as a yellow solid.

2-Hydroxy-4-nitrobenzaldehyde D3: 80% yield; silica gel TLC R_f 0.28 (EtOAc/n-hexane 20 % v/v); δ_H (400 MHz, DMSO-*d*$_6$): 7.75 (dd, *J* = 2.2, 8.8, 1H, Ar), 7.81 (d, *J* = 2.2, 1H, Ar), 7.88 (d, *J* = 8.8, 1H, Ar), 10.41 (s, 1H, C*H*O), 11.64 (s, 1H, exchange with D_2O, O*H*); δ_C (100 MHz, DMSO-*d*$_6$): 113.0, 114.6, 127.7, 130.5, 152.4, 161.7, 190.4. Experimental data in agreement with reported data.[226]

***General synthetic procedure of sulfocoumarin* D10-D12**.[141]

DBU (1.05 eq) was added to a solution of **D4-D6** (0.6 g, 1.0 eq) in dry DCM (10 ml) at 0°C under a nitrogen atmosphere and the reaction mixture was stirred at the same temperature until the consumption of the starting material (TLC monitoring). The reaction was quenched with a mixture of ice and HCl 6M and extracted with EtOAc (2 x 30 mL). The organic layer was dried over Na_2SO_4, filtered-off and concentrated under *vacuo* to yield the titled compounds **D10-D12** in mixture with the alcoholic intermediates **D7-D9** in different ratio.

$POCl_3$ (1.2 eq) was added to a solution of the mixture of **D7-D9** and the corresponding **D10-D12** in pyridine (4 mL) cooled to 0°C. The reaction was stirred for 3h at room temperature and then quenched with slush. The formed precipitate was collected by filtration and purified by silica gel column chromatography eluting with EtOAc in *n*-hexane to afford the titled compounds **D10-D12** as white solids.

Synthesis of benzo[e][1,2]oxathiine 2,2-dioxide **D10.**

Compound **D10** was obtained according the general procedure earlier reported using 2-formylphenyl methanesulfonate **D4** (0.6 g, 1.0 eq) and DBU (1.05 eq) in dry DCM (10 ml) and thereafter treating the obtained mixture with $POCl_3$ (1.2 eq) in pyridine (4 ml). The crude was purified by silica gel column chromatography eluting with 30% EtOAc in *n*-hexane.

Benzo[e][1,2]oxathiine 2,2-dioxide D10: 42% yield; m.p. 80-81°C; silica gel TLC R_f 0.23 (EtOAc/n-hexane 30 % v/v); δ_H (400 MHz, DMSO-d_6): 7.46 (m, 2H, Ar), 7.55 (d, J = 10.3, 1H, Ar), 7.62 (m, 1H, Ar), 7.74 (m, 2H, Ar); δ_C (100 MHz, DMSO-d_6): 118.4, 118.9, 122.7, 126.3, 130.0, 132.6, 136.6, 150.8; GC-MS (EI): m/z 182 $[M]^{+*}$.

Experimental data in agreement with reported data.[141]

Synthesis of 6-chlorobenzo[e][1,2]oxathiine 2,2-dioxide **D11.**

Compound **D11** was obtained according the general procedure earlier reported using 4-chloro-2-formylphenyl methanesulfonate **D5** (0.6 g, 1.0 eq) and DBU (1.05 eq) in dry DCM (10 ml) and thereafter treating the obtained mixture with $POCl_3$ (1.2 eq) in pyridine (4 ml). The crude was purified by silica gel column chromatography eluting with 30% EtOAc in *n*-hexane.

***6*-Chlorobenzo[e][1,2]oxathiine 2,2-dioxide D11:** 60% yield; m.p. 137-139°C; silica gel TLC R_f 0.28 (EtOAc/n-hexane 50 % v/v); δ_H (400 MHz, DMSO-d_6): 7.55 (d, J = 8.8, 1H, Ar), 7.69 (m, 3H, Ar), 7.91 (d, J = 2.4, 1H, Ar); δ_C (100 MHz, DMSO-d_6): 121.3, 121.4, 124.7, 130.3, 131.1, 132.9, 136.4, 150.3; GC-MS (EI): m/z 216 $[M]^{+*}$.

Synthesis of 7-nitrobenzo[e][1,2]oxathiine 2,2-dioxide **D12.**

Compound **D12** was obtained according the general procedure earlier reported using 5-nitro-2-formylphenyl methanesulfonate **D6** (0.6 g, 1.0 eq) and DBU (1.05 eq) in dry DCM (10 ml) and thereafter treating the obtained mixture with $POCl_3$ (1.2 eq) in pyridine (4 ml). The crude was purified by silica gel column chromatography eluting with 40% EtOAc in *n*-hexane.

7-Nitrobenzo[e][1,2]oxathiine 2,2-dioxide D12: 35% yield; m.p. 138-140°C; silica gel TLC R_f 0.38 (EtOAc/n-hexane 50 % v/v); δ_H (400 MHz, DMSO-d_6): 7.88 (m, 2H, Ar), 8.05 (d, J = 8.4, 1H, Ar), 8.30 (dd, J = 2.0, 8.4, 1H, Ar), 8.37 (d, J = 2.0, 1H, Ar); δ_C (100 MHz, DMSO-d_6): 115.2, 122.0, 125.0, 126.3, 132.3, 136.2, 149.7, 151.4; GC-MS (EI): m/z 227 $[M]^{+*}$.

Synthesis of 7-amminobenzo[e][1,2]oxathiine 2,2-dioxide **D13**.[141]

Iron powder (8.0 eq) was added to a solution of 7-nitrobenzo[e][1,2]oxathiine 2,2-dioxide **D12** (0.4 g, 1.0 eq) in acetic acid (0.06 ml), water (4.4 ml) and ethanol (2.9 ml) The mixture was stirred at 75 °C for 1 h, cooled to room temperature and treated with EtOAc (40 ml). The organic layer was washed with saturated $NaHCO_3$ solution (30 ml), dried over Na_2SO_4 and concentrated under *vacuo* to give **D12** which was further purified by silica gel column chromatography eluting with 50% EtOAc in *n*-hexane.

7-**Amminobenzo[e][1,2]oxathiine 2,2-dioxide D13:** 54% yield; m.p. 150-152°C; silica gel TLC R_f 0.32 (EtOAc/n-hexane 50 % v/v); δ_H (400 MHz, DMSO-d_6): 6.32 (bs, 2H, exchange with D_2O, NH_2), 6.45 (d, J = 2.0, 1H, Ar), 6.45 (dd, J = 2.0, 8.4, 1H, Ar), 6.95 (d, J = 10.2, 1H, Ar), 7.31 (d, J = 8.4, 1H, Ar), 7.44 (d, J = 10.2, 1H, Ar); δ_C (100 MHz, DMSO-d_6): 102.3, 107.8, 112.0, 115.7, 132.0, 138.1, 153.9, 154.2; GC-MS (EI): m/z 197 $[M]^{+*}$.

Synthesis of 7-chlorobenzo[e][1,2]oxathiine 2,2-dioxide **D14.**

7-Amminobenzo[e][1,2]oxathiine 2,2-dioxide (**D13**) (0.1 g, 1.0 eq) was added to a suspension of tert-butyl nitrite (6.0 eq) and $CuCl_2$ (6.0 eq) in dry CH_3CN (5 ml) under a nitrogen atmosphere and the reaction mixture was stirred r.t. until the consumption of the starting material (TLC monitoring). The reaction was quenched with HCl 1.0M and extracted with EtOAc (2 x 20 mL). The organic layers were washed with HCl 1.0M (2x15 ml), dried over Na_2SO_4, filtered-off and concentrated under *vacuo* to afford a solid that was purified by silica gel column chromatography eluting with 30% EtOAc in *n*-hexane to yield **D14** as a light yellow solid.

7-Chlorobenzo[e][1,2]oxathiine 2,2-dioxide D14: 55% yield; m.p. 125-127°C; silica gel TLC R_f 0.50 (EtOAc/n-hexane 50 % v/v); δ_H (400 MHz, DMSO-d_6): 7.56 (dd, J = 2.0, 8.4, 1H, Ar), 8.05 (d, J = 10.4, 1H, Ar), 7.74 (d, J = 2.0, 1H, Ar), 7.78 (m, 2H, Ar); δ_C (100 MHz, DMSO-d_6): 118.7, 119.7, 123.6, 127.4, 132.2, 136.8, 137.2, 152.0; GC-MS (EI): m/z 216 $[M]^{+*}$.

4.2.2 Carbonic Anhydrase Inhibition

The CA inhibitory profiles of compounds belonging to series **D** were obtained according to the general procedures described at the beginning of the experimental section.

4.2.3 Computational methods.

Docking studies for sulfocoumarin were performed according to the general procedures described at the beginning of the experimental section.

The docked pose was prepositioned in the model system, fully minimized at the DFT/B3LYP level of theory, LACVP* basis set, and then a transition state search with Jaguar was undertaken in the same experimental conditions with QST method. Starting from the fully minimized reactant and product structures, a guess at the transition state was built and optimized.

Single point calculation have been carried out at the DFT/B3LYP level of theory, LACVP^{**+} basis set, and the nature of stationary points as true minima or first order

saddle points was checked by frequency calculations and unscaled ZPE corrections were applied to the energy values.
The reaction energy, computed as the difference between the product and reactant energies, was determined. In a similar fashion, the activation barrier was determined as the difference between the transition state energy and the energy of the reactants.

4.3 N-Nitrosulfonamides: a new chemotype for carbonic anhydrase inhibition (Series D).

4.3.1 Chemistry.

The general chemistry protocols are reported at the beginning of the experimental section.

***General synthetic procedure of compounds* E1-E8.**[159]

NH_4NO_3 (1.1 eq) was added portion wise to a solution of aromatic sulfonamides **AS1-AS8** (1.2 mmol, 1.0 eq) in 95% H_2SO_4 (1 mL) at 0°C. The suspension was stirred at the same temperature for 15 min, then quenched with slush (8 ml) and the formed precipitate was filtered-off and washed with cold water.

Synthesis of N^1-nitro-2-amino-benzenesulfonamide **E1.**

N^1-Nitro-2-amino-benzenesulfonamide **E1** was obtained according the general procedure earlier reported using 2-aminobenzenesulfonamide **AS1** (0.2g, 1.0 eq) and NH_4NO_3 (1.1 eq) in conc H_2SO_4 (1 ml). The obtained residue was recrystallized from H_2O to afford the titled compound **E1** as a white solid.
N^1-Nitrosulfanilamide E1: 71 % yield; δ_H (400 MHz, DMSO-d_6): 6.92 (t, J = 7.8, 1H), 6.97 (d, J = 7.8, 1H), 7.37 (td, J = 1.0, 7.8, 1H), 7.66 (dd, J = 1.0, 7.8, 1H); δ_C (100 MHz, DMSO-d_6): 121.6, 122.9, 129.6, 131.5, 134.0, 139.3; *m/z* (ESI negative) 215.9 $[M-H]^-$
Experimental in agreement with reported data.[159]

Synthesis of N^1-nitro-3-amino-benzenesulfonamide **E2.**

N^1-Nitrosulfanilamide **E2** was obtained according the general procedure earlier reported using 3-aminobenzenesulfonamide **AS2** (0.2g, 1.0 eq) and NH_4NO_3 (1.1 eq) in conc H_2SO_4 (1 ml). The obtained residue was recrystallized from H_2O to afford the titled compound **E2** as an orange solid.

N^1-Nitro-2-amino-benzenesulfonamide E2: 68% yield; δ_H (400 MHz, DMSO-d_6): 7.33 (d, J = 7.4, 1H), 7.53 (t, J = 7.4, 1H), 7.77 (m, 2H); δ_C (100 MHz, DMSO-d_6): 122.6, 126.1, 127.1, 130.8, 134.2, 145.0; *m/z* (ESI negative) 215.9 $[M-H]^-$

Synthesis of N^1-nitrosulfanilamide **E3.**

N^1-Nitrosulfanilamide **E3** was obtained according the general procedure earlier reported using sulfanilamide **AS3** (0.2g, 1.0 eq) and NH_4NO_3 (1.1 eq) in conc. H_2SO_4 (1 ml). The obtained residue was recrystallized from H_2O to afford the titled compound **E3** as a white solid.

N^1-Nitrosulfanilamide E3: 68% yield; δ_H (400 MHz, DMSO-d_6): 7.01 (d, J = 8.4, 2H), 7.68 (d, J = 8.4, 2H); δ_C (100 MHz, DMSO-d_6): 118.8, 130.7, 135.9, 143.7; *m/z* (ESI negative) 215.9 $[M-H]^-$

Experimental in agreement with reported data.[159]

Synthesis of N,N-dimethyl-N^1-Nitrosulfanilamide **E4.**

N,N-Dimethyl-N^1-nitrosulfanilamide **E4** was obtained according the general procedure earlier reported using N,N-dimethylsulfanilamide **AS4** (0.24g, 1.0 eq) and NH_4NO_3 (1.1 eq) in conc. H_2SO_4 (1 ml). The obtained residue was recrystallized from H_2O to afford the titled compound **E4** as a white solid.

N,N-Dimethyl-N^1-nitrosulfanilamide E4: 64 % yield; δ_H (400 MHz, DMSO-d_6): 3.02 (s, 6H, 2 x CH_3), 6.80 (d, J = 9.0, 2H), 7.62 (d, J = 9.0, 2H); δ_C (100 MHz, DMSO-d_6): 41.2, 112.2, 129.0, 130.7, 152.6; *m/z* (ESI negative) 243.9 $[M-H]^-$

Experimental in agreement with reported data.[159]

Synthesis of N^1-nitro-4-aminomethyl-benzensulfonamide **E5.**

N^1-Nitrosulfanilamide **E5** was obtained according the general procedure earlier reported using 4-aminomethyl-benzensulfonamide hydrochloride **AS5** (0.26g, 1.0 eq) and NH_4NO_3 (1.1 eq) in conc. H_2SO_4 (1 ml). The obtained residue was recrystallized from H_2O to afford the titled compound **E5** as a white solid.

N^1-Nitro-4-aminomethyl-benzensulfonamide E5: 72 % yield; δ_H (400 MHz, DMSO-d_6): 4.14 (s, 2H, CH_2), 6.80 (d, J = 8.0, 2H), 7.85 (d, J = 8.0, 2H), 8.19 (bs, 3H, exchange with D_2O, NH_3^+) ; δ_C (100 MHz, DMSO-d_6):42.9, 129.0, 129.5, 138.1, 143.6; *m/z* (ESI negative) 230.0 $[M-H]^-$

Experimental in agreement with reported data.[159]

Synthesis of N^1-Nitro-N-propargylsulfanilamide **E6.**

N^1-Nitro-N-propargylsulfanilamide **E6** was obtained according the general procedure earlier reported using N-propargylsulfanilamide **AS6** (0.25g, 1.0 eq) and NH_4NO_3 (1.1 eq) in conc.H_2SO_4 (1 ml).

N^1-Nitro-N-propargylsulfanilamide E6: 33% yield; δ_H (400 MHz, DMSO-d_6): 3.12 (t, J = 2.2, 1H), 3.95 (d, J = 2.2, 2H, CH_2), 6.66 (d, J = 8.8, 2H), 7.54 (d, J = 8.8, 2H); δ_C (100 MHz, DMSO-d_6): 32.6, 74.2, 82.3, 112.0, 129.1, 130.6, 151.3; *m/z* (ESI negative) 253.9 $[M-H]^-$

Synthesis of N^1-Nitro-3-amino-4-hydroxy-benzenesulfonamide **E7.**

N^1-Nitro-3-amino-4-hydroxy-benzenesulfonamide **E7** was obtained according the general procedure earlier reported using 3-amino-4-hydroxy-benzenesulfonamide **AS7** (0.22g, 1.0 eq) and NH_4NO_3 (1.1 eq) in conc. H_2SO_4 (1 ml). The obtained residue was recrystallized from acetonitrile to afford the titled compound **E7** as a grey solid.

N^1-Nitro-3-amino-4-hydroxy-benzenesulfonamide E7: 42 % yield; δ_H (400 MHz, DMSO-d_6): 7.49 (d, J = 2.4, 1H), 7.67 (d, J = 2.4, 1H); δ_C (100 MHz, DMSO-d_6): 116.2, 121.3, 134.4, 135.8, 135.9, 145.3; *m/z* (ESI negative) 316.9 $[M-H]^-$

Synthesis of N^1-nitro-5-amino-1,3,4-thiadiazole-2-sulfonamide **E8.**

N^1-Nitro-5-Amino-1,3,4-thiadiazole-2-sulfonamide **E8** was obtained according the general procedure earlier reported using 5-amino-1,3,4-thiadiazole-2-sulfonamide hydrochloride **AS8** (0.26g, 1.0 eq) and NH_4NO_3 (1.1 eq) in conc. H_2SO_4 (1 ml). The obtained residue was recrystallized from EtOH to afford the titled compound **E8** as a white solid.

N^1-Nitro-5-amino-1,3,4-thiadiazole-2-sulfonamide E8: 58% yield; δ_C (100 MHz, DMSO-d_6): 158.8, 172.4; *m/z* (ESI negative) 223.8 $[M-H]^-$

Synthesis of N,N-dimethyl sulfanilamide **AS4.**

Iodomethane (2.0 eq) was added dropwise to a suspension of sulfanilamide **AS3** (0.5g, 1.0 eq) and potassium carbonate (2.0 eq) in dry DMF (2 ml). The mixture was stirred at 50°C for 1h, then cooled and quenched with H_2O (20 ml) and the formed precipitate was filtered-off, washed with H_2O and recrystallized from aceton to afford the titled compound **AS4** as a white solid.

N,N-Dimethyl-sulfanilamide AS4: 43% yield; silica gel TLC R_f 0.47 (EtOAc/*n*-hexane 50 % *v/v*); δ_H (400 MHz, DMSO-d_6): 3.34 (s, 6H, 2 x CH_3), 6.79 (d, J = 9.0, 2H), 6.98 (s, 2H, exchange with D_2O, SO_2NH_2), 7.63 (d, J = 9.0, 2H); δ_C (100 MHz, DMSO-d_6):38.6, 113.6, 125.2, 129.6, 153.4.

Synthesis of N-propargylsulfanilamide **AS6.**

Propargyl bromide (1.2 eq) was added to a suspension of sulfanilamide **AS3** (0.5 g, 1.0 eq) and pyridine (1.2 eq) in dry DMF (2 ml) under a nitrogen atmosphere and that was stirred at r.t. overnight. The reaction mixture was quenched with H_2O (10 ml) and the formed precipitate was filtered-off and purified by silica gel column chromatography eluting with 60% ethyl acetate in *n*-hexane to afford **AS6** as a yellow solid.

N-Propargylsulfanilamide AS6: 22% yield; silica gel TLC R_f 0.47 (MeOH/DCM 10 % *v/v*); δ_H (400 MHz, DMSO-d_6): 3.14 (t, J = 2.0, 1H), 3.97(dd, J = 2.0, 6.2, 2H), 6.73 (d, J = 8.8, 2H, Ar), 6.76 (t, J = 6.2, 1H, exchange with D_2O, N*H*), 6.99 (s, 2H, exchange with

D2O, SO_2NH_2), 7.59 (d, J = 8.8, 2H, Ar); δ_C (100 MHz, DMSO-d_6): 37.1, 77.5, 77.7, 112.9, 122.6, 130.2, 154.5.

4.3.2 Carbonic anhydrase inhibition.

The CA inhibitory profiles of compounds belonging to series **E** were obtained according to the general procedures described at the beginning of the experimental section.

4.3.3 Computational studies

Computational studies for compounds belonging to series **E** were performed according to the general procedures described at the beginning of the experimental section.

4.4. Structure-based evaluation of the binding mode of several chemotypes within the β-CA from the dandruff-producing fungi Malassezia globosa.

4.4.1. Chemistry

DTCs **F1–F21** used in the experiments were reported earlier.[101,102]
Phenols **G1–G22** were commercially available from Sigma-Aldrich (Milan, Italy) and were used without further purification.
MTCs **H1–17** used in the experiments were reported earlier.[104]
Benzoxaboroles **I1-I23** investigated in this study were prepared as previously reported.[167]

4.4.2 Carbonic anhydrase inhibition.

The CA inhibitory profiles of compounds belonging to series **F, G, H** and **I** were obtained according to the general procedures described at the beginning of the experimental section.

4.4.3 Computational methods.

The web-based SWISS-MODEL platform[227,228]and Prime[199d] were used in building homology models of MgCA (UniProt entry identifier A8Q1N3). The 3D structure of the fungal enzyme from C. neoformans, Can2 (PDB file 2W3N), which shows 36% amino acid sequence identity with the MgCA, was used as template.[21] Chain A of Can2 was selected for the modelling studies due to the lower number of missing amino acid side chain atoms (compared to chain B).[21] The dimeric quaternary structure was obtained by applying the correct crystallographic symmetry operators defined in the above mentioned PDB file. The GMQE (Global Model Quality Estimation) score of 0.68 reflected a good quality of the model. Global and local model quality were also evaluated basing on the QMEAN scoring function. Finally, the Ramachandran plot of the target and template enzymes were compared.

Computational studies for compounds belonging to series **F**, **G, H** and **I** were performed according to the general procedures described at the beginning of the experimental section.

4.5 Novel nitrogenous bases-bearing benzenesulfonamides as carbonic a nhydrase IX inhibitors

4.5.1 Chemistry.

The general chemistry protocols are reported at the beginning of the experimental section.

***General synthetic procedure of benzenesulfonamides* J3-J7.**

EDC hydrochloride (1.2 eq) was added to a solution of 1-carboxymethyl uracil **J2** (0.2 g, 1.0 eq), NHS or HOAt (1.2 eq) and DMAP (0.03 eq) in dry DMF (3 ml) under a nitrogen atmosphere and the reaction mixture was stirred at r.t. until the consumption of the starting material (TLC monitoring). Thereafter the proper aminobenzenesulfonamide (1.1 eq) was added to the reaction mixture, that was stirred at r.t. until the disappearance of the activated ester was observed (TLC monitoring) and then quenched with $HCl_{(aq)}$ 1M.

The formed precipitate was filtered under *vacuo*, washed with water and recrystallized from a 1/1 mixture of water and the proper alcohol.

Synthesis of 2-(2,4-dioxo-3,4-dihydropyrimidin-1(2H)-yl)-N-(3-sulfamoylphenyl)acetamide **J3.**

Compound **J3** was obtained according the general procedure earlier reported using 1-carboxymethyl uracil **J2** (0.2 g, 1.0 eq), HOAt (1.2 eq), DMAP (0.03 eq) and 3-aminobenzenesulfonamide (1.1 eq) in dry DMF (3 ml). The crude solid was recrystallized from a 1/1 mixture of H_2O/2-MeO-EtOH to afford **J3** as a white solid.

2-(2,4-Dioxo-3,4-dihydropyrimidin-1(2H)-yl)-N-(3-sulfamoylphenyl)acetamide J3: 77% yield; m.p. 230-231°C; silica gel TLC R_f 0.36 (MeOH/CH_2Cl_2 20 % v/v); δ_H (400 MHz, DMSO-d_6): 4.61 (s, 2H, CH_2), 5.65 (dd, J = 2.0, 7.6, 1H, CH), 7.42 (s, 2H, exchange with D_2O, SO_2NH_2), 7.56 (m, 2H, Ar), 7.67 (d, J = 7.6, 1H, CH), 7.74 (m, 1H, Ar), 8.20 (s, 1H, Ar), 10.64 (s, 1H, exchange with D_2O, CONH), 11.40 (s, 1H, exchange with D_2O, CONHCO); δ_C (100 MHz, DMSO-d_6): 51.1, 101.5, 117.1, 121.5, 122.8, 130.5, 139.8, 145.7, 147.4, 152.0, 164.7, 167.0; m/z (ESI negative) 322.9 $[M-H]^-$.

Synthesis of 2-(2,4-dioxo-3,4-dihydropyrimidin-1(2H)-yl)-N-(4-sulfamoylphenyl)acetamide **J4.**

Compound **J4** was obtained according the general procedure earlier reported using 1-carboxymethyl uracil **J2** (0.2 g, 1.0 eq), HOAt (1.2 eq), DMAP (0.03 eq) and 4-aminobenzenesulfonamide (1.1 eq) in dry DMF (3 ml). The crude solid was recrystallized from a 1/1 mixture of H_2O/2-MeO-EtOH to afford **J4** as a white solid.

2-(2,4-dioxo-3,4-dihydropyrimidin-1(2H)-yl)-N-(3-sulfamoylphenyl)acetamide J4: 68% yield; m.p. 224-225°C; silica gel TLC R_f 0.29 (MeOH/CH_2Cl_2 20 % v/v); δ_H (400 MHz, DMSO-d_6): 4.62 (s, 2H, CH_2), 5.65 (dd, J = 2.0, 7.6, 1H, CH), 7.32 (s, 2H, exchange with D_2O, SO_2NH_2), 7.67 (d, J = 7.8, 1H, CH), 7.80 (m, 4H, Ar), 10.69 (s, 1H, exchange with D_2O, CONH), 11.41 (s, 1H, exchange with D_2O, CONHCO); δ_C (100 MHz, DMSO-d_6): 51.1, 101.5, 119.6, 127.7, 139.6, 142.3, 147.4, 152.0, 164.7, 167.1; m/z (ESI negative) 322.9 $[M-H]^-$.

Synthesis of 2-(2,4-dioxo-3,4-dihydropyrimidin-1(2H)-yl)-N-(4-sulfamoylbenzyl)acetamide **J5.**

Compound **J5** was obtained according the general procedure earlier reported using 1-carboxymethyl uracil **J2** (0.2 g, 1.0 eq), NHS (1.2 eq), DMAP (0.03 eq), 4-(aminomethyl)benzenesulfonamide hydrochloride (1.1 eq) and DIPEA (1.1 eq) in dry DMF (3 ml). The crude solid was recrystallized from a 1/1 mixture of H_2O/IPA to afford **J5** as a white solid.

2-(2,4-dioxo-3,4-dihydropyrimidin-1(2H)-yl)-N-(4-sulfamoylbenzyl)acetamide J5: 50% yield; m.p. 238-239°C; silica gel TLC R_f 0.33 (MeOH/CH_2Cl_2 20 % v/v); δ_H (400 MHz, DMSO-d_6): 4.40 (d, J = 5.6, 2H, CH_2), 4.44 (s, 2H, CH_2), 5.61 (dd, J = 2.0, 8.0, 1H, CH), 7.34 (s, 2H, exchange with D_2O, SO_2NH_2), 7.48 (d, J = 8.4, 2H, Ar), 7.63 (d, J = 8.0, 1H, CH), 7.80 (d, J = 8.4, 2H, Ar), 8.79 (t, J = 5.2, 1H, exchange with D_2O, CONH), 11.32 (bs, 1H, exchange with D_2O, CONHCO); δ_C (100 MHz, DMSO-d_6): 42.7, 50.7, 101.5, 126.5, 128.4, 143.6, 144.1, 147.4, 152.0, 164.8, 168.0; m/z (ESI negative) 337.0 $[M-H]^-$.

Synthesis of 2-(2,4-dioxo-3,4-dihydropyrimidin-1(2H)-yl)-N-(4-sulfamoylphenethyl)acetamide **J6.**

Compound **J6** was obtained according the general procedure earlier reported using 1-carboxymethyl uracil **J2** (0.2 g, 1.0 eq), NHS (1.2 eq), DMAP (0.03 eq), 4-(aminoethyl)benzenesulfonamide (1.1 eq) in dry DMF (3 ml). The crude solid was recrystallized from a 1/1 mixture of H_2O/EtOH to afford **J6** as a white solid.

2-(2,4-dioxo-3,4-dihydropyrimidin-1(2H)-yl)-N-(4-sulfamoylphenthyl)acetamide J6: 61% yield; m.p. 212-213°C; silica gel TLC R_f 0.64 (MeOH/CH_2Cl_2 20 % v/v); δ_H (400 MHz, DMSO-d_6): 2.83 (t, J = 6.8, 2H, CH_2), 3.36 (q, J = 6.8, 2H, CH_2), 4.33 (s, 2H, CH_2), 5.60 (dd, J = 2.0, 7.8, 1H, CH), 7.35 (s, 2H, exchange with D_2O, SO_2NH_2), 7.45 (d, J = 8.0, 2H, Ar), 7.57 (d, J = 7.8, 1H, CH), 7.78 (d, J = 8.0, 2H, Ar), 8.33 (t, J = 5.2, 1H, exchange with D_2O, CONH), 11.32 (bs, 1H, exchange with D_2O, CONHCO); δ_C (100

MHz, DMSO-d_6): 35.5, 40.7, 50.4, 101.4, 126.6, 130.1, 143.1, 144.4, 147.5, 152.0, 164.8, 167.8; m/z (ESI negative) 351.0 $[M-H]^-$.

Synthesis of 2-(2,4-dioxo-3,4-dihydropyrimidin-1(2H)-yl)-N-(2-hydroxy-5-sulfamoylphenyl)acetamide **J7.**

Compound **J7** was obtained according the general procedure earlier reported using 1-carboxymethyl uracil **J2** (0.2 g, 1.0 eq), HOAt (1.2 eq), DMAP (0.03 eq) and 3-amino-4-hydroxybenzenesulfonamide (1.1 eq) in dry DMF (3 ml). The crude solid was recrystallized from a 1/1 mixture of H_2O/2-MeO-EtOH to afford **J3** as a white solid.

2-(2,4-dioxo-3,4-dihydropyrimidin-1(2H)-yl)-N-(2-hydroxy-5-sulfamoylphenyl)acetamide J7: 71% yield; m.p. 262-263°C; silica gel TLC R_f 0.07 (MeOH/CH_2Cl_2 10 % v/v); δ_H (400 MHz, DMSO-d_6): 4.69 (s, 2H, CH_2), 5.63 (dd, J = 2.0, 7.6, 1H, CH), 7.03 (d, J = 8.5, 1H, Ar), 7.16 (s, 2H, exchange with D_2O, SO_2NH_2), 7.45 (dd, J = 2.4, 8.5, 1H, Ar), 7.67 (d, J = 7.6, 1H, CH), 8.50 (d, J = 2.4, 1H, Ar), 7.79 (s, 1H, exchange with D_2O, OH), 10.85 (s, 1H, exchange with D_2O, CONH), 11.36 (s, 1H, exchange with D_2O, CONHCO); δ_C (100 MHz, DMSO-d_6): 51.1, 101.4, 115.5, 120.5, 123.5, 126.7, 135.4, 147.5, 151.2, 152.0, 164.7, 167.1; m/z (ESI negative) 338.9 $[M-H]^-$.

Synthesis of 1-carboxymethyl uracil **J2.** [229]

An aqueous solution of bromoacetic acid (1.2 eq in 3 ml of water) was added dropwise to a solution of uracil **J1** (1.0 g, 1.0 eq) and KOH (2.0 eq) in water (6 ml) at 60°C. The reaction mixture was stirred for 4h at the same temperature, then cooled to r.t. and acidified to pH 2. The formed precipitate was collected by filtration and washed with water and Et_2O to afford the titled compound **J2** as a white powder.

1-Carboxymethyl uracil J2: 82% yield; m.p. 288-290°C; silica gel TLC R_f 0.10 (MeOH/$CHCl_3$ 10 % v/v); δ_H (400 MHz, DMSO-d_6): 4.45 (s, 2H, CH_2), 5.63 (d, J = 7.8, 1H, CH), 7.65 (d, J = 7.8, 1H, CH), 11.40 (s, 1H, exchange with D_2O, CONHCO), 13.12 (bs, 1H, exchange with D_2O, COOH); δ_C (100 MHz, DMSO-d_6): 49.6, 101.8, 147.0, 152.0, 164.8, 170.6.

Experimental in agreement with reported data.[229]

General synthetic procedure of triazole benzenesulfonamides J11-J12 and J15-J16.[230]

The proper azidobenzenesulfonamide **J9, J10 (A2)** (1.1 eq) was added to a solution of the propargyl derivate **J8** or **J14** (0.1 g, 1.0 eq) in H_2O/*tert*-BuOH 1/1 (8 ml) at r.t., followed by a suspension of $CuSO_4$ (0.1 eq) and Na ascorbate (0.5 eq) in water (0.5 ml). The reaction mixture was stirred at r.t. or 40°C until the consumption of the starting material (TLC monitoring). then quenched with H_2O (20 ml) and the formed precipitate was filtered-off and washed with Et_2O. A solution of the raw solid in DMF (5 ml) was filtered through Celite 521® and then treated with water (20 ml) to obtain a precipitate that was filtered-off to afford the titled compounds **J11-J12 and J15-16.**

Synthesis of 3-(4-((2,4-dioxo-3,4-dihydropyrimidin-1(2H)-yl)methyl)-1H-1,2,3-triazol-1-yl)benzenesulfonamide **J11.**

Compound **J11** was obtained according the general procedure earlier reported using 1-propargyl uracil **J8** (0.1 g, 1.0 eq), 3-azidobenzenesulfonamide (1.1 eq), $CuSO_4$ (0.1 eq) and Na ascorbate (0.5 eq) in H_2O/*tert*-BuOH 1/1 (8 ml). The reaction mixture was stirred for 6h at r.t. to afford the titled compound **J11** as a light yellow solid.

3-(4-((2,4-dioxo-3,4-dihydropyrimidin-1(2H)-yl)methyl)-1H-1,2,3-triazol-1-yl)benzenesulfonamide J11: 37% yield; m.p. >300°C; silica gel TLC R_f 0.12 (MeOH/CH_2Cl_2 10 % v/v); δ_H (400 MHz, DMSO-d_6): 5.10 (s, 2H, CH_2), 5.67 (dd, J = 2.0, 8.0, 1H, C*H*), 7.56 (s, 2H, exchange with D_2O, SO_2NH_2), 7.85 (d, J = 8.0, 1H, C*H*), 8.05 (d, J = 8.6, 2H, Ar), 8.17 (d, J = 8.6, 2H, Ar), 8.94 (s, 1H, C*H*), 11.40 (s, 1H, exchange with D_2O, CON*H*CO); δ_C (100 MHz, DMSO-d_6): 43.3, 102.4, 118.1, 122.9, 124.0, 126.5, 131.8, 137.5, 145.0, 146.4, 146.7, 151.7, 165.7; m/z (ESI negative) 347.0 $[M-H]^-$.

Synthesis of 4-(4-((2,4-dioxo-3,4-dihydropyrimidin-1(2H)-yl)methyl)-1H-1,2,3-triazol-1-yl)benzenesulfonamide **J12.**

Compound **J12** was obtained according the general procedure earlier reported using 1-propargyl uracil **J8** (0.1 g, 1.0 eq), 4-azidobenzenesulfonamide (1.1 eq), $CuSO_4$ (0.1 eq) and Na ascorbate (0.5 eq) in H_2O/*tert*-BuOH 1/1 (8 ml). The reaction mixture was stirred for 6h at r.t. to afford the titled compound **J12** as a light yellow solid.

4-(4-((2,4-dioxo-3,4-dihydropyrimidin-1(2H)-yl)methyl)-1H-1,2,3-triazol-1-yl)benzenesulfonamide J12: 43% yield; m.p. >300°C; silica gel TLC R_f 0.28 (MeOH/CH_2Cl_2 20 % v/v); δ_H (400 MHz, DMSO-d_6): 5.10 (s, 2H, CH_2), 5.67 (dd, J = 2.0, 8.0, 1H, CH), 7.61 (s, 2H, exchange with D_2O, SO_2NH_2), 7.85 (m, *2*H, CH + Ar), 8.05 (d, J = 8.6, 2H, Ar), 7.95 (d, J = 8.5, 1H, Ar), 8.17 (dd, J =1.4, 8.5, 1H, Ar), 8.40 (t, J = 1.4, 1H, Ar), 8.93 (s, 1H, CH), 11.40 (s, 1H, exchange with D_2O, CONHCO); δ_C (100 MHz, DMSO-d_6): 43.3, 102.4, 121.2, 122.8, 128.4, 139.4, 144.8, 145.0, 146.3, 151.7, 164.6; m/z (ESI negative) 346.9 $[M-H]^-$.

Synthesis of 3-(4-((6-amino-9H-purin-9-yl)methyl)-1H-1,2,3-triazol-1-yl)benzenesulfonamide **J15.**

Compound **J15** was obtained according the general procedure earlier reported using 9-propargyl adenine **J14** (0.1 g, 1.0 eq), 3-azidobenzenesulfonamide (1.1 eq), $CuSO_4$ (0.1 eq) and Na ascorbate (0.5 eq) in H_2O/*tert*-BuOH 1/1 (8 ml). The reaction mixture was stirred o.n. at 40°C to afford the titled compound **J15** as a light yellow solid.

3-(4-((6-amino-9H-purin-9-yl)methyl)-1H-1,2,3-triazol-1-yl)benzenesulfonamide J15: 77% yield; m.p. >300°C; silica gel TLC R_f 0.15 (MeOH/CH_2Cl_2 20 % v/v); δ_H (400 MHz, DMSO-d_6): 5.60 (s, 2H, CH_2), 7.38 (bs, 2H, exchange with D_2O, NH_2), 7.60 (s, 2H, exchange with D_2O, SO_2NH_2), 7.60 (t, J = 7.7, 1H, Ar), 7.95 (d, J = 7.7, 1H, Ar), 8.14 (d, J = 7.7, 1H, Ar), 7.60 (t, J = 7.8, 1H, Ar), 8.38 (bs, 3H, Ar), 8.98 (s, 1H, CH); δ_C (100 MHz, DMSO-d_6): 39.00, 116.9, 118.1, 122.9, 123.2, 124.1, 126.4, 131.7, 137.5, 142.2, 145.2, 146.6, 153.3, 157.0; m/z (ESI negative) 370.1 $[M-H]^-$.

Synthesis of 4-(4-((6-amino-9H-purin-9-yl)methyl)-1H-1,2,3-triazol-1-yl)benzenesulfonamide **J16.**

Compound **J16** was obtained according the general procedure earlier reported using 9-propargyl adenine **J14** (0.1 g, 1.0 eq), 4-azidobenzenesulfonamide (1.1 eq), $CuSO_4$ (0.1 eq) and Na ascorbate (0.5 eq) in H_2O/*tert*-BuOH 1/1 (8 ml). The reaction mixture was stirred o.n. at 40°C to afford the titled compound **J16** as a light yellow solid.

4-(4-((6-amino-9H-purin-9-yl)methyl)-1H-1,2,3-triazol-1-yl)benzenesulfonamide

J16: 70% yield; m.p. >300°C; silica gel TLC R_f 0.21 (MeOH/CH_2Cl_2 20 % v/v); δ_H (400 MHz, DMSO-d_6): 5.63 (s, 2H, CH_2), 7.36 (bs, 2H, exchange with D_2O, NH_2), 7.55 (s, 2H, exchange with D_2O, SO_2NH_2), 8.03 (d, J = 8.4, 2H, Ar), 8.14 (d, J = 8.4, 2H, Ar), 8.40 (bs, 2H, Ar), 8.96 (s, 1H, C*H*); δ_C (100 MHz, DMSO-d_6): 39.0, 120.3, 121.3, 123.1, 128.3, 128.5, 139.4, 142.2, 144.8, 145.3, 153.4, 157.0; m/z (ESI negative) 370.1 $[M-H]^-$.

Synthesis of 1-propargyl uracil **J8.**[231]

Propargyl bromide (1.0 eq) was added dropwise to a solution of uracil **J1** (0.5 g, 1.0 eq) and DBU (1.0 eq) in dry CH_3CN (7 ml) at 0°C under a nitrogen atmosphere. The reaction mixture was refluxed for 1.5h, then quenched with $HCl_{(aq)}$ 1M (15 ml) and extracted with EtOAc (25 ml). The organic layer was dried over Na_2SO_4, filtered-off and concentrated under *vacuo* to give a residue that was purified by silica gel coloumn chromatography eluting with 70 % EtOAc in *n*-hexane to afford the title compound **J8** as white solid.

1-Propargyl uracil J8: 40% yield; m.p. 169–170°C; silica gel TLC R_f 0.23 (EtOAc/*n*-hexane 50 % v/v); δ_H (400 MHz, DMSO-d_6): 3.47 (t, J = 2.0, 1H, *CH*), 4.54 (d, J = 3.0, 2H, CH_2), 5.66 (d, J = 7.8, 1H, C*H*), 7.74 (d, J = 7.8, 1H, C*H*), 11.44 (bs, 1H, exchange with D_2O, CON*H*CO); δ_C (100 MHz, DMSO-d_6): 37.6, 76.8, 79.4, 102.6, 145.5, 151.3, 164.5.

Experimental in agreement with reported data.[231]

Synthesis of 9-propargyl adenine **J14.**[232]

Propargyl bromide (1.0 eq) was added dropwise to a suspension of adenine **J13** (1.0 g, 1.0 eq) and K_2CO_3 (1.0 eq) in dry DMF (6 ml) at 0°C under a nitrogen atmosphere. The reaction mixture was stirred overnight at r.t. and then quenched with slush (20 ml). The

formed precipitate was filtered-off and purified by silica gel coloumn chromatography eluting with 5 % MeOH in DCM to afford the title compound **J14** as white solid.

9-Propargyl adenine J14: 23% yield; m.p. 209-210°C; silica gel TLC R_f 0.57(MeOH/CH_2Cl_2 10 % v/v); δ_H (400 MHz, DMSO-d_6): 3.43 (t, J = 2.0, 1H, *CH*), 4.98 (d, J = 3.2, 2H, CH_2), 7.26 (s, 2H, exchange with D_2O, NH_2), 8.12 (s, 1H, C*H*), 8.15 (s, 1H, C*H*); δ_C (100 MHz, DMSO-d_6): 32.8, 76.4, 78.9, 119.0, 140.6, 149.6, 153.2, 156.5.
Experimental in agreement with reported data.[232]

General synthetic procedure of azidobenzenesulfonamides J9, J10 (A2).

The proper aminobenzenesulfonamide (0.5 g, 1.0eq) was dissolved in a 2M HCl aqueous solution (5 ml). $NaNO_2$ (1.2 eq) was slowly added at 0°C and the reaction mixture was stirred at the same temperature for 0.5h. Thereafter NaN_3 (1.5 eq) was added portion-wise and the mixture was stirred at r.t. for 0.5h. The obtained precipitate was filtered-off and washed with water to afford the corresponding azidobenzenesulfonamides **J9, J10 (A2)**.

Synthesis of 3-azido-benzenesulfonamide **J9.**[233]

Compound **J9** was obtained according the general procedure earlier reported.

3-Azidobenzenesulfonamide J9: 60% yield; m.p. 110°C; silica gel TLC *Rf* 0.35 (EtOAc/*n*-hexane 50 % *v/v*); δ_H (400 MHz, DMSO-d_6): 7.37 (m, 2H, Ar), 7.48 (s, 2H, exchange with D_2O, SO_2NH_2), 7.52 (s, 1H, Ar), 7.63 (m, 1H, Ar); δ_C (100 MHz, DMSO-d_6): 117.2, 123.1, 123.5, 131.8, 141.4, 146.9.
Experimental in agreement with reported data.[233]

General synthetic procedure of benzenesulfonamides J22-J25 and J26-J29.

The proper 2-chloro-acetamido benzenesulfonamide **J18-J21** (1.1 eq) was added to a suspension of N,N-dimethyl-N'-(9H-purin-6-yl)formimidamide **J17** (0.2 g, 1.0 eq) and K_2CO_3 (1.2 eq) in dry DMF (5 ml) under a nitrogen atmosphere and the reaction mixture was stirred at r.t. until the consumption of the starting material (TLC monitoring). The reaction was quenched with slush (20 ml) and the formed precipitate was filtered-off

under vacuo, washed with water and recrystallized from the proper solvent to afford the titled compounds **J22-J25**.

Benzenesulfonamide **J22-J25** (0.2 g, 1.0 eq) was suspended in HCl 1.25M in MeOH (6 ml) in sealed tube and the reaction mixture stirred at 80°C until the consumption of the starting material (TLC monitoring). The solution was concentrated under vacuo and the residue triturated with aceton. The obtained hydrochloric salt was treated with a $NaHCO_3$ aqueous solution (5 ml) to give a powder that was filtered-off and washed with water to afford the titled derivatives **J26-J29.**

Synthesis of 2-(6-(((dimethylamino)methylene)amino)-9H-purin-9-yl)-N-(3-sulfamoylphenyl)acetamide **J22.**

Compound **J22** was obtained according the general procedure earlier reported using N,N-dimethyl-N'-(9H-purin-6-yl)formimidamide **J17** (0.2 g, 1.0 eq)**,** K_2CO_3 (1.2 eq) and 2-chloro-N-(3-sulfamoylphenyl)acetamide (1.1 eq) **J18** in dry DMF (5 ml). The crude solid was recrystallized from a IPA to afford **J22** as a white solid.

2-(6-(((dimethylamino)methylene)amino)-9H-purin-9-yl)-N-(3-sulfamoylphenyl)acetamide J22: 50% yield; m.p. 248-249°C; silica gel TLC R_f 0.21 (MeOH/CH_2Cl_2 20 % v/v); δ_H (400 MHz, DMSO-d_6): 3.00 (s, 3H, CH_3), 3.14 (s, 3H, CH_3), 5.48 (s, 2H, CH_2), 7.40 (s, 2H, exchange with D_2O, SO_2NH_2), 7.55 (m, 2H, Ar), 7.70 (m, 1H, Ar), 8.16 (m, 1H, Ar), 8.37 (s, 1H, C*H*), 8.47 (s, 1H, C*H*), 8.87 (s, 1H, C*H*), 10.70 (bs, 1H, exchange with D_2O, CON*H*); δ_C (100 MHz, DMSO-d_6): 35.4, 41.5, 50.6, 117.0, 118.3, 121.4, 122.7, 130.4, 139.9, 145.7, 148.5, 152.8, 155.6, 157.3, 161.6, 167.2; m/z (ESI negative) 401.1 $[M-H]^-$.

Synthesis of 2-(6-(((dimethylamino)methylene)amino)-9H-purin-9-yl)-N-(4-sulfamoylphenyl)acetamide **J23.**

Compound **J23** was obtained according the general procedure earlier reported using N,N-dimethyl-N'-(9H-purin-6-yl)formimidamide **J17** (0.2 g, 1.0 eq), K_2CO_3 (1.2 eq) and 2-chloro-N-(4-sulfamoylphenyl)acetamide **J19** (1.1 eq) in dry DMF (5 ml). The crude solid was recrystallized from a IPA to afford **J23** as a white solid.

2-(6-(((dimethylamino)methylene)amino)-9H-purin-9-yl)-N-(4-sulfamoylphenyl)acetamide J23: 47% yield; m.p. 238-239°C; silica gel TLC R_f 0.22 (MeOH/CH_2Cl_2 10 % v/v); δ_H (400 MHz, DMSO-d_6): 3.00 (s, 3H, CH_3), 3.14 (s, 3H, CH_3), 5.49 (s, 2H, CH_2), 7.30 (s, 2H, exchange with D_2O, SO_2NH_2), 7.73 (d, J = 8.8, 2H, Ar), 7.80 (d, J = 8.8, 2H, Ar), 8.37 (s, 1H, CH) ,8.47 (s, 1H, CH), 8.80 (s, 1H, CH), 10.77 (bs, 1H, exchange with D_2O, CONH); δ_C (100 MHz, DMSO-d_6): 35.7, 41.5, 50.6, 118.3, 119.5, 127.7, 139.5, 142.5, 148.4, 152.8, 155.6, 157.3, 161.6, 167.4; m/z (ESI negative) 401.1 $[M-H]^-$.

Synthesis of 2-(6-(((dimethylamino)methylene)amino)-9H-purin-9-yl)-N-(4-sulfamoylbenzyl)acetamide **J24.**

Compound **J24** was obtained according the general procedure earlier reported using N,N-dimethyl-N'-(9H-purin-6-yl)formimidamide **J17** (0.2 g, 1.0 eq)**,** K_2CO_3 (1.2 eq) and 2-chloro-N-(4-sulfamoylbenzyl)acetamide **J20** (1.1 eq) in dry DMF (5 ml). The crude solid was recrystallized from a IPA to afford **J24** as a white solid.

2-(6-(((dimethylamino)methylene)amino)-9H-purin-9-yl)-N-(4-sulfamoylbenzyl)acetamide J24: 75% yield; m.p. 255-256°C; silica gel TLC R_f 0.17 (MeOH/CH_2Cl_2 20 % v/v); δ_H (400 MHz, DMSO-d_6): 2.97 (s, 3H, CH_3), 3.20 (s, 3H, CH_3), 4.37 (d, J = 6.0, 2H, CH_2), 5.32 (s, 2H, CH_2), 7.36 (s, 2H, exchange with D_2O, SO_2NH_2), 7.42 (d, J = 8.0, 2H, Ar), 7.74 (d, J = 8.8, 2H, Ar), 8.35 (s, 1H, CH) , 8.47 (s, 1H, CH), 8.72 (t, J = 6.0, 1H, exchange with D_2O, CONH), 8.92 (s, 1H, CH); δ_C (100 MHz, DMSO-d_6): 35.5, 41.5, 42.8, 50.0, 118.2, 126.3, 128.4, 143.6, 144.1, 148.5, 152.7, 155.6, 157.2, 161.6, 168.4; m/z (ESI negative) 415.1 $[M-H]^-$.

Synthesis of 2-(6-(((dimethylamino)methylene)amino)-9H-purin-9-yl)-N-(4-sulfamoylphenethyl)acetamide **J25.**

Compound **J25** was obtained according the general procedure earlier reported using N,N-dimethyl-N'-(9H-purin-6-yl)formimidamide **J17** (0.2 g, 1.0 eq)**,** K_2CO_3 (1.2 eq) and 2-chloro-N-(4-sulfamoylphenethyl)acetamide **J21** in dry DMF (5 ml). The crude solid was recrystalized from a IPA to afford **J25** as a white solid.

2-(6-(((dimethylamino)methylene)amino)-9H-purin-9-yl)-N-(4-sulfamoylphenethyl)acetamide J25: 44% yield; m.p. 227-228°C; silica gel TLC R_f 0.23 (MeOH/CH_2Cl_2 20 % v/v); δ_H (400 MHz, DMSO-d_6): 2.81 (t, J = 7.2, 2H, CH_2), 3.01 (s, 3H, CH_3), 3.20 (s, 3H, CH_3), 3.33 (q, J = 7.2, 2H, CH_2), 5.23 (s, 2H, CH_2), 7.34 (s, 2H, exchange with D_2O, SO_2NH_2), 7.41 (d, J = 8.0, 2H, Ar), 7.75 (d, J = 8.8, 2H, Ar), 8.28 (t, J = 6.0, 1H, exchange with D_2O, CONH), 8.30 (s, 1H, CH), 8.46 (s, 1H, CH),), 8.92 (s, 1H, CH); δ_C (100 MHz, DMSO-d_6): 35.6, 40.0, 40.8, 41.5, 49.9, 118.2, 126.6, 129.9, 143.0, 144.4, 148.5, 152.7, 155.6, 157.2, 161.5, 168.1; m/z (ESI negative) 429.2 $[M-H]^-$.

Synthesis of 2-(6-amino-9H-purin-9-yl)-N-(3-sulfamoylphenyl)acetamide **J26.**

Compound **J26** was obtained according the general procedure earlier reported treating compound **J22** with HCl 1.25M in MeOH and successively with $NaHCO_{3(aq)}$.

2-(6-amino-9H-purin-9-yl)-N-(3-sulfamoylphenyl)acetamide J26: 72% yield; m.p. >300°C; silica gel TLC R_f 0.09 (MeOH/CH_2Cl_2 20 % v/v); δ_H (400 MHz, DMSO-d_6): 5.36 (s, 2H, CH_2), 6.88 (s, 2H, exchange with D_2O, NH_2), 7.40 (s, 2H, exchange with D_2O, SO_2NH_2), 7.55 (m, 2H, Ar), 7.75 (m, 1H, Ar), 8.21 (s, 1H, Ar), 8.23 (s, 1H, CH), 8.32 (s, 1H, CH), 10.67 (s, 1H, exchange with D_2O, CONH); δ_C (100 MHz, DMSO-d_6): 50.1, 112.8, 117.2, 121.6, 122.9, 130.5, 139.7, 145.7, 147.7, 152.5, 153.0, 160.6, 167.0; m/z (ESI negative) 346.0 $[M-H]^-$.

Synthesis of 2-(6-amino-9H-purin-9-yl)-N-(4-sulfamoylphenyl)acetamide **J27.**

Compound **J27** was obtained according the general procedure earlier reported treating compound **J23** with HCl 1.25M in MeOH and successively with $NaHCO_{3(aq)}$.

2-(6-amino-9H-purin-9-yl)-N-(4-sulfamoylphenyl)acetamide J27: 41% yield; m.p. >300°C; silica gel TLC R_f 0.09 (MeOH/CH_2Cl_2 10 % v/v); δ_H (400 MHz, DMSO-d_6): 5.37 (s, 2H, CH_2), 6.88 (s, 2H, exchange with D_2O, NH_2), 7.30 (s, 2H, exchange with D_2O, SO_2NH_2), 7.79 (m, 4H, Ar), 8.37 (s, 1H, CH), 8.23 (s, 1H, CH), 8.31 (s, 1H, CH), 10.69 (bs, 1H, exchange with D_2O, CONH); δ_C (100 MHz, DMSO-d_6): 50.1, 112.8, 119.7, 127.7, 139.7, 142.3, 147.7, 152.4, 153.0, 160.6, 167.2; m/z (ESI negative) 346.0 $[M-H]^-$.

Synthesis of 2-(6-amino-9H-purin-9-yl)-N-(4-sulfamoylbenzyl)acetamide **J28.**

Compound **J28** was obtained according the general procedure earlier reported treating compound **J24** with HCl 1.25M in MeOH and successively with $NaHCO_{3(aq)}$.

2-(6-amino-9H-purin-9-yl)-N-(4-sulfamoylbenzyl)acetamide J28: 81% yield; m.p. >300°C; silica gel TLC R_f 0.11 ($MeOH/CH_2Cl_2$ 20 % v/v); δ_H (400 MHz, DMSO-d_6): 4.42 (d, J = 6.0, 2H, CH_2), 5.21 (s, 2H, CH_2), 6.88 (s, 2H, exchange with D_2O, NH_2), 7.35 (s, 2H, exchange with D_2O, SO_2NH_2), 7.49 (d, J = 8.0, 2H, Ar), 7.74 (d, J = 8.8, 2H, Ar), 8.23 (s, 1H, CH) ,8.26 (s, 1H, CH), 8.81 (t, J = 6.0, 1H, exchange with D_2O, CONH); δ_C (100 MHz, DMSO-d_6): 43.0, 49.7, 112.8, 126.6, 128.5, 143.8, 147.6, 152.6, 153.2, 160.7, 160.8, 168.1; m/z (ESI negative) 360.0 $[M-H]^-$.

Synthesis of 2-(6-amino-9H-purin-9-yl)-N-(4-sulfamoylphenethyl)acetamide **J29.**

Compound **J29** was obtained according the general procedure earlier reported treating compound **J25** with HCl 1.25M in MeOH and successively with $NaHCO_{3(aq)}$.

2-(6-amino-9H-purin-9-yl)-N-(4-sulfamoylphenetyl)acetamide J29: 72% yield; m.p. >300°C; silica gel TLC R_f 0.13 ($MeOH/CH_2Cl_2$ 20 % v/v); δ_H (400 MHz, DMSO-d_6): 2.84 (t, J = 7.2, 2H, CH_2), 3.35 (q, J = 7.2, 2H, CH_2), 5.06 (s, 2H, CH_2), 6.85 (s, 2H, exchange with D_2O, NH_2), 7.33 (s, 2H, exchange with D_2O, SO_2NH_2), 7.41 (d, J = 8.0, 2H, Ar), 7.75 (d, J = 8.0, 2H, Ar), 8.20 (s, 1H, CH), 8.23 (s, 1H, CH), 8.43 (t, J = 6.0, 1H, exchange with D_2O, CONH); δ_C (100 MHz, DMSO-d_6): 35.4, 40.9, 49.7, 112.6, 126.6, 130.0, 143.0, 144.2, 147.4, 152.6, 153.1, 160.6, 167.9; m/z (ESI negative) 374.1 $[M-H]^-$.

Synthesis of N,N-dimethyl-N'-(9H-purin-6-yl)formimidamide **J17.**[234]

Dimethylformamide dimethyl acetal (1.2 eq) was added to a suspension of adenine (1.0 g, 1.0 eq) in DMF (8 ml). The reaction mixture was stirred overnight at 50°C and then treated with aceton (20 ml). The precipitate was filtered-off under vacuo to afford the titled compound **J17** as a white solid.

N,N-Dimethyl-N'-(9H-purin-6-yl)formimidamide J17: 90% yield; m.p. 252-255°C; silica gel TLC R_f 0.50 (MeOH/CH_2Cl_2 20 % v/v); δ_H (400 MHz, DMSO-d_6): 3.18 (s, 3H, CH_3), 3.23 (s, 3H, CH_3), 8.32 (s, 1H, C*H*) ,8.45 (s, 1H, C*H*), 8.93 (s, 1H, C*H*), 13.04 (bs, 1H, exchange with D_2O, N*H*); δ_C (100 MHz, DMSO-d_6): 36.1, 41.2, 125.3, 144.6, 152.4, 153.8, 156.7, 160.8.
Experimental in agreement with reported data.[234]

General synthetic procedure of 2-chloro-acetamido benzenesulfonamide J18-J21. [235]

Chloroacetyl chloride (1.2 eq) was added dropwise to a suspension of the proper aminobenzenesulfonamide (1.0 g, 1.0 eq) and K_2CO_3 (1.2 eq) in acetone (20 ml) at 0°C and the reaction mixture was stirred for 0.5h at the same temperature. The reaction mixture was concentrated under vacuo and the quenched with cold HCl $1M_{(aq)}$ (20 ml) and the formed precipitate was filtered-off under vacuo and washed with water to afford the titled compounds **J18-J21**.

Synthesis of 2-chloro-N-(3-sulfamoylphenyl)acetamide **J18.**

Compound **J18** was obtained according the general procedure earlier reported using 3-aminobenzenesulfonamide (1.0 g, 1.0 eq)**,** K_2CO_3 (1.2 eq) and chloroacetyl chloride (1.2 eq) in acetone (20 ml).
2-Chloro-N-(3-sulfamoylphenyl)acetamide J18: 83% yield; silica gel TLC R_f 0.30 (MeOH/CH_2Cl_2 10 % v/v); δ_H (400 MHz, DMSO-d_6): 4.32 (s, 2H, CH_2), 7.43 (s, 2H, exchange with D_2O, SO_2NH_2), 7.58 (m, 2H, Ar), 7.78 (m, 1H, Ar), 8.20 (d, J = 1.6, 1H, Ar), 10.63 (s, 1H, exchange with D_2O, CON*H*); δ_C (100 MHz, DMSO-d_6): 44.4, 117.3, 121.9, 123.2, 130.6, 139.7, 145.7, 166.0.

Synthesis of 2-chloro-N-(4-sulfamoylphenyl)acetamide **J19.**

Compound **J19** was obtained according the general procedure earlier reported using 4-aminobenzenesulfonamide (1.0 g, 1.0 eq)**,** K_2CO_3 (1.2 eq) and chloroacetyl chloride (1.2 eq) in acetone (20 ml).

2-chloro-N-(4-sulfamoylphenyl)acetamide **J19:** 75% yield; silica gel TLC R_f 0.37 (MeOH/CH_2Cl_2 10 % v/v); δ_H (400 MHz, DMSO-d_6): 4.34 (s, 2H, CH_2), 7.31 (s, 2H, exchange with D_2O, SO_2NH_2), 7.80 (m, 4H, Ar), 10.67 (s, 1H, exchange with D_2O, CONH); δ_C (100 MHz, DMSO-d_6): 44.4, 119.9, 127.7, 139.9, 142.3, 166.1.
Experimental in agreement with reported data.[235]

Synthesis of 2-chloro-N-(4-sulfamoylbenzyl)acetamide **J20.**

Compound **J20** was obtained according the general procedure earlier reported using 4-(aminomethyl)benzenesulfonamide hydrochloride (1.0 g, 1.0 eq), K_2CO_3 (2.2 eq) and chloroacetyl chloride (1.2 eq) in acetone (20 ml).
2-Chloro-N-(4-sulfamoylbenzyl)acetamide J20: 50% yield; silica gel TLC R_f 0.26 (MeOH/CH_2Cl_2 10 % v/v); δ_H (400 MHz, DMSO-d_6): 4.18 (s, 2H, CH_2), 4.41 (d, J = 5.8, 2H, CH_2), 7.34 (s, 2H, exchange with D_2O, SO_2NH_2), 7.48 (d, J = 8.4, 2H, Ar), 7.81 (d, J = 8.4, 2H, Ar), 8.85 (t, J = 5.8, 1H, exchange with D_2O, CONH); δ_C (100 MHz, DMSO-d_6): 43.0, 43.5, 126.6, 128.5, 143.7, 143.8, 167.1.

Synthesis of 2-chloro-N-(4-sulfamoylphenethyl)acetamide **J21.**

Compound **J21** was obtained according the general procedure earlier reported using 4-(aminoethyl)benzenesulfonamide (1.0 g, 1.0 eq), K_2CO_3 (1.2 eq) and chloroacetyl chloride (1.2 eq) in acetone (20 ml).
2-Chloro-N-(4-sulfamoylphenethyl)acetamide J21: 93% yield; silica gel TLC R_f 0.26 (MeOH/CH_2Cl_2 10 % v/v); δ_H (400 MHz, DMSO-d_6): 2.85 (t, J = 7.2, 2H, CH_2), 3.40 (q, J = 5.6, 2H, CH_2), 4.07 (s, 2H, CH_2), 7.33 (s, 2H, exchange with D_2O, SO_2NH_2), 7.44 (d, J = 8.4, 2H, Ar), 7.78 (d, J = 8.4, 2H, Ar), 8.34 (t, J =5.6, 1H, exchange with D_2O, CONH); δ_C (100 MHz, DMSO-d_6): 35.4, 41.0, 43.5, 126.6, 130.0, 143.0, 144.3, 166.8.

4.5.2 Carbonic anhydrase inhibition

The CA inhibitory profiles of compounds belonging to series **J** were obtained according to the general procedures described at the beginning of the experimental section.

4.5.3 X-ray Crystallography

Due to the challenges in expressing, purifying, and crystallizing wild type hCA IX, an hCA IX-mimic was utilized for structural studies. The hCA IX-mimic was produced by mutating seven active site residues of hCA II to mimic the active site of hCA IX (A65S, N67Q, E69T, I91L, F131V, K170E, L204A). HCA II and hCA IX-mimic were purified as previously described.[236] Briefly, the protein was overexpressed in BL21(DE3) cells via induction with IPTG and then purified from the cell lysate using affinity chromatography with a *p*-(aminomethyl)benzenesulfonamide resin. Protein purity was confirmed utilizing SDS-PAGE. Crystals were grown via the hanging drop vapor diffusion method with a mother liquor consisting of 1.6M sodium citrate and 50mM Tris-HCl, pH 7.8. Crystals were observed within 3 days. The crystals were soaked in ~10mM inhibitor for 5 min prior to freezing in liquid nitrogen for shipment.

Diffraction data was collected on a Pilatus 6M detector at the Cornell High Energy Synchrotron Source (CHESS) F1 beamline (λ = 0.977 Å). Data was collected with a crystal-to-detector distance of 250 or 270 mm, 1° oscillation angle, and 1 or 3 sec exposure time for CA IX-mimic and CA II, respectively, for a total of 270 images. The program *HKL2000*[237] was utilized to index, integrate, and scale the data. Phase determination (molecular replacement with using PDB: 3KS3[238] as a search model), refinement, and generation of restraint files were completed in *Phenix*[239]. The graphical programs *Coot*[240] and *Pymol*[241] were used to analyze protein inhibitor interactions and generate figures.

Table EXP2.

Summary of Data Collection and Atomic Model Refinement Statistics for compounds J29

Complex	CA II_**J29**	CA IX-mimic_**J29**
PDB Code	**-**	**-**
Space Group **Cell Dimensions (Å;°)**	$P2_1$ a = 42.6, b = 41.7, c = 72.6; β= 104.2	$P2_1$ a = 42.0, b = 41.2, c = 71.8; β= 103.7
Resolution (Å)	40.2–1.6 (1.69–1.64)	29.0 – 1.6 (1.68 – 1.63)
Total Reflections	37,853	31,540
I/Iσ	20.6 (2.0)	17.6 (1.3)
Redundancy	3.7 (3.8)	2.5 (2.8)
Completeness (%)	83.8 (83.8)	84.4 (82.9)
Rcryst (%)	14.0 (22.5)	15.5 (25.9)
Rfree (%)	17.1 (28.1)	20.1 (36.0)
Rsym (%)	5.2 (57.2)	4.7 (5.9)
Rpim	2.9 (34.0)	3.3 (46.2)
# of Protein Atoms	4,079	4,062
# of Water Molecules	156	130
# of Ligand Atoms	43	43
Ramachandran stats (%): Favored, allowed, generously allowed	97.7, 2.3, 0	96.9, 3.1, 0
Avg. B factors (Å^2): Main-chain, Side-chain, Ligand	13.9, 20.2, 29.7	13.8, 20.9, 30.0
rmsd for bond lengths, angles (Å,º)	0.009, 1.109	0.010, 1.118

4.5.4 Cell culture, treatments and Cell viability assay

Human colon cancer cell lines HT-29 were obtained from American Type Culture Collection (Rockville, MD). HT-29 were cultured in DMEM high glucose with 10% FBS in 5% CO_2 atmosphere at 37° C. Media contained 2 mM L-glutamine, 1% essential amino acid mix, 100 IU ml^{-1} penicillin and 100 μg ml^{-1} streptomycin (Sigma, Milan, Italy). HT-29 cells were plated in 96-wells cell culture ($1 \cdot 10^4$/well) and, 24 h after, treated with the tested compounds (0-300 μM) for 16 and 48 h. Low oxygen conditions were acquired in a hypoxic workstation (Concept 400 anaerobic incubator, Ruskinn Technology Ltd., Bridgend, UK). The atmosphere in the chamber consisted of 0.1% O_2 (hypoxia), 5% CO_2, and residual N_2. In parallel, normoxic (20% O_2) dishes were incubated in air with 5% CO_2.

HT-29 cell viability was evaluated by the reduction of 3-(4,5-dimethylthiozol-2-yl)-2,5-diphenyltetrazolium bromide (MTT) as an index of mitochondrial compartment functionality. Cells were plated and treated as described. Post-treatments, after extensive washing, 1 mg/ml MTT was added into each well and incubated for 30 minutes at 37 °C. After washing, the formazan crystals were dissolved in 200 µl DMSO. The absorbance was measured at 550 nm. Experiments were performed in quadruplicate on at least three different cell batches.

4.6 In vitro evaluation and computational studies on novel 4/3-((4-oxo-5-(2-oxoindolin-3-ylidene)thiazolidin-2-ylidene)amino) benzenesulfonamides (series K).

4.6.1 Chemistry

Derivatives of series **K** were synthesized by Prof. Eldehna group according to the procedures reported in Eldehna, W.M. et al. *Eur. J. Med. Chem.* **2017**,*139*, 250-262.

4.6.2 Carbonic anhydrase inhibition

The CA inhibitory profiles of compounds belonging to series **K** were obtained according to the general procedures described at the beginning of the experimental section.

4.6.3 Computational studies

Computational studies for compounds belonging to series **K** were performed according to the general procedures described at the beginning of the experimental section.

Chapter 5. Conclusions

In conclusion, the research activity carried out during my three-years PhD period led to the discovery of novel inhibitors, also belonging to new chemotypes, for different isoforms of the zinc-enzymes carbonic anhydrase and to the identification of new and promising candidates for the treatment of glaucoma, cancer and bacterial/fungal/parasitic infections. Indeed, considering the variety of human physiological-pathological processes showing abnormal levels or activities of these enzymes, as well as the essential role of CAs in the life cycle of pathogens, CA isozymes have acquired growing interest for the design of inhibitors with biomedical applications.

SBDD tools were applied for the design of new derivatives as well as for the rationalization of the experimental inhibitory profile measured for the synthesized and screened derivatives.

The "Click Chemistry approach" represented a topic of the research program and was widely applied to synthesize novel CAIs belonging to the sulfonamide, coumarin and sulfocoumarin type. The inhibitory profile of the designed and synthesized derivatives pointed out interesting potential candidates for the treatment of pathologies, such as glaucoma or tumors. The binding mode of the triazole sulfonamide derivatives within hCAs was studied by means of computational and crystallographic methods.

By means of quantum-mechanical (QM) computational methods applied to a cluster CA-model, we were able to define a multi-step mechanism for the CA-mediated sulfocoumarin hydrolytic process. The detailed knowledge of sulfocoumarin mechanism of action will be meaningful to rationalize the particular CA inhibitory profile this class of inhibitors are endowed with and to further design innovative derivatives.

New chemotypes were studied for CA inhibition. Primarily, N-nitrosulfonamides were validated as new chemotype possessing CA inhibitory properties. Promising results obtained for an initial set of compounds, screened on different CA isoforms, were followed by computational binding mode evaluation, which depicted a novel Zn-binding approach. Subsequently, a variety of hCAIs belonging to different chemotypes present in our libraries were screened as inhibitors of the β-CA from the dandruff-producing fungus *Malassetia Globosa*. A homology model of MgCA was built using the crystal structure of Can2 as template in order to evaluate the binding mode of such chemotypes within

MgCA. A large series of benzoxaboroles was tested additionally as inhibitors of CgNce103 and Can2 and their binding mode in this latter evaluated by means of computational studies. The SBDD binding mode evaluation carried out to rationalize the inhibitory profile exhibited by four different chemotypes toward MgCA (also Can2 and CgNce103 for benzoxaboroles) shed light on the ligand/target interactions established at the molecular level and represents a starting point to further the research of non-sulfonamide, effective CAIs targeting MgCA or different fungal isoforms.

A set of derivatives was designed and synthesized by incorporating a purine/pyrimidine pharmacophore as the tail of a classical CAI with a benzenesulfonamide ZBG scaffold in order to both modulate the interaction with CA isozymes and exploit an intrinsic anti-tumor effect in parallel and synergic to the inhibition of hCA IX. The compounds were investigated for their inhibition of cytosolic hCA I and II and transmembrane hCA IV and IX. X-ray crystallography demonstrates the binding mode of a nitrogenous base within the active site of hCA II and a hCA IX-mimic. Finally, the most effective compounds were evaluated for their anti-proliferative activity against HT-29 colon cancer cell lines. The analysis of the trend of the obtained results allowed us to ascribe the responsibility for the observed cytotoxic effects to either multiple, not yet identified mechanisms of action, or the inhibition of the tumor-associated hCA IX, depending on the treatment time and the applied hypoxic or normoxic conditions.

Additional computational studies and biological evaluation carried out during the three-years PhD period allowed to study and explore the inhibitory action and binding mode of several derivatives with a variety of CA isoforms.

References

1. Supuran, C. T. Carbonic anhydrases: novel therapeutic applications for inhibitors and activators. *Nat. Rev. Drug Discovery* **2008**, *7*, 168-181.
2. Alterio,V.; Di Fiore, A.; D'Ambrosio, K.; Supuran, C.T.; De Simone, G. Multiple binding modes of inhibitors to carbonic anhydrases: how to design specific drugs targeting 15 different isoforms? *Chem. Rev*. **2012**, *112*, 4421-4468.
3. Drug Design of Zinc-Enzyme Inhibitors: Functional, Structural, and Disease Applications; Supuran, C. T.; Winum, J.-Y. Eds.; Wiley: Hoboken, NJ, **2009**; Part II.
4. Xu, Y.; Feng, L.; Jeffrey, P. D.; Shi, Y.; Morel, F. M. Structure and metal exchange in the cadmium carbonic anhydrase of marine diatoms. *Nature* **2008**, 452, 56-61.
5. Lane, T. W.; Saito, M. A.; George, G. N.; Pickering, I. J.; Prince, R. C.; Morel, F. M. Biochemistry: a cadmium enzyme from a marine diatom. *Nature* **2005**, 435, 42.
6. Maren, T. H. Carbonic anhydrase: chemistry, physiology, and inhibition. *Physiol. Rev.* **1967**, 47, 595-781.
7. Del Prete, S.; Vullo, D.; Fisher, G.M.; Andrews, K.T.; Poulsen, S.A.; Capasso, C.; Supuran, C. T. Discovery of a new family of carbonic anhydrases in the malaria pathogen Plasmodium falciparum-the η-carbonic anhydrases. *Bioorg. Med. Chem. Lett.* **2014**, *24*, 4389-4396.
8. Tripp, B. C.; Smith, K.; Ferry, J. G. Carbonic anhydrase: new insights for an ancient enzyme. *J. Biol. Chem.* **2001**, 276, 48615-48618.
9. Ferry, J. F. The gamma class of carbonic anhydrases. *Biochim. Biophys. Acta* **2010**, 1804, 374-381.
10. Smith, K.S.; Jakubzick, C.; Whittam, T. S.; Ferry, J.G. Carbonic anhydrase is an ancient enzyme widespread in prokaryotes. *Proc. Natl. Acad. Sci. U.S.A.* **1999**, *96*, 15184–15189.
11. Kikutani, S.; Nakajima, K.; Nagasato, C.; Tsuji, Y.; Miyatake, A.; Matsuda, Y. Thylakoid luminal θ-carbonic anhydrase critical for growth and photosynthesis in the marine diatom Phaeodactylum tricornutum. *Proc. Natl. Acad. Sci. U.S.A.* **2016**, *113*, 9828–9833.
12. Capasso, C.; Supuran, C. T. An overview of the alpha-, beta- and gamma-carbonic anhydrases from Bacteria: can bacterial carbonic anhydrases shed new light on evolution of bacteria? *J. Enzyme Inhib. Med. Chem.* **2015**, *30*, 325–332.
13. Meldrum, N. U.; Roughton, F. J. Carbonic anhydrase. Its preparation and properties. *J. Physiol.* **1933,** *80*, 113-142.
14. Edsall, J. T. Multiple molecular forms of carbonic anhydrase in erythrocytes. *Ann. N. Y. Acad. Sci.* **1968**, *151*, 41-63.
15. Capasso, C.; Supuran, C. T. Bacterial, fungal and protozoan carbonic anhydrases as drug targets. *Expert Opin. Ther. Targets.* **2015**, *19*, 1689-1704.
16. Boron, W. F. Evaluating the role of carbonic anhydrases in the transport of $HCO3^-$- related species. *Biochim. Biophys. Acta.* **2010**, *1804*, 410-421.
17. Krishnamurthy, V. M.; Kaufman, G. K.; Urbach, A. R.; Gitlin, I.; Gudiksen, K. L.; Weibel, D. B.; Whitesides, G. M. Carbonic anhydrase as a model for biophysical and physical-organic studies of proteins and protein-ligand binding. *Chem. Rev*. **2008**, *108*, 946-1051.
18. Tanc, M.; Carta, F.; Scozzafava, A.; Supuran, C. T. α-Carbonic Anhydrases Possess Thioesterase Activity. *ACS Med. Chem. Lett*. **2015**, *6*, 292-295.
19. Nishimori, I.; Minakuchi, T.; Kohsaki, T.; Onishi, S.; Takeuchi, H.; Vullo, D.; Scozzafava, A.; Supuran, C. T. Carbonic anhydrase inhibitors: the beta-carbonic anhydrase from Helicobacter pylori is a new target for sulfonamide and sulfamate inhibitors. *Bioorg. Med. Chem. Lett.* **2007**, *17*, 3585-3594.
20. Supuran, C. T. Structure and function of carbonic anhydrases. *Biochem. J*. **2016**, 473, 2023-2032.

21. Schlicker, C.; Hall, R. A.; Vullo, D.; Middelhaufe, S.; Gertz, M.; Supuran, C. T.; Muehlschlegel, F. A.; Steegborn, C. Structure and Inhibition of the CO2-Sensing Carbonic Anhydrase Can2 from the Pathogenic Fungus Cryptococcus neoformans. *J. Mol. Biol.* **2009**, 385, 1207-1220.
22. Clare, B. W.; Supuran, C. T. A perspective on quantitative structure-activity relationships and carbonic anhydrase inhibitors. *Expert. Opin. Drug. Metab. Toxicol.* **2006**, *2*, 113-137.
23. Carbonic Anhydrase: Its Inhibitors and Activators; Supuran, C. T., Scozzafava, A., Conway, J., Eds.; CRC Press: Boca Raton, FL, 2004.
24. Supuran, C. T. Carbonic anhydrases as drug targets-an overview. *Curr. Top. Med. Chem.* **2007**, *7*, 825-833.
25. Supuran, C. T.; Scozzafava, A.; Casini, A. Carbonic anhydrase inhibitors. *Med. Res. Rev.* **2003**, *23*, 146-189.
26. Supuran, C. T.; Scozzafava, A. Carbonic anhydrases as targets for medicinal chemistry. *Bioorg. Med. Chem.* **2007**, *15*, 4336-4350.
27. Temperini, C.; Scozzafava, A.; Supuran, C. T. In Drug Design of Zinc-Enzyme Inhibitors: Functional, Structural, and Disease Applications; Supuran, C. T., Winum, J.-Y., Eds.; Wiley: Hoboken, NJ, **2009**; p 473.
28. Gao, B. B.; Clermont, A.; Rook, S.; Fonda, S. J.; Srinivasan, V. J.; Wojtkowski, M.; Fujimoto, J. G.; Avery, R. L.; Arrigg, P. G.; Bursell, S. E.; Aiello, L. P.; Feener, E. P. Extracellular carbonic anhydrase mediates hemorrhagic retinal and cerebral vascular permeability through prekallikrein activation. *Nat. Med.* **2007**, *13*, 181-188.
29. Mincione, F.; Scozzafava, A.; Supuran, C. T. The development of topically acting carbonic anhydrase inhibitors as antiglaucoma agents. *Curr. Pharm. Des.* **2008**, *14*, 649-654.
30. Supuran, C. T. Diuretics: from classical carbonic anhydrase inhibitors to novel applications of the sulfonamides. *Curr. Pharm. Des.* **2008**, *14*, 641-648.
31. De Simone, G.; Scozzafava, A.; Supuran, C. T. Which carbonic anhydrases are targeted by the antiepileptic sulfonamides and sulfamates? *Chem. Biol. Drug Des.* **2009**, *74*, 317-321.
32. Basnyat, B.; Gertsch, J. H.; Johnson, E. W.; Castro-Marin, F.; Inoue, Y.; Yeh, C. Efficacy of low-dose acetazolamide (125 mg BID) for the prophylaxis of acute mountain sickness: a prospective, double-blind, randomized, placebo-controlled trial. *High Alt. Med. Biol.* **2003**, *4*, 45-52.
33. Swenson, E. R.; Teppema, L. J. Prevention of acute mountain sickness by acetazolamide: as yet an unfinished story. *J. Appl. Physiol.* **2007**, *102*, 1305-1307.
34. Barreiro, E.; Hussain, S. N. A. Protein carbonylation in skeletal muscles: impact on function. *Antioxid. Redox Signal.* **2010**, *12*, 417-429.
35. Matsui, H.; Murakami, M.; Wynns, G. C.; Conroy, C. W.; Mead, A.; Maren, T. H.; Sears, M. L. Membrane carbonic anhydrase (IV) and ciliary epithelium. Carbonic anhydrase activity is present in the basolateral membranes of the non-pigmented ciliary epithelium of rabbit eyes. *Exp. Eye Res.* **1996**, *62*, 409-417.
36. Tang, Y.; Xu, H.; Du, X.; Lit, L.; Walker, W.; Lu, A.; Ran, R.; Gregg, J. P.; Reilly, M.; Pancioli, A.; Khoury, J. C.; Sauerbeck, L. R.; Carrozzella, J. A.; Spilker, J.; Clark, J.; Wagner, K. R.; Jauch, E. C.; Chang, D. J.; Verro, P.; Broderick, J. P.; Sharp, F. R. Gene expression in blood changes rapidly in neutrophils and monocytes after ischemic stroke in humans: a microarray study. *J. Cereb. Blood Flow Metab.* **2006**, *26*, 1089-1102.
37. De Simone, G.; Supuran, C. T. In Drug Design of Zinc-Enzyme Inhibitors: Functional, Structural, and Disease Applications; Supuran, C. T., Winum, J.-Y., Eds.; Wiley: Hoboken, NJ, **2009**; p 241.
38. Liu, C.; Wei, Y.; Wang, J.; Pi, L.; Huang, J.; Wang, P.; Carbonic anhydrases III and IV autoantibodies in rheumatoid arthritis, systemic lupus erythematosus, diabetes, hypertensive renal disease, and heart failure. *Clin. Dev. Immunol.* **2012**, 2012, 354594.
39. Margheri, F.; Ceruso, M.; Carta, F.; Laurenzana, A.; Maggi, L.; Lazzeri, S.; Simonini, G.; Annunziato F.; Del Rosso M.; Supuran C. T.; Cimaz, R. Overexpression of the transmembrane

carbonic anhydrase isoforms IX and XII in the inflamed synovium. *J. Enzyme Inhib. Med. Chem.* **2016**, *31*, 60-63.

40. De Simone, G.; Di Fiore, A.; Supuran, C. T. Are carbonic anhydrase inhibitors suitable for obtaining antiobesity drugs? *Curr. Pharm. Des.* **2008**, *14*, 655-660.
41. De Simone, G.; Supuran, C. T. Antiobesity carbonic anhydrase inhibitors. *Curr. Top. Med. Chem.* **2007**, *7*, 879-884.
42. Supuran, C. T.; Di Fiore, A.; De Simone, G. Carbonic anhydrase inhibitors as emerging drugs for the treatment of obesity. *Expert Opin. Emerg. Drugs.* **2008**, *13*, 383-392.
43. Nishimori, I.; Minakuchi, T.; Onishi, S.; Vullo, D.; Scozzafava, A.; Supuran, C. T. Carbonic anhydrase inhibitors. DNA cloning, characterization, and inhibition studies of the human secretory isoform VI, a new target for sulfonamide and sulfamate inhibitors. *J. Med. Chem.* **2007**, *50*, 381-388.
44. Kivelä, J.; Parkkila, S.; Parkkila, A. K.; Rajaniemi, H. A low concentration of carbonic anhydrase isoenzyme VI in whole saliva is associated with caries prevalence. *Caries Res.* **1999**, *33*, 178-184.
45. Ruusuvuori, E.; Li, H.; Huttu, K.; Palva, J. M.; Smirnov, S.; Rivera, C.; Kaila, K.; Voipio, J. Carbonic anhydrase isoform VII acts as a molecular switch in the development of synchronous gamma-frequency firing of hippocampal CA1 pyramidal cells. *J. Neurosci.* **2004**, *24*, 2699-2707.
46. Aspatwar, A.; Tolvanen, M. E.; Ortutay, C.; Parkkila, S. Carbonic anhydrase related protein VIII and its role in neurodegeneration and cancer. *Curr. Pharm. Des.* **2010**, *16*, 3264-3276.
47. Nishimori, I. In Carbonic Anhydrase: Its Inhibitors and Activators; Supuran, C. T., Scozzafava, A., Conway, J., Eds.; CRC Press: Boca Raton, FL, **2004**; p 25.
48. Neri, D.; Supuran, C.T. Interfering with pH regulation in tumours as a therapeutic strategy. *Nat. Rev. Drug Discov.* **2011**, *10*, 767-777.
49. Pastorekova, S.; Parkkila, S.; Zavada, J. Tumor-associated carbonic anhydrases and their clinical significance. *Adv. Clin. Chem.* **2006**, *42*, 167-216.
50. De Simone, G.; Supuran, C. T. Carbonic anhydrase IX: Biochemical and crystallographic characterization of a novel antitumor target. *Biochim. Biophys. Acta* **2010**, *1804*, 404-409.
51. Battke, C.; Kremmer, E.; Mysliwietz, J.; Gondi, G.; Dumitru, C.; Brandau, S.; Lang, S.; Vullo, D.; Supuran, C. T.; Zeidler, R. Generation and characterization of the first inhibitory antibody targeting tumour-associated carbonic anhydrase XII. *Cancer Immunol. Immunother.* **2011**, *60*, 649-658.
52. Liao, S. Y.; Ivanov, S.; Ivanova, A.; Ghosh, S.; Cote, M. A.; Keefe, K.; Coca-Prados, M.; Stanbridge, E. J.; Lerman, M. I. Expression of cell surface transmembrane carbonic anhydrase genes CA9 and CA12 in the human eye: overexpression of CA12 (CAXII) in glaucoma. *J. Med. Genet.* **2003**, *40*, 257-261.
53. Pastorek, J., Pastorekova, S. Hypoxia-induced carbonic anhydrase IX as a target for cancer therapy: From biology to clinical use. *Semin. Cancer Biol.* **2015**, *31*, 52−64.
54. Monti, S. M.; Supuran, C. T.; De Simone, G. Anticancer carbonic anhydrase inhibitors: a patent review (2008 -2013). *Expert Opin. Ther. Pat.* **2013**, *23*, 737−749.
55. Lehtonen, J.; Shen, B.; Vihinen, M.; Casini, A.; Scozzafava, A.; Supuran, C. T.; Parkkila, A. K.; Saarnio, J.; Kivelä, A. J.; Waheed, A.; Sly, W. S.; Parkkila, S. Characterization of CA XIII, a novel member of the carbonic anhydrase isozyme family. *J. Biol. Chem.* **2004**, *279*, 2719-2727.
56. Shah, G. N.; Ulmasov, B.; Waheed, A.; Becker, T.; Makani, S.; Svichar, N.; Chesler, M.; Sly, W. S. Carbonic anhydrase IV and XIV knockout mice: roles of the respective carbonic anhydrases in buffering the extracellular space in brain. *Proc. Natl. Acad. Sci .U.S.A.* **2005**, *102*, 16771-16776.
57. Ogilvie, J. M.; Ohlemiller, K. K.; Shah, G. N.; Ulmasov, B.; Becker, T. A.; Waheed, A.; Hennig, A. K.; Lukasiewicz, P. D.; Sly, W. S. Carbonic anhydrase XIV deficiency produces a functional defect in the retinal light response. *Proc. Natl. Acad. Sci. U.S.A.* **2007**, *104*, 8514-8519.

58. Alterio, V.; Di Fiore, A.; D'Ambrosio, K.; Supuran, C. T.; De Simone, G. In Drug Design of Zinc-Enzyme Inhibitors: Functional, Structural, and Disease Applications; Supuran, C. T., Winum, J.-Y., Eds.; Wiley: Hoboken, NJ, **2009**; p 73.
59. Eriksson, A. E.; Kylsten, P. M.; Jones, T. A.; Liljas, A. Crystallographic studies of inhibitor binding sites in human carbonic anhydrase II: a pentacoordinated binding of the SCN- ion to the zinc at high pH. *Proteins* **1988**, *4*, 283-293.
60. Boriack-Sjodin, P. A.; Heck, R. W.; Laipis, P. J.; Silverman, D. N.; Christianson, D. W. Structure determination of murine mitochondrial carbonic anhydrase V at 2.45-A resolution: implications for catalytic proton transfer and inhibitor design. *Proc. Natl. Acad. Sci. U.S.A.* **1995**, *92*, 10949-10953.
61. Eriksson, A. E.; Liljas, A. Refined structure of bovine carbonic anhydrase III at 2.0 A resolution. *Proteins* **1993**, *16*, 29-42.
62. Stams, T.; Nair, S. K.; Okuyama, T.; Waheed, A.; Sly, W. S.; Christianson, D. W. Crystal structure of the secretory form of membrane-associated human carbonic anhydrase IV at 2.8-A resolution. *Proc. Natl. Acad. Sci. U.S.A.* **1996**, *93*, 13589-13594.
63. Whittington, D. A.; Waheed, A.; Ulmasov, B.; Shah, G. N.; Grubb, J. H.; Sly, W. S.; Christianson, D. W. Crystal structure of the dimeric extracellular domain of human carbonic anhydrase XII, a bitopic membrane protein overexpressed in certain cancer tumor cells. *Proc. Natl. Acad. Sci. U.S.A.* **2001**, *98*, 9545-9550.
64. Whittington, D. A.; Grubb, J. H.; Waheed, A.; Shah, G. N.; Sly, W. S.; Christianson, D. W. Expression, assay, and structure of the extracellular domain of murine carbonic anhydrase XIV: implications for selective inhibition of membrane-associated isozymes. *J. Biol. Chem.* **2004**, *279*, 7223-7228.
65. Duda, D. M.; Tu, C.; Fisher, S. Z.; An, H.; Yoshioka, C.; Govindasamy, L.; Laipis, P. J.; Agbandje-McKenna, M.; Silverman, D. N.; McKenna, R. Human carbonic anhydrase III: structural and kinetic study of catalysis and proton transfer. *Biochemistry* **2005**, *44*, 10046-10053.
66. Di Fiore, A.; Monti, S. M.; Hilvo, M.; Parkkila, S.; Romano, V.; Scaloni, A.; Pedone, C.; Scozzafava, A.; Supuran, C. T.; De Simone, G. Crystal structure of human carbonic anhydrase XIII and its complex with the inhibitor acetazolamide. *Proteins* **2008**, *74*, 164-175.
67. Alterio, V.; Hilvo, M.; Di Fiore, A.; Supuran, C.T.; Pan, P.; Parkkila, S.; Scaloni, A.; Pastorek, J.; Pastorekova, S.; Pedone, C.; Scozzafava, A.; Monti, S.M.; De Simone, G. Crystal structure of the catalytic domain of the tumor-associated human carbonic anhydrase IX *Proc. Natl. Acad. Sci. U.S.A.* **2009**, *106*, 16233-16238.
68. Di Fiore, A.; Truppo, E.; Supuran, C. T.; Alterio, V.; Dathan, N.; Bootorabi, F.; Parkkila, S.; Monti, S. M.; De Simone, G. Crystal structure of the C183S/C217S mutant of human CA VII in complex with acetazolamide. *Bioorg. Med. Chem. Lett.* **2010**, *20*, 5023-5026.
69. Capasso, C.; Supuran C.T. Anti-infective carbonic anhydrase inhibitors: a patent and literature review. *Expert Opin. Ther. Pat.* **2013**, *23*, 693-704.
70. Chirica, L.C.; Petersson, C.; Hurtig, M.; Jonsson, B.H.; Borén, T.; Lindskog, S. Expression and localization of alpha- and beta-carbonic anhydrase in Helicobacter pylori. *Biochim. Biophys. Acta.* **2002**, *1601*, 192-199.
71. Nishimori, I.; Minakuchi, T.; Morimoto, K.; Sano, S.; Onishi, S.; Takeuchi, H.; Vullo, D.; Scozzafava, A.; Supuran, C. T. Carbonic anhydrase inhibitors: DNA cloning and inhibition studies of the alpha-carbonic anhydrase from Helicobacter pylori, a new target for developing sulfonamide and sulfamate gastric drugs. *J. Med. Chem*. **2006**, *49*, 2117-2126.
72. Shahidzadeh, R.; Opekun, A.; Shiotani, A; Graham D. Y. Effect of the carbonic anhydrase inhibitor, acetazolamide, on Helicobacter pylori infection in vivo: a pilot study. *Helicobacter* **2005**, *10*, 136-138.

73. Del Prete, S.; Isik, S.; Vullo, D.; De Luca, V.; Carginale, V.; Scozzafava, A.; Supuran C.T.; Capasso, C. DNA cloning, characterization, and inhibition studies of an alpha-carbonic anhydrase from the pathogenic bacterium Vibrio cholerae. *J. Med. Chem.* **2012**, *55*, 10742-10748.
74. Vullo, D.; Isik, S.; Del Prete, S.; De Luca, V.; Carginale, V.; Scozzafava, A.; Supuran, C.T.; Capasso, C. Anion inhibition studies of the alpha-carbonic anhydrase from the pathogenic bacterium Vibrio cholerae. *Bioorg. Med. Chem. Lett.* **2013**, *23*, 1636-1638.
75. Innocenti, A.; Hall, R. A.; Schlicker, C.; Scozzafava, A.; Steegborn, C.; Mühlschlegel, F. A.; Supuran, C.T. Carbonic anhydrase inhibitors. Inhibition and homology modeling studies of the fungal beta-carbonic anhydrase from Candida albicans with sulfonamides. *Bioorg. Med. Chem.* **2009**, *17*, 4503-4509.
76. Monti, S.M.; Maresca, A.; Viparelli, F.; Carta, F.; De Simone, G.; Mühlschlegel, F.A.; Scozzafava, A.; Supuran, C. T. Dithiocarbamates are strong inhibitors of the beta-class fungal carbonic anhydrases from Cryptococcus neoformans, Candida albicans and Candida glabrata. *Bioorg. Med. Chem. Lett.* **2012**, *22*, 859-862.
77. Cottier, F.; Leewattanapasuk, W.; Kemp, L.R.; Murphy, M.; Supuran, C. T.; Kurzai, O.; Mühlschlegel, F. A. Carbonic anhydrase regulation and CO(2) sensing in the fungal pathogen Candida glabrata involves a novel Rca1p ortholog. *Bioorg. Med. Chem.* **2013**, *21*, 1549-1554.
78. Davis. R. A.; Hofmann, A.; Osman, A.; Hall, R. A.; Mühlschlegel, F.A.; Vullo, D.; Innocenti, A.; Supuran, C. T.; Poulsen, S.A. Natural product-based phenols as novel probes for mycobacterial and fungal carbonic anhydrases. *J. Med. Chem.* **2011**, *54*, 1682-1692.
79. Isik, S.; Kockar, F.; Arslan, O.; Guler, O. O.; Innocenti, A.; Supuran, C. T. Carbonic anhydrase inhibitors. Inhibition of the beta-class enzyme from the yeast Saccharomyces cerevisiae with anions. *Bioorg. Med. Chem. Lett*. **2008**, *18*, 6327-6331.
80. Hewitson, K. S.; Vullo, D.; Scozzafava. A.; Mastrolorenzo, A.; Supuran, C. T. Molecular cloning, characterization, and inhibition studies of a beta-carbonic anhydrase from Malassezia globosa, a potential antidandruff target. *J. Med. Chem.* **2012**, *55*, 3513-3520.
81. Krungkrai, J.; Scozzafava, A.; Reungprapavut, S.; Krungkrai, S. R.; Rattanajak, R.; Kamchonwongpaisan, S.; Supuran C. T. Carbonic anhydrase inhibitors. Inhibition of Plasmodium falciparum carbonic anhydrase with aromatic sulfonamides: towards antimalarials with a novel mechanism of action? *Bioorg. Med. Chem.* **2005**, *13*, 483-489.
82. Krungkrai, S. R; Suraveratum, N.; Rochanakij, S.; Krungkrai, J. Characterisation of carbonic anhydrase in Plasmodium falciparum. *Int. J. Parasitol* **2001**, *31*, 661-668.
83. Supuran CT, Capasso C. The eta-class carbonic anhydrases as drug targets for antimalarial agents. *Expert Opin. Ther. Targets* **2015**, *19*, 551-563.
84. Pan, P.; Vermelho, A. B.; Capaci Rodrigues, G.; Scozzafava, A.; Tolvanen, M. E.; Parkkila, S.; Capasso, C.; Supuran, C. T. Cloning, characterization, and sulfonamide and thiol inhibition studies of an alphacarbonic anhydrase from Trypanosoma cruzi, the causative agent of Chagas disease. *J. Med. Chem.* **2013**, *56*, 1761-1771.
85. Guzel-Akdemir, O.; Akdemir, A.; Pan, P.; Vermelho, A. B.; Parkkila, S.; Scozzafava, A.; Capasso, C.; Supuran, C. T. A class of sulfonamides with strong inhibitory action against the alpha-carbonic anhydrase from Trypanosoma cruzi. *J. Med. Chem.* **2013**, *56*, 5773-5781.
86. Syrjanen, L.; Vermelho, A. B.; Rodrigues Ide, A.; Corte-Real, S.; Salonen, T.; Pan, P.; Vullo, D.; Parkkila, S.; Capasso, C.; Supuran, C. T. Cloning, characterization, and inhibition studies of a beta-carbonic anhydrase from Leishmania donovani chagasi, the protozoan parasite responsible for leishmaniasis. *J. Med. Chem* **2013**, *56*, 7372-7381.
87. Supuran, C. T. Structure-based drug discovery of carbonic anhydrase inhibitors. *J. Enzyme Inhib. Med. Chem.* **2012**, *27*, 759–772.
88. Supuran, C. T. Carbonic anhydrase inhibitors. *Bioorg. Med. Chem. Lett*. **2010**, *20*, 3467–3474.
89. Carta, F.; Supuran, C.T.; Scozzafava, A. Sulfonamides and their isosters as carbonic anhydrase inhibitors. *Future Med. Chem.* **2014**, *6*, 1149-1165.

90. Winum, J.Y.; Supuran, C.T. Recent advances in the discovery of zinc-binding motifs for the development of carbonic anhydrase inhibitors. *J. Enzyme Inhib. Med. Chem*. **2015**, *30*, 321-324.
91. Supuran, C.T. How many carbonic anhydrase inhibition mechanisms exist? *J. Enzyme Inhib. Med. Chem*. **2016**, *31*, 345-360.
92. Keilin, D.; Mann, T. Carbonic anhydrase. Purification and nature of the enzyme. *Biochem. J.* **1940**, *34*, 1163-1176.
93. Winum, J.-Y.; Monter, J,-L.; Scozzafava, A.; Supuran, C. T. In Drug Design of Zinc-Enzyme Inhibitors: Functional, Structural, and Disease Applications; Supuran, C. T., Winum, J.-Y., Eds.; Wiley: Hoboken, NJ, **2009**; p 39.
94. Carbonic Anhydrases as Biocatalysts: From Theory to Medical and Industrial Applications; Supuran, C. T., De Simone. Eds.; Elsevier. **2015**.
95. Bozdag, M.; Ferraroni, M.; Nuti, E.; Vullo, D.; Rossello, A.; Carta, F.; Scozzafava, A.; Supuran, C. T. Combining the tail and the ring approaches for obtaining potent and isoform-selective carbonic anhydrase inhibitors: solution and X-ray crystallographic studies. *Bioorg. Med. Chem.* **2014**, *22*, 334−340.
96. Scozzafava, A.; Menabuoni, L.; Mincione, F.; Briganti, F.; Mincione, G.; Supuran, C. T. Carbonic anhydrase inhibitors. Synthesis of water-soluble, topically effective, intraocular pressure-lowering aromatic/heterocyclic sulfonamides containing cationic or anionic moieties: Is the tail more important than the ring? *J. Med. Chem.* **1999**, *42*, 2641−2650.
97. Menchise, V.; De Simone, G.; Alterio, V.; Di Fiore, A.; Pedone, C.; Scozzafava, A.; Supuran, C. T. Carbonic anhydrase inhibitors: stacking with Phe131 determines active site binding region of inhibitors as exemplified by the X-ray crystal structure of a membrane-impermeant antitumor sulfonamide complexed with isozyme II. *J. Med. Chem*. **2005**, *48*, 5721-5727.
98. Scozzafava, A.; Briganti, F.; Ilies, M. A.; Supuran, C. T. Carbonic anhydrase inhibitors: synthesis of membrane-impermeant low molecular weight sulfonamides possessing in vivo selectivity for the membrane-bound versus cytosolic isozymes. *J. Med. Chem.* **2000**, *43*, 292-300.
99. Pacchiano, F.; Carta, F.; McDonald, P. C.; Lou, Y.; Vullo, D.; Scozzafava, A.; Dedhar, S.; Supuran, C. T. Ureido-substituted benzenesulfonamides potently inhibit carbonic anhydrase IX and show antimetastatic activity in a model of breast cancer metastasis. *J. Med. Chem.* **2011**, *54*, 1896−1902.
100. ClinicalTrials.gov, https://clinicaltrials.gov/ct2/results?term=slc-0111&Search=Search (Accessed on October 15th 2017).
101. Carta, F.; Aggarwal, M.; Maresca, A.; Scozzafava, A.; McKenna, R.; Supuran, C. T. Dithiocarbamates: a new class of carbonic anhydrase inhibitors. Crystallographic and kinetic investigations. *Chem. Commun. (Camb).* **2012**, *48*, 1868-1870.
102. Carta, F.; Aggarwal, M.; Maresca, A; Scozzafava, A.; McKenna, R.; Masini, E.; Supuran, C. T. Dithiocarbamates strongly inhibit carbonic anhydrases and show antiglaucoma action in vivo. *J. Med. Chem.* **2012**, 55,1721-1730.
103. Carta, F.; Akdemir, A.; Scozzafava, A.; Masini, E; Supuran, C. T. Xanthates and trithiocarbonates strongly inhibit carbonic anhydrases and show antiglaucoma effects in vivo. *J. Med. Chem.* **2013**, *56*, 4691-4700.
104. Vullo, D.; Durante, M.; Di Leva, F. S.; Cosconati, S.; Masini, E.; Scozzafava, A.; Novellino, E.; Supuran, C. T.; Carta, F. Monothiocarbamates Strongly Inhibit Carbonic Anhydrases in Vitro and Possess Intraocular Pressure Lowering Activity in an Animal Model of Glaucoma. *J. Med. Chem.* **2016**, *59*, 5857-5867.
105. Mori, M.; Cau, Y.; Vignaroli, G.; Laurenzana, I.; Caivano, A.; Vullo, D.; Supuran, C. T.; Botta, M. Hit recycling: discovery of a potent carbonic anhydrase inhibitor by in silico target fishing. *ACS Chem. Biol.* **2015**, *10*, 1964–1969.

106. Innocenti, A.;Vullo, D.; Scozzafava, A.; Casey, J. R.; Supuran, C. T. Carbonic anhydrase inhibitors. Interaction of isozymes I, II, IV, V and IX with carboxylates. *Bioorg. Med. Chem. Lett.* **2005**, *15*, 573–578.
107. Scozzafava, A.; Supuran, C. T. Hydroxyurea is a carbonic anhydrase inhibitor. *Bioorg. Med. Chem.* **2003**, *11*, 2241–2246.
108. Di Fiore, A.; Maresca, A.; Supuran, C. T.; De Simone, G. Hydroxamate represents a versatile zinc binding group for the development of new carbonic anhydrase inhibitors. *Chem. Commun. (Camb.)* **2012**, *48*, 8838–8840.
109. Nair, S. K.; Ludwig, P. A.; Christianson, D. W. Two-site binding of phenol in the active site of human carbonic anhydrase II: structural implications for substrate association. *J. Am. Chem. Soc.* **1994**, *116*, 3659–3660.
110. Innocenti, A.; Vullo, D.; Scozzafava, A.; Supuran, C. T. Carbonic anhydrase inhibitors. Interactions of phenols with the 12 catalytically active mammalian isoforms (CA I–XIV). *Bioorg. Med. Chem. Lett*. **2008**, *18*, 1583–1587.
111. Carta, F.; Temperini, C.; Innocenti, A.; Scozzafava, A.; Kaila, K.; Supuran, C. T. Polyamines inhibit carbonic anhydrases by anchoring to the zinc-coordinated water molecule. *J. Med. Chem.* **2010,** *53*, 5511–5522.
112. Innocenti, A.; Ozturk Sarkaya, S. B.; Gulcin, I.; Supuran, C. T. Carbonic anhydrase inhibitors. Inhibition of mammalian isoforms I-XIV with a series of natural product polyphenols and phenolic acids. *Bioorg. Med. Chem.* **2010**, *18*, 2159–2164.
113. Davis, R. A.; Hofmann, A.; Osman, A.; Hall, R. A.; Mühlschlegel, F. A.; Vullo, D.; Innocenti, A.; Supuran, C. T.; Poulsen, S. A. Natural product-based phenols as novel probes for mycobacterial and fungal carbonic anhydrases. *J. Med. Chem.* **2011**, *54*, 1682–1692.
114. Martin, D.P.; Cohen, S. M. Nucleophile recognition as an alternative inhibition mode for benzoic acid based carbonic anhydrase inhibitors. *Chem. Commun. (Camb.)* **2012**, *48*, 5259–5261.
115. Tars, K.; Vullo, D.; Kazaks, A.; Leitans, J.; Lends, A.; Grandane, A.; Zalubovskis, R.; Scozzafava, A.; Supuran, C. T. Sulfocoumarins (1,2- benzoxathiine-2,2-dioxides): a class of potent and isoform-selective inhibitors of tumor-associated carbonic anhydrases. *J. Med. Chem.* **2013**, *56*, 293–300.
116. Buchieri, M.V.; Riafrecha, L.E.; Rodrıguez, O. M.; Vullo, D.; Morbidoni, H. R.; Supuran, C. T.; Colinas, P. A. Inhibition of the b-carbonic anhydrases from Mycobacterium tuberculosis with C-cinnamoyl glycosides: identification of the first inhibitor with anti-mycobacterial activity. *Bioorg. Med. Chem. Lett.* **2013;** *23*, 740–743.
117. Maresca, A.; Temperini, C.; Vu, H.; Pham, N. B.; Poulsen, S. A.; Scozzafava, A.; Quinn, R. J. Supuran, C. T. Non-zinc mediated inhibition of carbonic anhydrases: coumarins are a new class of suicide inhibitors. *J. Am. Chem. Soc.* **2009**, *131*, 3057–3062.
118. Maresca, A.; Temperini, C.; Pochet, L.; Masereel, B.; Scozzafava, A.; Supuran, C. T. Deciphering the mechanism of carbonic anhydrase inhibition with coumarins and thiocoumarins. *J. Med. Chem.* **2010**, *53*, 335–344.
119. Temperini, C.; Innocenti, A.; Scozzafava, A.; Parkkila, S.; Supuran, C. T. The coumarin binding site in carbonic anhydrase accommodates structurallydiverse inhibitors: the antiepileptic lacosamide as an example and lead molecule for novel classes of carbonic anhydrase inhibitors. *J. Med. Chem*. **2010**, *53*, 850–854.
120. Touisni, N.; Maresca, A.; McDonald, P. C.; Lou, Y.; Scozzafava, A.; Dedhar, S.; Winum, J. Y.; Supuran, C. T. Glycosyl coumarin carbonic anhydrase IX and XII inhibitors strongly attenuate the growth of primary breast tumors. *J. Med. Chem.* **2011**, *54*, 8271–8277.
121. Bonneau, A; Maresca, A.; Winum, J. Y.; Supuran, C. T. Metronidazolecoumarin conjugates and 3-cyano-7-hydroxy-coumarin act as isoform-selective carbonic anhydrase inhibitors. *J. Enzyme Inhib. Med. Chem.* **2013**, *28*, 397–401.

122. Sharma, A.; Tiwari, M.; Supuran, C. T. Novel coumarins and benzocoumarins acting as isoform-selective inhibitors against the tumor-associated carbonic anhydrase IX. *J. Enzyme Inhib. Med. Chem.* **2014**, *29*, 292–296.
123. Maresca, A.; Supuran, C. T. Coumarins incorporating hydroxy- and chloro- moieties selectively inhibit the transmembrane, tumor-associated carbonic anhydrase isoforms IX and XII over the cytosolic ones I and II. *Bioorg. Med. Chem. Lett.* **2010**, *20*, 4511–4514.
124. Maresca, A.; Scozzafava, A.; Supuran, C. T. 7,8-Disubstituted- but not 6,7-disubstituted coumarins selectively inhibit the transmembrane, tumor-associated carbonic anhydrase isoforms IX and XII over the cytosolic ones I and II in the low nanomolar/subnanomolar range. *Bioorg. Med. Chem. Lett.* **2010**, *20*, 7255–7258.
125. Wilkinson, B. L.; Bornaghi, L. F.; Houston, T. A.; Innocenti, A.; Supuran, C. T.; Poulsen, S.-A. A novel class of carbonic anhydrase inhibitors: glycoconjugate benzene sulfonamides prepared by "click-tailing". *J. Med. Chem*. **2006**, *49*, 6539-6548.
126. Lopez, M.; Salmon, A. J.; Supuran, C. T.; Poulsen, S.-A. Carbonic anhydrase inhibitors developed through "click tailing" *Curr. Pharm. Des*. **2010**, *16*, 3277-3287.
127. Wilkinson, B. L.; Bornaghi, L. F.; Houston, T. A.; Innocenti, A.; Vullo, D.; Supuran, C. T.; Poulsen, S.-A. Carbonic anhydrase inhibitors: inhibition of isozymes I, II, and IX with triazole-linked O-glycosides of benzene sulfonamides. *J. Med. Chem*. **2007**, *50*,1651-1657.
128. Pala, N.; Micheletto, L.; Sechi, M.; Aggarwal, M.; Carta, F.; McKenna, R.; Supuran, C.T. Carbonic anhydrase inhibition with benzenesulfonamides and tetrafluoro-benzenesulfonamides obtained via Click Chemistry. *ACS Med. Chem. Lett.* **2014**, *5*, 927−930.
129. Christopher, D. H.; Xin-Ming, L.; Dong, W. Click chemistry, a powerful tool for pharmaceutical sciences. *Pharm. Res.* **2008**, *25*, 2216–2230.
130. Weinreb, R.N.; Aung, T.; Medeiros, F.A. The pathophysiology and treatment of glaucoma: a review. *JAMA* **2014**, *311*, 1901-1911.
131. Masini, E.; Carta, F.; Scozzafava, A.; Supuran, C. T. Antiglaucoma carbonic anhydrase inhibitors: A patent review. *Expert Opin. Ther. Pat.* **2013**, *23*, 705−716.
132. Scozzafava, A.; Supuran, C. T. Glaucoma and the applications of carbonic anhydrase inhibitors. *Subcell Biochem.* **2014**, *75*, 349-359.
133. Carta, F.; Supuran, C. T.; Scozzafava, A. Novel therapies for glaucoma: a patent review 2007−2011. *Expert Opin. Ther. Pat.* **2012**, *22*, 79−88.
134. Scozzafava, A.; Menabuoni, L.; Mincione, F.; Supuran, C.T. Carbonic anhydrase inhibitors. A general approach for the preparation of water soluble sulfonamides incorporating polyamino-polycarboxylate tails and of their metal complexes possessing long lasting, topical intraocular pressure lowering properties. *J. Med. Chem.* **2002**, *45*, 1466-1476.
135. Khalifah, R. G. The carbon dioxide hydration activity of carbonic anhydrase. *J. Biol. Chem.* **1971**, *246*, 2561−2573.
136. Tanc, M.; Carta, F.; Bozdag, M.; Scozzafava, A.; Supuran, C. T. 7-Substituted-sulfocoumarins are isoform-selective, potent carbonic anhydrase II inhibitors. *Bioorg. Med. Chem.* **2013,** *15*, 4502–4510.
137. Grandane, A.; Tanc, M.; Zalubovskis, R.; Supuran, C. T. 6-Triazolylsubstituted sulfocoumarins are potent, selective inhibitors of the tumor associated carbonic anhydrases IX and XII. *Bioorg. Med. Chem. Lett.* **2014**, *5*, 1256–1260.
138. Grandane, A.; Tanc, M.; Zalubovskis, R.; Supuran, C. T. Synthesis of 6-tetrazolylsubstituted sulfocoumarins acting as highly potent and selective inhibitors of the tumor-associated carbonic anhydrase isoforms IX and XII. *Bioorg. Med. Chem.* **2014**, *22*, 1522–1528.
139. Grandane, A.; Tanc, M.; Di Cesare Mannelli, L.; Carta, F.; Ghelardini, C.; Žalubovskis, R.; Supuran, C. T. 6-substituted sulfocoumarins are selective carbonic anhdydrase IX and XII inhibitors with significant cytotoxicity against colorectal cancer cells. *J. Med. Chem.* **2015**, *58*, 3975–3983

140. Tanc, M.; Carta, F.; Scozzafava, A.; Supuran, C. T. 6-substituted 1,2-benzoxathiine- 2,2-dioxides are isoform-selective inhibitors of human carbonic anhydrases IX, XII and VA. *Org. Biomol. Chem.* **2015**, *13*, 77–80
141. Grandane, A.; Belyakov, S.; Trapencieris, P.; Žalubovskis, R. Facile synthesis of coumarin bioisosteres 1,2-benzoxathiine 2,2-dioxides. *Tetrahedron* **2012**, 68, 5541–5546.
142. Krebs, H. A. Inhibition of carbonic anhydrase by sulfonamides. *Biochem. J.* **1948**, *43*, 525-528.
143. Supuran, C. T.; Scozzafava, A.; Briganti, F. Carbonic anhydrase inhibitors: N-cyanosulfonamides, a new class of high affinity isozyme II and IV inhibitors. *J. Enzym. Inhib.* **1999**, 4, 289-306.
144. Duffel, M.; Silwai-Ing, I.; Segarra, T.; Dixson, J.; Barfknecht, C.; Schoenwald, R. N-Substituted sulfonamide carbonic anhydrase inhibitors with topical effects on intraocular pressure. *J. Med. Chem.* **1986**, 29, 1488-1494.
145. Briganti, F.; Pierattelli, R.; Scozzafava, A.; Supuran, C. T. Carbonic anhydrase inhibitors. Part 37. Novel classes of isozyme I and II inhibitors and their mechanism of action. Kinetic and spectroscopic investigations on native and cobalt-substituted enzymes. *Eur. J. Med. Chem.* **1996**, *31*, 1001-1010.
146. Di Fiore, A.; Maresca, A.; Alterio, V.; Supuran, C. T.; De Simone, G. Carbonic anhydrase inhibitors: X-ray crystallographic studies for the binding of N-substituted benzenesulfonamides to human isoform II. *Chem. Commun.* (Camb.) **2011**, *47*, 11636-11638.
147. Mahon, B. P.; Hendon, A. M.; Driscoll, J. M.; Rankin, G. M.; Poulsen, S. A.; Supuran, C. T.; McKenna, R. Saccharin: a lead compound for structure-based drug design of carbonic anhydrase IX inhibitors. *Bioorg. Med. Chem.* **2015**, 23, 849-854.
148. Moeker, J.; Peat, T. S.; Bornaghi, L. F.; Vullo, D.; Supuran, C. T.; Poulsen, S. A. Cyclic secondary sulfonamides: unusually good inhibitors of cancer-related carbonic anhydrase enzymes. *J. Med. Chem.* **2014,** 57, 3522-3531.
149. Carradori, S.; Secci, D.; De Monte, C.; Mollica, A.; Ceruso, M.; Akdemir, A.; Sobolev, A. P.; Codispoti, R.; De Cosmi, F.; Guglielmi, P.; Supuran, C. T. A novel library of saccharin and acesulfame derivatives as potent and selective inhibitors of carbonic anhydrase IX and XII isoforms. *Bioorg. Med. Chem.* **2016,** 24, 1095-1105.
150. D'Ascenzio, M.; Carradori, S.; De Monte, C.; Secci, D.; Ceruso, M.; Supuran, C. T. Design, synthesis and evaluation of N-substituted saccharin derivatives as selective inhibitors of tumor-associated carbonic anhydrase XII. *Bioorg. Med. Chem.* **2014**, *22*, 1821-1831.
151. Mollica, A.; Costante, R.; Akdemir, A.; Carradori, S.; Stefanucci, A.; Macedonio, G.; Ceruso, M.; Supuran, C. T. Exploring new Probenecid-based carbonic anhydrase inhibitors: Synthesis, biological evaluation and docking studies. *Bioorg. Med. Chem.* **2015**, *23*, 5311.
152. D'Ascenzio, M.; Carradori, S.; Secci, D.; Vullo, D.; Ceruso, M.; Akdemir, A.; Supuran, C. T. Selective inhibition of human carbonic anhydrases by novel amide derivatives of probenecid: synthesis, biological evaluation and molecular modelling studies. *Bioorg. Med. Chem.* **2014**, *22*, 3982-3988.
153. Minksztym, K. Synthesis of Aromatic Aminosulfonic Acid Nitroamides. *Synthesis* **2007**, *12*, 1819-1822.
154. Mathews, B. R. Benzene Sulfon nitramide, Toluene-4-sulfonnitramide, 2-nitroluene-4-sulfonnitranimide and Some of their Salts *J. Phys. Chem.* **1920**, *24*, 108.
155. Tian, G.; Liu, Y. Mechanistic insights into the catalytic reaction of ferulic acid decarboxylase from Aspergillus niger: a QM/MM study. *Phys. Chem. Chem. Phys.*, **2017**, *19*, 7733-7742.
156. Janoš, P.; Trnka, T.; Kozmon, S.; Tvaroška, I.; Koča, J. Different QM/MM Approaches To Elucidate Enzymatic Reactions: Case Study on ppGalNAcT2. *J. Chem. Theory. Comput.* **2016,** *13*, 6062-6076.
157. Georgieva, P.; Himo, F. Density functional theory study of the reaction mechanism of the DNA repairing enzyme alkylguanine alkyltransferase. *Chemical Physics Letters* **2008**, *463*, 214–218.

158. Pelmenschikov, V.; Blomberg, M. R.; Siegbahn, P. E. A theoretical study of the mechanism for peptide hydrolysis by thermolysin. *J. Biol. Inorg. Chem.* **2002**, *7*, 284-298.
159. Navrátil, V.; Klusák, V.; Rulíšek, L. Theoretical aspects of hydrolysis of peptide bonds by zinc metalloenzymes. *Chemistry* **201**3, *19*, 16634-16645.
160. Liao, R. Z.; Yu, J. G.; Himo, F. Reaction mechanism of the trinuclear zinc enzyme phospholipase C: a density functional theory study. *J. Phys. Chem. B.* **2010,** *114*, 2533-2540.
161. Dawson, T. L. Jr. Malassezia globosa and restricta: breakthrough understanding of the etiology and treatment of dandruff and seborrheic dermatitis through whole-genome analysis. *J. Invest. Dermatol. Symp. Proc.* **2007**, *12*, 15−19.
162. Guillot, J.; Hadina, S.; Gueho, E. The genus Malassezia: old facts and new concepts. *Parassitologia* **2008**, *50*, 77−79.
163. Del Prete, S.; Vullo, D.; Osman, S. M.; AlOthman, Z.; Capasso, C.; Supuran, C. T. Anion inhibition studies of the dandruff-producing fungus Malassezia globosa β-carbonic anhydrase MgCA. *Bioorg. Med. Chem. Lett.* **2015**, *25*, 5194-5198.
164. Del Prete, S.; De Luca, V.; Vullo, D.; Osman, S. M.; AlOthman, Z.; Carginale, V.; Supuran, C. T.; Capasso, C. A new procedure for the cloning, expression and purification of the β-carbonic anhydrase from the pathogenic yeast Malassezia globosa, an anti-dandruff drug target. *J. Enzyme Inhib. Med. Chem.* **2016**, *31*, 1156-1561.
165. Hay, R. J. Malassezia, dandruff and seborrhoeic dermatitis: an overview. *Br. J. Dermatol.* **2011**, *165*, 2-8.
166. Greene, D. L.; McCormick, B. J.; Pierpont, C. G. Amine adducts of thiocarbamate complexes. crystal and molecular structure of bis(cyc1opentamethylene thiocarbamato)bis(piperidine)zinc(II). *Inorg. Chem*. **1973**, *12*, 2148–2152.
167. Alterio, V.; Cadoni, R.; Esposito, D.; Vullo, D.; Fiore, A. D.; Monti, S. M.; Caporale, A.; Ruvo, M.; Sechi, M.; Dumy, P.; Supuran, C. T.; De Simone, G.; Winum, J. Y. Benzoxaborole as a new chemotype for carbonic anhydrase inhibition. *Chem. Commun.* **2016**, *52*, 11983-11986.
168. Pałasz, A.; Dariusz, Ciez. In search of uracil derivatives as bioactive agents. Uracils and fused uracils: Synthesis, biological activity and applications. *Eur. J. Med. Chem.* **2015**, *97*, 582-611.
169. Legraverend, M.; Grierson, D. S. The purines: Potent and versatile small molecule inhibitors and modulators of key biological targets. *Bioorg. Med. Chem.* **2006**, *14*, 3987–4006.
170. Parker, W. B. Enzymology of Purine and Pyrimidine Antimetabolites Used in the Treatment of Cancer. *Chem. Rev.* **2009,** *109*, 2880–2893.
171. Calderón-Arancibia, J.; Espinosa-Bustos, C.; Cañete-Molina, A.; Tapia, R.A.; Faúndez, M.; Torres, M.J.; Aguirre, A.; Paulino, M.; Salas, C.O. Synthesis and Pharmacophore Modelling of 2,6,9-Trisubstituted Purine Derivatives and Their Potential Role as Apoptosis-Inducing Agents in Cancer Cell Lines. *Molecules* **2015**, *20*, 6808-6826.
172. Raic-Malic, S.; Svedruzic, D.; Gazivoda, T.;Marunovic, A.; Hergold-Brundic, A.; Nagl, A.; Balzarini, J.; De Clercq, E.; Mintas, M. Synthesis and Antitumor Activities of Novel Pyrimidine Derivatives of 2,3-O,O-Dibenzyl-6-deoxy-L-ascorbic Acid and 4,5-Didehydro-5,6- dideoxy-L-ascorbic Acid. *J. Med. Chem.* **2000,** *43*, 4806-4811.
173. Nepali, K.; Sharma, S.; Sharma, M.; Bedi, P. M. S.; Dhar, K. L. Rational approaches, design strategies, structure activity relationship and mechanistic insights for anticancer hybrids. *Eur. J. Med. Chem.* **2014**, *77*, 422-487.
174. Gediya, L. K.; Njar, V. C. Promise and challenges in drug discovery and development of hybrid anticancer drugs. *Expert Opin. Drug Discov*. **2009**, *4*, 1099-1111.
175. Krištafora, S.; Bistrovic, A.; Plavec, J.; Makuc, D.; Martinovic, T.; Pavelic, S. K.; Raic-Malic, S. One-pot click synthesis of 1,2,3-triazole-embedded unsaturated uracil derivtives and hybrids of 1,5- and 2,5-disubstituted tetrazoles and pyrimidines. *Tetrahedron Letters*, **2015**, *56*, 1222–1228.
176. Eldehna, W. M.; Fares, M.; Ceruso, M.; Ghabbour, H. A.; Abou-Seri, S. M.; Abdel-Aziz, H. A.; El Ella, D. A.; Supuran, C. T. Amido/ureidosubstituted benzenesulfonamides-isatin conjugates

as low nanomolar/ subnanomolar inhibitors of the tumor-associated carbonic anhydrase isoform XII. *Eur. J. Med. Chem.* **2016**, *110*, 259-266.

177. Güzel-Akdemir, Ö.; Akdemir, A.; Karalı, N.; Supuran, C. T. Discovery of novel isatin-based sulfonamides with potent and selective inhibition of the tumor associated carbonic anhydrase isoforms IX and XII. *Org. Biomol. Chem.* **2015**, *13*, 6493–6499.
178. Ibrahim, H. S.; Abou-Seri, S. M.; Tanc, M.; Elaasser, M. M.; Abdel-Aziz, H. A.; Supuran, C. T. Isatin-pyrazole benzenesulfonamide hybrids potently inhibit tumor-associated carbonic anhydrase isoforms IX and XII. *Eur. J. Med. Chem.* **2015**, *103*, 583-593.
179. Abdel-Hamid, M. K.; Abdel-Hafez, A. A.; El-Koussi, N. A.; Mahfouz, N. M.; Innocenti, A.; Supuran, C. T. Design, synthesis, and docking studies of new 1,3,4-thiadiazole-2-thione derivatives with carbonic anhydrase inhibitory activity. *Bioorg. Med. Chem.* **2007**, *15*, 6975–6984.
180. Ibrahim, H. S.; Abou-Seri, S. M.; Abdel-Aziz, H. A. 3-Hydrazinoindolin-2-one derivatives: Chemical classification and investigation of their targets as anticancer agents. *Eur. J. Med. Chem.* **2016**, *122*, 366-381.
181. Kidwai, M.; Jahan, A.; Mishra, N. K. Isatins: A diversity orientated biological profile. *Med. Chem.* **2014**, *4*, 451-468.
182. Goodman, V. L.; Rock, E. P.; Dagher, R.; Ramchandani, R. P.; Abraham, S.; Gobburu, J. VS.; Booth, B. P. Approval summary: sunitinib for the treatment of imatinib refractory or intolerant gastrointestinal stromal tumors and advanced renal cell carcinoma. *Clin. Cancer Res.* **2007**, *13*, 1367–1373.
183. McCormack, P. L.; Nintedanib: first global approval. *Drugs* **2015**, *75*, 129–139.
184. Eldehna, W. M.; Almahli, H.; Al-Ansary, G. H.; Ghabbour, H. A.; Aly, M. H.; Ismael, O. E.; Al-Dhfyan, A.; Abdel-Aziz, H. A. Synthesis and in vitro anti-proliferative activity of some novel isatins conjugated with quinazoline/phthalazine hydrazines against triple-negative breast cancer MDA-MB-231 cells as apoptosis-inducing agents. *J. Enzyme Inhib. Med. Chem.* **2017**, *32*, 600-613.
185. Eldehna, W. M.; Altoukhy, A.; Mahrous, H.; Abdel-Aziz, H. A. Design, synthesis and QSAR study of certain isatin-pyridine hybrids as potential anti-proliferative agents. *Eur. J. Med. Chem.* **2015,** *90*, 684-694.
186. Eldehna, W. M.; Fares, M.; Ibrahim, H. S.; Aly, M. H.; Zada, S; Ali, M. M.; Abou-Seri, S. M.; Abdel-Aziz, H. A.; El Ella, D.A.A. Indoline ureas as potential anti-hepatocellular carcinoma agents targeting VEGFR-2: Synthesis, *in vitro* biological evaluation and molecular docking. *Eur. J. Med. Chem.* **2015**, *100*, 89-97.
187. Havrylyuk, D.; Zimenkovsky, B.; Vasylenko, O.; Gzella, A.; Lesyk, R. Synthesis of New 4‐Thiazolidinone-, Pyrazoline-, and Isatin-Based Conjugates with Promising Antitumor Activity. *J. Med. Chem.* **2012**, *55*, 8630-8641.
188. Kaminskyy, D.; Khyluk, D.; Vasylenko, O.; Zaprutko, L.; Lesky, R. A Facile Synthesis and Anticancer Activity Evaluation of Spiro[Thiazolidinone-Isatin] Conjugates. *Sci Pharm.* **2011**, *79*, 763-777.
189. Wang, S.; Zhao, Y.; Zhang, G.; Lv, Y.; Zhang, N.; Gong, P. Design, synthesis and biological evaluation of novel 4-thiazolidinones containing indolin-2-one moiety as potential antitumor agent. *Eur. J. Med. Chem.* **2011**, *46*, 3509-3518.
190. Ramshid, P. K.; Jagadeeshan, S.; Krishnan, A.; Mathew, M.; Nair, S.A.; Pillai, M. R. Synthesis and *In Vitro* Evaluation of Some Isatin-Thiazolidinone Hybrid Analogues as Anti-Proliferative Agents. *Med. Chem.* **2010**, *6*, 306-312.
191. Leitans, J.; Kazaks, A.; Balode, A.; Ivanova, J.; Zalubovskis, R.; Supuran, C. T.; Tars, K. Efficient Expression and Crystallization System of Cancer-Associated Carbonic Anhydrase Isoform IX. *J. Med. Chem.* **2015**, *58*, 9004-9009.

192. Csermely, P.; Agoston, V.; Pongor, S. The efficiency of multi-target drugs: the network approach might help drug design. *Trends Pharmacol. Sci.* **2005**, *26*, 178-182.
193. Espinoza-Fonseca, L. M. The benefits of the multi-target approach in drug design and discovery. *Bioorg. Med. Chem*. **2006,** *14*, 896-897.
194. Zimmermann, G. R.; Lehár, J.; Keith, C. T. Multi-target therapeutics: when the whole is greater than the sum of the parts. *Drug Discov. Today.* **2007**, *12*, 34-42.
195. Sikazwe, D. M. N. The Multi-Target Drug Design Era is Here, Consider it. *Drug Design* **2012**, *1*, 1000-1101.
196. Dsouza, R. N.; Pischel, U.; Nau, W. M. Fluorescent dyes and their supramolecular host/guest complexes with macrocycles in aqueous solution. *Chem. Rev.* **2011**, *111*, 7941–7980.
197. Rudat, B.; Birtalan, E.; Thomè, I.; Kolmel, D. K.; Horhoiu, V. L.; Wissert, M. D.; Lemmer, U.; Eisler, H. J.; Balaban, T. S.; Brase, S. Novel pyridinium dyes that enable investigations of peptoids at the single-molecule level. *J. Phys. Chem. B.* **2010**, *114*, 13473-13480.
198. Guise, C. P.; Mowday, A. M.; Ashoorzadeh, A.; Yuan, R.; Lin, W. H.; Wu, D. H.; Smaill, J.B.; Patterson, A.V.; Ding, K. Bioreductive prodrugs as cancer therapeutics: targeting tumor hypoxia. *Chin. J. Cancer* **2014**, *33*, 80-86.
199. Schrödinger Suite Release 2016-1, Schrödinger, LLC, New York, NY, 2016: (a) Maestro v.10.5; (b) Epik, v.3.5; (c) Impact, v.7.0; (d) Prime, v.4.3; (e) Macromodel v.11.1. (f) Glide, v.7.0; (g) Jaguar, v.9.1;
200. (a) Kaminski, G. A.; Friesner, R. A.; Tirado-Rives, J.; Jorgensen, W. L. Evaluation and Reparametrization of the OPLS-AA Force Field for Proteins via Comparison with Accurate Quantum Chemical Calculations on Peptides. *J. Phys. Chem. B.* **2001**, *105*, 6474-6487; (b) Hornak, V.; Abel, R.; Okur, A.; Strockbine, B.; Roitberg, A.; Simmerling, C. Comparison of multiple Amber force fields and development of improved protein backbone parameters *Proteins* **2006**, *65*, 712-725.
201. Li, J.; Abel, R.; Zhu, K.; Cao, Y.; Zhao, S.; Friesner, R. A. The VSGB2.0 model: a next generation energy model for high resolution protein structure modeling. *Proteins*, **2011**, *79*, 2794−2812.
202. Orbisaglia, S.; Jacques, B.; Braunstein, P.; Hueber, D.; Pale, P.; Blanc, A.; de Fremont, P. Synthesis, characterization, and catalytic activity of cationic NHC gold(III) pyridine complexes. *Organometallics* **2013**, *32*, 4153−4164.
203. Wang, Y.; Kegong, J.; Sylvester, L.; Zhang, L. Rapid access to chroman-3-ones through gold-catalyzed oxidation of propargyl aryl ethers. *Angew. Chem. Int. Ed.* ***2012***, *51*, 1915–1918.
204. Zhang, W.; Li, Z.; Zhou, M.; Wu, F.; Hou, X.; Luo, H.; Liu, H.; Han, X.; Yan, G.; Ding, Z.; Li, R. Synthesis and biological evaluation of 4-(1,2,3-triazol-1-yl) coumarin derivatives as potential antitumor agents. *Bioorg. Med. Chem. Lett.* **2014**, *24*, 799–807.
205. Lindè, A.; Kruger, L.; Backvall, J. Highly selective sulfoxidation of allylic and vinylic sulfides by hydrogen peroxide using a flavin as catalyst. *J. Org. Chem*. **2003**, *68*, 5890-5896.
206. Dinges, J.; Albert, D.; Arnold, L.; Ashworth, K.; Akritopoulou-Zanze, I. 1,4-Dihydroindeno[1,2-c]pyrazoles with acetylenic side chains as novel and potent multitargeted receptor tyrosine kinase inhibitors with low affinity for the hERG ion channel. *J. Med. Chem*. **2007**, *50*, 2011-2029.
207. Roy, U. K.; Roy, S. SnCl2 mediated efficient N,N-dialkylation of azides to tertiary-amine via potential stannaimine intermediate. *J. Organomet. Chem.* **2006**, *71*, 1525–1530.
208. Carta, F.; Mannelli, L.; Pinard, M.; Ghelardini, C.; Scozzafava, A.; McKenna, R.; Supuran, C. T. A class of sulfonamide carbonic anhydrase inhibitors with neuropathic pain modulating effects. *Bioorg. Med. Chem.* **2015**, *23*, 1828–1840.
209. Kwok, S.; Fotsing, J.; Fraser, R.; Rodionov, V.; Fokin, V. Transition-metal-free catalytic synthesis of 1,5-diaryl-1,2,3-triazoles. *Org. Lett*. **2010**, *12*, 4217–4219.
210. Wilkening, I.; Del Signore, G.; Hackenberger, C. Synthesis of phosphonamidate peptides by Staudinger reactions of silylated phosphinic acids and esters. *Chem. Commun*. **2011**, *47*, 349–351.

211. Ciocoiu, C.; Nikolic, N.; Nguyen, H.; Thoresen, H.; Aasen, A.; Hansen, T. Synthesis and dual PPARa/d agonist effects of 1,4-disubstituted 1,2,3-triazole analogues of GW 501516. *Eur. J. Med. Chem.* **2010**, *45*, 3047-3055.
212. Baron, A.; Herrero, C.; Quaranta, A.; Charlot, M.; Leibl, W.; Vauzeilles, B.; Aukauloo, A. Click chemistry on a ruthenium polypyridine complex. An efficient and versatile synthetic route for the synthesis of photoactive modular assemblies. *Inorg. Chem*. **2012**, *51*, 5985−5987.
213. Jawalekar, A.; Meeuwenoord, N., Cremers, G.; Overkleeft, H.; van der Marel, G.; Rutjes, G.; van Delft, F. L. Conjugation of nucleosides and oligonucleotides by [3+2] cycloaddition. *J. Org. Chem*. **2008**, *73*, 287-290.
214. Zhu, Z.; Li, Y.; Wei, C.; Wen, X.; Xi, Z.; Yi, L. Multi-Fluorinated Azido Coumarins for Rapid and Selective Detection of Biological H2 S in Living Cells. *Chem. Asian J*. **2016**, *11*, 68 -71.
215. Dai, Z.; Chen, Y.; Zhang, M.; Kun Li, S; Yang, T.; Shen, L.; Wang, J.; Qian, S.; Zhue H.; Hao Ye, Y. Synthesis and antifungal activity of 1,2,3-triazole phenylhydrazone derivatives. *Org. Biomol. Chem*., **2015**, *13*, 477–486.
216. Suwal, S.; Pflum, M. Phosphorylation-Dependent Kinase–Substrate Cross-Linking. *Angew. Chem. Int. Ed*. **2010**, *49*, 1627-1630.
217. Leslie, A. G. W.; Powell, H. R. Processing diffraction data with mosflm. In *Evolving Methods for Macromolecular Crystallography*. NATO Science Series II: Mathematics, Physics and Chemistry, Vol. 245; Springer Netherlands: Dordrecht, The Netherlands, **2007**; pp 41-51.
218. Murshudov, G. N.; Vagin, A. A.; Dodson, E. J. Refinement of macromolecular structures by the maximum-likelihood method. *Acta Crystallogr.* **1997**, *53*, 240-255.
219. Emsley P.; Lohkamp B.; Scott W.; Cowtan K. Features and development of coot. *Acta Crystallogr.* **2010**, *66*, 486-501.
220. Lamzin, V. S.; Perrakis, A.; Wilson, K. S.; In *International Tables for Crystallography. Vol. F: Crystallography of Biological Macromolecules*; Rossmann, M. G., Arnold, E., Eds.; Kluwer Academic Publishers: Dordrecht, The Netherlands, **2001**; pp 720-722.
221. Lovell, S. C.; Davis, I. W.; Arendall, W. B.; de Bakker, P. I. W.; Word, J. M.; Prisant, M. G.; Richardson, J. S.; Richardson, D. C. Structure validation by Calpha geometry: phi,psi and Cbeta deviation. *Proteins: Struct. Funct. Genet.* **2003**, *50*, 437-450.
222. Pettersen, E. F.; Goddard, T. D.; Huang, C. C.; Couch, G. S.; Greenblatt, D. M.; Meng, E. C.; Ferrin, T. E. UCSF Chimera--a visualization system for exploratory research and analysis. *J. Comput. Chem.* **2004**, *25*, 1605-1612.
223. Rutkauskas, K.; Zubrienė, A.; Tumosienė, I.; Kantminienė, K.; Kažemėkaitė, M.; Smirnov, A.; Kazokaitė, J.; Morkūnaitė, V.; Čapkauskaitė, E.; Manakova, E.; Gražulis, S.; Beresnevičius, Z. J.; Matulis, D. 4-amino-substituted benzenesulfonamides as inhibitors of human carbonic anhydrases. *Molecules* **2014**, 19, 17356-17380.
224. Krauss, A. H. P.; Impagnatiello, F.; Toris, C. B.; Gale, D. C.; Prasanna, G.; Borghi, V.; Chiroli, V.; Chong, W. K. M.; Carreiro, S. T.; Ongini, E. Ocular hypotensive activity of BOL-303259-X, a nitric oxide donating prostaglandin F2α agonist, in preclinical models. *Exp. Eye Res.* **2011**, *93*, 250−255.
225. Kilkenny, C.; Browne, W. J.; Cuthill, I. C.; Emerson, M.; Altman, D. G. Improving bioscience research reporting: the ARRIVE guidelines for reporting animal research. *J. Pharmacol. Pharmacother.* **2010**, *1*, 94–99.
226. Takakura, H.; Sasakura, K.; Ueno, T; Urano, Y.; Terai, T.; Hanaoka, K.; Tsuboi, T.; Nagano, T. Development of Luciferin Analogues Bearing an Amino Group and Their Application as BRET Donors. *Chem. Asian J.* **2010**, *5*, 2053-2061.
227. Biasini, M.; Bienert, S., Waterhouse, A.; Arnold, K.; Studer, G.; Schmidt, T.; Kiefer, F.; Gallo Cassarino T.; Bertoni, M.; Bordoli, L.; Schwede, T. SWISS-MODEL: modelling protein tertiary and quaternary structure using evolutionary information. *Nucleic Acids Res.* **2014**, *42*, W252-258.

228. Arnold, K.; Bordoli, L.; Kopp, J.; Schwede, T. The SWISS-MODEL workspace: a web-based environment for protein structure homology modelling. *Bioinformatics.* **2006**, *22*, 195-201.
229. Liu, X. J.; Chen, R. Y.; Weng, L. H.; Leng, X. B. Synthesis and Structure of Novel Phosphonodipeptides Containing a Uracil or Thymine Group. *Heteroatom Chemistry* **2000**, *11*, 422-427.
230. Himo, F.; Lovell, T.; Hilgraf, R., Rostovtsev, V. V.; Noodleman, L.; Sharpless, K. B.; Fokin. V. V. Copper(I)-catalyzed synthesis of azoles. DFT study predicts unprecedented reactivity and intermediates. *J. Am. Chem. Soc.* **2005**, *127*, 210-216.
231. Hakimelahi, G. H.; Gassanov, G. S.; Hsu, M. H.; Hwua, J. R.; Hakimelahib, S. A Novel Approach Towards Studying Non-Genotoxic Enediynes as Potential Anticancer Therapeutics. *Bioorg. Med. Chem.* **2002**, *10*, 1321–1328.
232. Prajapati, R. K.; Kumar, J.; Verma, S. Silver-catalyzed intramolecular cyclization of 9-propargyladenine via N3 alkylation. *Chem. Commun.* **2010**, *46*, 3312–3314.
233. Carta, F.; Ferraroni, M.; Scozzafava, A.; Supuran, C. T. Fluorescent sulfonamide carbonic anhydrase inhibitors incorporating 1,2,3-triazole moieties: Kinetic and X-ray crystallographic studies. *Bioorg. Med. Chem.* **2016**, *24*, 104-112.
234. Umura, K.; Oine, T.; Yamada, Y.; Tomie, M.; Adachi, T.; Nagura, T.; Kawazu, M.; Mizoguchi, T.; Inoue, I. Synthetic Studies on Eritadenine. I. Reactions of Some Purines with the 2,3-0-Protected Dihydroxybutyrolactone. *J. Org. Chemistry* **1971**, *36*, 1573-1579.
235. Alafeefy, A. M.; Ceruso, M.; Al-Tamimi, A. S.; Del Prete, S.; Capasso, C.; Supuran, C. T. Quinazoline–sulfonamides with potent inhibitory activity against the a-carbonic anhydrase from Vibrio cholerae. *Bioorg. Med. Chem.* **2014**, *22*, 5133–5140.
236. Pinard, M. A.; Boone, C. D.; Rife, B. D.; Supuran, C. T.; McKenna, R. Structural study of interaction between brinzolamide and dorzolamide inhibition of human carbonic anhydrases. *Bioorg. Med. Chem.* **2013**, *21***,** 7210–7215.
237. Otwinowski, Z. & Minor, W. [20] Processing of X-ray diffraction data collected in oscillation mode. in *Methods in Enzymology* (ed. Charles W. Carter, J.) **Volume 276,** 307–326 (Academic Press, 1997).
238. Avvaru, B. S.; Kim, C.U.; Sippel, K. H.; Gruner, S. M.; Agbandje-McKenna, M.; Silverman, D. N.; McKenna, R. A short, strong hydrogen bond in the active site of human carbonic anhydrase II. *Biochemistry* **2010**, *49***,** 249–251.
239. Adams, P. D., Afonine, P. V.; Bunkóczi, G.; Chen, V. B., Davis, I. W.; Echols, N.; Headd, J. J., Hung, L.W.; Kapral, G. J.; Grosse-Kunstleve, R. W.; McCoy, A. J.; Moriarty, N.W.; Oeffner, R.; Read, R.J.; Richardson, D. C.; Richardson, J. S.; Terwilliger, T.C.; Zwart, P. H. *PHENIX* : a comprehensive Python-based system for macromolecular structure solution. *Acta Crystallogr. D Biol. Crystallogr.* **2010**, *66***,** 213–221.
240. Emsley, P.; Cowtan, K. *Coot* : model-building tools for molecular graphics. *Acta Crystallogr. D Biol. Crystallogr.* **2004**, *60***,** 2126–2132.
241. The PyMOL Molecular Graphics System, Version 1.5.0.4 Schrödinger, LLC.